ELECTROSTATIC STABILIZATION OF SUSPENSIONS IN NON-AQUEOUS MEDIA

PROMOTOR:

Dr. J. Lyklema hoogleraar in de fysische chemie, met bijzondere aandacht voor de grensvlak- en kolloïdchemie

Ph.C. van der Hoeven

ELECTROSTATIC STABILIZATION OF SUSPENSIONS IN NON-AQUEOUS MEDIA

PROEFSCHRIFT
TER VERKRIJGING VAN DE GRAAD VAN DOCTOR
IN DE LANDBOUW- EN MILIEUWETENSCHAPPEN
OP GEZAG VAN DE RECTOR MAGNIFICUS,
DR. H.C. VAN DER PLAS,
IN HET OPENBAAR TE VERDEDIGEN
OP WOENSDAG 19 JUNI 1991
DES NAMIDDAGS TE VIER UUR IN DE AULA
VAN DE LANDBOUWUNIVERSITEIT TE WAGENINGEN.

STELLINGEN

behorende bij het proefschrift

ELECTROSTATIC STABILIZATION OF SUSPENSIONS IN NON-AQUEOUS MEDIA

van

Ph.C. van der Hoeven

1. Als gevolg van de aanwezigheid van verontreinigen worden in vele industriële niet-ionogene oppervlakte-actieve stoffen hoge geleidbaarheden gemeten. Gezien de daaruit af te leiden aanwezigheid van aanzienlijke ionenconcentraties lijkt het gebruik van de naam 'nonionics' voor deze vloeistoffen nauwelijks terecht. *Dit proefschrift, hoofdstuk 2.*

2. Tot nog toe is slechts weinig aandacht besteed aan kolloïdale eigenschappen in niet-waterige media van dispersies van in water oplosbare vaste stoffen, zoals die bijvoorbeeld gebruikt worden in was- en reinigingsmiddelen. Gezien het maatschappelijk belang van deze stoffen wekt deze geringe aandacht bevreemding, te meer daar wel veel aandacht wordt besteed aan kolloïdale eigenschappen in deze media van in water onoplosbare stoffen. *Dit proefschrift, hoofdstuk 2.*

3. De stelling dat vlokking aanleiding geeft tot separatie is correct voor verdunde kolloïdale systemen. In geconcentreerde suspensies geeft meer vlokking juist aanleiding tot minder separatie. *Dit proefschrift, hoofdstukken 2 en 3.*

4. De suggestie dat de Hamaker constante van een anorganisch zout tijdens een kristalisatieproces invloed zou hebben op de kristalgroei en op de porositeit van poederdeeltjes verkregen uit een waterige dispersie verdient meer onderzoek. *Dit proefschrift, hoofdstuk 3.*

5. Het vinden van buitengewoon lage geleidbaarheden in apolaire koolwaterstoffen heeft tot de misvatting geleid dat in alle niet-waterige media de ionenconcentraties eveneens zo laag zijn dat geen electrostatische stabilisatie van kolloïdale systemen zou mogen worden verwacht. *Dit proefschrift, hoofdstuk 4.*

6. De toepassing van de theorie van G.R. Féat and S. Levine (*J. Colloid Interface Sci.* **1976**, 54, 34) over electrostatische stabilisatie in apolaire koolwaterstoffen door J.H. Green and G.D. Parfitt (*Colloids Surf.* **1988**, 29, 391) op kolloïdale suspensies met toegevoegde dispersiemiddelen, is onjuist. *Dit proefschrift, hoofdstuk 4.*

7. Onder invloed van licht in het nabije-ultraviolet kan zwaveldioxide fotochemisch worden aangeslagen tot een hogere en reaktievere energietoestand (J.G. Calvert and J.N. Pitts. **Photochemistry.** (J. Wiley, New York), **1965**, p. 210). Dit geeft aanleiding tot substitutie van zwaveldioxide in een reactie met polaire media (J.R. Nooi, Ph.C van der Hoeven (*Tetrahedron Letters,* **1970**, 29, p. 2531; *Recueil* **1972**, 91, p.161); in alkanen in aanwezigheid van zuurstof moet echter, gezien een geconstateerde kwantumopbrengst van alkylsulfonzuur van ongeveer 4000, een radicaal kettingreactie worden aangenomen.

8. De veronderstelling dat de waswerking van een wasmiddel kan worden beoordeeld aan de hand van experimenten met proeflapjes in een laboratoriumopstelling gaat voorbij aan de grote invloed op de waswerking van variabele factoren die te maken hebben met consumentengedrag en vuilconcentratie.

9. Een progressief energie-tariefstelsel stimuleert zonder twijfel de ontwikkeling van energiezuiniger wasprocessen.

10. De ontkleuring van hydrofiele chromoforen door oxydatie met perazijnzuur kan met kleine hoeveelheden van een sterke complexant voor overgangsmetaalionen zeer aanzienlijk worden versneld.

11. Calciumzeep complexen hebben een zodanig lage oplosbaarheid in water dat ze, na adsorptie op een kristalletje van een in water-oplosbare vaste stof, in staat zijn de oplossnelheid van die vaste stof in water zeer sterk te verlagen.

12. De naambekendheid die door Lever zou kunnen worden verworven met een speciaal ontwikkeld middel voor de reiniging van gevels van belangrijke cultuurmonumenten, zoals bijvoorbeeld die van het Vaticaan, is zo groot dat financiële experts een dergelijk project zouden bestempelen als 'low-risk, high-pay'.

13. De significante verschillen die tussen diverse, willekeurig gekozen proteasen worden gevonden bij de ontkleuring in alkalisch milieu van eiwithoudende vlekken, maakt het aannemelijk dat verder onderzoek moet leiden tot de ontdekking van nog meer effectieve proteasen.

14. Het gebruik in een zeepziederij van proceswater, dat afkomstig is uit de rivier, zodat het zout-gehalte in het proceswater afhankelijk is van de getijdebeweging, leidt tot de schijnbaar onwetenschappelijke doch juiste conclusie dat 'zeepzieden bij volle maan de beste zeep oplevert'. Conclusies als deze tonen aan dat het streven van de stichting 'Skepsis' om parafysische beweringen op hun merites te onderzoeken een juist streven is.

15. De keuze die de overheid maakt tot bezuiniging in de gezondheidszorg is betreurenswaardig gezien de noodzaak voor meer onderzoek bij een nog steeds geleidelijke toename van het aantal gevallen van acute myeloïde leukemie in onze samenleving en de huidige machteloosheid van medici bij de behandeling van deze ziekte en van andere ongeneeslijke ziekten van het afweersysteem.

16. De beperking van het aantal letters in de titels van computerbestanden tot acht kan op den duur leiden tot een afname van de meer dan achtletterige woorden in onze taal.

17. De noodzaak dat hoboïsten het hout van hun riet enige tijd ter zwelling in water moeten laten weken, met het doel het opwekken van trillingen in het riet te vereenvoudigen en daarmee het door de hoboïst geproduceerde geluid te verbeteren, creëert bij musiceren in oude kerken een probleem. Dit kan worden beschouwd als een bijzonder voorbeeld van problemen die kunnen ontstaan in een niet-waterige omgeving.

18. Het begrip 'pasta-achtig' voor het aangeven van de aggregatietoestand van een stof kan leiden tot verwarring bij de kenners van de Italiaanse keuken.

19. Uit emancipatorische overwegingen dient de zegswijze 'Kleren maken de man' te worden herzien. Deze uitdrukking kan ten onrechte het vermoeden wekken dat alleen de man kleren nodig heeft om het te maken.

Opgedragen aan

Marianne

David

Ter herinnering aan

Eddo

CHAPTERS

VOORWOORD

Het werk beschreven in dit proefschrift is een onderdeel van het 'Detergents research' programma van het Unilever Research Laboratorium in Vlaardingen. Het is uitgevoerd in de sectie 'Liquids' van de 'Detergents' divisie.

Fysisch-chemisch onderzoek binnen een industriële onderzoeksgroep zoals onze wasmiddeldivisie is, anders dan een buitenstaander misschien zou vermoeden, niet zo heel erg verschillend van datgene wat plaats vindt in niet-industriële onderzoekscentra. De werkwijzen en meetinstrumenten zijn in grote mate dezelfde en ook de drang van de onderzoeker naar het vinden van de 'wetenschappelijke waarheid' is niet anders. Ook de gehanteerde methoden bij het onderzoek zijn in principe niet verschillend en volgen vaak de bekende route van de opstelling van een meest waarschijnlijke werkhypothese, na het uitvoeren van de experimenten de vergelijking van het resultaat met de hypothese, de verwerping van de hypothese of de aanvaarding of uitbreiding daarvan, enzovoorts. Deze werkwijze is sterk gelijkend op die toegepast in disciplines waar men te maken heeft met door de natuur veroorzaakte variaties in omstandigheden of 'materialen', zoals in de landbouwkunde, de levensmiddelenwetenschappen of in de geneeskunde.

Natuurlijk is de doelstelling wel verschillend. Die heeft in de industrie praktisch altijd een toegepaste achtergrond. Onderzoek moet leiden tot een nieuwe technologie, een nieuw produkt, een verbetering van de veiligheid van een bestaand produkt of van een gebruikt proces, of tot een kostenbesparing. Het moet oplossingen aandragen voor de gevolgen van een iets andere samenstelling van de grondstof, enzovoorts. Daar deze doelstelling zonder een verder inzichtelijk onderzoek vaak niet kan worden bereikt is daarmee de basis gelegd voor een researchinstituut zoals het onze. De researchinstelling fungeert daarbij als kennisbank voor de werkmaatschappijen.

Een ander gevolg van deze randvoorwaarde voor de fysisch-chemisch onderzoeker is het gebruik van materialen die direct afkomstig zijn uit het produktieproces, dat wil zeggen zonder verdere omvorming of zuivering. Deze processen zouden leiden tot een gedrag van de grondstof dat niet meer geheel representatief is voor de in de praktijk gebruikte grondstof en wordt daarom in 'exploratief' zowel als in 'toegepast' onderzoek zoveel mogelijk gemeden. Een gevolg daarvan is dat de stoffen waarmee we werken vaak minder goed zijn gedefinieerd en dat we bij onze resultaten te maken kunnen hebben met de invloeden van experimentele ruis. Er is dan veel experimenteel werk nodig om de 'praktische' onderliggende relaties te ontdekken. Zonder dit zal echter het echt begrip nodig om aan onze doelstellingen te voldoen niet worden verkregen.

Bij het onderzoek beschreven in dit proefschrift is voortdurend een poging gedaan relaties te vinden tussen het gedrag van de praktische grondstoffen en het gedrag zoals dat volgens de bestaande kennis of theorie zou mogen worden voorspeld. Om precies te weten wat we in handen hadden, was het daarom nodig de gebruikte grondstoffen niet alleen wat betreft hun chemische samenstelling, maar juist ook wat betreft hun fysische vorm uitgebreid te analyseren. Als gevolg daarvan is het

aantal verbindingen waarmee dit onderzoek is uitgevoerd, beperkt gebleven. Het is de oprechte hoop van de schrijver van dit proefschrift dat met verdere studies op het gebied van de dispersies in de 'laag-polaire nonionics', deze kennis verder zal worden uitgebouwd.

MET DANK AAN...

Een omvangrijke studie als deze was niet mogelijk geweest zonder de steun, begeleiding en hulp van een groot aantal personen. Op deze plaats wil ik graag iedereen bedanken die door zijn beslissing of medewerking mij in staat gesteld heeft tot het doen van dit onderzoek en tot het schrijven van dit proefschrift.

Op de allereerste plaats betreft dit mijn promotor Prof. Dr. Hans Lyklema. Hans, ik ben je zeer dankbaar voor de medewerking die je van het begin tot aan het eind aan dit ongewone promotieonderzoek hebt willen geven. Ik heb buitengewoon veel geleerd van je inspirerende en altijd opbouwende kritiek. Voor mij was dit een tot voorbeeld strekkende ervaring. Het is mij duidelijk geworden waarom de vakgroep Fysische- en Kolloïdchemie in Wageningen onder jouw leiding zo'n toonaangevende positie in de wereld heeft veroverd. Ik ben er trots op juist bij jou te mogen promoveren.

Mijn dank betreft natuurlijk vervolgens mijn werkgever, in de personen van Dr. Hans Broekhoff, Senior Research Member van de 'Detergents Management Group', de directeur 'Detergents' van het Unilever Research Laboratorium in Vlaardingen Dr. Tony Lee en mijn Division-Manager Ir. Henk Vonkeman, die mij de gelegenheid hebben gegeven tot het doen van dit onderzoek. Verder betreft mijn dank mijn Section-Managers Dr. Terry Clarke en Dr. Hans Dröge, die de ruimte voor dit onderzoek hebben gecreëerd en het hardnekkig tegen velerlei aanvallen hebben verdedigd. Hans, Tony, Henk, Terry en nogmaals Hans, dank voor het vertrouwen dat jullie van het begin af aan in het slagen van deze onderneming hebben getoond.

Op deze plaats wil ik verder vooral bedanken de medewerkers in mijn afdeling die op zo'n enthousiaste wijze aan dit hele project hebben meegewerkt. Zonder anderen tekort te willen doen, noem ik daarbij speciaal Ing. Peter Versluis, die van het begin af aan betrokken is geweest bij dit project en die mij heeft ingewijd in de geheimen van de reologie, en Gert-Jan van den Oever, mijn ervaren gesprekspartner die het nooit moe werd met mij over de elektrische en diëlektrische eigenschappen van niet-waterige media te discussiëren. Ook wil ik noemen Piet van Reeven en Kees Zuijdervliet, die bergen experimenteel werk hebben verzet. Zoals dat ook het geval is in de niet-industriële laboratoria is ook onderzoek in een industrieel laboratorium een zaak van teamwerk en goede sfeer in de werkomgeving. Het is te gemakkelijk te zeggen dat ieder eenvoudig zijn werk heeft gedaan. Zonder jullie betrokkenheid en motivatie waren we niet zo ver gekomen. Ook de andere medewerkers van de sectie 'Liquids' wil ik in deze dank betrekken.

Verschillende medewerkers van de secties 'Spectroscopy', 'Analytical Chemistry', 'Catalysis' en 'Liquids Processing' en van de 'Technical Applications Unit' hebben aan dit onderzoek door experimenteel werk of door discussie bijgedragen, evenals verschillende leden van de sectie 'Physical Chemistry' onder leiding van Dr. Wim Agterof. Hiervoor allen mijn dank. In het bijzonder echter wil ik noemen Dr. Jan Bus en Kest Hissink van de afdeling 'Radiochemistry', die de methode van de γ-straling-absorptie speciaal voor onze suspensies hebben ontwikkeld en Dr. Michiel Gribnau en Henrie van Aalst van de afdeling 'Nuclear Magnetic Resonance' die de pfg-nmr-metingen speciaal voor dit onderwerp naar ons laboratorium hebben gehaald. Uit het feit dat beide methoden nu ook voor andere soortgelijke onderzoeken worden gebruikt, kunnen we concluderen dat onze aanpak niet alleen voor ons werk een nuttige is geweest. Ook wil ik op deze plaats niet nalaten te noemen de medewerkers van de afdeling 'Electron Microscopy' en met name Ing. Han Blonk, voor het maken van de 'Scanning EM' opnamen. Ook Ing. Piet van der Vlist, die ons zeer heeft geholpen bij de meting van de brekingsindices met behulp van de immersie-methode, wil ik daarvoor dankzeggen.

Van de medewerkers van ons laboratorium wil ik ten slotte bedanken Dr. Mark Houghton voor de correcties van het Engels van mijn manuscript hoofdstukken, Martin Pols en John Deij voor de adviezen over de vormgeving en druk, en Mari van der Giessen voor het omslagontwerp.

Natuurlijk wil ik niet eindigen zonder ook mijn vrouw en vriendin Marianne in het openbaar te bedanken voor de hulp verleend tijdens het schrijven van dit proefschrift. Hulp die ze gaf naast een drukke werkkring, maar die haar er niet van weerhield een tegelijk begonnen academische studie in recordtijd succesvol af te ronden. De aanleiding voor ons beiden om met onze activiteiten te beginnen, was ongewoon en droevig. Gelukkig hebben wij beiden, ook dank zij de hulp van Dr. Roos van de Mast, weer een draad kunnen vinden waaraan we ons hebben kunnen optrekken om verder te gaan. Ten slotte dank ik ook mijn zoon David, die zoveel begrijpt, en die met zijn wijze houding ervoor zorgde dat we zo nu en dan ook nog wat rust namen.

CONTENTS

Chapter 1

INTRODUCTION

1.1 LIQUID PRODUCTS FOR WASHING

At present there is a trend for consumers of detergent products to have an increasing preference for products in a liquid form. In the last few years many new liquid detergent products have appeared on the market, which gradually replace the detergent powders. For users, as well as for the manufacturing industry, the liquid product form has advantages. Liquid products tend to dissolve more rapidly, are easier to use and do not dust during preparation and application. Also in washing machines utilizing automatic dosing from containers, liquid products have good opportunities for application.

All detergent powders on the market contain a blend of 'actives' mixed with a variety of other solid adjuncts. Actives are surfactant molecules which help to remove the soil during a washing process. The solids applied, sometimes in patent literature referred to as 'detergency adjuvant solids' or simply 'detergent solids', have a variety of other functions. Normally, in detergent powders a calcium binder or 'builder' is present, which improves the efficiency of the washing process by binding the calcium ions that give rise to the water-hardness. Other solid adjuncts that can be present are bleaches and enzymes. They contribute to the oxidative or enzymatic removal of stains. Bleach stabilizers, enzyme stabilizers, anti-redeposition aids and pH-buffers are also solids and commonly applied in detergent powder formulations.

Liquid detergent products are usually emulsions or suspensions, in which water is the continuous liquid medium. They contain mainly actives and a limited number of dissolved or suspended solids as detergency adjuncts. The current study deals with suspensions of (detergent-related) solids in a **non-aqueous liquid**, i.e. in a liquid nonionic surfactant.

1.2 NON-AQUEOUS LIQUID DETERGENT PRODUCTS

When water is evaporated from an aqueous liquid detergent product, eventually a non-aqueous mixture of non-volatile actives and solids results. If the actives applied are liquid at room temperature, the mixture formed is a concentrated (pasty) suspension of solids with surfactants as continuous phase. As a detergent product, such a non-aqueous liquid detergent suspension can be advantageous. It can be made very concentrated and allows, in contrast to aqueous products, the combination of water sensitive bleaching agents and enzymes in one product. Preparations of such detergent suspensions have been considered for more than 20 years and are now researched for practical application.

Various nonionic surfactants are available which are liquid at room temperature and which can be used as a liquid medium. Most nonionics are mild in contact with the human skin and are biodegradable. Therefore it is particularly advantageous to develop detergent products in which the continuous phase is a liquid nonionic surfactant. A typical example of a non-aqueous liquid detergent composition with a nonionic as the liquid phase is given in Table 1.1

Table 1.1: Example of a composition of a non-aqueous liquid detergent product for fabric washing. From European patent 266 199 (1986).

Component:	% w/w
Nonionic (Plurafac RA30)	43.5
Na triphosphate	30.0
Na carbonate	4.0
Na perborate	15.5
T.A.E.D.[a]	4.0
Proteolytic enzyme	0.6
E.D.T.A.[b], silica, etc.	2.4
Total	100.0

[a] T.A.E.D.: N,N,N,N Tetraacetyl ethylene diamine; [b] E.D.T.A.: Di-sodium ethylene diamine tetraacetic acid.

The composition given in Table 1.1 is a practical example and was developed for fabric washing in drum-type washing machines. It contains sodium triphosphate as builder and soda ash (anhydrous sodium carbonate) as buffer. Sodium perborate combined with N,N,N,N Tetraacetyl ethylenediamine forms the bleach system. Further the product contains a proteolytic enzyme.

To avoid tactile grittiness in liquid products the average particle diameter of the suspended solids must be lower than about 25 μm. Since granulated detergent grade raw materials generally contain particles with greater diameters, in the production process usually a milling operation has to be included. At a typical particle size the solids volume fraction ϕ of the non-aqueous liquid suspensions ranges from 0.35 to 0.53 and the particle number concentrations is approximately 10^{15} to 10^{17} m^{-3}. The non-aqueous liquid detergent products therefore belong to the domain of concentrated suspensions.

1.3 'SETTING' OF PROTOTYPE NON-AQUEOUS LIQUID PRODUCTS

One considerable drawback of a product with the composition given in Table 1.1 is that the viscosity of the product increases with time. On storage over a period of a few weeks products can set completely solid and become unpourable (Table 1.2, 1st row). This process, which is denoted 'setting', occurs more rapidly at higher temperatures. As products are in practice sometimes stored at elevated temperatures and as the period between production and use is sometimes longer than two months, setting leads to unacceptable products.

In the course of the development of non-aqueous liquid products setting was interpreted as a consequence of instability in the colloid chemical sense. In

colloidally unstable systems, interacting suspended particles attract each other so strongly that they coagulate or flocculate. Being diffusion controlled this process progresses further with time. According to this picture, the observed viscosity rise is seen as a consequence of a continued coagulation of the suspended particles causing an increase of volume fraction of solids and of the viscosity due to immobilization by inclusion of the continuous phase.

Table 1.2: Setting and pourability after storage of a non-aqueous liquid product with and without added DoBS acid. From European patent 266 199 (1986).

DoBS acid	Setting in %*	Pourability
Absent	75	poor
Present	0	good

* Setting was measured after 2 weeks at 37 °C by tilting a bottle with product and observing the percentage which remained in an unchanged position.

When indeed setting is due to colloidal instability, reduction of the attraction between the particles, i.e. colloidal stabilization, should decrease setting and give a maintenance of control over the physical properties of the suspension. For suggestions regarding suspension stabilization in non-aqueous media a literature study was carried out. The number of papers dealing with dispersion stabilization is considerable. Surveys dealing with practical and theoretical aspects and with control of physical properties have been given by Parfitt (1981) [1.1] and Tadros (1980) [1.2], (1986) [1.3]. Elementary principles have been discussed in the textbook of Hiemenz (1986) [1.4]. Reviews on dispersions in non-aqueous media have been given by Lyklema (1968) [1.5], Parfitt and Peacock (1978) [1.6] and McKay (1984) [1.7]. The fundamentals and kinetics of agglomeration and their effects on viscosity, or more in general on rheology, are discussed by Sonntag and Strenge (1987) [1.8]. Discussions and suggestions for stabilizers for colloidal systems have been given by Napper (1983) [1.9], Tadros (1982, 1987) [1.10] and Lyklema (1985) [1.11]. However, the routes mentioned did not offer an adequate solution to our problem and did not made it possible to us to stabilize a wide range of solid ingredients suspended in nonionic.

1.4 SUSPENSIONS WITH ADDED DODECYLBENZENE SULPHONIC ACID

In our attempts to obtain control over the physical properties of solids at high volume fractions ϕ suspended in a liquid nonionic surfactant, a number of surprising observations have been made. It was found that addition of a small amount of a soluble acid derived from an organic anionic active, viz. dodecylbenzene sulphonic acid (DoBS acid or HDoBS), changed the physical properties of these suspension considerably: On pouring, no inhomogeneities, but a regular flow was observed. Also, after prolonged storage, setting was no longer occurring (see Table 1.2, 2nd row).

Similar effects were observed in suspensions of single ingredients. For example, on addition of DoBS acid to a concentrated suspension of sodium triphosphate in

the same nonionic as used for the product (Plurafac LFRA30), the viscosity decreases markedly from pasty to pourable (Fig. 1.1). The effect was already found with small amounts of added acid and is particularly large at low shear rates. At higher levels of DoBS acid the viscosity rises again, owing to the rise of the viscosity of the continuous phase.

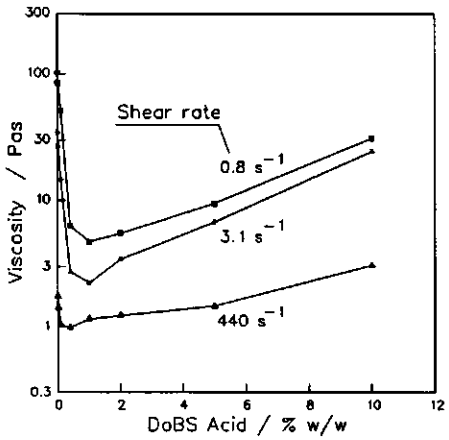

Fig. 1.1: The viscosity drop resulting from addition of DoBS acid to a concentrated suspension of sodium triphosphate in nonionic (Plurafac LFRA30) (ϕ : 0.39).

Another observation is that DoBS acid effects the sedimentation behaviour (Fig. 1.2). In the absence of DoBS acid, the uninhibited attraction between particles has the result that colliding particles agglomerate rapidly. This causes the equilibrium sediment volume to be rapidly achieved and the formation of a solid sediment. First encounters of particles are already sufficient for sticking. After addition of DoBS acid, however, the suspended particles not only sediment more slowly with time, but also form a denser sediment. The system behaves as if the particles are less strongly bound and are moving more freely (Fig. 1.3).

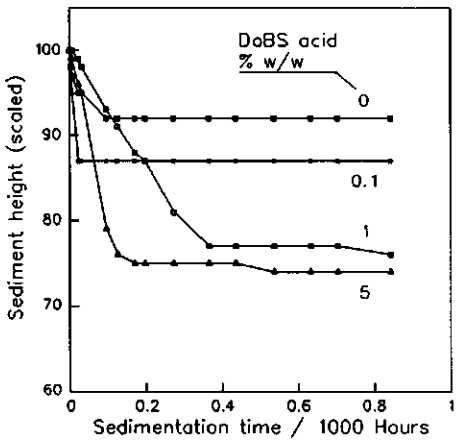

Fig. 1.2: Change in sedimentation pattern at addition of DoBS acid to a concentrated suspension of sodium triphosphate in nonionic (Plurafac LFRA30) (ϕ : 0.38).

With sodium triphosphate suspensions, with an initial ϕ of 0.38 and in the absence of acid, sedimentation leads to an increase of the average volume fraction of the sediment to 0.42. On dosing of DoBS acid to a level of 0.1 % w/w they rise to ϕ = 0.44 and on dosing to a level of 1 % of acid further to ϕ = 0.51. Addition of higher levels of acid has only limited additional influence on the final sediment volume, but has a diminishing influence on the sedimentation rate (Fig. 1.2).

The observations imply that DoBS acid achieves some degree of deflocculation and the creation of a stabilization against agglomeration of the suspended particles in nonionic liquid.

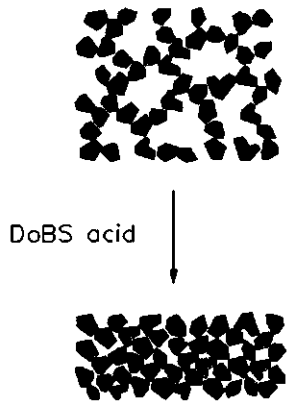

Fig. 1.3: Deflocculation model (in the lower diagram) of a coagulated suspension at addition of DoBS acid.

This is further supported by the observation that after addition of DoBS acid to a concentrated suspension of sodium triphosphate in Plurafac nonionic, the relative viscosity does not increase significantly with temperature (Fig. 1.4), whereas the viscosity of the suspension without acid as function of the temperature strongly rises. These results clearly illustrate the achievement of and maintained control over the physical properties by acid addition. The results given in this chapter demonstrate that the effect of addition of DoBS acid can be quite striking in that the physical properties of nonionic suspensions are changed dramatically.

1.5 WORKING HYPOTHESIS AND SCOPE OF STUDY

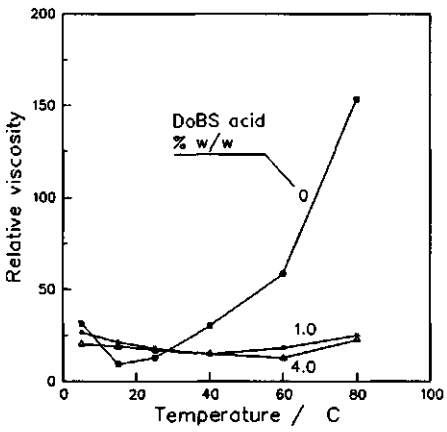

Fig. 1.4: Viscosity dependence on temperature. Influence of the addition of DoBS acid to a concentrated suspension of sodium triphosphate in nonionic (ϕ = 0.40).

Although the results cited strongly supports the assertion that a stabilizing effect is obtained from the added acid, the issue is now whether the acid acts as a steric or as an electrostatic stabilizer. Surprising as it may seem in view of the literature on non-aqueous systems, during our research the hypothesis developed that the stability is of an electrostatic nature. This was firstly based on the observation that the addition of small amounts of DoBS acid, i.e. $\leq$ 1 %, already gave the observed effects. Based on this hypothesis a further programme was established with the objective of generalizing the mechanism of suspension stabilization in nonionic surfactant media by systematic observation, paying particular attention to the possibilities and consequences of electrical double layer formation.

The subject-matter of the present study is the suspension behaviour of stabilized non-aqueous suspensions of individual (detergent-related) solids, in various nonionic surfactants as liquid phases. The experimental methods we have applied to the particles are size analysis and shape characterization. In addition we have

also measured the dielectric constants and refractive indices of the solids. On supernatants obtained after decanting we have applied elemental analyses and conductometry. Further we measured on supernatants dielectric constants and pulse nuclear magnetic resonance. Electrophoresis was carried out on particles suspended in supernatants. The suspension properties were investigated by γ-ray absorption, by (laser-) light- and electron- microscopy and by rheological methods. These techniques allowed us to determine not only such important characteristics as electrolyte dissociation and charge present on particle surfaces, but also allowed us to evaluate the Hamaker constants of the solids in suspension. Attempts are made to relate the electrostatic repulsions obtained in these systems with suspension properties in equilibrated sediments and also under shear.

It will be demonstrated that the insights obtained support the hypothesis of an electrostatic stabilization mechanism in non-aqueous nonionic surfactant media. It is the primary objective of this work that the results give solutions to problems met in the various stages of development of detergent products. Although nonionic surfactants are a mixture of compounds and the systems are therefore rather complex, the work has allowed us to draw conclusions which have scientific interest well beyond the scope of detergent applications.

1.6 SUMMARY

Concentrated suspensions of detergent powder solids in a liquid nonionic surfactant are considered for practical application as liquid detergent products. However, for practical purposes such suspensions cannot be prepared by simple mixing of the ingredients. The reason is that during storage the viscosity of the suspensions increases and the pourability drops. It is supposed that this effect is due to colloidal instability, causing the suspended particles to coagulate and agglomerate on storage.

It has been found that after addition of a small amount of dodecylbenzene sulphonic acid (DoBS acid), good pourability is maintained on storage. All the effects obtained with suspensions in nonionic surfactants suggest that the addition of DoBS acid prevents coagulation and improves colloidal stability. Based on the small amounts of DoBS acid required it was hypothesized that the colloidal stability obtained is of an electrostatic nature. In a liquid non-aqueous medium this is unexpected. The hypothesis was used to form the basis of a further study of the mechanism of stabilization.

1.7 BIBLIOGRAPHY

1.1 **Dispersions of Powders in Liquids (2nd Ed.)**. Parfitt G.D.; Editor. (Applied Science Publishers, London). **1981**.

1.2 **Physical stability of suspension concentrates.** Tadros, Th.F.. *Adv. Colloid Interface Sci.* **1980,** 12, 141-261.

1.3 **Control of the properties of suspensions.** Tadros, Th.F.. *Colloids Surf.* **1986,** 18, 137-173.

1.4 **Principles of colloid and surface chemistry. Second edition. Revised and expanded.** Hiemenz, P.C.. (Marcel Dekker, New York) **1986.**

1.5 **Principles of the Stability of Lyophobic Colloidal Dispersions in Non-Aqueous Media.** Lyklema, J.. *Adv. Colloid Interface Sci.* **1968,** 2, 65-114.

1.6 **Surface and Colloid Science. Vol. 10: Stability of Colloidal Dispersions in Non-aqueous Media.** Parfitt, G.D.; Peacock, J.; Editors (Plenum Press, London, UK). **1978.**

1.7 **Surfactant Science Series. Vol 21: Pigment Dispersion in Apolar Media. [Ch.9: In Interfacial Phenomena in Apolar Media].** McKay, R.B.. Eicke, H.F.; Parfitt, G.D.; Editors. (Marcel Dekker, New York) **1984.**

1.8 **Coagulation Kinetics and Structure Formation.** Sonntag, H.; Strenge, K.. (Plenum Press, London). **1987.**

1.9 **Polymeric stabilizations of colloidal dispersions.** Napper, D.H.. (Academic Press, London). **1983.**

1.10 a. **The effect of polymers on dispersion properties.** Tadros, Th. F..(Academic Press, London, UK). **1982**; b. **Application of surfactants and polymers in pesticidal suspension concentrates.** Tadros, Th. F.. *Spec. Publ.- R. Soc. Chem.* **1987**, 59, 102-125.

1.11 **Flocculation, sedimentation and consolidation. How polymers adsorb and effect colloid stability.** Lyklema, J.. Moudgil, B.M.; Somasundran, P.; Editors. (Am. Eng. Foundation). **1985.**

Chapter 2

COAGULATION IN CONCENTRATED SUSPENSIONS

2.1 INTRODUCTION AND DEFINITIONS

Suspensions in non-aqueous media that are most commonly studied are virtually all based on hydrocarbons (xylene or benzene) or alcohols as the liquid phase. They mainly involve three groups: 1. insoluble oxides of metals or metalloids, represented by rutile (TiO_2) and silica (SiO_2), 2. particles of organic polymeric origin, represented by various types of organic polymer latexes, and 3. a group of miscellaneous compounds including for example carbon black or salts of Ca, such as $CaCO_3$, or Ba, exemplified by $BaTiO_3$. This selection of water-insoluble solids for studies in non-aqueous liquids may suggest that water-soluble solids cannot be easily dispersed in apolar media. Although, they have to our knowledge not yet been discussed in the literature, we noticed that concentrated suspensions of various water-soluble crystalline sodium salts in non-ionic surfactants can be readily prepared. In this chapter we start with a brief description of the materials applied in this study and of a few basic features of the suspensions. Further aspects considered in this chapter are the influence of attraction on coagulation between particles and its effects on the physical properties of a suspension as a whole. Frequently a comparison will be made with the related colloidal dispersions of small sub-micron size particles.

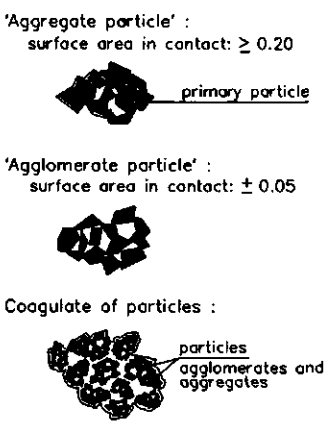

Fig. 2.1: Particles (aggregates and agglomerates) formed of primary particles, and a coagulate of particles.

The terminology applied is based, with some adaptations, upon that proposed by Parfitt (1981) [2.1]. Solids in suspension are considered to consist basically of: 1. primary particles, usually crystals with a size of a few tens of nm (nm = nanometer = 10^{-9} m), 2. 'aggregate particles' and 3. 'agglomerate particles' (Fig. 2.1). An **aggregate** is a collection of **primary particles** sintered together so that their surface area is significantly less than the sum of the areas of their constituent particles (Fig. 2.1). An **agglomerate** is formed from primary particles firmly joined at edges and corners, and gives less loss of the surface area. Agglomerates and

aggregates are porous and both contain voids, but agglomerates at a higher fraction than aggregates. Usually, aggregate particles and agglomerate particles is the species we recognize under a optical microscope as the particles in a powder. The term **dispersion** is used for the mixture of particles in a liquid irrespective of the size of the particles and so also includes colloidal-size particles. The term **suspension** is reserved for systems where the dispersed particles have larger dimensions than colloidal, i.e. larger than 1 μm (μm = micrometer = 10^{-6} m). In suspensions, particle settling under the influence of gravity leads to the formation of a **sediment** with a **clear layer** on top; the term **sedimentation** is used for the particle settling process.

The terms used to describe the formation in suspension of relatively weak clusters from aggregates or agglomerates is **flocculation**, when influenced by the presence of polymer, or **coagulation**, when influenced by electrostatics. By definition, small pressures giving low shear, such as applied during pouring or mild shaking, are sufficient to distort coagulates and flocs, but not to disintegrate the agglomerates or aggregates. Crumbling of aggregates or agglomerates occurs under influence of larger shear forces, for example such as those occurring during centrifugation. **De-flocculation and de-coagulation** are the terms used for the breakdown of flocs and coagulates into smaller entities. **Packing** is defined as the space occupied in a sediment (V_{sed}) by a volume of solid particles (V_{sol}). The **packing fraction** is equivalent to the inverse of the **solids volume fraction** ϕ (Eq. 2.1).

$$\text{Packing fraction} = \frac{V_{\text{sediment}}}{V_{\text{solids}}} = \frac{1}{\phi} \qquad [2.1]$$

For non-homodisperse particles, when not specified differently, the 'surface-weighted' mean particle radius ($a_{3,2}$) is used (for particle radius nomenclature see for example Alderliesten, 1984) [2.2]).

2.2 MATERIALS

2.2.1 The nonionics

Nonionic surfactants, or briefly nonionics, are organic molecules and usually contain no other elements than C, H and O. Alkyl ethers of polyethylene glycol are used the most frequent in present detergent formulations and contain an aliphatic tail besides this polar, polyethylene part. Examples of representative nonionic structures are given in Fig. 2.2. Nonionics are synthesized in a condensation reaction with ethylene-oxide (-CH_2-CH_2-O-: EO or E) and can have a range of molecular weights. Optionally they can be co-polymerized with propylene-oxide groups (-CH_2-$CH(CH_3)$-O-: PO or P). Alkyl chain lengths and numbers of EO or PO groups determine the properties of nonionics. Their composition is usually abbreviated to $C_nE_mP_p$, in which n, m and p stand for the average number of carbon atoms of the alkyl chain, for the number of EO groups and for the number of PO groups, respectively. In current detergent products, nonionics with $9 \leq n \leq 18$ and $3 \leq m \leq 9$ are usually preferred. Nonionic surfactants usually contain

water at a level of approximately 0.5 to 0.8 %. Specific densities are close to 1 $\times 10^3$ kg m^{-3} and their conductivity K can be as high as 10^{-4} S m^{-1} (S = Siemens = Ω^{-1}), due to the presence of ionic impurities. Nonionic surfactants are considered to be solvents with a **low polarity**. Their relative dielectric constant ranges between 4 and 12. The alkylene oxide groups give these molecules good surface active properties and good miscibility with water.

A comprehensive introduction to nonionics, their structure, composition and manufacturing has been given by Schönfeldt (1969) [2.3] and more recently by Cross (1987) [2.4]. By cation and anion exchange (using Biorad AG/1X2 and Biorad AG 50W/X8 resins) followed by microwave drying, ionogenic matter and water levels in nonionics can be

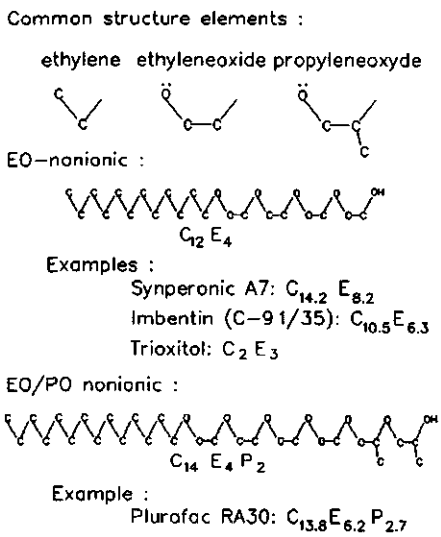

Fig. 2.2: Models and common structure elements of examples of EO and EO/PO nonionics. For clarity H-atoms are omitted.

Table 2.1: Properties of two purified and dried nonionics.

		Imbentin C91/35[a]	Plurafac LFRA30[b]
Molecular weight (M)	/10^{-3} kg Mol^{-1}	419	687
Specific density (ρ)	/10^3 kg m^{-3}	0.979	0.976
Water content	% w/w	0.03	0.06
Conductivity (K)	/10^{-6} S m^{-1}	2.84	0.30
Dielectric constant (ε)		6.23	5.70
Refractive index (25°C) (n)		1.4528	1.4529
Viscosity (η)	/10^{-3} Pa s	33.6	51.6

[a] ex ICI (UK); [b] ex Kolb (CH).

reduced considerably. Physical data after purification and drying of two representative nonionics applied in the current studies (Plurafac LFRA30 and Imbentin C91/35) are given in Table 2.1.

2.2.2 The solids

The solids used in this study involve those usually applied in current detergent powders and were used without further purification. Typical examples are the inorganic 'builder' salts soda ash (sodium carbonate), STP (sodium triphosphate), Soluble M (sodium trisilicate) or 'activated' Zeolite 4A (a sodium aluminium-silicate with 5 % water). Other examples are perborate monohydrate (sodium perborate) and calcite (calcium carbonate). A list of solids and some physical data have been given in Table 2.2. A small number of synthetic oxides such as Periclase, Lime, Anatase and Alumina have also been applied in some of the studies.

Table 2.2: Specific density, particle size and water content of the solids applied in the current study.

	Solid	Chemical Formula	ρ /10^3 kg m^{-3}	$a_{3,2}$[j] /10^{-6} m	Water content % w/w
1	Anatase[b]	TiO_2	3.81	3.8	0.2
2	Alumina[c]	Al_2O_3	3.40	4.2	< 0.1
3	Periclase[d]	MgO	2.96	3.6	0.5
4	Lime[e]	CaO	3.22	2.1	< 0.1
5	Calcite[f]	$CaCO_3$	2.57	2.6	3.0
6	Perborate[ag]	$NaBO_3.H_2O$	2.14	4.4	1.1
7	Zeolite 4A[g]	$Na_2O.Al_2O_3.(SiO_2)_2$	1.68	4.4	3.3
8	Soda ash[ah]	Na_2CO_3	2.47	4.8	0.6
9	STP[ad]	$Na_5P_3O_{10}$	2.47	6.6	0.4
10	Soluble M[ai]	$Na_2O.(SiO_2)_3$	1.95	8.4	11.6

[a] Dry-milled. [b] ex BDH [c] Merck [d] Rhone Poulenc [e] Baker [f] Interox
[g] Degussa [h] AKZO [i] Crossfield [j] Experimental results (Malvern sizer).

Solids were chosen that had an average 'surface-weighted' particle radius of 2 to 5 μm. If necessary we milled to that size. From Table 2.2 it can be seen that these attempts were reasonably successful. Under the microscope, after milling, the particles show irregular surfaces, but with an approximate spherical shape and

width to length ratios of ≤ 0.6. To a good approximation, the particles can therefore be considered as spheres. The densities measured in a pycnometer under ambient conditions in nonionic liquid were found to range between 1.7 and 3.4 $\times 10^3$ kg m^{-3}. In the cases where literature values are available these values are in good agreement, indicating that in the density measurements the voids are sufficiently large to become completely filled with nonionic liquid. The water levels of the solids are usually low although they are not completely anhydrous. Their dielectric constants range between 4 and 15 and shows them to be poor conductors. Dielectric data of the individual solids are given in Chapter 6.

The measured density of 'activated' Zeolite 4A (1.68 $\times 10^3$ kg m^{-3}) is considerably lower than the literature value given for conventional Zeolite 4A (2.1 $\times 10^3$ kg m^{-3}) given by Kimura et. al. (1987) [2.5] or for sodium aluminium silicate (2.62 $\times 10^3$ kg m^{-3}). This is ascribed to the presence of small pores of 0.4 nm in crystalline primary particles of 'activated' Zeolite 4A (Breck, 1956) [2.6], being too small to be filled with nonionic liquid.

2.2.3 Suspensions in nonionics

After mixing of solids with nonionics, chemical analysis of the supernatants showed that the solids have a limited solubility. For example, with sodium triphosphate (STP), atomic absorption measurements of a (millipore filtered) supernatant showed that sodium concentrations increase only to a level of 6 mM at most (mM = millimolar = 10^{-3} M) after a period of four months (Table 2.3). Phosphorous levels remained below the detection limit of 0.1 mM. The limited increase in specific conductivity also confirmed this. Similar observations were made with suspensions of the other solids. From microscopic observations of

Table 2.3: Solubility of STP in nonionics. Concentrations (Na, P and H_2O) and conductivity (K) in the supernatant, four months after suspension making.

		Imbentin C91/35		Plurafac RA30	
		-	+ STP*	-	+ STP
K	/10^{-6} S m^{-1}	2.84	25.8	0.30	0.80
Na	mM	0.03	5.8	0.01	0.8
P	mM	n.d.	n.d.	n.d.	n.d
Water	% w/w	0.04	0.36	0.03	0.27

* STP: sodium triphosphate; n.d.: non detectable.

solids isolated from the suspensions it can be further concluded that the particles neither visibly swell nor dissolve. These suspensions are colloidally unstable. The particles attract each other due to van der Waals attraction forces and, if present at all, repulsive forces are not sufficient to prevent coagulation.

2.2.4 The DoBS acid additive

The DoBS acid additive we used at low levels in our studies of the nonionic suspensions is n-dodecylbenzene sulphonic acid (Marlon AS3, ex Hüls) with the average chemical formula: $C_{12}H_{25}C_6H_4SO_3H$. This sulphonic acid, a strong Brønsted acid, is obtained by sulphonation with SO_3 of 'alkylate', i.e. a product formed by catalytic reaction of benzene and linear C_{12} alkene. In the catalytic reaction a mixture of isomers is formed whereby the benzene group is substituted fairly evenly among the secondary carbon atoms in the alkane chain (Agozzino, et al, 1986) [2.7]. Its 'average' structure is represented in Fig. 2.3. Commercial grades of the DoBS acid have a purity $\geq$ 96.5 %; as impurities they contain ca. 2 % of sulphuric acid and some non-converted organic matter. A discussion of linear alkylbenzene sulphonate, i.e. the 'anionic' sodium salt derived from DoBS acid, its manufacture and properties has been given by Kumar and Bhat (1987) [2.8] and by Drozd and Gorman (1988) [2.9].

The sodium salt of DoBS acid, i.e. sodium dodecylbenzene sulphonate, has some structural similarity to Aerosol OT (sodium di-2-ethyl- hexyl sulphosuccinate, Na AOT) a well-known anionic dispersant, which has been found to give surface charging and ionization in non-aqueous dispersions (Parfitt and Peacock, 1978) [2.10]. Sodium alkylbenzene sulphonate is worldwide the most frequently applied anionic in detergent powders and liquids.

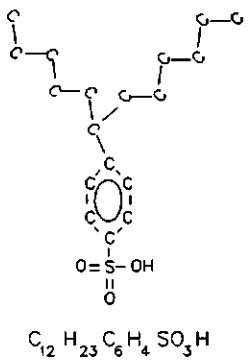

Fig. 2.3: Molecular structure of DoBS acid. For clarity H-atoms are omitted.

2.3 ATTRACTION AND ITS INFLUENCE ON COAGULATION

2.3.1 Attraction strength and sediment type

Particles in a lyophobic suspension attract each other as a consequence of van der Waals attraction between dispersed particles. A quantitative discussion of the van der Waals attraction between the solids in a nonionic suspension will be given in Chapter 3. Anticipating this, a more qualitative discussion of the consequences of van der Waals forces for suspension properties is given here.

By approximation it can be said that the van der Waals attraction energy (V_a) for a pair of interacting particles is larger for big particles than for small ones and that it increases when particles approach each other. Mathematically, this relation can be represented by

$$V_A \propto -\frac{a}{H} \qquad [2.2]$$

if a is the particle radius and H the interparticle distance. When two suspended particles approach each other, for example under the influence of gravity, their first points of encounter are the edges and asperities. The energy gain obtained could be considered as a type of an interparticle 'bonding energy', where the edges and asperities are the primary interacting parts. The situation of such interacting surface parts of two macrobodies may be compared with that of chemically interacting groups of two encountering macromolecules in a solution.

When the van der Waals bonding energy is large it can be supposed that the bonds between two particles are formed almost immediately at their first encounter. In this situation small areas of contact between particles can already be sufficient to immobilize them completely with respect to each other ('hit-and- stick'). Further encounters of such formed pairs lead to the formation of a strongly coagulated, open structure in three dimensions, where a limited number of contact points per particle is present (Fig 2.4 a). If all the particles are connected a network of cross-linked particles will be formed immobilizing and encompassing the full continuous phase. However, if the bonding energy is small, sufficient immobilization is achieved only after more bonding has occurred. To achieve this a re-orientation of the interacting particle surfaces is necessary. Many unsuccessful encounters may be needed between two approaching particles before this has happened and before they are bound rigidly to each other. Alternatively, contacting pairs can slide along each other till such a rigid bond has established itself. For micron-size particles this implies that the time-scale of sedimentation under gravity becomes shorter than the time-scale of interparticle bonding. Therefore the first bonding, and also the further bonding of the pairs to larger coagulates, only occurs slowly so that the particles become densely packed in a sediment (Fig. 2.4b).

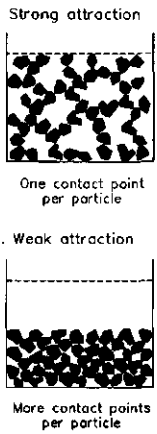

Fig. 2.4: Sedimentation of (a) an unstable suspension and (b) a stable or slightly unstable suspension.

The weak coagulates with a more dense structure and the strong coagulates with a more open structure can in this respect be compared with the formation from primary particles (Fig. 2.1) of densely packed particle aggregates or of more loosely packed particle agglomerates, respectively. In the discussion of the sediment model the extreme situations have been described, viz. strong versus weak bonding energies. Intermediate values of bonding energy, will lead to sediments in between the two extremes.

In sect. 1.3, it was mentioned that coagulation due to colloidal instability was responsible for the large sediment volume (Fig. 1.2) as well as for the high viscosity (Fig. 1.1). Moreover, it was found that the suspensions were not stable during storage or at elevated temperatures (Fig. 1.4), which was ascribed to progressive coagulation. Addition of the DoBS acid evidently changed various properties of the suspensions and at elevated temperatures no viscosity increase was observed any more. Apparently, the state of the suspension was changed from coagulated to less coagulated or even to stability. In the next section the origin of this effect will be discussed further.

2.3.2 Reduced attraction and colloidal stabilization

Attraction by van der Waals forces causes an energetically favourable situation when particles approach each other; it results in bonds with a more negative value of V_a (Eq. 2.2). The reduction in potential energy can be represented by a curve, showing that the closer the surfaces approach the larger the lowering (Fig. 2.5; see also sects. 3.2.2 and 3.2.3). If at some distance from the surface of a particle some 'obstruction' is created that hinders a closer approach, the energy at that distance is more favourable (lower) than that at infinite separation. In Fig. 2.5 this is represented by $V_a^{(a)}$. When the range of the obstruction is shorter this causes an even higher energy of 'bonding'. In Fig. 2.5 this is represented by $V_a^{(b)}$.

From colloid chemistry it is known that such an obstruction can be created by a repulsive barrier. For dispersions of colliding colloidal-size particles it results in a reduction of the rate of coagulation (see for example Hiemenz, 1986) [2.11]. It is found that for dispersed systems a repulsive barrier can be obtained basically by an electrostatic or by a steric effect, or by combinations of these two. The first effect is based on the creation of an electrostatic repulsive force. The second is based on the formation of a steric obstruction to a closer approach, for example from an adsorbed, bulky polymeric molecule. The repulsive effect is being generated as soon as adsorbed layers begin to overlap.

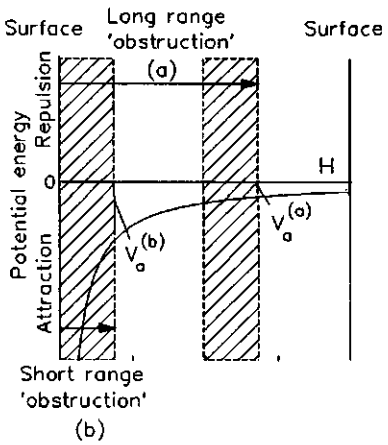

Fig. 2.5: The effect of obstruction on potential energy of attraction (V_a) for two approaching surfaces.

Both these routes render coagulation less favourable. Hence, they reduce the rate of the coagulation process and lead to a situation where the original number of particles (and their properties) are longer maintained. In colloid chemistry therefore usually they are referred to as **'electrostatic stabilization'** (Overbeek, 1981, 1987)[2.12]and as **'steric stabilization'** (Heller and Pugh, 1960)

[2.13]. In situations of adsorbed polyelectrolytes this may lead to combinations of electrostatic and steric stabilization (Fowkes, 1983 [2.14]; Lyklema, 1985 [2.15]). Electrostatic or charge stabilization is widely applied in aqueous systems, when ions from dissociated electrolytes are present and can charge the particles. Steric stabilization is currently applied in non-aqueous media, where electrolyte dissociations are usually low, but also in aqueous media.

For stable colloidal particles with large repulsive barriers and small remaining attractions, Brownian motion caused by thermal energy is large in comparison to the bonding energy. However, particles with an average size in the micron-range are so large that gravity-induced settling is only to a minor degree influenced by Brownian movements. It leads to the formation of a sediment irrespective of the preponderance of attractive or repulsive forces, although the compactness of the sediment will differ. The interparticle distance after sedimentation, where the particles are at rest, is the distance at which the sum of all forces is zero and where the repulsions withstand the gravitational force. The energy or force required to cause a sediment to flow must be larger than the sum of the van der Waals bonding energy and the potential energy due to gravitation. The flow is the easier, the longer the range of the repulsion and the smaller the contribution of the attraction to this sum is.

2.3.3 DLVO theory

The magnitudes of attraction and of repulsion, created by electrostatic or steric effects, is usually represented in potential energy-distance or force-distance curves. Such graphs describe the energies or forces of each of these attractive and repulsive interaction as a function of the distance between the interacting surfaces. A simple addition of all these functions allows one to obtain the complete picture and permits one to find which of the two effects at a certain distance dominates over the other. Examples of two typical extreme patterns are given in Fig. 2.6.

By its nature the range of the attraction is always larger than that of the repulsion (Fig. 2.6). The combination of the attraction with an extinguishing repulsive energy causes a **secondary minimum** in the energy- distance curves. When particle surfaces approach each other up to very short distances, i.e. in the atomic distance range, Born effects cause very strong repulsions between the particle surfaces. The combination of Born repulsion with the van der Waals attraction causes the development of another minimum in the energy-distance curve, viz. the **primary minimum**. Since the attraction is particularly strong at small distances (Eq. 2.2), the primary minimum is much deeper than the secondary minimum (see Fig. 2.6).

The theory describing the additivity of attractive- and repulsive-electrostatic forces is named "DLVO theory" after Deryagin, Landau, Verwey and Overbeek, who formulated this theory more than 40 years ago. A review of the theory has been given by Kitahara and Watanabe (1984) [2.16], or can be found in the

textbook of Hiemenz (1986) [2.11]. An original discussion is given by Verwey and Overbeek (1948) [2.17].

Particles which are so close to each other that they are positioned at the distance of their **primary minimum** are in an energetically extremely favourable situation and are rigidly bound to each other. Suspensions consisting of such particles are completely solid and unpourable. However, when between particles only **'secondary minimum coagulation'** occurs this gives rise to a more 'liquid' behaviour of the suspensions. Thus, the strength of the interparticle attractions determines the physical properties of a suspension (sect. 2.3.2).

The interparticle attractions can be strong or weak depending completely on the size and range of the repulsive barrier: A high repulsive barrier inhibits the (strong) primary minimum coagulation. A short range of the repulsive barrier causes a deeper secondary minimum. It induces an energetically more favourable position for the particles (in the secondary minimum) and gives faster coagulation to form loose and open coagulates. On the other hand a long range of the repulsive barrier causes a shallow secondary minimum at a relatively large interparticle distance. It causes weak coagulation with dense packing (see Fig. 2.6).

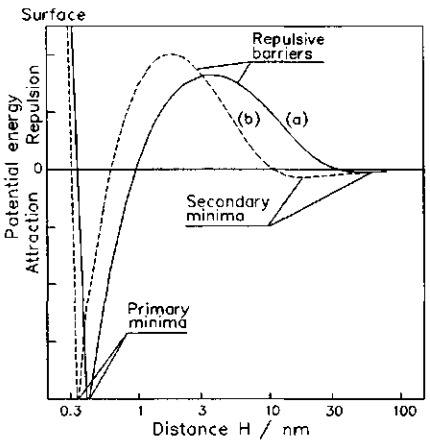

Fig. 2.6: DLVO curves (a) for a short range repulsion and (b) for a long range repulsion.

Strong, primary minimum coagulation is assumed to occur when the depth of the minimum is > 10 kT-units, i.e. > 4.12×10^{-20} J (J = Joule; at room temperature 1 kT-unit = 4.12×10^{-20} J). Secondary minimum coagulation is supposed if the value is ≤ 10 kT, whereas strong and weak secondary minimum coagulation can be distinguished further. Apart from the depth of the secondary minimum also the range of the area in the vicinity of the secondary minimum is mentioned to be important (Vincent, 1987) [2.18]. Hence, when the magnitude of the attraction could be manipulated by varying the size and range of the repulsion, this would directly influence the degree of coagulation. The methods by which the magnitude of the attraction can be affected will be discussed in sect. 2.5. First it will be discussed in what way the type of coagulation influences the physical properties of a suspension.

2.4 COAGULATION AND SUSPENSION PHYSICAL PROPERTIES

2.4.1 Sedimentation

The coagulation, occurring as a result of attraction between particles, influences various physical aspects of concentrated suspensions, viz. the rate of sedimentation, the final sediment volume, the viscosity and the network- and shear- moduli of the sediment formed (see Chapter 7).

According to the coagulation model given (sect. 2.3.1), strong net overall attraction between particles could explain the large sediment volume observed in the absence of acid for the concentrated suspension of sodium triphosphate in Plurafac nonionic (Fig. 1.2). The reduction of the sediment volume resulting from addition of DoBS acid is explained from the a creation of a repulsion leading to weaker attraction and more densely packed coagulates.

The strength of the attraction has also an effect on the compressibility of sediments under pressure. Compressibilities of sediments formed by strongly attracting particles will be larger than those of weakly attracting particles. This consideration leads to the apparent contradiction that in concentrated suspensions stronger attraction leads not only to larger average interparticle distances but also to weaker suspensions, which are more easily distorted. If it were possible to reduce the attractive dispersion forces, we would observe the opposite, viz. creation of a denser and better packed sediment and with a lower compression. Such effects are obtained from the creation of an effective resistance against coagulation by colloidal stabilization.

The slower rate of sedimentation found after the addition of DoBS acid to concentrated sodium triphosphate suspensions can also be ascribed to a reduction of the attractive forces between coagulates. According to the model, if the attractive forces between coagulates are reduced, more encounters or more sliding in the sediment can occur before further coagulation causes the complete immobilization of the coagulates. Since the addition of DoBS acid has lead to a reduction in degree of coagulation its effect can be interpreted as a de-coagulation. An order of magnitude estimation of the lowest secondary minimum energy minimally necessary to have no visible sedimentation in our nonionic suspensions can be made by the sedimentation experiment (Fig.1.2): After an initial stage where sedimentation is visible, there follows a stage during which no measurable sedimentation occurs any more. As the accuracy of the visual observation of the sediment height is ca. 1 mm, over the 850 hours of observation the sedimentation rate in the later stage was maximally 1 mm, which is equivalent to 3×10^{-10} m s^{-1}. For particles with a radius a of 5 μm this would correspond to a relative shear rate $d\gamma/dt$ (often short-hand written as $\dot{\gamma}$) of 6×10^{-5} s^{-1}. The hydrodynamic energy (V_H) required to displace a particle over a distance $3a/4$, is given by Eq. 2.3 (Blom, Jongschaap, van Gelder; 1987) [2.19])

$$V_H = 9\pi \ \eta_c a^3 \dot{\gamma} \qquad [2.3]$$

On using this equation it is found that, for particles or coagulates with a radius of 5 μm and a continuous phase viscosity (η_c) of 60 mPa s (milliPascal second), V_H amounts 1.2 $\times 10^{-20}$ J or 3 kT. This gives the order of the minimum attractive energy in the secondary minimum necessary to have no visible sedimentation and is a fairly high value. If the actual attractive energy is higher this could not lead to a lower rate of clear layer formation, but it would give a higher low shear rate viscosity. It is further important to realize that if the particles would have a radius of 10 μm instead of 5 μm the minimum bonding energy needed to have no visible sedimentation would have been 8 times as high.

2.4.2 Viscosity

Concentrated suspensions are non-Newtonian liquids. This means that their viscosity, which is defined as the quotient of shear stress and shear rate, is dependant on the shear rate applied. They are 'shear thinning', implying that they have a higher viscosity at low shear rates than at high shear rates. For a discussion of the viscosity behaviour of concentrated suspensions the reader is referred to the recent book of Barnes, Hutton and Walters (1989) [2.20]. A more extensive discussion on viscosity is given in Chapter 7.

At the high shear rates the viscosity of a suspensions is not affected by coagulation any more because under those conditions the hydrodynamic forces are dominant over the effects of the (weak or strong) interactive forces. However, especially at the low shear rates the effects of coagulation are reflected in the viscosity. Characteristic patterns for strongly and weakly flocculating particles are given in Fig. 2.7.

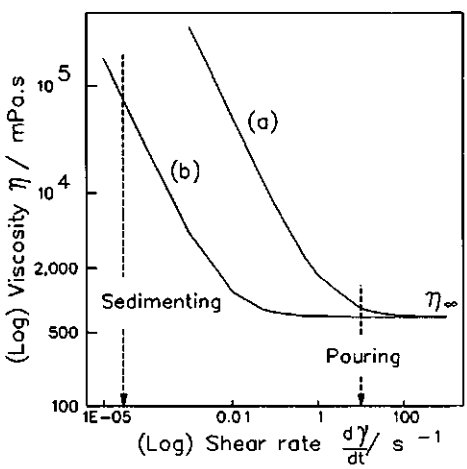

Fig. 2.7: Viscosity - shear rate patterns of concentrated suspensions (a) with strongly and (b) weakly attracting particles, both at equal volume fraction solids.

The shear rate representative of that occurring on tilting a suspension or on pouring is in the order of 1 to 10 s^{-1} (Fig. 2.7). At these shear rates, at given volume fraction solids, interparticle force effects are noticeable and can lead to differences in viscosities. Practical experience shows that at this shear rate a high viscosity, i.e. $\geq$ 2000 mPa s, points to a fairly strong secondary minimum coagulation, whereas with weaker secondary minimum coagulation, viscosities as low as 600 mPa s can be found. It

makes all the difference between a hardly pourable, 'thick' suspension and a 'liquid suspension' with an easy flow.

The shear rate representative of particle sedimentation is much lower and is approximately 10^{-4} to 10^{-5} s^{-1} (sect. 2.3.2) (Fig. 2.7). This low shear rate regime is still accessible to a number of modern rheometers. At that low shear rate the viscosities are higher and are strongly influenced by the strength of the interparticle forces. Since this shear rate region is more discriminating, it is the best area for studying differences in attractions between particles.

The observation that **at high shear rates** interparticle forces have no effect on the viscosity can lead to an apparent contradiction when we do not compare systems with equal volume fractions, because viscosities also increase with volume fraction solids.

2.5 COLLOIDAL STABILIZATION IN NONIONIC SUSPENSIONS

As demonstrated before, creation of colloidal stabilization would influence the degree of coagulation and offers a way to influence a number of important physical properties. The available stabilization methods by which the size and range of the secondary minimum coagulation in non-aqueous systems can be manipulated is discussed in this section.

2.5.1 Steric stabilization

Steric stabilization plays a role if dispersed particles have adsorbed layers of macromolecules (sect. 2.3.2). These cause a steric hinderance and an obstruction against closer approach as soon as adsorbed layers begin to overlap. Studies, theoretical and practical, on steric stabilization are large in number. Surveys have been given by Vincent (1974) [2.21], Osmond and Waite (1975) [2.22], Tadros (1982) [2.23], Napper (1983) [2.24], Fleer and Lyklema, 1983 [2.25] and Lyklema (1985) [2.26]. Suitable macromolecules for steric stabilization used in practice are copolymers, having one or more groups with a sufficient affinity for the solid to keep the macromolecules strongly 'anchored' on the solid surface and have one or two dangling tails with a large affinity for the solvent.

In the last decade a large variety of polymers have been developed which are applied as steric stabilizers in all sorts of practical colloidal products. They have found wide application particularly in the areas where dispersion stabilization is important for intermediates or end-products. Examples are dispersions of pigments, paints, pesticides, ceramics and pharmaceutical preparations.

For systems of colloidal particles, it has been overwhelmingly demonstrated that by proper choice of the polymer type and the size of the steric layer, that the attractive force can be reduced to a value where it is so low that translational

Brownian motion is already sufficient to counterbalance the rate of coagulation. This results in an improved colloidal stability.

2.5.2 Stabilization of micron-size particles

For a discussion on the effectivity of steric stabilization of micron-size particles it is important to realize that for such particles, which attract each other more strongly than small particles, higher molecular sizes of polymer are necessary to keep the particles sufficiently apart (Fowkes, 1984) [2.14]. However, high molecular sizes of polymer will enhance the risk of bridging flocculation. Other drawback of polymer stabilization mentioned are its temperature sensitivity and its sensitivity for small differences in the solvent quality. These considerations indicate that polymer stabilization to obtain 'liquid', non- or weakly flocculated suspensions of micron-size particles, is not easy. If possible at all stabilization has to be carried out only with high molecular weight polymers with few, but strong anchoring properties.

Due to its amphiphilic character, the nonionic active molecule is well able to adsorb on the polar solid surfaces of a colloid. Examples of such adsorptions of nonionics from aqueous media to hydrophilic surfaces have been reported a.o. by Akers and Riley (1988) [2.27], by Partyka et al. (1984) [2.28] and by Glazman et al. (1986) [2.29]. In all these cases steric effects are due to an adsorbed nonionic layer on the surface. However, the results of concentrated sodium triphosphate suspension in Plurafac (Fig. 1.1, 1.2 and 1.4) suggest that if a steric layer is formed at all, it is not large enough to avoid a rather strong degree of coagulation.

Because of the presence of a polar headgroup, anionic surfactant molecules also have an anchoring ability for hydrophilic surfaces in non-aqueous media and could give some steric stabilization to colloidally size particles (Tadros, 1987) [2.30]. However, because surfactant molecules are much smaller in size than macromolecules, their steric range is too small to have a sufficient reduction of the attraction (Fowkes and Pugh (1984) [2.31]). Apparently, in our suspensions no large numbers of adsorbed surfactant molecular layers were present so that no steric contribution to stability could ensue (sect. 1.4). This consideration has guided us to the hypothesis that the stabilizing effect from DoBS acid is electrostatic in nature.

2.5.3 Electrostatic stabilization

On various places it has been reported that in non-aqueous media electrostatic effects do not play an important role in the stabilization of dispersions (Osmond and Waite, 1975 [2.22], Tadros, 1982 [2.23]; Napper, 1983 [2.24]) (see sect. 4.3.1.1). This is contrary to aqueous dispersions where in many cases electrostatic effects have been observed. The general reason given for the lack of electrostatic effects in low polar media is that the Debye lengths are very large, so that overlap

of the double layers does not lead to a significant potential drop and being therefore not able to create a significant repulsion. Fowkes and Pugh (1984) [2.32] have already pointed out that this statement can lead to misconceptions. Anticipating a discussion on double layer formation in non-aqueous media in sect. 4.2.2, one important aspect will be mentioned here.

The following expression (Eq.2.4) can be derived from the definition of the Debye screening length $1/\kappa$ at 298 K (see sect. 4.2)

$$\frac{1}{\kappa} = 0.034 \sqrt{\frac{\varepsilon}{c_i}} \qquad [2.4]$$

In Eq. 2.4 ε represents the dielectric constant of the liquid phase and c_i the ionic strength. The value for $1/\kappa$ is obtained in nm (nanometres = 10^{-9} m), if c_i is given in M (Mol dm^{-3}). The expression shows that, when $1/\kappa$ is large in non-aqueous media, this is not due to the low dielectric constant, but due to the low electrolyte dissociation. Thus, if in a non-aqueous medium the usually poor dissociation could be improved, shorter Debye lengths are obtained. In these media also large electrostatic repulsions could be obtained, provided that ion concentrations are sufficiently high and provided that one of the ionic species adsorbs specifically at the surface. The crucial feature is therefore the dissociation of an electrolyte and the surface charging.

Factors which influence the dissociations of electrolytes in non-aqueous media have been discussed in the past (Koelmans and Overbeek, 1954 [2.32]; Klinkenberg and van der Minne, 1958 [2.33]). They suggest a dependency of the dissociation on the electrolyte structure and size (see sect. 4.3.2.1). It is possible to estimate a dissociation constant (K_D), making several assumptions, based on the theory of ion pair formation as developed by Bjerrum and Fuoss. This can be done with aid of the 'Fuoss equation' (1958) [2.34]

$$K_D = \frac{10^3}{\frac{4}{3}\pi r^3 N_A} \exp\left(-\frac{e^2}{4\pi \varepsilon_0 k_B T} \frac{1}{\varepsilon r}\right) \qquad [2.5]$$

In this equation N_A is Avogadro's constant, ε_0 the dielectric constant in vacuum, e the unit of charge, k_B Boltzmann's constant and T the temperature. The equation shows that the dissociation constant is a function of the radius r of the dissociating electrolyte ion-pair, and of the dielectric constant of the liquid ε. Using Eq. 2.5 it can be calculated that for example for a dissociating anionic molecule with an ion-pair radius of 0.5 nm, in a nonionic with $\varepsilon = 6$, that $K_D = 2.4 \times 10^{-8}$ dm^3 M^{-1}. From this dissociation constant it can be calculated that, an arbitrarily chosen, 10 mM solution of a 1 : 1 dissociating molecule would give an ionic concentration c_i of 1.5×10^{-5} M, corresponding with a degree of dissociation $\alpha = 0.0015$.

The magnitude of this ion concentration is considerably higher than values reported for Aerosol OT in non-polar media, i.e. with $\varepsilon \leq 4$, which were found to be of the order of 10^{-10} M (Kitahara, 1967) [2.35]. Correspondingly, at such high ion concentrations, from Eq. 2.4, Debye lengths can be calculated which are about 22 nm. These Debye length are much smaller than those given by Kitahara (1967), which are in the range between 1 and 95 μm. In comparison to the Debye lengths in aqueous media this is not an extreme value at all.

When dissociating electrolytes in a non-aqueous solvent give rise to a certain concentration of positive and negative ions, it is only a small further step to a specific adsorption of one of the ions on the particle surface. The consequences are a charging of the surface, an electric surface potential, the building up of a double layer and the development of an electrostatic repulsion when these double layers overlap.

The above considerations are the basis for the suggestion that in the systems containing solids, nonionics and DoBS acid we might have to deal with an electrostatic stabilization mechanism. Three conditions have to be fulfilled for suspensions in nonionics before we can conclude that an electrostatic mechanism operates. These three conditions are 1. that the particles have become charged, 2. that the electrolyte dissociations are sufficiently large and 3. that the van der Waals attraction is not too high, so that at a specific distance the attraction can be overcompensated by an electrostatic repulsion. Only under these conditions could electrostatic parameters be used to manipulate the attraction reducing factors. This would allow us to influence the repulsion, the size and depth of the secondary minimum and thus the degree of coagulation and the physical properties of suspension in our non-aqueous media. The quantitative aspects of the three conditions mentioned will be discussed more systematically in the coming chapters.

2.6 SUMMARY

Nonionics used in this study are condensates of long chain alcohols and 3 to 9 alkylene oxide units. The dispersed solids are the salts present in current detergent powders or oxides. They are aggregates or agglomerates of smaller primary particles and consist of irregular spheroids. Solid sodium salts can be suspended in nonionic at relatively high volume fractions. Analysis of supernatants indicated only very limited dissolution. Hence, the suspensions are lyophobic. In our studies we applied n-dodecylbenzenesulphonic acid (DoBS acid or HDoBS), the acid form of a frequently applied anionic detergent.

Sedimentation rate, sediment volume and viscosity are important physical characteristics of concentrated nonionic suspensions. These properties depend on the interactions between the suspended particles. The interactions are governed by the balance between factors on one hand which cause an energy gain on interparticle approach, i.e. the attractive van der Waals forces and gravity, and attraction reducing, 'stabilizing' factors on the other. Although the origin of the stabilization created by addition of DoBS acid is unknown, in the non-aqueous

nonionic medium an electrostatic stabilization mechanism is feasible. Brownian movement does not play a large role in the stabilization in these systems due to the large particle sizes.

2.7 BIBLIOGRAPHY

2.1 a. **Dispersions of powders in liquids. Third edition.** Parfitt, G.D.. (Applied Science Publishers, London, UK). **1981;** b. **Chemistry of interfaces.** Jaycock, M.J.; Parfitt, G.D..(John Wiley and sons, New York, USA). **1981.**

2.2 **A nomenclature for mean particle diameters.** Alderliesten, M.. *Anal. Proc.* **1984,** 21, 167-171.

2.3 **Surface active ethylene oxide adducts.** Schönfeldt, K..(Pergamon Press, Oxford, UK). **1969.**

2.4 **Surfactant Science Series. Vol.19: Nonionic Surfactants: Chemical Analysis.** Cross, J.; Editor (Marcel Dekker, New York, USA). **1987.**

2.5 **Effect of zeolite on the dispersion stability of particles.** Kimura, M; Komaki, M.; Nakajima, T.. *Textile Res. J.* **1987,** 57 (2), 82-87.

2.6 **Crystalline zeolites. I The properties of a new synthetic zeolite, type A.** Breck, D.W.; Eversole, W.G.; Milton, R.M.; Reed, T.B.; Thomas, T.L.. *J. Amer. Chem. Soc.* **1956,** 78 (23), 5965-5970.

2.7 **Sodium p-alkylbenzenesulfonates: A simple and fast characterization by electron impact mass spectrometry.** Agozzino, P; Ceraulo, L.; Ferrugia, M.; Caponetti, E.; Intravaia, F.; Triolo, R.. *J. Colloid Interface Sci.* **1986,** 114 (1), 26-31.

2.8 **Studies of surface activity of linear alkylbenzene sulfonates II: Effect of water hardness.** Kumar, R.; Bhat, S.G.T.. *J. Amer. Oil Chem. Soc.* 64 (4), 556-561, **1987.**

2.9 **Formulating characteristics of high and low 2-phenyl linear alkylbenzene sulphonates in liquid detergents.** Drozd, J.C.; Gorman, W.. *J. Am. Oil Chem. Soc.* **1988,** 65 (3), 398-404.

2.10 **Surface and Colloid Science. Vol. 10: Stability of Colloidal Dispersions in Non-aqueous Media.** Parfitt, G.D.; Peacock, J.; Editors (Plenum Press, London, UK). **1978.**

2.11 **Principles of colloid and surface chemistry. 2nd ed. Revised and Expanded.** Hiemenz, P.C.; Editor (Marcel Dekker, New York, USA). **1986.**

2.12 a.**Colloidal Dispersions: Colloids, A Fascinating Subject. Introductory Lecture.** Overbeek, J.Th.G.. Goodwin, J.W.; Editor (R. Soc. Chem. - Spec. Pub. 43, London, UK) **1981;** b. **Modern trends of colloid science in chemistry and**

biology: Birth, life and death of colloids. Overbeek, J.Th.G.. Eicke, H.-F.; Editor. (Birkhäuser Verlag, Basel) **1985.**

2.13 **'Steric' stabilization of colloidal solutions by adsorption of flexible macromolecules.** Heller, W.; Pugh, T.J.. *J. Poly. Sci.* **1960,** 47, 203-209.

2.14 **The dispersibility and stability of carbon black in media of low dielectric constant. 1. Electrostatic and steric contributions to colloidal stability.** Pugh, R.J.; Matsunaga, T.; Fowkes, F.M.. *Colloids Surf.* **1983,** 7, 183-207.

2.15 **Modern trends in colloid chemistry and biology. Adsorption of polyelectrolytes and their effect on the interaction of colloid particles.** Lyklema, J.. J.Th.G.. Eicke, H.-F.; Editor. (Birkhäuser Verlag, Basel). **1985.**

2.16 **Surfactant Science Series. Vol.15: Electrical Phenomena at Interfaces. Fundamentals, Measurements, and Applications.** Kitahara, A.. Kitahara, A.; Watanabe, A.; Editors. (Marcel Dekker, New York, USA). **1984.**

2.17 **Theory of the stability of lyophobic colloids. The interaction of sol particles having an electric double layer.** Verwey, E.J.W.; Overbeek, J.Th.G.. (Elsevier, Amsterdam). **1948.**

2.18 **Phase separation in dispersions of weakly interacting particles.** Vincent, B.. *Chem. Engng. Sci.* **1987,** 42 (2), 779-86.

2.19 **Inleiding in de reologie.** Blom, C,; Jongschaap, R.J.J; Mellema, J.. (Kluwer, Deventer, The Netherlands). **1987.**

2.20 **An introduction to rheology.** Barnes, H.A.; Hutton, J.F.; Walters, K.. (Elsevier, Amsterdam). **1989.**

2.21 **The effect of adsorbed polymers on dispersion stability.** Vincent, B.. *Adv. Colloid Interface Sci.* **1974,** 4, 193-277.

2.22 **Dispersion Polymerization in Organic Media. The Theoretical Basis for the Steric Stabilization of Polymer Dispersions Prepared in Organic Media.** Osmond, D.W.J.; Waite, F.A.. Barrett, K.E.J.; Editor. (John Wiley, New York, USA). **1975.**

2.23 **Polymer Adsorption and Dispersion Stability. The Effect of Polymers on Dispersion Properties.** Tadros, Th.F.. Tadros, Th.F.; Editor (Academic Press, London). **1982.**

2.24 **Polymeric Stabilizations of Colloidal Dispersions. Basic Concepts of Colloid Stability.** Napper, D.H.; Editor. (Academic Press, London). **1983.**

2.25 **Adsorption From Solution at the Solid/Liquid interface. Ch.4: Adsorption of Polymers.** Fleer, G.J.; Lyklema, J.. Parfitt G.D.; Rochester C.H.; Editors. (Acad. Press., London). **1983.**

2.26 **Flocculation, sedimentation and Consolidation. How polymers adsorb and affect colloid stability.** Lyklema, J.. Moudgil, B.M.; Somasundaran, P.. Editors (Amer. Eng. Foundation). **1985.**

2.27 **The adsorption of polyoxyethylene alkyl-phenols onto calcium carbonate from aqueous solution.** Akers, R.J.; Riley, P.W.. *J. Colloid Interface Sci.* **1974,** 48(1), 162-164.

2.28 **The adsorption of non-ionic surfactants on a silica gel.** Partyka, S.; Zaini, S.; Lindheimer, M.; Brun, B.. *Colloids Surf.* **1984,** 12, 255-270.

2.29 **The effect of nonionic surface-active agents on the stability and coagulation of ferric hydroxide sol.** Glazman, Yu.M.; Botsaris, G.D.; Dansky, P.. *Colloids Surf.* **1986,** 21, 431-446.

2.30 **Application of surfactants and polymers in pesticidal suspension concentrates.** Tadros, Th.F.. *Spec. Publ. - R. Soc. Chem.* **1987,** 59, 102-125.

2.31 **Polymer adsorption and Dispersion Stability. Steric and Electrostatic Contributions to the Colloidal Properties of Non-aqueous Dispersions.** Fowkes, F.M.; Pugh, R.J.. *Amer. Chem. Soc. - Symp. Series* 240, **1984.**

2.32 **Stability and electrophoretic deposition of suspensions in non-aqueous media.** Koelmans, H.; Overbeek, J.Th.G.. *Disc. Faraday Soc.* **1954,** 18, 52-63.

2.33 **Electrostatics in the petroleum industry. The prevention of explosion hazards.** Klinkenberg, A; van der Minne, J.L.. Shell Research and Development Report. (Elsevier, Amsterdam). **1958.**

2.34 **Ionic association. III. The equilibrium between ion pairs and free ions.** Fuoss, R.M.. *J. Amer. Chem. Soc.* **1958,** 80, 5059-5060.

2.35 **The effect of water on electrokinetic potential and stability of suspensions in non-polar media.** Kitahara, A.; Karasawa, S; Yamada, H.. *J. Colloid Interface Sci.* **1967,** 25, 490-495.

Chapter 3

PARTICLE ATTRACTION IN SUSPENSIONS

3.1 INTRODUCTION

Three conditions have to be fulfilled before we can decide whether we have to deal with electrostatic stabilization in the non-aqueous system consisting of solids dispersed in nonionic in the presence of DoBS acid (see sect. 2.5.3). These conditions are:
1. the solid particles obtain a surface charge,
2. the electrolyte dissociation in nonionic is sufficiently large so as to give Debye lengths of the right order, and
3. the van der Waals attraction between particles is sufficiently small, so that a particle distance can be found, beyond which the attraction is more than compensated by the electrostatic repulsion.

Before this can be analyzed quantitatively, the van der Waals attraction has to be known. Basically the attraction between solids in a liquid depends on the nature of the materials, as reflected in the 'Hamaker constant', on the geometry of the particles (size, surface roughness) and on the interparticle distance. In the first part of this chapter the effects of geometry and distance are discussed. The consequences for a suspension of micron-size spheroidal, roughly shaped particles suspended in liquid nonionic surfactant are considered in particular. In the second part of this chapter the material properties are considered. A modified version of the 'microscopic theory' has been elaborated to enable an evaluation of the Hamaker constants. Some aspects of the 'macroscopic theory' are also discussed. Both theories have been applied to calculate the Hamaker constants of our solids from their refractive indices and dielectric constants.

In the further chapters of this thesis attractions and repulsions are formulated in terms of interaction energies (V_A and V_R) of pairs of particles and not in terms of ensembles of many particles. To compare the van der Waals forces with the shear forces induced by gravity, attraction and repulsion are also discussed in terms of forces (F_A and F_R).

3.2 THE GEOMETRICAL FACTOR IN THE VAN DER WAALS ATTRACTION

3.2.1 The general form of the equations

Any pair of identical atoms or molecules attract each other by London-van der

Waals forces. The energy of this attraction u at a distance r, is given by

$$u(r) = -\frac{\beta}{r^6} \qquad [3.1]$$

where β is a positive constant related to the nature of the molecules, and r is the distance between the centres of the molecules. Equation 3.1 is valid for distances from a few tenths of nm to about 15 nm. This theory on attraction between simple atoms has been developed by London (1937) [3.1]. At a first approximation, the London-van der Waals dispersion forces are additive. The theory in which this was worked out has, amongst others, been reviewed by Gregory (1969) [3.2] and Visser (1972) [3.3]. More recent overviews can be found in the textbooks of Israelachvili (1985) [3.4] and Hunter (1987) [3.5].

For a pair of macrobodies, each consisting of many identical molecules, the van der Waals energy can be approximated by a simple summation or integration of all interacting pairs. This is given by

$$V_A(r) \approx -\sum_{\text{all pairs}} \frac{\beta}{r^6} \approx -\int_{V_1}\int_{V_2} \frac{\beta q^2}{r^6}\, dV_1\, dV_2 \qquad [3.2]$$

where V_1 and V_2 represent the volumes of particles 1 and 2, and q the number of atoms per unit volume of the particle material. Hamaker and de Boer (see Hamaker, 1937 [3.6]; de Boer, 1936 [3.7]) and others have solved the integral of Eq. 3.2 for various geometries. Independent of the geometry for two macrobodies of type 1, all solutions have the general form

$$V_A = -A_{11}\, f(\text{geometry}) \qquad [3.3]$$

In this expression the proportionality constant A_{11} is the Hamaker constant. It is a constant with a magnitude of 1 to 100 $\times 10^{-20}$ J, depending on the nature of the material. It is defined by

$$A_{11} = \pi^2 q^2 \beta \qquad [3.4]$$

The subscripts 11, in Eqs. 3.3 and 3.4, indicate that we are dealing with interactions between two identical particles of material 1 in vacuum, whereas f(geometry) stands for a geometrical function related to the shape and distance of the macrobodies involved in the interaction. In the forthcoming sections first the geometrical factor will be discussed, assuming one particular material type with a Hamaker constant A_{11}.

3.2.2 The energy of attraction; plates and spheres models

When the interacting macrobodies consist of two flat parallel plates ('slabs'), with thickness greater than the separation distance between the plates H (Fig. 3.1a), the

van der Waals energy of attraction $V_A^{(flat)}$ between unit area of one plate and the entire other plate (in J per unit area) is approximated by

$$V_A^{(flat)} = -A_{11} \frac{1}{12\pi} \frac{1}{H^2} \qquad [3.5]$$

which shows that on approach the attraction energy increases with the square of the distance. Owing to the additive contribution of all the molecules in the macrobody, the decay of the van der Waals attraction energy with distance is much slower than that of the individual molecules, which decreases as the sixth power of the distance (Eq. 3.1).

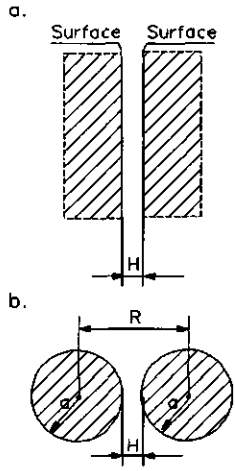

Fig. 3.1: Geometric parameters a. for two interacting infinitely large plates and b. for two interacting spheres.

For a pair of equal spheres with radius a (Fig. 3.1b), particle centre to centre distance R, distance of closest approach between the spherical surfaces H ($= R - 2a$) and defining $s = R/a$, the van der Waals energy of attraction is given by Eq. 3.6

$$V_A^{(spheres)} = -\frac{A_{11}}{6}\left(\frac{2}{s^2-4} + \frac{2}{s^2} + \ln\frac{s^2-4}{s^2}\right) \qquad [3.6]$$

Since in this equation the geometrical function is dimensionless, the dimensions of $V_A^{(spheres)}$ are the same as those of the Hamaker constant A_{11}, i.e. Joules. The expression shows implicitly that the van der Waals attraction energy rises proportionally with the radius a of the suspended particle at a given distance of separation (Fig. 3.2). It takes thus more energy to separate large particles than smaller ones, or for that matter, the energy gain obtained on approach is larger for big than for small particles.

For short distances of approach, i.e. $H << a$, Eq. 3.6 can be approximated by Eq. 3.7

$$V_A^{(spheres)} = -\frac{A_{11}}{12}\frac{a}{H} \qquad [3.7]$$

showing that $V_A^{(spheres)}$ is now inversely proportional to the distance H. This change is even slower than that for flat plates or for spherical particles at distances $H \approx a$. Now, the attractive energy $V_A^{(spheres)}$ is proportional to a/H, meaning that $V_A^{(spheres)}$ is larger when the particle size a is larger and when the distance H is smaller. This proportionality was used earlier in Eq. 2.2.

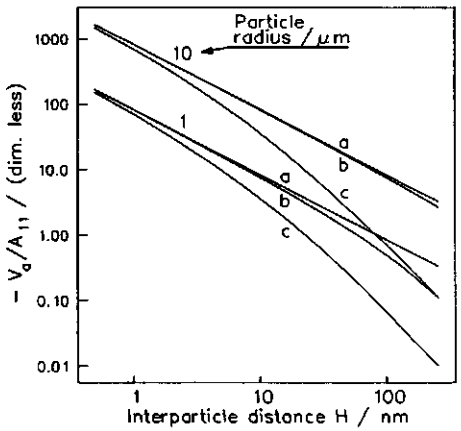

Fig. 3.2: V_a/A_{11} as a function of H for spherical, micron-size particles; comparison of Eqs. 3.7 (a) and 3.6 (b). Curve c shows the influence of retardation (see Eq. 3.9).

A comparison of Eqs. 3.7 (Fig. 3.2a) and 3.6 (Fig. 3.2b) shows that for micron-size particles and not too large values of H, the differences between the two equations are small: for example for particles with a radius of 10 μm they remain small up to a separation of 100 nm. However, for colloidal particles the differences become substantial at distances of $\geq$ 10 nm. For our further analytical calculations Eq. 3.7 has been used; for the numerical computations the more complex Eq. 3.6 has been applied.

Equations 3.6 and 3.7 are solutions for interacting equal spheres. For interactions of two spherical particles of unequal size, when a_1 and a_2 are the radii of particles 1 and 2, respectively, the expression becomes as given in Eq. 3.8

$$V_A^{(\text{spheres})} = -\frac{A_{11}}{6}\left(\frac{2a_1a_2}{H^2+2a_1H+2a_2H} + \frac{2a_1a_2}{H^2+2a_1H+2a_2H+4a_1a_2} + \ln\frac{H^2+2a_1H+2a_2H}{H^2+2a_1H+2a_2H+4a_1a_2}\right) \quad [3.8]$$

Apart from flat plates and spheres Eq. 3.2 has further been solved for many other geometries. Examples are those between spheres and flat surfaces and between parallel and crossed cylinders. A useful summary of the various equations has been given by Israelachvili (1985) [3.4] and Hunter (1987) [3.5]. For our systems sphere-sphere interactions and flat plate-flat plate interactions are the most relevant.

3.2.3 The effect of retardation

London-van der Waals forces differ from Keesom- and Debye-van der Waals forces that the former exhibit the phenomenon of retardation, which leads to a stronger decay with distance when this distance is large. Consequently, at larger distances of separation of atoms or molecules this will lead to retardation of the dispersion forces. It causes a decay with r^7 instead of with r^6 as predicted by Eq. 3.1. For interactions between atoms or molecules this is of little consequence. However, for interactions between macroscopic particles, where the forces can still be significant at large distances, the effect of retardation should be taken into

account. The theory of retardation, being a quantummechanical phenomenon and originally developed by Casimir and Polder (1948) [3.8], was elaborated by Lifshitz (1960) [3.9]; empirical correction factors to the London dispersion energy, for spheres and slabs, were developed by Overbeek (1952/1966) [3.10]. An interesting review, although with a disturbing number of errors, has been given by Sonntag and Strenge (1987) [3.11].

The correction factors given by Overbeek had as a drawback that different expressions were necessary to cover the total range of distances. Later attempts were successful in deriving a correction function that overcomes this problem (see for example Rabinovich, 1978) [3.12]. A simple and elegant empirical correction has been worked out by Gregory who defined a correction which was found to be valid over the total range of distances (Gregory, 1981) [3.13] and which, for separations smaller than the particle radius, applied for plates as well as for spheres. According to Gregory the retardation correction as a function of (plate or sphere) distance H for the van der Waals attractive energy V_A is given by

$$V_A^{(ret.)} = [1 - 5.32\frac{H}{\lambda_L} \ln(1 + \frac{1}{5.32\frac{H}{\lambda_L}})]\, V_A \qquad [3.9]$$

where λ_L is the London wavelength, being typically 100 nm or thereabouts. On using Eq. 3.9 for macrobodies Gregory found that the results for the attractive energy agreed fairly well with the 'exact' computations from small distances up to about 20 % of the particle radius.

Using Gregory's correction equation (Eq. 3.9) attractive energies corrected for retardation, i.e. $(-V_A^{(ret.)}/A)$ for spheres, as function of the interparticle separation H, have been computed and are depicted in Fig. 3.3 (and in Fig. 3.2).

As can be seen from this graph the reductions of the attraction at longer distances, in comparison with results of Eq. 3.6, are significant. Due to retardation, at a distance of 20 nm, the van der Waals attraction energy is only ca. 30 % of the value obtained with Eq. 3.6; at 80 nm this value is still only 10 %.

An implication of retardation is that the changes in energy on approach become more sensitive to the

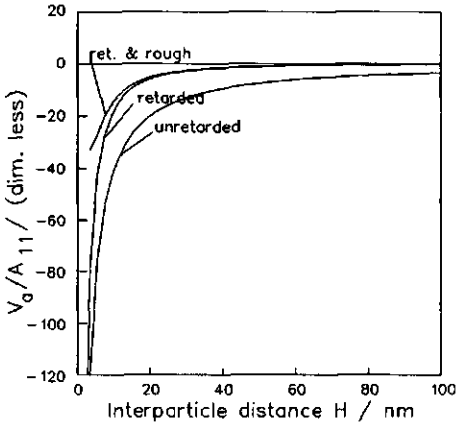

Fig. 3.3: V_a/A_{11} as a function of H: Eq. 3.6, effect of retardation (Eq. 3.9) and the combined effect of retardation and surface roughness (Eq. 3.12). Particle radius: 5 μm.

interparticle distance. With big particles, which have larger attractive energies, the effects are of particular importance and will cause the bonding energies to be even more dominated by the interactions of the protrusions at the closest points of contact. Another consequence related to surface roughness is that protrusions cause particles in sediments to remain more separated than when they are smooth. Hence, the average van der Waals binding energy obtained at these more remote distances will be low and cause particles to be weakly bound. However, small changes in position of the particles, causing a reduction of particle separation, can thus largely increase the van der Waals bonding energy.

3.2.4 The effects of surface roughness

The expressions given sofar (Eqs. 3.5 to 3.9) are derived for particles with smooth surfaces. However, all our micron-size particles have rough surfaces (sect. 3.2.2) which may influence the van der Waals attractions considerably. The theory of the latter problem has been discussed by Czarnecki and Itschenskij (1984, 1986) [3.14] and also by Rabinovich, Charnetski and Itchenskii (1987, 1989) [3.15]. The theory and its consequences for our particles is briefly discussed below.

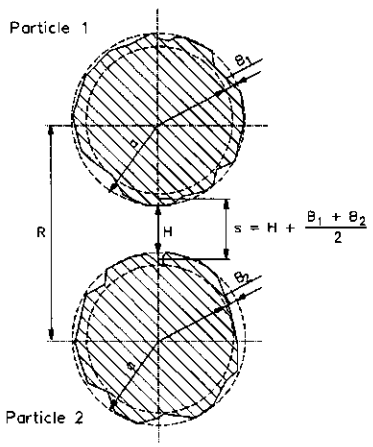

Fig. 3.4: Surface roughness parameters for two interacting spherical particles.

Following the theory of Czarnecki and Itschenskij it is assumed that for two particles 1 and 2 any surface irregularity is confined to a shell of thickness B_1 and B_2 (Fig. 3.4). Each particle may then be considered to consist of a solid core with constant density and a shell with some radial density distribution. Therefore, the total van der Waals interaction can be expressed as the sum of four terms, namely the interactions between core 1 and core 2, between core 1 and shell 2, between core 2 and shell 1 and between shell 1 and shell 2. The integration, taking all these interactions into account, was carried out for the interaction of roughly shaped particles by Rabinovich, Charnetski and Itchenskii (1989) [3.15]. For equal spheres with equal roughness $B_1 = B_2 = B$, the expression found (Eq. 3.10) gives the reduction of the van der Waals attraction energy, relative to that of particles with smooth surfaces as function of interparticle distance

$$V_A^{(rough)} = \frac{1}{(1 + \frac{B}{H})} f(H, B)\, V_A \qquad [3.10]$$

In Eq. 3.10, the notation $V_A^{(spheres)}$ in Eqs. 3.6 and 3.7 has been abbreviated to V_A. It refers to the non-retarded attractive energy for smooth, spherical particles

with a radius a and with a shortest surface distance H, calculated (for example) using Eqs. 3.6 or 3.7. It is valid over any distance and roughness ($0 < H,B < \infty$).

The function $f(H,B)$ in Eq. 3.10 is rather complex. It is given in full detail by Czarnecki and Itschenskij (1984, 1986) [3.15]. They demonstrated, however, that from the plot of log $(V_A/V_A^{(rough)})$ versus log $(H+B)/H$, it could be derived that $f(H,B) \approx 1$, so that Eq. 3.10 approximates to

$$V_A^{(rough)} \approx \frac{1}{(1 + \frac{B}{H})} V_A \qquad [3.11]$$

Our solids consist of particles (aggregates and agglomerates) with an average size ≥ 1 μm. The surfaces may have two types of irregularities: 1. protuberances of primary particles, having a size of the order of those of the primary particles, i.e. $B > 20$ to 50 nm, and 2. roughness due to unevenness in the crystalline surfaces, with an estimated magnitude of $B \leq 2$ nm.

The first irregularity is larger than the size of the double layers in our systems. For an influence on attraction and repulsion between particles it will therefore be of minor importance. However, the roughness due to unevenness in the crystalline surfaces is in the same order as the thickness of the double layers (see sect. 6.2.4). To evaluate the magnitude of the roughness it should be compared to the magnitude of the distances of the nearest points of contact between the particles. This will be in the order of the Debye length and hence depend on the ion concentration. From Eq. 3.11 it can be calculated that at a distance of 20 nm, the reduction amounts to ca. 10 %. Hence, at that distance this effect is much smaller than the effect of retardation. However, with closer approaches the roughness correction does become more important. Also at higher ion concentrations, causing lower Debye lengths, the reduction becomes larger. In the case the distances are ca. 5 nm, it can be derived from Eq. 3.11 that for $B = 2$ at that distance the reduction would be as large as ca. 30 %. When the corrections for retardation and for surface roughness are combined, this leads to an expression (Eq. 3.12) which contains the total correction of the van der Waals attractive energy (Sonntag and Strenge, 1987) [3.11]

$$V_A^{(ret.,rough)} \approx [1 - 5.32\frac{H}{\lambda_L} \ln(1 + \frac{1}{5.32\frac{H}{\lambda_L}})] \frac{1}{(1+\frac{B}{H})} V_A \qquad [3.12]$$

The resulting reduction for particles with a radius of 5 μm, in the case of $B = 2$ nm, when these effects are combined, can be read from Fig. 3.3 (curve c). It demonstrates that this surface roughness reduces the attraction between particles considerably, particularly at short distances.

3.2.5 The force of attraction

The force of attraction between two macrobodies can be obtained from (the negative value of) the first derivative with respect to the distace of the energy of attraction

$$F_A = - \frac{dV_A}{dH} \qquad [3.13]$$

where F_A has the dimensions N (= Newton), when the energy is expressed in J and the distance between the surfaces is given in m.

For flat plates, differentiation of Eq. 3.5 gives

$$F_A^{(flat)} = -A_{11} \frac{1}{6\pi} \frac{1}{H^3} \qquad [3.14]$$

For spherical particles, the following analytical solution was found by van Mil, et al. (1984) [3.16]

$$F_A^{(spheres)} = - A_{11} \frac{32}{3} \frac{1}{as^3(s^2-4)^2} \qquad [3.15]$$

For $H << a$, differentiation of Eq. 3.7, leads to

$$F_A^{(spheres)} = - A_{11} \frac{1}{12} \frac{a}{H^2} \qquad [3.16]$$

Analogously to the route applied to calculate the energy, the effect of retardation on the force can be obtained. After differentiation of Eq. 3.9, this leads to

$$F_A^{(ret.)} = \frac{1}{(1 + 5.32 \frac{H}{\lambda_L})} F_A \qquad [3.17]$$

Results of computations of van der Waals forces and the effects of retardation and surface roughness are presented in Fig. 3.5, for particles with a radius of 5 μm and for B = 2 nm. For the combined influences of retardation and surface roughness on the force we could not find an analytical solution. The combined correction of retardation and surface roughness, was therefore computed numerically. Further, in this graph a comparison is made between the numerically computed derivative of Eq. 3.6 with respect to H, and the analytical solution given by Eq. 3.15. The results of the calculations show that retardation, at the distances of interest, i.e. between 5 and 20 nm, causes a significant reduction of the interparticle forces. At such distances the effect of a surface roughness $B \leq 2$ nm is less important. In the further calculations the effect of the surface roughness is therefore ignored. The consequence is that the attractions evaluated are maximum

attractions and in situation where particles have a large surface roughness the actual effective attractions will be smaller.

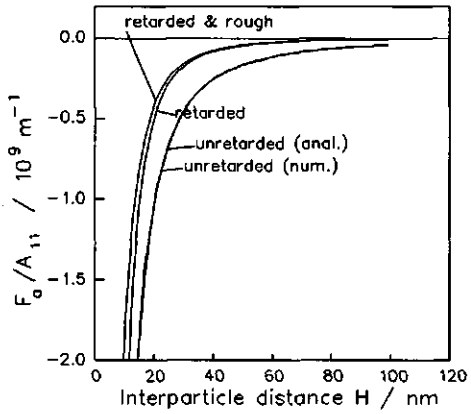

Fig. 3.5: F_a/A_{11} as a function of H: unretarded (from Eqs. 3.15 and 3.6), with retardation correction (Eq. 3.17) and with retardation and roughness correction (from Eq. 3.12).

3.3 THE HAMAKER CONSTANT

Up to now in this discussion we have restricted ourselves to the geometric function in the van der Waals attraction formulae. The Hamaker constants A_{11}, which reflect the material properties, have not been discussed yet. From the few dozen Hamaker constants (in air) of solids and liquids given in the literature (Vincent, 1973) [3.17]; Hough and White, 1980 [3.18]; Israelachvili, 1985 [3.4] or Hunter, 1987 [3.5]) it is evident that the Hamaker constants of the various solids can differ considerably: Hamaker constants in air for organics (solids and liquids) have magnitudes of $6 \pm 1 \times 10^{-20}$ J and are reported to be lower than those of inorganic salts ($9 \pm 3 \times 10^{-20}$ J), which are again lower than those of metal oxides ($13 \pm 4 \times 10^{-20}$ J) (Visser, 1976) [3.19]. More or less accurately known are the Hamaker constants of some metal oxides, but of the liquid nonionics and of our inorganic solids, with the exception of calcite (Hough and White, 1980) [3.18], no data are available. Hence we must find a procedure for computing them.

Methods are reported which allows an estimation based on the 'macroscopic' theory of Lifshitz (Hough and White, 1980), [3.18] (Israelachvili, 1985) [3.4]. These require a knowledge of the absorption spectrum and the dispersion, i.e. the refractive index $n(\omega)$ and/or the dielectric permittivity as a function of frequency $\varepsilon(\omega)$. In addition, another method was applied which uses the classical Hamaker-de Boer 'microscopic' summation approach. This method is based on the subdivision of the inorganic solid molecules into atoms, which all have an average composition and polarizability, identical to that of the solids molecule. The method requires, apart from the refractive indexes and dielectric constants, the molecular weights and the specific densities of the materials involved. A brief description of these two methods is given in the next sections.

3.3.1 The 'macroscopic', Lifshitz theory

The most straightforward way to calculate the Hamaker constant A_{11} is by following the theory of Lifshitz, reviewed and discussed by Mahanty and Ninham (1976) [3.20], Hough and White (1980) [3.18] and Israelachvili (1985) [3.4]. For two interacting, like macrobodies in vacuum, Israelachvili derived the

following expression with which it is possible to approximate the Hamaker constant

$$A_{11} \approx \frac{3}{4} k_B T \frac{(\varepsilon - 1)^2}{(\varepsilon + 2)^2} + \frac{3 h \nu_e}{16\sqrt{2}} \frac{(n^2 - 1)^2}{(n^2 + 1)^{\frac{3}{2}}} \qquad [3.18]$$

In this equation, instead of integration over the whole frequency area, $\varepsilon(\omega)$ and $n(\omega)$ in the original equations are replaced respectively by two static values, one at low frequencies, i.e. the static dielectric constant ε, and one at high frequency, i.e. the refractive index of the medium in visible light n. In this expression ν_e is the main electronic absorption frequency, typically around 3×10^{15} s^{-1} (i.e. λ_{abs} ca. 200 nm); h and k_B are Planck's and Boltzmann's constant, respectively, and T the temperature in K.

Equation 3.18 is very useful and allows the direct estimation of Hamaker constants of inorganic as well as organic substances from experimentally accessible parameters, provided that the main electronic absorption frequencies have all the typical value of 3×10^{15} s^{-1}. For a number of liquids Israelachvili has shown that the results of Eq. 3.18 are accurate within a few percent when compared with the results of exact computations (Israelachvili, 1985; Table XV) [3.4]. For the solids Eq. 3.18 tends to give values which systematically underestimate the exact solutions by a few tens of percents. With a single exception, dielectric parameters ε and n of the relevant solids for this study are not available in literature. Therefore they had to be measured. The measuring methods will be discussed in the sects. 5.2.2, 5.3.2.1 and 5.3.2.2, the results in sect. 6.4.

Considering the large differences in chemical composition, it is unlikely that our inorganic solid salts and nonionics all have the same ν_e value of 3×10^{15} s^{-1}. To enable calculation of the Hamaker constant more accurately, a more rigorous approach is necessary. This approach involves a need for the complete dielectric spectra for the materials and numerical calculation. Unfortunately, for our materials such spectra are not available.

3.3.2 The Hamaker-de Boer 'microscopic' approach

3.3.2.1 Hamaker constants for atoms and molecules

Basically, for monoatomic macrobodies, Hamaker constants also can be calculated by the summation method given in Eq. 3.4 by substituting appropriate values of q and β_{11}. In this equation q is the number density of atoms that form the macrobody. It is defined by

$$q = \frac{N_A \rho}{M} \qquad [3.19]$$

where N_A Avogadro's number, ρ the specific density of the solid and M the relative atomic mass.

The calculation of β_{11}, the London constant, is more complex. According to the London theory for 'hydrogen-like' atoms the following expression is valid (Gregory, 1969) [3.2]

$$\beta_{11} = \frac{3}{4} h \nu_0 \left(\frac{\alpha_0}{4\pi\varepsilon_0}\right)^2 \qquad [3.20]$$

where ε_0 is the dielectric permittivity in vacuum, ν_0 is the frequency of the electron in the ground state and α_0 the static electronic polarizability of the atom (dimension: $C^2J^{-1}M^2$). For ν_0 we may write

$$\nu_0 = \frac{e}{2\pi\sqrt{m_e}} \frac{1}{\sqrt{\alpha_0}} \qquad [3.21]$$

where m_e is the mass of the electron. Substitution of the values of the natural constants, gives

$$\nu_0 = 2.67 \times 10^{-5} \frac{1}{\sqrt{\alpha_0}} \qquad [3.22]$$

The electronic polarizability α_0, can be calculated from the refractive index using the Lorenz-Lorentz equation

$$\alpha_0 = 4\pi\varepsilon_0 \frac{M}{\frac{4\pi}{3} N_A \rho} \frac{n^2 - 1}{n^2 + 2} \qquad [3.23]$$

For materials consisting of more complex atoms or molecules an expression can be derived which is identical to Eq. 20, except that ν_0 is replaced by a 'characteristic frequency' of the UV part of the absorption spectrum ν_v (Gregory, 1969) [3.2]

$$\beta_{11} = \frac{3}{4} h \nu_v \left(\frac{\alpha_0}{4\pi\varepsilon_0}\right)^2 \qquad [3.24]$$

Except Anatase, our inorganic solids have a dielectric constant between 4 and 10 and belong therefore to the poor conductors. They have a (small) energy gap between the valence and conduction bands and have only low intensity, separate bands in the visible part of the electromagnetic spectrum. This is also apparent from their clear, colourless appearance (Bohren and Huffman, 1983) [3.21]. The electrons in the energy range responsible for chemical bonding will cause much stronger absorptions in the higher energy part of the spectrum.

These absorptions are, as Hough and White emphasized (1980) [3.18], of overwhelming importance for the dispersion forces. Values of ν_v (Eq. 3.24) can therefore be derived from the absorption spectrum of the molecules involved and

correspond with the high absorption at the main electronic frequency in the UV. Typical values of ν_v are 1.5 to 3.5 $\times 10^{15}$ s^{-1}, corresponding with an absorption in the UV of a wavelength λ_{abs} of ca. 100 to 200 nm (Calvert and Pitts, 1966) [3.22]. [Note that the quantity $h\nu_v$ in Eq. 3.24 may be regarded as some energy which characterizes the material. It is sometimes approximated by the ionization energy $I = h\nu_v$, from which the absorbtion frequency can be derived and compared with absorption frequencies obtained in other ways.]

When s is regarded as the 'effective number of dispersion electrons' of the atom or molecule, ν_0 and ν_v are related by

$$s = (\frac{\nu_v}{\nu_0})^2 \qquad [3.25]$$

Substitution of Eq. 3.25 in Eq. 3.24 yields the 'Slater-Kirkwood' equation

$$\beta_{11} = \frac{3}{4}\sqrt{s}\, h\nu_0 (\frac{\alpha_0}{4\pi\varepsilon_0})^2 \qquad [3.26]$$

Thus, for more complex atoms and molecules, β_{11} may be calculated when s is known. However, estimation of s is not simple. It is possible to determine s experimentally from a dispersion plot (a so-called 'Cauchy-plot'), i.e. a plot of the refractive index as a function of the frequency (Gregory, 1969 [3.2]; Hough and White, 1980 [3.18]).

Unfortunately, for many solids these data are not available. Slater and Kirkwood (1931) [3.23] proposed that s is equivalent to the outer shell electrons suggesting that all 'bonding electrons' contribute equally to the dispersion forces. This theory, or further modified versions (Moelwyn-Hughes, 1961 [3.24]; Salem, 1960 [3.25]) have found no further application because of the availability of the 'macroscopic' Lifshitz theory (sect. 3.1). Based on the Hamaker-de Boer additivity approach, discussed in this section, in the following section a method is proposed which allows the calculation of the Hamaker constants of our solids. The results of this approach have been applied to check the results obtained using the approximated equation from the 'macroscopic' theory.

3.3.2.2 Hamaker-de Boer approach for inorganic solids

For our inorganic solids the London constants have been calculated from a modification of the Slater-Kirkwood equation, i.e. Eq. 3.26. The proposed route is based upon a subdivision of the solid molecules into atoms, which all have an average composition and polarizability identical to that of the solid molecule. The London constants are then calculated from these average atomic polarizabilities. In this approach it is further supposed that the 'average atoms' are all bonded by semi-polar bonds and that only the (single or double) bond-forming electrons contribute to the higher energetic waves contributing to the dispersion forces.

Following this line of thinking Eq. 3.19 may be read as

$$\overline{q}(\text{atom}) = n_a \frac{N_A \rho}{M} \qquad [3.27]$$

which gives the total number of 'average atoms' per volume, when n_a is the number of atoms in the molecule and $\overline{q}$ represents the average atomic volume. Introduction of n_a in the Lorenz-Lorentz equation (Eq. 3.23) also allows the calculation of the average polarizability of the atoms in the solid

$$\overline{\alpha_0}(\text{atom}) = 4\pi\varepsilon_0 \frac{M}{n_a \frac{4\pi}{3} N_A \rho} \frac{n^2 - 1}{n^2 + 2} \qquad [3.28]$$

Now, from Eq. 21, the atomic absorption frequency ν_a can be calculated. It represents the oscillator frequency of the bonding electrons in the ground state. Substitution of $\overline{\alpha}_0$(atom) derived from Eq. 3.28 in Eq. 3.29 (i.e. the equivalent of Eq. 3.26) and substitution of a value of s allows the calculation of β_{11}

$$\overline{\beta_{11}} = \frac{3}{4} \sqrt{s}\, h \nu_0 \left(\frac{\overline{\alpha_0}(\text{atom})}{4\pi\varepsilon_0} \right)^2 \qquad [3.29]$$

The value of s represents now the average number of bonding electrons per atom. It is obtained simply from the summation of the single and double bond forming electrons involved in atomic bonding, divided by the number of atoms in the molecule. For example, for sodium carbonate the total number of bonding electrons is 12 and the number of atoms is 6, yielding an average s value of 2. Although in this manner the choice of s seems rather arbitrary, in physical terms the procedure may be considered as equivalent to a correction factor taking into account the ionization energy of the second step of ionization.

Using the values of β_{11} obtained finally the Hamaker constant A_{11} can be calculated. The Hamaker constants resulting from the macroscopic 'Lifshitz-Israelachvili' method (Eq. 3.18) and from the microscopic 'modified Slater-Kirkwood' method (Eqs. 3.29, 3.27 and 3.4) for a number of solids (inorganic salts and oxides, see Table 2.2) are plotted against each

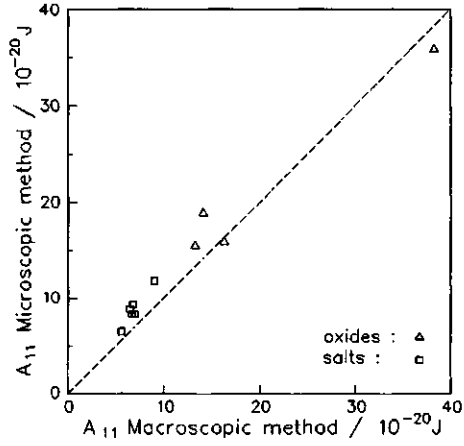

Fig. 3.6: Hamaker constants (A_{11}) of inorganic solids obtained from the 'macroscopic' theory (Eq. 3.18) compared with those from the 'microscopic' theory (Eqs. 3.29, 3.27 and 3.4).

other in Fig. 3.6, showing the differences between the two methods. The comparison indicates that the microscopic method leads to Hamaker constants which are systematically a few tens of a percent higher than the macroscopic method, but the trends are similar. Considering the great differences between the two approaches the outcome is gratifying and indicates the margins between which our Hamaker constants are established.

3.3.3 Hamaker constants in condensed media

So far, van der Waals interactions between particles in vacuum have been considered. If particles are embedded in a condensed liquid medium, which is the case for our solid particles in nonionic liquid, the attraction-reducing influence of the medium has to be taken into account in Eqs. 3.5 to 3.17. For the case of interacting alike particles of material 1 dispersed in a medium 3, following an idea of Hamaker and de Boer, the Berthelot principle can be applied (Israelachvili, 1985 [3.4]). Hence, the Hamaker constant for the interaction of the two particles in a liquid medium, $A_{11(3)}$, can be approximated by

$$A_{11(3)} = (\sqrt{A_{11}} - \sqrt{A_{33}})^2 \qquad [3.30]$$

where A_{33} refers to the Hamaker constant of the liquid medium in a vacuum. An alternative expression has been derived from the macroscopic theory (Israelachvili, 1985) [3.4]. It reads

$$A_{11(3)} \approx \frac{3}{4} k_B T \frac{(\varepsilon_1 - \varepsilon_3)^2}{(\varepsilon_1 + \varepsilon_3)^2} + \frac{3 h \nu_e}{16\sqrt{2}} \frac{(n_1^2 - n_3^2)^2}{(n_1^2 + n_3^2)^{\frac{3}{2}}} \qquad [3.31]$$

in which the symbols represent the same as in Eq. 3.18. For this equation to be valid it is supposed that ν_e does not change when the particles are surrounded by a condensed medium.

Thus, Hamaker constants in a medium can be calculated
a. directly from Eq. 3.31 (i.e. purely macroscopically),
b. from Eq. 3.18, the Israelachvili equation, combined with Eq. 3.30 (i.e. mixed macroscopically and microscopically) and
c. from Eq. 3.29, the modified Slater-Kirkwood equation, combined with Eq. 3.30 (i.e. purely microscopically).

The Hamaker constant of liquids can, with an accuracy of a few percent, be obtained directly from Eq. 3.18 (Israelachvili, 1985; Table XV) [3.4]. Hence, for nonionics, Eq. 3.18 is applied to calculate the Hamaker constant from their refractive indexes and dielectric constants. Since the error in the Hamaker constants of inorganic solids in vacuum is already a few tens of a percent, the error in the Hamaker constant when these solids are in a condensed phase is rather high, particularly when the difference between Hamaker constants of liquid and

solid is small. In such cases the results cannot be expected to be better than giving an order of magnitude.

Hamaker constants evaluated for inorganic solids (nature 1) dispersed in nonionic liquid (nature 3) will be reported in sect. 6.4.3. Anticipating this, it can be remarked that values obtained by the microscopic method tend to be systematically higher than those obtained from the macroscopic method. This was also found for Hamaker constants across vacuum (Fig. 3.6). Values of $A_{11(3)}$ of our inorganic salts, found by the macroscopic method, range between 0.02 and 0.4 $\times 10^{-20}$ J, whereas those found by the microscopic method range between 0.2 and 1.0 $\times 10^{-20}$ J. In spite of the differences it can be concluded that these values of $A_{11(3)}$ are all relatively low and are in the same range as the literature values for the systems dodecane-water-dodecane: 0.5 $\times 10^{-20}$ J or quartz(SiO_2)-octane-quartz(SiO_2): 0.1 $\times 10^{-20}$ J (Hough and White, 1980 [3.19]; Israelachvili, 1985 [3.4]). These low Hamaker constants enable suspensions of the inorganic salts in nonionic to be relatively easily stabilized. Moreover, when stabilized, dense sediments with high volume fractions of solids can be formed (sect. 2.3.1). In the nonionic liquid phase, solid oxides have higher Hamaker constants than the inorganic salts. Hence, they lead to more voluminous sediments and are more difficult to stabilize.

3.3.4 Hamaker constants for porous macrobodies

3.3.4.1 Agglomerates and aggregates in suspension

Some inorganic solids are formed of irregularly shaped, spheroid macrobodies which may contain a considerable amount of voids. In suspension, these voids are usually filled with the nonionic liquid. Hence, we have to deal with interactions of mixtures of substances. For the calculation of the Hamaker constants for interactions between such particles, porosity may be taken into account by the expression

$$A_{(1313)} = A_{11}\phi_p + A_{33}(1 - \phi_p) \qquad [3.32]$$

where ϕ_p stands for the estimated internal solids volume fraction of the particle and A_{1313} the 'effective' Hamaker constant for the porous particle of medium 1, with the pores filled with medium 3, interacting with an alike particle across vacuum. This method is basically identical with that proposed by Hough and White (1980) [3.19].

Hamaker constants of organic nonionic liquids are lower than those of the dispersed inorganic solids. Porosity will therefore have a reducing influence on the interparticle attraction in suspension. Aggregates (sect. 2.2.1) will thereby show a smaller effect than the more porous agglomerates. When, as is the case for example with 'activated' Zeolite 4A, the pores are too small to be filled with the liquid molecules, for A_{33} in Eq. 3.30, the value for vacuum (or air) has to be substituted, which reduces in a nonionic suspension the attraction between 'activated' Zeolite particles considerably.

3.3.4.2 Coagulates in suspension

Having given the expressions for single (aggregate or agglomerate) particles in suspension, it makes sense to realize that the theory given in this chapter is similarly applicable to composites of particles, i.e. to coagulates or flocs (sect. 2.2.1). As the radii of coagulates, involving a number of particles, are larger than those of the particles, this implies that, due to the increase of the geometric factor in the energy and force equations (for example Eqs. 3.6 and 3.15), also the 'inter-coagulate' energies and forces would become larger. This does not seem logical. It would mean that the links **between the particles** in the coagulates would become weaker than those **between the coagulates**. In that case application of shear would more readily lead to an internal breakdown of coagulates than to interruption of the bonds between the coagulates. This is unlikely and does not occur.

The reason that this does not occur has its origin in the 'effective' Hamaker constants of the coagulates. By definition, coagulates are composed of solids and enclosed immobilized liquid phase. The extent of the immobilized phase is solely determined by the way in which the solids in the coagulates are packed. Consequently, the effective Hamaker constants of coagulates will be considerably lower than those of pure solids. In coagulation-redispersion equilibrium the coagulates will have equal internal and external attractive energies. When the Hamaker constant of the dispersed solid is relatively large, i.e. when the difference with the continuous phase is large, internal attractions between the solid particles inside a coagulate are stronger and, consequently, the coagulates have to grow more to reach an equal external attraction with other coagulates. In sediments this will coincide with a more open structured, voluminous solid packing. Conversely, when the difference in Hamaker constants is small, already at a smaller size the flocs have an equal internal and external attractive energy.

The importance of this consideration is that it shows that, with equal geometrical factors, mechanical properties of suspensions can be related to the Hamaker constant, which is a material property. Theorists may be able to work out this concept further. From the solids volume fraction, for example expressed in a fractal dimension of the coagulates, the chance could be calculated that somewhere the structure, determined by the number of bonds between coagulates and the strength per bond, is disrupted by shear.

3.3.5 The Hamaker constant as a function of temperature

The London contribution to the dispersion forces is virtually independent of the temperature. Therefore, in alkane-like non-polar systems, no increase of the attraction energy with temperature is found (Mahanty and Ninham, 1976) [3.21]. An expression which shows the effect of temperature on the Hamaker constant of two alike macrobodies of nature 1 across a liquid medium of nature 3 is Eq. 3.29. The first term on the right hand side of this equation, containing the zero-frequency dielectric constant, gives the purely entropic contribution $A_{\nu=0}$ (Israelachvili, 1985) [3.4]. From this part of the equation the magnitude of the

temperature effect can be estimated. Differences in dielectric constants between our solids (nature 1) and the nonionic liquid (nature 3) are maximally a factor two. This difference gives a value of the first term of 6×10^{-23} J, at a temperature of 298 K, a value which hardly increases if the temperature rises to 343 K (70 °C). These values are much smaller than the values of $A_{11(3)}$ mentioned in sect. 3.3. They demonstrate that in our systems the temperature dependent contribution to the dispersion forces (and to the Hamaker constant) is very small and can be ignored. Hence, the observed rise in viscosity with increase of temperature of the suspension of sodium triphosphate in Plurafac nonionic (see Fig. 1.4) could not be ascribed to an increase in attractive energy.

3.4 SUMMARY:

The literature on the van der Waals attraction (energy and forces) between particles in suspension is discussed. For particles in the micron-size range, geometrical parameters (differences in particle size, interparticle distance, retardation and surface roughness) are of more importance than in colloidal systems. This means that the van der Waals bonding energy obtained on approach is larger and as a function of increasing interparticle distances decays more rapidly. Retardation causes large reductions of van der Waals attractions at distances $\geq$ 20 nm, i.e. beyond approximately the Debye length in a nonionic suspension. Surface roughness, due to unevenness in the crystalline surface, causes reductions at short distances of approach.

In the van der Waals attraction, material properties are reflected in the Hamaker constant. Hamaker constants for the inorganic crystalline solids considered in this study are not available in the literature. Therefore it was necessary to evaluate them theoretically. Two theories have been applied: a macroscopic, 'Lifshitz-Israelachvili' theory and a microscopic theory. The latter is a modification of the Hamaker-de Boer-Slater-Kirkwood theory. From a comparison it appeared that the two methods give identical results within a few tens of a percent. The Hamaker constants for the inorganic salts suspended in nonionic are found to be relatively low and lower than those of the metal oxides.

3.5 BIBLIOGRAPHY

3.1 London, F.. *Trans. Faraday Soc.* **1937**, 33, 8-26.

3.2 **The Calculation of Hamaker Constants.** Gregory, J.. *Adv. Colloid Interface Sci.* 1969, 2, 396-411.

3.3 **On Hamaker constants: A comparison between Hamaker constants and Lifshitz-van der Waals constants.** Visser, J.. *Adv. Colloid Interface Sci.* **1973**, 3, 331-363.

3.4 **Intermolecular and surface forces. With applications to colloidal and biological systems.** Israelachvili, J.N.. (Academic Press, London). **1985.**

3.5 **Foundations of colloid science. Vol.1. The Theory of van der Waals forces.** Hunter, R.J; Editor. (Clarendon Press, Oxford) **1987.**

3.6 Hamaker, H.C.. *Physica* **1937,** 4, 1058.

3.7 de Boer, J.H.. *Trans. Faraday Soc.* **1936,** 32, 11-21.

3.8 Casimir H.B.G.; Polder D.. *Phys. Rev.* **1948**, 73, 360.

3.9 Dzyaloshinskii, I.E.,; Lifshitz, E.M.; Pitaevskii, L.P.. *Sovjet Physics JETP.* **1960,** 10, 161.

3.10 a. **Colloid science. Vol.1.** Overbeek, J.Th.G.. Kruyt, H.R.; Editor. (Elsevier, Amsterdam) **1952;** b. **...** Overbeek, J.Th.G.; Silhout, A. van. *Proc. Koninkl. Akad. Wetensch.* **1966**, B.69, 501.

3.11 **Coagulation Kinetics and Structure Formation.** Sonntag, H.; Strenge, K.. (Plenum Press, London, UK). **1987.**

3.12 **Approximate method for calculation of Hamaker constants with allowance for the effect of electromagnetic lag.** Rabinovich, Ya.I.. *Kolloidn. Zh.* **1978,** 41 (6), 965-969.

3.13 **Approximate Expressions for Retarded van der Waals Interaction.** Gregory, J.. *J. Colloid Interface Sci.* **1981**, 83 (1), 138-145.

3.14 a. **Van der Waals Attraction Energy between Unequal Rough Spherical Particles.** Czarnecki, J.; Itschenskij, V.. *J. Colloid Interface Sci.* **1984**, 98 (2), 590-591; b. **The effects of surface inhomogeneities on the interactions in colloidal systems and colloidal stability.** Czarnecki, *Adv. Colloid Interface Sci.* **1986**, 24, 283-319.

3.15 a. **Calculation and measurement of the forces of the dispersive interactions of bodies with rough surfaces.** Rabinovich, Ya. I.; Charnetski, Ya.; Ichenskii, V.. *Kolloidn. Zh.* **1987**, 49 (2), 262-265; b. **Two approaches to calculation of the energy of the dispersion interaction of rough bodies in a vacuum.** Rabinovich, Ya.I.; Charnetski, Ya.; Ichenskii, V.. *Kolloidn. Zh.* **1989**, 51 (2), 259-265.

3.16 **Stability of coarse suspensions in non-polar media: Effect of gravity on the interactions between particles.** Mil, P.J.J.M. van ; Crommelin, D.J.A.; Wiersema, P.H.. *J. Colloid Interface Sci.* **1984**, 98 (1), 61-71.

3.17 **The van der Waals Attraction Between Colloid Particles Having Adsorbed Layers. II Calculation of Interaction Curves.** Vincent, B.. *J. Colloid Interface Sci.* **1973**, 42 (2), 270-285.

3.18 **The calculation of Hamaker constants from Lifshitz theory with application to wetting phenomena.** Hough, D.B.; White, L.R.. *Adv. Colloid Interface Sci.* **1980**, 14, 3-41.

3.19 **Surface and colloid science. Vol. 8. Chapter 1: Adhesion of colloidal particles.** Visser, J.. Mateijevic, E.. Editor. (John Wiley, New York) **1976.**

3.20 **Dispersion forces.** Mahanty J.; Ninham B.W.. (Academic Press, New York) **1976.**

3.21 **Absorption and scattering of light by small particles. Chapter 9: Classical theories of optical constants.** Bohren C.F.; Huffman D.R.. (John Wiley, New York). **1983.**

3.22 **Photochemistry. Chapter 5: Photochemistry of polyatomic molecules.** Calvert J.G.; Pitts J.N.. (John Wiley, New York). **1966.**

3.23 **The van der Waals forces in gases.** Slater J.C.; Kirkwood J.G.. *Phys. Rev.* **1931**, 37, 682-97.

3.24 **Physical Chemistry. 2nd Ed.** Moelwyn-Hughes, E.A.. (Pergamom Press, New York). **1961.**

3.25 Salem L., *Mol. Phys.* **1960**, 441, 3.

Chapter 4

ELECTROSTATIC REPULSION IN NON-AQUEOUS MEDIA

4.1 INTRODUCTION

Three basic conditions have to be fulfilled before we can decide whether we are dealing with electrostatic stabilization in a low-polar system containing solids, nonionic and DoBS acid (sect. 2.5.3). These conditions are:
1. the particles obtain a surface charge,
2. the electrolyte dissociation is sufficiently large to give small Debye lengths, and
3. the van der Waals attraction between particles is such that there are distances where the attraction is more than compensated by electrostatic repulsion.

The van der Waals attraction in a concentrated suspension of crystalline solids in nonionic liquid can be calculated by the theory elaborated in Chapter 3. In this chapter the theory of electrostatic repulsion is dealt with. It is the aim to decide whether electrostatic obstruction can become sufficient to create stabilization.

Similarly to attraction, repulsion is discussed for pairs of particles and not for sets of many particles. As usual, the expressions for repulsion are primarily given in terms of **energies** (V_R). To be able to compare them with other forces (gravity, shear) repulsion will also be expressed in terms of **forces** (F_R) (for spheres) or **pressures** (P_R) (for flat plates).

Basically, electrostatic repulsion is a consequence of interactions involving the ionic layers surrounding the particles. Consequently, at given surface charge, the electrostatic repulsion does not depend on the nature of the solids. For the electrostatic repulsion the charge distribution in the ionic layers plays a dominant role, particularly in the radial direction. This distribution is supposed to follow classical Poisson-Boltzmann statistics. In this part we will deal first with these ionic layers and the repulsion which develops on their interactions. Attention will thereby be given especially to the effects of a dissociating, monovalent electrolyte in non-aqueous solvents. According to the DLVO theory (sect. 2.3.3), summation of the attraction and the repulsion as a function of distance leads to the net total interaction energy (V_T) between two particles.

4.2 DOUBLE LAYERS AND ELECTROSTATIC REPULSION

4.2.1 Double layers and Debye lengths

4.2.1.1 Double layers

When a solid is introduced into an electrolyte solution, the solid surface becomes charged if there is an unequal adsorption of positive and negative ions at the surface. Coulombic forces caused by the adsorbed ions keep the counterions in the vicinity of the surface, whereas Brownian motion counteracts that effect and causes them to be distributed diffusely over the liquid phase. The theory of the effect of surface charging has been extensively discussed in the classic book of Verwey and Overbeek (1948) [4.1] and also more recently by Usui and Hachisu (1984) [4.2].

Surfaces can become charged in a number of different ways, such as dissociation of molecules adsorbed from solution or dissociation of covalently bound groups in the solid itself. In essence, however, double layers can always be considered as being the result of a spontaneous, entropy-driven dissociation of molecules present at the surface. A schematic representation of the distribution of a monovalent electrolyte over surface and solution is given in Fig. 4.1. In this example it is assumed that the surface is becoming positively charged due to the adsorption of an electrolyte, of which the anions are desorbed. The combination of surface charge, counterion and co-ion layers is usually referred to as the electrostatic 'double-layer'. Double layer formation in aqueous systems is the subject matter of a vast amount of literature. For a more extensive discussions of double layer formation, apart from the references already mentioned, see for example the review given by Lyklema (1981) [4.3] and the books of Israelachvili (1985) [4.4], Hiemenz (1986) [4.5] and Hunter (1987) [4.6].

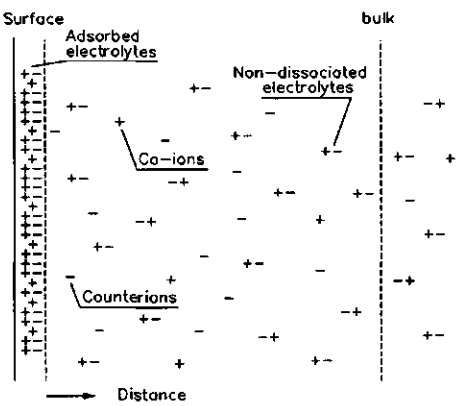

Fig. 4.1: Dissociation of a monovalent electrolyte giving co-ions and counter-ions. Ions adsorbed give rise to a surface charge and counterions. The solvent molecules are not shown.

Concentration profiles of negative and positive ions as a function of distance from the surface are shown in Fig. 4.2. The ion concentrations are calculated supposing a Poisson-Boltzmann type of distribution. It is supposed for these calculations that the solution has a low dielectric constant ($\varepsilon = 6$) (see sect. 2.2.1). Furthermore we

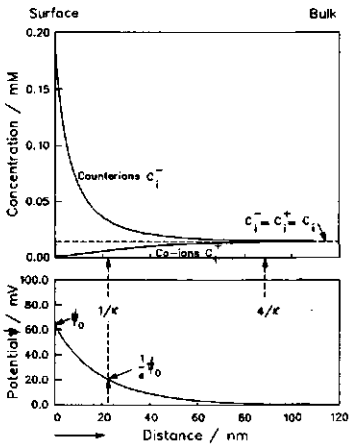

Fig. 4.2: Ionic density profiles and electric potential near the surface for a monovalent electrolyte. Parameters: $\varepsilon = 6$, $c_i = 0.015$ mM and $\psi_0 = 65$ mV.

have assumed a bulk ionic strength c_i of a monovalent electrolyte as derived from the Fuoss equation of 1.5×10^{-5} M (see sect. 2.5.3, Eq. 2.5) and an electrical potential at the beginning of the diffuse part of the double layer of ca. 65 mV. (The basis for the latter assumption will be discussed in sect. 4.3.1). These parameters are typical for our systems and will also be used in further parts of this chapter. Henceforth they are referred to as 'reference' parameters.

From Fig. 4.2 (top curve) it can be seen that, the difference between the counterion concentration (in the example in Fig. 4.1 the negative ions) and co-ion concentration (the positive ions) is the largest close to the surface. With increasing distance from the solid surface the concentration differences become smaller. The double layer ends at the distance where negative and positive ion concentrations are equal and are equal to the bulk ion concentration, which happens in principle at infinite distance. For practical purposes thicknesses of double layers are measured in units of the Debye lengths. Double layers can be discussed in terms of charge separation, ion concentration distributions, or in terms of the electrical potential ψ. The potential as a function of distance (for a flat surface) has also been given in Fig. 4.2 (bottom curve).

The extensions of double layers can be affected by the bulk ion concentrations in the bulk. When raised, the concentrations of both the positive and negative ions in the double near the surfaces increase. This causes a more rapid decay of the ion concentration as a function of distance in the double layer. Thus, increase of bulk ion concentration reduces the thickness of the double layer and conversely.

4.2.1.2 Debye lengths

The thickness of the double layer around a charge can be characterised by the so-called 'Debye length' $1/\kappa$, where κ is the Debye-Hückel screening parameter. For a monovalent symmetric 1 : 1 electrolyte, κ can be defined as

$$\kappa = \sqrt{\frac{2\, e^2}{\varepsilon_0\, k_B T}\, n_i} \qquad [4.1]$$

where ε_0 is dielectric permittivity in vacuum, k_B Boltzmann's constant, T the temperature in Kelvin, e the elementary charge and ε the (dimensionless) relative static permittivity, i.e. the dielectric constant. In Eq. 4.1, n_i is the ionic number concentration in the bulk of the solution (dimension: m^{-3}). It is equivalent to

$$n_i = N_A\, 10^3\, c_i \qquad [4.2]$$

with c_i the bulk molar ionic strength (dimension: M) and N_A Avogadro's constant. Substitution of Eq. 4.2 in Eq. 4.1 leads to an equation from which the Debye length $1/\kappa$ can be calculated from the experimentally accessible parameters c_i and ε

$$\frac{1}{\kappa} = \sqrt{\frac{k_B T\, \varepsilon_0}{2 \times 10^3 e^2 N_A} \frac{\varepsilon}{c_i}} \qquad [4.3]$$

When the natural constants in Eq. 4.3 are substituted and T is taken at 298 K, this gives the expression for the Debye length, which was used in sect. 2.5.3 (Eq. 2.4).

In terms of electrical potential ψ, the basic equation of the potential distribution is the Poisson equation. Taking all ions i into account and when the solvent is considered as homogeneous and continuous, for monovalent electrolytes it reads

$$-\varepsilon_0 \varepsilon \nabla^2 \psi = 4\pi \sum_i e\, n_i \exp\left(-\frac{e\,\psi}{k_B T}\right) \qquad [4.4]$$

where ∇^2 is the Laplace operator and $\psi = \psi(x)$ the potential at a distance x from the surface. In this equation it is assumed that ε is independent of x, a constancy which is generally fulfilled for non-aqueous systems (Lyklema, 1968) [4.7]. From the Poisson equation, when the potential at the beginning of the double layer is denoted ψ_0, it can be derived for flat double layers

$$\tanh \frac{e\,\psi}{4\, k_B T} = \tanh \frac{e\,\psi_0}{4\, k_B T} \exp(-\kappa x) \qquad [4.5]$$

which approximates for small potentials to

$$\psi = \psi_0 \exp(-\kappa x) \qquad [4.6]$$

The Poisson equation for spherical double layers has no analytical solution. However, often use is made of an analytical solution which can be obtained for low potentials, i.e. the Debye-Hückel approximation

$$\psi = \psi_0 \frac{a}{r} \exp(-\kappa(r - a)) \qquad [4.7]$$

where $\psi = \psi(r)$ is the potential at a distance r from the particle centre and a is the particle radius. From Eq. 4.6 it can be derived that the Debye-length $1/\kappa$ can be defined as the distance over which ψ is dropped to a value $1/e \approx 0.367$ of its value at the surface ψ_0 (Fig. 4.2, bottom curve). In general, $1/\kappa$ is a useful parameter to describe the extension of double layers.

Equation 4.3 illustrates that the Debye length $1/\kappa$ increases with decreasing c_i. For example for water with an approximate dielectric constant ε of 78, containing a monovalent electrolyte at an ionic strength c_i of 1 mM, a Debye length of about 10 nm is obtained, whereas for 100 mM it is only ca. 1 nm. By using lower electrolyte concentrations, it is possible to have more extended double layers in water. From Eq. 4.3 it is also seen that the Debye length $1/\kappa$ is small when the dielectric constant ε of the liquid is low. If this were the only effect, in media with a low dielectric constant Debye lengths ought to be lower than in water. However, in such media the double layers are nevertheless usually extended. The reason for this is the commonly poor electrolyte dissociation causing that the low value of c_i outweighs the value of ε.

4.2.2 Double layer overlap and 'electrostatic' repulsion; flat plates model

Overlap of double layers can occur in situations when macrobodies surrounded by double layers come in the vicinity of each other (Fig. 4.3). In suspensions, for example, this can occur under the influence of external forces, such as gravity or shear. Overlap of two double layers leads to the development of an electrostatic force, directed against any applied external force and is consequently experienced as a repulsion. The magnitude is related to the extent of the overlap. The full theory used to calculate the magnitude and extent of the electrostatic repulsive forces or free energies was already developed more than 40 years ago (Verwey and Overbeek, 1948 [4.1]). Although it was at first instance developed particularly for aqueous systems, it is also applicable for non-aqueous media at low ionic strengths (Koelmans and Overbeek, 1954 [4.8], Lyklema, 1968 [4.7], Parfitt and Peacock, 1978 [4.9], Kitahara, 1984 [4.10]). The theory demonstrates that the electrostatic repulsions can be calculated (by good approximation) from parameters, which are experimentally accessible.

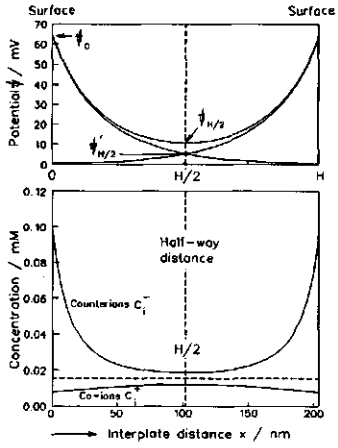

Fig. 4.3: Ion distribution and electric potential profiles for two overlapping double layers. Calculated using the 'reference' parameters of Fig. 4.2. ($\psi_{H/2}$ = ca. 12 mV).

In the following parts of this section the expressions for repulsion will be given in terms of pressures and energies, first for the model situation of flat plates. The approximations which lead to analytical solutions of the equations, are also given. Using the approximated equations, the repulsions can be calculated from only three parameters, viz. the dielectric constant of the liquid continuous phase ε, the ionic strength in the bulk c_i and the electrical potential at the beginning of the double

layer ψ_0. For the exact computations also the electric potential half-way between the plates $\psi_{H/2}$ (see Fig. 4.3) is needed. The application of the theory for non-aqueous media will be also discussed.

4.2.2.1 Exact repulsive pressure from $\psi_{H/2}$

Between two flat surfaces with overlapping double layers there are two pressure: one of **osmotic** origin P_{Osm} and one of **electrostatic** origin P_{El}.

The **osmotic** component P_{Osm} is the result of differences between ion concentrations in the double layer and the bulk of the solution. It can be described at any point between the surfaces by

$$P_{Osm} = (n_i^+(x) + n_i^-(x))\, k_B T - 2\, n_i\, k_B T \qquad [4.8]$$

In this equation $n_i^+(x)$ and $n_i^-(x)$ represent the number concentrations of positive and negative ions at any distance x in the double layer, respectively, and $n_i^+(\infty) = n_i^-(\infty) = n_i$ is the ion number concentration in the bulk (see Fig. 4.2). When the positive and negative ions in the double-layer follow a Poisson-Boltzmann type distribution function, P_{Osm} can be expressed in terms of the electric potential between the plates ψ by

$$P_{Osm} = 2\, n_i\, k_B T(\cosh\frac{e\,\psi}{k_B T} - 1) \qquad [4.9]$$

The **electrostatic** component P_{El} follows from elementary electrostatic field theory and the expression for energy storage in an electric field. For an electric field $d\psi/dx$, present at any point in the double layer, the pressure is equal to the energy per unit volume stored at that point. In formula

$$P_{El} = -\frac{1}{2}\, \varepsilon_0 \varepsilon\, (\frac{d\psi}{dx})^2 \qquad [4.10]$$

Analogous to Eq. 4.8, the electrostatic component can be expressed in terms of the bulk ion concentration n_i and in the potential ψ. For this purpose the potential gradient $d\psi/dx$ is written as functions of ψ and the potential in the overlap region half-way the two plates $\psi_{H/2}$ (see Fig. 4.3). Again for a Poisson-Boltzmann type of ion distribution pattern, it can be derived

$$\frac{d\frac{e\,\psi}{k_B T}}{d(\kappa x)} = -\sqrt{2\,(\cosh\frac{e\,\psi}{k_B T} - \cosh\frac{e\,\psi_{H/2}}{k_B T})} \qquad [4.11]$$

[Note: A derivation of Eq. 4.11 is given by Verwey and Overbeek (1948) [4.1], p. 67; the equation follows after integration over the plate distance of a second order differential equation, describing the variation of the potential between two plates]. Equation 4.11 is an elliptic integral of the first kind, for which no analytical solution is available. When integration is carried out between the limits $x = 0$ and

$x = H/2$, and between $\psi = \psi_0$ and $\psi = \psi_{H/2}$, numerical integration of Eq. 4.11 leads to the electric potential half-way between the plates $\psi_{H/2}$.

The expression required for P_{El} is found after substitution of Eqs. 4.11 and 4.1 and after some rearrangement. It reads

$$P_{El} = -2 n_i k_B T \left(\cosh\frac{e\psi}{k_B T} - \cosh\frac{e\psi_{H/2}}{k_B T}\right) \qquad [4.12]$$

P_{El} has a negative sign, meaning that it is attractive (Usui and Hachisu, 1984) [4.2]. However, since it is smaller than P_{Osm} (Eq. 4.9) the net effect of the two contributing components to the total pressure is always repulsive.

For a given system, a condition for equilibrium at any point between two flat plates is that the total pressure, i.e. the (positive) sum of the electro-static and the osmotic pressure, is independent of position.

$$P_R^{(flat)} = P_{Osm} + P_{El} = \text{Constant} \qquad [4.13]$$

After substitution of Eqs. 4.9 and 4.12 in Eq. 4.13 it is finally found that

$$P_R^{(flat)} = 2 n_i k_B T \left(\cosh\frac{e\psi_{H/2}}{k_B T} - 1\right) \qquad [4.14]$$

Equation 4.14 is a simple and important expression. It can be used to predict the effects of changes in ion concentration and in potential half-way the two plates $\psi_{H/2}$ on the magnitude of the electrostatic repulsion. The equation remains applicable for surfaces of any other than flat geometry. It shows that the repulsive pressure rises when the surfaces approach each other, i.e. when the overlap potential $\psi_{H/2}$ of their double layers increases or, at constant overlap, that the repulsive pressure also increases when the bulk ion concentration n_i increases. It has to be noted, however, that at higher ion concentrations the double layers are thinner. To maintain a constant overlap, it is thus necessary that the surfaces have to come closer together (see sect. 4.3.1.2).

4.2.2.2 Exact repulsive energy from $\psi_{H/2}$

An exact equation for the potential energy of repulsion between two flat surfaces can be found from the Gibbs free energies. A complete derivation of the equation has been given by Verwey and Overbeek (1948) [4.1]. The route they applied is only briefly discussed here.

The Gibbs energy G of two interacting surfaces at distance H (see Fig. 4.3) can be obtained from integration with respect to the distance of both the electrostatic and osmotic pressure components. Hence, from Eqs. 4.9 and 4.10

$$G = -2 n_i k_B T \int_0^{H/2} (\cosh\frac{e\psi}{k_B T} - 1) dx + \\ -\frac{1}{2} \varepsilon_0 \varepsilon \int_0^{H/2} (\frac{d\psi}{dx})^2 dx \qquad [4.15]$$

The first of these two integrals can be solved analytically. After substitution of Eq. 4.1 and some rearrangement Eq. 4.15 becomes

$$G = -2 n_i k_B T \frac{H}{2} (\cosh\frac{e\psi_{H/2}}{k_B T} - 1) + \\ -2 n_i k_B T \frac{1}{\kappa} \int_0^{H/2} (\frac{d\frac{e\psi}{k_B T}}{d(\kappa x)})^2 d(\kappa x) \qquad [4.16]$$

For the second integral in Eq. 4.16 there is no analytical solution. After substitution of Eq. 4.9, Eq. 4.16 can be rewritten giving

$$G = -\frac{2 n_i k_B T}{\kappa} \{\kappa \frac{H}{2} (\cosh\frac{e\psi_{H/2}}{k_B T} - 1) + \\ - \int_0^{\kappa\frac{H}{2}} 2 (\cosh\frac{e\psi}{k_B T} - \cosh\frac{e\psi_{H/2}}{k_B T}) d(\kappa x)\} \qquad [4.17]$$

The total Gibbs free energy between two flat surfaces can now be found after integration of Eq. 4.17. It gives the total gain in Gibbs energy, when the surfaces are moved from their original positions at distance H to infinity

$$V_R^{(flat)} = 2 (G_{H/2} - G_\infty) = -2 G_\infty + 2 G_{H/2} \qquad [4.18]$$

The energy of the plates at infinite distance can be derived directly. Since at infinite distance $\psi_{H/2} \to 0$, G_∞ follows from integration of Eq. 4.17 for $x \to \infty$, giving

$$G_\infty = -2 n_i k_B T \frac{1}{\kappa} (4 \cosh\frac{e\psi_0}{k_B T} - 4) \qquad [4.19]$$

The total repulsive Gibbs energy for a system of two parallel flat plates ($V_R^{(flat)}$) can than be written as

$$V_R^{(flat)} = \frac{4\, n_i\, k_B T}{\kappa} \{(4\cosh\frac{e\psi_0}{k_B T} - 4) - \kappa\frac{H}{2}(\cosh\frac{e\psi_{H/2}}{k_B T} - 1) + \\ - \int_0^{\kappa\frac{H}{2}} 2(\cosh\frac{e\psi}{k_B T} - \cosh\frac{e\psi_{H/2}}{k_B T})\, d(\kappa x)\} \qquad [4.20]$$

which finally gives, after substitution of Eq. 4.1,

$$\frac{V_R^{(flat)}}{\kappa} = 2\,\varepsilon_0\,\varepsilon\,(\frac{k_B T}{e})^2 \{(4\cosh\frac{e\psi_0}{k_B T} - 4) + \\ - \kappa\frac{H}{2}(\cosh\frac{e\psi_{H/2}}{k_B T} - 1) + \qquad [4.21] \\ - \int_0^{\kappa\frac{H}{2}} 2(\cosh\frac{e\psi}{k_B T} - \cosh\frac{e\psi_{H/2}}{k_B T})\, d(\kappa x)\}$$

Since $\kappa H/2$ is a function of $\psi_{H/2}$ and ψ_0, the right-hand-side of Eq. 4.21 contains only ε, $\psi_{H/2}$ and ψ_0 as the variables. Hence, in shorthand notation it can be written

$$\frac{V_R^{(flat)}}{\kappa} = \frac{2(G_H - G_\infty)}{\kappa} = f(\varepsilon, \psi_{H/2}, \psi_0) \qquad [4.22]$$

From Eq. 4.21, for a medium with a known relative dielectric constant ε, $V_R^{(flat)}/\kappa$ can be calculated numerically as a function of $\kappa H/2$, when $\psi_{H/2}$ and ψ_0 are known. For aqueous media, values of $f(\varepsilon_{water}, \psi_0, \psi_{H/2})$, for a number of different values of $\kappa H/2$ have been reported by Verwey and Overbeek (1948) [4.1] (p. 82, Table XI) or Hunter [4.6] (Table 7.1), using $\varepsilon_{water} = 78.55$. These values allow the calculation of $V_R^{(flat)}/\kappa$ for aqueous systems at various plate distances. From Eq. 4.21 it can be seen that $V_R^{(flat)}/\kappa$ is proportional to the dielectric constant. Hence, to compute $V_R^{(flat)}/\kappa$ for media with other dielectric constants, $f(\varepsilon, \psi_0, \psi_{H/2})$ can be obtained by simply multiplying the tabulated data of $f(\varepsilon_{water}, \psi_0, \psi_{H/2})$ with $\varepsilon/\varepsilon_{water}$.

4.2.2.3 Approximated repulsive pressure from ψ_0

Although accurate, Eq. 4.21 is not very practical because of the fact that $\psi_{H/2}$ is not experimentally accessible. However, an equation has been derived (Verwey and Overbeek, 1948 [4.1]), which allows, by approximation, calculation of the repulsive pressure from ψ_0. For the situation that the plates are not too close so where the potential in the overlap region is only small, i.e. $\psi_{H/2}$ is $\leq$ ca. 25 mV, it can be shown that Eq. 4.14 reduces to

$$P_R^{(flat)} \approx n_i k_B T \left(\frac{e \psi_{H/2}}{k_B T}\right)^2 \qquad [4.23]$$

For small potentials half-way between the plates it can be further assumed that, at the half-way distance, the overlap potential is approximately equal to the sum of the individual electrical potentials $\psi'_{H/2}$ of both surfaces (see Fig. 4.3, top graph)

$$\psi_{H/2} \approx 2 \psi'_{H/2} \qquad [4.24]$$

Using the Debye-Hückel theory for small potentials, a relation between ψ_0 and $\psi'_{H/2}$ can be given by

$$\psi'_{H/2} \approx 4 \frac{k_B T}{e} \gamma \exp(-\kappa \frac{H}{2}) \qquad [4.25]$$

where γ is a function of ψ_0

$$\gamma = \tanh \frac{e \psi_0}{4 k_B T} \qquad [4.26]$$

After substitution of Eq. 4.24 in Eq. 4.23 this finally leads to

$$P_R^{(flat)} \approx 64 n_i k_B T \gamma^2 \exp(-\kappa H) \qquad [4.27]$$

This equation is the result of the 'weak overlap' approximation (Eq. 4.24). It allows an (approximate) calculation of the repulsive pressure $P_R^{(flat)}$ as a function of the distance between the plates H for different bulk ionic number concentrations n_i and surface potential ψ_0. κ can be obtained from Eq. 4.1 and is also a function of n_i and ε.

4.2.2.4 Approximated repulsive energy from ψ_0

The total repulsive Gibbs energy for the interaction between flat plates ($V_R^{(flat)}$) can be obtained after integration of the pressure ($P_R^{(flat)}$) bringing the plates from an infinite distance to a final distance H

$$V_R^{(flat)} = -\int_{\infty}^{H} P_R^{(flat)} \, dH \qquad [4.28]$$

When $P_R^{(flat)}$ from Eq. 4.27 is substituted in Eq. 4.28 this leads to an equation, which is valid for small half-way potentials

$$V_R^{(flat)} \approx 64 n_i k_B T \gamma^2 \frac{1}{\kappa} \exp(-\kappa H) \qquad [4.29]$$

Comparison of equations 4.27 and 4.29 demonstrates that the pressure and the energy are related simply by

$$V_R^{(flat)} = \frac{1}{\kappa} P_R^{(flat)} \qquad [4.30]$$

This equation allows us to obtain the energy directly from the pressure.

In the case that not only the overlap potential $\psi_{H/2}$ is small, but also the surface potential ψ_0, i.e. when both $e\psi_0/k_BT \leq 1$ and $e\psi_{H/2}/k_BT \leq 1$, Eq. 4.29 can be approximated further to a number of more or less equivalent expressions which are frequently encountered in the literature

$$V_R^{(flat)} \approx 2\,\varepsilon_0\varepsilon\,\psi_0^2\,\kappa\frac{\exp(-\kappa H)}{(1+\exp(-\kappa H))}$$

$$\approx 2\,\varepsilon_0\varepsilon\,\psi_0^2\,\kappa\exp(-\kappa H) \qquad [4.31]$$

$$\approx 2\,n_i\,k_B T\left(\frac{e\psi_0}{k_B T}\right)^2\frac{1}{\kappa}\left(1-\tanh\left(\kappa\frac{H}{2}\right)\right)$$

In Fig. 4.4 a comparison is made between the exact and the approximated equations for repulsions applying to our 'reference' conditions. The exact result of the repulsive energy ($V_R^{(flat)}$) is obtained by numerical integration of Eq. 4.21, whereas Eq. 4.11 is used for the calculation of $\psi_{H/2}$ and $H/2$. The results are plotted in Fig. 4.4a. The approximated repulsive energies are obtained from Eqs. 4.29 and 4.31. For the calculation of the repulsive pressures ($P_R^{(flat)}$) the exact results are obtained from Eq. 4.14, again combined, for the calculation of the plate distance H, with the results of Eq. 4.11. The results are given in Fig. 4.4b. The approximated pressures are obtained from Eq. 4.27.

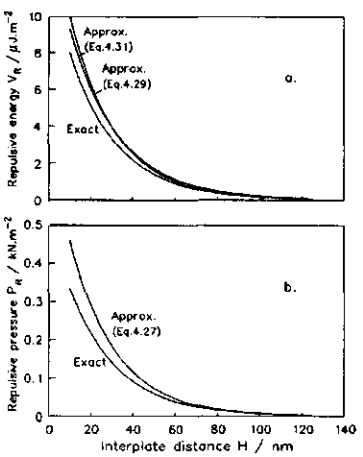

Fig. 4.4: Repulsive energies (a) and pressures (b) as a function of H. Comparison of results of exact and approximated equations, using the 'reference' parameters for nonionics (Fig. 4.2).

The results confirm that the approximate equations give the closest agreement with the exact results in the 'weak overlap' situation. The approximated equations tend overestimate at small plate distances, probably due to the ignorance of higher order terms in Eq. 4.23. For larger double layer overlap, at a distance of 10 nm, the approximate equations give values that overestimate the exact calculations by about 20 %.

4.2.3 Electrostatic repulsion for spheres

The elaborations in the previous sections lead to expressions for the repulsive energies and pressures for flat parts of interacting surfaces. In this section we deal with interactions, in which surface curvature is taken into account.

In our suspensions we use particles with an average radius $a \geq 1$ μm (see sect. 2.2.2, Table 2.2), whereas Debye lengths $1/\kappa$ of approximately 20 nm may occur in these systems (see sections 2.5.3 and 4.2.1.2). Hence, the theory of repulsion for spherical particles for situations where $\kappa a > 5$ should be applied. The theory for particles with relatively extended double layers, which is often applied in non-aqueous media, is less relevant for our systems and is therefore not discussed here. For the theories for $1 \leq \kappa a \leq 5$ the reader is referred to Verwey and Overbeek (1948) [4.1] or to van Mil, Crommelin and Wiersema (1984) [4.11]. We shall now discuss the expressions for the repulsive energy and force for two interacting spherical double layers in the case of large κa.

4.2.3.1 Exact energy and pressure from $\psi_{H/2}$

According to an approximation, elaborated by Deryagin, the repulsive energy between two curved surfaces is considered to consist of additive contributions of infinitesimal, parallel concentric rings, each pair of rings contributing to the potential energy by an amount equal to $2\pi h\,(2G_{H'} - 2G_{\infty})\mathrm{d}h$, where $2G$ is the Gibbs free energy per unit of surface (at distances H' and at infinite distance respectively) and h is the radius of the ring (see Fig. 4.5). The total repulsive energy can now be found by integrating these energies per unit of surface over the whole surface of the curved body (see Verwey and Overbeek (1948) [4.1], Israelachvili (1984) [4.4], Usui and Hachisu (1984) [4.2])

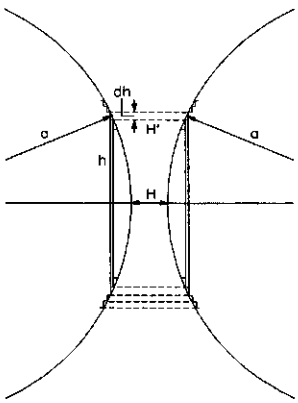

Fig. 4.5: Building up of the repulsion between two spheres from the repulsion between parallel rings.

$$V_R^{(curved)} = 2\pi \int_0^{\infty} h\,(2G_{H'} - 2G_{\infty})\,\mathrm{d}h \qquad [4.32]$$

Since for spherical particles with a large particle radius a and with small values of h: $(H' - H)/2 \approx a\,\mathrm{d}H'$ (see Fig. 4.5), the repulsive energy for two interacting spheres can now be written as

$$V_R^{(sphere)} = 2\pi a \int_H^\infty 2\,(G_{H'} - G_\infty)\,d\frac{H'}{2} \qquad [4.33]$$

As was shown in Eq. 4.21, the difference of free energies ($2G_{H'} - 2G_\infty$) can be written as a (rather complicated) function of ε, $\psi_{H/2}$ and ψ_0. A shorthand notation was given by Eq. 4.22. After substitution of Eq. 4.21, Eq. 4.33 can be written, as

$$V_R^{(sphere)} = \pi a \kappa \int_H^\infty f(\varepsilon, \psi_{H/2}, \psi_0)\,dH' \qquad [4.34]$$

From Eq. 4.34, the interaction energy for two spheres ($V_R^{(sphere)}$), with radius a and Debye length $1/\kappa$, can now be computed by numerical integration between the limits H and ∞. The method is basically analogous to that applied for Eq. 4.21 and implies the numerical integration of Eq. 4.11, giving, at a value of the surface potential ψ_0, the value of $H/2$ at any electric potential $\psi_{H/2}$. The value of $f(\varepsilon,\psi_{H/2},\psi_0)$ follows after numerical computation from Eq. 4.21. Values of $f(\varepsilon_{water},\psi_{H/2},\psi_0)$ can be obtained from Verwey and Overbeek [4.1] (Table XI) or Hunter [4.6] (Table 7.1).

The repulsive force for a pair of interacting spherical particles ($F_R^{(sphere)}$) can be obtained directly from

$$F_R^{(sphere)} = -\frac{dV_R^{(sphere)}}{dH'} \qquad [4.35]$$

After carrying out the differentiation, the exact following exact expression is obtained

$$F_R^{(sphere)} = \pi a \kappa f(\varepsilon, \psi_{H/2}, \psi_0) \qquad [4.36]$$

Computation from Eq. 4.36 of the repulsive force for spheres can now be carried out in the same way as mentioned before for the repulsive energy. Results will be given in Fig. 4.6. In the expressions for spheres, the distance H is the shortest distance between the surfaces of the interacting spheres (Fig. 4.5).

The equations for the energy and the force (Eqs. 4.34 and 4.36, respectively), indicate that the repulsion is proportional to the particle radius. Thus, at given distance double layers surrounding large particles create more resistance to approach than those around small particles. This conclusion is also reflected in the approximated equations to be derived in the next section.

4.2.3.2 Approximated energy and pressure from ψ_0

An interesting relation is found when Eqs. 4.36 and 4.22 are combined

$$F_R^{(sphere)} = \pi\ a\ V_R^{(flat)} \qquad [4.37]$$

This relation is a result of the 'Deryagin approximation'. It shows that the force between two spheres with equal radius a and at a distance H may immediately be derived from the energy equation for flat plates also at a distance H. This equation is very useful for a derivation of the approximated equations for spheres or other geometries from those of the flat plates, given in sects. 4.2.2.3 and 4.2.2.4.

Regarding the force, as for the flat plate geometry, we start with the approximated equation for weak overlap of double layers (i.e. for low $\psi_{H/2}$). On substitution of Eq. 4.29 in Eq. 4.37, we obtain

$$F_R^{(sphere)} \approx \pi a\ 64\ n_i k_B T\ \gamma^2\ \frac{1}{\kappa} \exp(-\kappa H) \qquad [4.38]$$

For the situation that $\psi_{H/2}$ and ψ_0 are both small after substitution of Eq. 4.31 gives

$$F_R^{(sphere)} \approx \pi a\ 2\ \varepsilon_0 \varepsilon\ \psi_0^2\ \kappa \frac{\exp(-\kappa H)}{(1 + \exp(-\kappa H))} \qquad [4.39]$$

$$\approx \pi a\ 2\ \varepsilon_0 \varepsilon\ \psi_0^2\ \kappa \exp(-\kappa H)$$

Of course, Eq. 4.39 is less correct for systems with high surface potentials than Eq. 4.38. For systems with low surface potentials, however, these equations are frequently applied (see for example Israelachvili, 1985) [4.4].

Finally we will give the approximation of the energy of interaction for two spheres. This equation can also be derived from the equations for flat plates. From Eqs. 4.18 and 4.33 it is follows that

$$V_R^{(sphere)} = \pi a \int_H^\infty V_R^{(flat)}\, dH \qquad [4.40]$$

Once again, this equation explicitly shows that the total interaction of two spheres is interpreted as the sum of all contributions of an infinite number of infinitely thin interacting rings that constitute the total sphere. Equation 4.40 is used to derive approximated equations for the repulsive energy for spheres ($V_R^{(sphere)}$) from those for the repulsive energy for flat plates ($V_R^{(flat)}$).

The approximation for 'weak overlap', i.e. for $\psi_{H/2}$ small is first discussed. Substitution of Eq. 4.29, i.e. the weak overlap energy equation for flat plates, in Eq. 4.40 and integration between the limits H and ∞ gives

$$V_R^{(sphere)} \approx \pi a\, 64 n_i k_B T\, \gamma^2\, \frac{1}{\kappa^2} \exp(-\kappa H) \qquad [4.41]$$

From a comparison of the approximate equations for the force (Eqs. 4.38) and for the energy (Eq. 4.41) of spheres, it follows that these equations are related. Their relation (Eq. 4.22) is analogous to that between the force and energy for the flat plates (Eq. 4.30).

$$V_R^{(sphere)} = \frac{1}{\kappa} F_R^{(sphere)} \qquad [4.42]$$

Hence, for spherical particles, in the situation of weak overlap, multiplication of the (approximated) force by $1/\kappa$ leads to the energy of interaction.Combination of Eqs. 4.30, 4.37 and 4.42 leads to two other equations, particularly useful for the conversion of the energies and forces for spheres to that of flat plates, viz.

$$P_R^{(flat)} = \frac{\kappa^2}{\pi a} V_R^{(sphere)} \qquad [4.43]$$

which allows the conversion of the repulsive energy between two spherical particles to a pressure, and

$$P_R^{(flat)} = \frac{\kappa}{\pi a} F_R^{(sphere)} \qquad [4.44]$$

which gives the relation of the force between two spherical particles and the pressure.

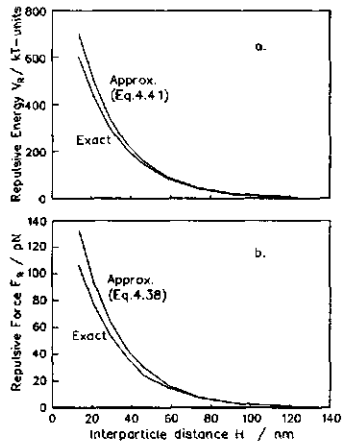

Fig. 4.6: Repulsive energy (a) and force (b) between a pair of spheres as a function of distance. Comparison of results of exact and approximate equations, using the reference parameters given in Fig. 4.2.

If, in addition to $\psi_{H/2}$, also ψ_0 is small, from substitution of Eq. 4.31 in Eq. 4.40 and integration between H and ∞ (Verwey and Overbeek, 1948) [4.1] it follows

$$V_R^{(sphere)} \approx \pi a\, 2 \varepsilon_0 \varepsilon\, \psi_0^2 \ln(1 + \exp(-\kappa H)) \qquad [4.45]$$

or

$$V_R^{(sphere)} \approx \pi a\, 2 \varepsilon_0 \varepsilon\, \psi_0^2 \exp(-\kappa H) \qquad [4.46]$$

which are both well-known equations (Israelachvili, 1985) [4.4].

Exact and approximated equations for the energy and force for interacting spheres, using the usual reference parameters of a low-polar medium (Fig. 4.2), have been given in Fig. 4.6. Since for the example reference parameters a value of ψ_0 of ca. 65 mV was chosen, in these calculations the (approximated) equations for a high surface potential (and a weak overlap) were used. For the force and for the Gibbs energy this was Eq. 4.38 and Eq. 4.41, respectively. As can be seen from Fig. 4.6 the approximated results are ca. 20 % too high when the distances are 10 nm or smaller. However, the agreement is much better at larger distances. Obviously, the approximated equations for weak overlap apply very well for our non-aqueous systems. They will be applied further in this work.

4.3 ELECTROLYTES IN NON-AQUEOUS MEDIA.

4.3.1 Dissociation and electrostatic stabilization

It can be read directly from Figs. 4.4 and 4.6, that for our system significant electrostatic repulsion can develop, when the 'reference' parameters are used. The choice for $\varepsilon = 6$ as example parameter is because it is representative for the nonionic surfactants (see Table 2.1). The choice of $c_i = 0.015$ mM is based on the Fuoss equation and can be considered as the typical ionic strength in a medium with $\varepsilon = 6$ obtained with an electrolyte with a molar radius of 0.5 nm and at a concentration c_0 of 10 mM (see sect. 2.5.3). Anticipating our results in nonionic surfactants the choice of an electric surface potential ψ_0 of 65 mV is also realistic (sect. 6.3). Surface potentials of this magnitude in non-aqueous media are rather normal. Various researchers reported potentials of this magnitude for non-aqueous media (Koelmans and Overbeek, 1954 [4.8]; Albers and Overbeek, 1959 [4.12]; McGown, Parfitt and Willis, 1965 [4.13]; Kitahara, 1967 [4.14], 1973 [4.15] and 1977 [4.16]; Novotny, 1981 [4.17]; van Mil et al., 1984, [4.11]; Pugh, Matsunaga and Fowkes, 1983 [4.18]; Green and Parfitt, 1985-1988, [4.19] and Labib and Williams, 1984/1986 [4.20], 1988 [4.21]). [It has to be noted that in all these papers electrokinetic (ζ-)potentials are given and no electric surface potentials ψ_0. However, in media of low ε the differences between ψ_0 and ζ-potentials are small (Lyklema, 1968, [4.7]; Kitahara, 1984 [4.10]). This is not the case in aqueous systems, i.e systems of high ε, in which there can be large differences between the electrokinetic potential and the electric surface potential.]

On using these reference conditions, we found that spherical particles with a size of 5 μm have repulsive energies of the order of a few hundreds of kT-units. They develop repulsive forces of a few tens of Pn at interparticle distances of about the Debye length. Between flat surface parts repulsive pressures develop which become easily as high as a few hundreds Pa. Particularly the forces and pressures, reflecting the slopes of the energy curves, are so large that it is to be expected that electrostatic effects do play a role in the stabilization of our non-aqueous suspensions, certainly when the ionic strengths could be further increased on using higher concentrations of dissociating electrolyte. These results, however, seem in conflict

with the scepticism on the contribution of electrostatic forces to suspension stabilization in non-aqueous media (see also sect. 2.5.3).

4.3.1.1 Sceptic and supportive opinions

Up to now attention paid to the possibility of electrostatic stabilization in non-aqueous media has been rather limited, particularly in comparison with the overwhelming number of studies on steric stabilization of colloidal systems in non-aqueous media and the large variety of taylor-made polymers available for that purpose. The reason for this limited attention is not obvious. It could be the conclusions of a theoretical study in which it was derived for dispersed TiO_2 particles in non-polar media that "double layer effects alone will not stabilize a highly concentrated dispersion in a hydrocarbon medium" (Féat and Levine, 1975) [4.22]. It could also be due to "the wealth of practical experience that points to the conclusion that electrostatic stabilization is less effective in non-aqueous dispersion media than it is in aqueous media", or that "steric stabilization is usually the preferred method of stabilization in non-aqueous dispersion media" (Osmond and Waite, 1975 [4.23]; Napper, 1983 [4.24]).

However, this scepticism is not met everywhere. There are also a number of 'believers' in the role of electrostatics in non-aqueous media. Already in the fifties the relevance of electrostatic stabilization effects in hydrocarbon media, particularly for large particles, was mentioned (Koelmans and Overbeek, 1954) [4.8]. In the course of time, a number of review papers appeared. In these papers, in spite of the scepticism, the option of electrostatics for dispersion stabilization was kept open (Lyklema (1968) [4.7], Parfitt and Peacock, 1978 [4.9], Kitahara, 1984 [4.10]). Fowkes et al. even fulminated against the "wide-spread scepticism concerning the importance of electrostatics in organic media" and warned against its negligence (Fowkes et al., 1982 [4.25]). He went even further by saying that readers should be "wary of any claims of steric stabilization unless the electrostatic contribution has been measured" (Fowkes and Pugh, 1984) [4.26].

We think that the general scepticism on electrostatic effects may have to do with the fact that little is known of the nature of the charging mechanism and of the charge-carrying species dissolved in organic liquids. Other reasons could be the difficulties in measuring the important electrostatic parameters: ionic strengths, dielectric constants and electric surface potentials. The fact that the number of electrolytes suited for non-aqueous systems has been rather limited could also have inhibited progress in the area.

4.3.1.2 Electrostatic stabilization in non-polar media

As in aqueous media, in non-aqueous media the ionic strengths can been derived from a measurement of conductivity. The procedure is described by various authors (Klinkenberg and van der Minne (1958) [4.27], Kitahara et al. (1967) [4.14], (1973/1974) [4.15] and van Mil et al. (1982) [4.28]) and will be discussed more extensively in Chapter 5. Kitahara reported that in 'non-polar'

hydrocarbon media with $\varepsilon = 2.3$ (cyclohexane, hexane and benzene) and at a concentration of approximately 10 mM of Na Aerosol OT (Na AOT), conductivities as low as 1×10^{-9} S m^{-1} were found. Ionic strengths of the order of 1×10^{-10} M were evaluated from these conductivities. [Note that these ionic strengths are close to the 5×10^{-11} M predicted by the Fuoss equation (sect. 2.5.3, Eq. 2.5). This supports the value of this equation.]

Kitahara's results show that the electrolyte Na AOT is extremely poorly dissociated. Hence, the double layers are extended and the Debye lengths $1/\kappa$ have values of hundreds of microns. Kitahara mentioned values of $1/\kappa$ even ranging between 1×10^3 and 0.95×10^5 nm [corrected by van Mil to between 6×10^2 and 1.28×10^4 nm (van Mil et al., 1982 [4.28])]. Values of a similar order of magnitude were reported by Koelmans and Overbeek (1954) [4.8]. From Eq. 4.14 it can be derived that for systems with such extremely low ionic strengths the repulsive pressures will be very small. Only when the surface potential ψ_0 is extremely high, at the closest approach, can the result of $\cosh(\psi_{H/2}\text{-}1)$ become sufficiently large to compensate for the low value of the ionic strengths. However, such high surface potentials are rarely encountered and have only been reported by Fowkes and Pugh (1984 [4.26]). [Note that, even at the highest overlap, since $\psi_{H/2} \leq \psi_0$, in Eq. 4.14 the value of $\cosh(\psi_{H/2}\text{-}1)$ normally cannot compensate for the very low value of the ionic strength.] Thus, at 'normal' surface potentials only with high ionic strengths a contribution to colloidal stabilization is feasible. Hence, it will not be easy to obtain a significant electrostatic contribution to stabilization in fully non-polar media.

Electrostatic effects in situations with extremely low ionic strengths were theoretically described in the frequently cited paper of Féat and Levine (1975) [4.22]. These authors considered a system consisting of a non-polar solvent ($\varepsilon = 2$ to 3), with TiO_2 particles as the dispersed solid and Na AOT as the electrolyte. They supposed that only adsorbed Na AOT molecules dissociated and that no other electrolyte contributed to the ionic strength in the bulk. In such systems the ionic strength is simply related to the particle number concentration or the surface area delivering the counterions. [Note that in such (extreme) conditions the size of the double layer is obtained from an equation which differs from Eq. 4.3 in the sense that the factor two under the root is replaced by one.] Féat and Levine assumed the negative ion concentration to be of the order of 1×10^{-7} M and evaluated very small repulsions indeed. Completely in line with Eq. 4.14 they concluded that double layer repulsion only will not stabilize (highly concentrated) suspensions in a hydrocarbon medium.

However, in a number of other media with a dielectric constant between 2 and 5, indications for electrostatic stabilization were reported. It was suggested that in xylene not the small colloidal particles but only the larger coagulates of the primary particles were stabilized (McGown, Parfitt and Willis, 1965 [4.13], Green and Parfitt, 1985/1988 [4.19]). These authors pointed out that the chances to a larger role of electrostatic stabilization in non-aqueous media increase when the colloidal particles coagulate to larger entities. This effect of particle size was already earlier observed by Koelmans and Overbeek (1954 [4.8]) and is also

reported more recently by van Mil, et al. (1984 [4.11]), who found indications for stabilization with coarse micron-size particles in xylene and in hexane/liquid paraffin mixtures, respectively.

In our suspensions we are dealing with large particles. But based on the considerations given above, for larger and practically more useful electrostatic stabilization the dissociations of electrolyte have to be higher than in media with a dielectric constant between 2 and 5. In the next sections the role of the medium and the dissociations will be elaborated further. This with particular attention to the differences in behaviour between fully non-polar, non-aqueous media on the one hand side and non-aqueous media with a slightly higher dielectric constant on the other.

4.3.1.3 The distinction between 'non-polar' and 'low-polar' solvents

It can be derived from Fuoss's equation (Eq. 2.5) that, for media with low ε, small differences in dielectric constants have large effects on electrolyte dissociation. Using Fuoss's equation for the calculation of the dissociation constant K_D and applying further the equation of the Debye-Hückel activity coefficient $\gamma_\pm$ for a monovalent dissociating electrolyte, viz.

$$-\log \gamma_\pm = \frac{1.812 \times 10^6 (\varepsilon T)^{-\frac{3}{2}} c_i^{\frac{1}{2}}}{1 + 5.0288 \times 10^{11} r (\varepsilon T)^{-\frac{1}{2}} c_i^{\frac{1}{2}}} \qquad [4.47]$$

where ε is the dielectric constant, T the temperature (K) and r the radius of the dissociating ion pair (m). At known concentrations of dissociating electrolyte c_0, the ionic strength c_i can be evaluated from

$$c_i = \frac{\sqrt{K_D^2 + 4 \gamma_\pm^2 K_D c_0} - K_D}{2 \gamma_\pm^2} \qquad [4.48]$$

Using these equations the Debye lengths $1/\kappa$ have been calculated (from Eq. 4.3) at different values of ε. The results are plotted in Fig. 4.7. The calculations have been carried out for $r = 0.5$ nm, i.e. an estimated value for NaDoBS, and using two rather arbitrary electrolyte concentrations c_0 of 10 and 30 mM, i.e. 0.3 and 1 % NaDoBS, respectively.

The results shown in Fig. 4.7 demonstrate that, when ε is 2, the Debye length has an extreme magnitude of approximately 1×10^5 nm. This corresponds well with the observations of Kitahara (1967, [4.14]). However, on increasing the dielectric constant from 2 to 5, $1/\kappa$ drops by three orders of magnitude, whereas the results for the two electrolyte concentrations are not very different. At a dielectric constant ≥ 5, Debye lengths are < 40 nm and approach the range that is normally found in aqueous systems. Thus, in media with $\varepsilon \geq 5$ significant dissociations and

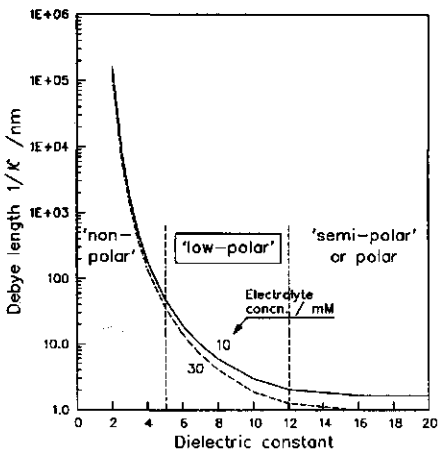

Fig. 4.7: Debye length $1/\kappa$ as a function of dielectric constant ε of a monovalent electrolyte (10 and 30 mM). $r = 0.5$ nm.

electrostatic contributions to suspension stabilization can be expected. In media with $\varepsilon > 12$, as in aqueous media, the dissociation of electrolytes is almost complete. In these media the Debye lengths are controlled by the electrolyte amounts dissolved.

Based on the patterns observed for the Debye lengths we propose to call the group with $5 < \varepsilon \leq 12$ 'low-polar'. In these liquids more electrolyte dissociation occurs than in 'non-polar' media. Furthermore in these media the dissociation is controlled largely by the dielectric constant ε of the solvent. We distinguish them from the non-polar solvents with $\varepsilon \leq 5$ and from the semi-polar or polar solvent with $\varepsilon > 12$. Following this proposal nonionics are classified as low-polar solvents (see Table 4.1); liquid hydrocarbons based solely on hydrocarbon (cyclohexane, benzene, etc.) and organic ethers belong to the group of the non-polar solvents, whereas the liquid alcohols are semi-polar or polar.

The acknowledgment that in concentrated suspensions in non-polar media the Debye lengths can extend over many particle diameters has promoted the development of theories which take into account multiparticle interactions (Albers and Overbeek, 1959 [4.12]; Féat and Levine, 1975 [4.22]). However, since in our low-polar nonionic media the Debye lengths are much shorter (Fig. 4.7), these theories are less relevant for our systems.

4.3.2 Dissociation enhancing effects

4.3.2.1 Electrolyte structure

Up to now we have said little about the specific nature of the dissociating species. From an inventory by Parfitt and Peacock made in 1978 [4.9] it appeared that in a almost half of the studies carried out in non-aqueous media the electrolyte used is Na AOT. Since then the situation has not much changed. Na AOT or Na Aerosol OT, i.e. sodium di-2-ethylhexyl sulphosuccinate, is an anionic surfactant salt. On dissociation it produces a sulphonate anion and a sodium cation.

Of the remaining part of the electrolytes used in non-aqueous media the majority are other anionic salts. They vary from simple, well-defined ingredients such as sodium stearate, oleate or other salts (calcium-, magnesium-, barium- or aluminium-) of di-2-ethylhexyl sulphosuccinate, to molecules such as aluminium diisopropylsalicylate (Al Dips), tetra(isoamyl)ammonium picrate (Tiap) and calcium

stearylcyclohexyl-benzene sulphonates. More complex macromolecules such as 'Span 80' (sorbitan monopalmitate), 'alkyd resin', 'melamine resin' or polyisobutene succinimide (OLOA 1200) have also been mentioned, but for these there may be an additional steric contribution to the stabilization. Usually only less than a few percent of these ingredients is already sufficient to obtain a large effect on the conductivity and other physical properties of the suspension.

From the literature it can be concluded that, in addition to the dielectric constant, the nature of the electrolyte plays a significant role in determining the dissociation in non-aqueous media. Two, not entirely independent influences can be distinguished, viz.: a. that of the size of the dissociating ion pair and b. that of the contribution from solvating the resulting positive and negative ions.

The effect of the size of the dissociating species follows directly from elementary electrostatic considerations and is easily demonstrated by the Fuoss equation (Eq. 2.5). From this equation it follows that greater dissociation can be expected from ion-pair species with larger ionic radii. Hence, in non-aqueous media, higher ionic strengths are expected from larger than from smaller (anionic and cationic) electrolyte molecules. The contribution of solvation of ions to the dissociation can be quantified with the aid of microcalorimetry; some qualitative remarks are made in the next section.

Table 4.1: Dielectric constants of non-ionics compared to those of some non-aqueous solvents.

Solvent	ε (25°C)
Non-polar	
n-Hexane	1.89
n-Dodecane	2.02
Benzene	2.27
p-Xylene	2.3
1,4 Dioxane	2.2
Diethyl ether	4.3
Dimethyl ether	5.0
Low-polar	
$C_{14}E_6P_3$ (Plurafac)	5.7*
$C_{11}E_6$ (Imbentin)	6.2*
C_4E_2	10.1*
C_2E_3 (Trioxitol)	11.0*
(Semi-)polar	
1-Hexanol	13.3
1-Butanol	17.8
1-Ethanol	24.3

* Experimental results of this work (see also Table 2.1). The other values are from the CRC Handbook (1986/1987).

4.3.2.2 Ion solvation; 'Crown complexation'

When ions in a condensed phase complexes with the solvent molecules we can speak of solvation. For example, for sodium chloride dissolved in methanol, methanol inhibits the re-association of sodium cations with chlorine anions by solvation of the sodium ions. This solvating effect of methanol for sodium cations is predominantly induced by ion-dipole, ion-quadrupole, and ion-induced dipole type interaction. The solvent molecules can be considered to form complexes with the inorganic cations; a phenomenon which reduces their mobility and which stabilizes them (Popovych and Tomkins, 1981 [4.29]).

It has been known since 1949 that polyether chains of nonionics and inorganic cations can form complexes (Doscher, 1949 [4.30]). Various analytical-chemical methods for the determination of polyoxyethylene compounds are based on the formation of such complexes. Increase of the EO length of these molecules increases the cation complexing power, but also influences the complex forming selectivity for the various ions. For dimethyl ethers of polyethyleneglycol ('glymes'), optimal EO chain lengths for complex formation have been defined: for the small lithium cation the 1 : 1 complex constant is the highest when the EO number is 4, for sodium ions this is so when the EO number is 5-6 and for potassium ions when the number is 6-7. In this respect analogies have often been drawn with the 'crown complexes' formed between macrocyclic polyethers and group I and IIa metal ions (Cross, 1987 [4.31]).

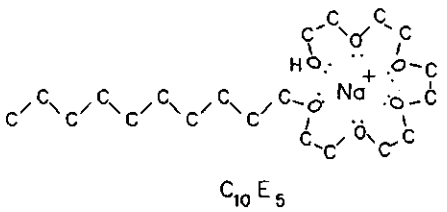

Fig. 4.8: Factors that potentially can enhance electrolyte dissociation in nonionics: Solvation by 'crown complexation' of a sodium cation by a $C_{10}E_5$ nonionic.

Analogous observations have been reported for nonionics and polyethylene glycol. In addition to the ether groups the terminal -OH group has been mentioned as being a particularly strong contributor to complex formation. Following the observation in 'glymes' it is expected that for sodium cations strong complexing would be found in nonionics with EO chains consisting of 4-5 ether groups. A graphical image of a 'crown-complex' formed from a cation with a nonionic molecule is given in Fig. 4.8. It has to be noted here that solvation by complex formation comes on top of the dissociation given by the Fuoss equation and was not taken into account in the estimation of the ionic concentration used so far. A contribution of solvation to the dissociation would thus lead to higher ionic strengths and smaller Debye lengths than those calculated.

4.3.2.3 'Triple ions' and inverse micelles

Other factors may further stimulate dissociation in low-polar nonionic media. In hydrocarbons formation of triple ions from dissociating Na AOT has been convincingly demonstrated to contribute to ion dissociation (van Mil, et al. 1982 [4.28]). The suggested reaction path is depicted in Fig. 4.9a. They found that, particularly in the low electrolyte concentration range, increasing the electrolyte concentration from 1×10^{-4} to 1 mM, the dissociation increased significantly due to the ion stabilizing contribution of the triple ions.

Green and Parfitt (1985) [4.19] applied the theory of Féat and Levine to dispersions of TiO_2 and carbon black particles in p-xylene. These dispersions were stabilized with Na AOT in the concentration range 1 to 100 mM. When it is supposed, in accordance with the theory of Féat and Levine, that only the dissociation of adsorbed Na AOT molecules contributes to the ionic strength, the applica-

tion of this theory is correct. It is more likely, however, that Na AOT in the bulk has also contributed to the total ionic strength in their systems. This would have lead to higher ionic strengths, to shorter Debye lengths and to higher repulsive pressures than now supposed by them. Absence of conductivity data in the work of Green and Parfitt makes it impossible, however, to verify this point.

A further contribution to dissociation of anionics stems from the formation of ion clusters or inverse micelles at higher anionic concentrations. Inverse micelles are associates formed of ionic molecules, with an agglomeration number varying between 20 and 1000.

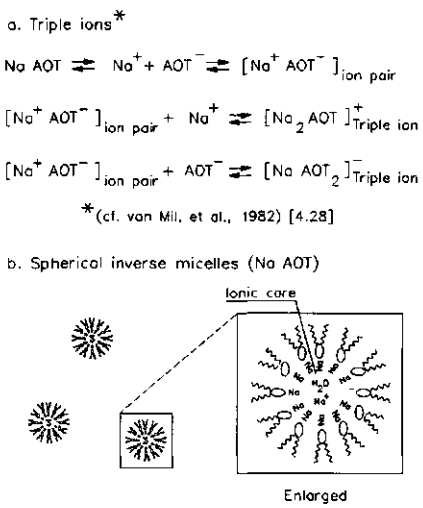

Fig. 4.9: Factors that may enhance electrolyte dissociation in non-aqueous media: Formation of a.'Triple-ions', b. Spherical inverse micelles. Example electrolyte: Na Aerosol OT.

When they associate to spheres the ionic groups are directed to the centre and the hydrophobic tails are directed outward. A schematic presentation of spherical inverse Na AOT micelles is given in Fig. 4.9b. Ionic components, i.e. traces of water or cations, accumulate preferentially in the ionic core. It has been suggested long ago that, in liquid non-polar hydrocarbons, inverse micelles can contribute to ion-stabilization and enhance electrolyte dissociation (Klinkenberg and van der Minne, 1958 [4.27]); Fowkes, 1967 [4.32]). The existence of inverse micelles in such media have been demonstrated (Shinoda, 1963 [4.33]; Konno et al., 1987 [4.34]).

4.4 ELECTROSTATIC STABILIZATION IN NON-AQUEOUS SUSPENSIONS

4.4.1 DLVO energy curves

4.4.1.1 Repulsive barriers and secondary minima

In sect. 2.3.3 an example of an 'energy-DLVO' curve, obtained after addition of the attractive energy (V_A) and the repulsive energy (V_R) curves leading to (V_T), has already been given. Another example is given in Fig. 4.10, where the distance axis is logarithmic. The curve is constructed on using Eqs. 3.6, 3.9 and 4.41, for: $\varepsilon = 6$, $\psi_0 = 65$ mV and $a = 5$ μm, whereas $c_i = 1$ mM. This is in the range of ionic strengths between 0.02 and 2 mM experimentally found. For the suspended detergent solid particles in nonionic the Hamaker constant $A_{11(3)}$ is chosen at 0.3×10^{-20} J (see sect. 6.4.3.1). The curves have been drawn for distances ≥ 2 nm.

It can be seen from Fig. 4.10 that with the chosen combination of parameters, for H between 2 and 15 nm, the repulsion energy exceeds the attraction energy, causing the formation of a repulsive barrier. V_T rises sharply with decreasing distance between the particle surfaces, eventually leading to a repulsion that can become as high as 500 kT at 2 nm. Minimum values in the secondary minimum area, which is depicted enlarged in the inset in Fig. 4.10, are of an order of only 3 kT. The minima are found at distances of ca. 20 nm. Due to the influence of retardation (sect. 3.2.3) the secondary minimum energy is only small.

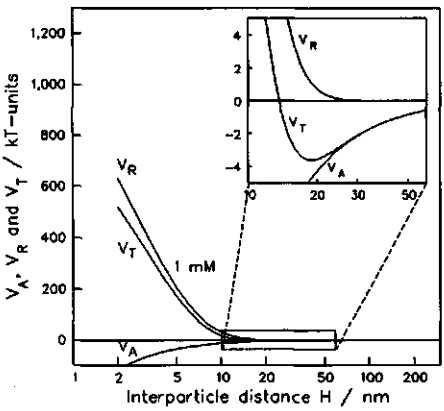

Fig. 4.10: Example of a DLVO-energy curve in a 'low-polar' medium giving the total energy of interaction (V_T) as a function of H. For parameters see text.

4.4.1.2 Influence of five governing variables

The DLVO curves are determined by the following five parameters: the **dielectric constant** ε, the **ionic strength** c_i, the **surface potential** ψ_0, the **Hamaker constant** $A_{11(3)}$ and **the particle radius** a. In this sequence the effects of these variables will now be demonstrated.

The influence of the nature of the solvent is evaluated, by varying the **dielectric constant** ε from 6 to 10. Results are graphically represented in Fig. 4.11. The other parameters used were kept constant at: $c_i = 0.5$ mM, $\psi_0 = 65$ mV, $A_{11(3)} = 0.3 \times 10^{-20}$ J and $a = 5$ μm. The decrease of the repulsive barrier with decreasing ε, which follows also directly from Eq. 4.41, is significant. The depth of the secondary minimum increases when ε becomes smaller. Hence, with lower ε, stronger secondary minimum coagulation is expected.

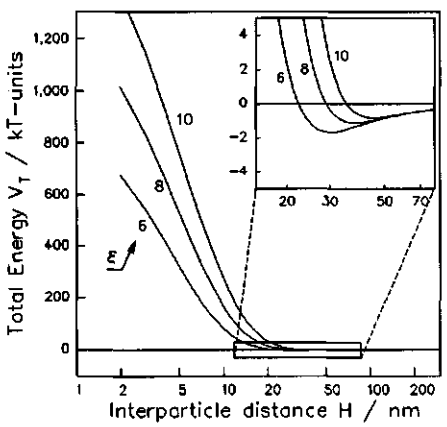

Fig. 4.11: DLVO-energy curve for particles in a low-polar medium; the effect of **dielectric constant** ε. For parameters see text.

The influence of the **ionic strength** c_i, in the range from 0.1 to 1 mM, is shown in Fig. 4.12. The constant parameters were: $\varepsilon = 6$, $\psi_0 = 65$ mV,

$A_{11(3)} = 0.3 \times 10^{-20}$ J and $a = 5$ μm. The graph demonstrates that the repulsive energy decreases with increasing ionic strength, whereas the secondary minimum becomes deeper and moves toward shorter distance. These results clearly demonstrate that, provided there is a surface charge, there is no problem at all in creating large repulsive energy barriers in such non-aqueous media. The problem is rather that of also creating steep slopes in the energy curve, that is, to create large repulsive forces. From the considerations given before it is clear that larger repulsive forces can be obtained only at high ionic strengths, i.e. at sufficient electrolyte dissociations (see sects. 4.3.1.2 and 4.4.2).

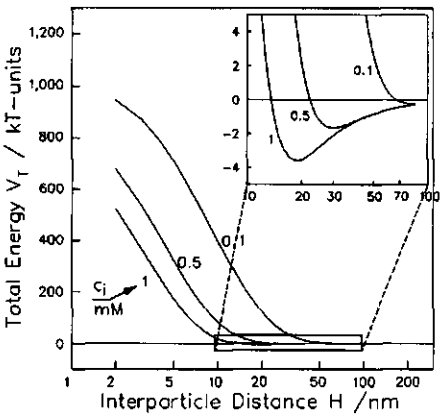

Fig. 4.12: DLVO-energy curve for particles in a low-polar medium; the effect of **ionic strength** c_i. For parameters see text.

The third effect considered is that of a varying **surface potential** ψ_0. Curves have been given in Fig. 4.13 for surface potentials of 65, 50, 35 and 20 mV. The calculations have been carried out for $\varepsilon = 6$, for an ionic strength $c_i = 0.1$ mM, for $A_{11(3)} = 0.3 \times 10^{-20}$ J and for $a = 5$ μm. From Fig. 4.13 it can be seen that with a surface potential of 20 mV significant repulsive barriers of a few dozen kT are found. It has been mentioned that, to stabilize colloidal systems, a repulsive energy barrier of $\geq$ 15 kT is necessary (Koelmans and Overbeek, 1954 [4.7]). When this value is applicable to our suspended micron-size particles, surface potentials of around 20 mV will already be enough to ensure colloidal stability. Figure 4.13 shows that the effect of lowering of the surface potential on the secondary minimum is small.

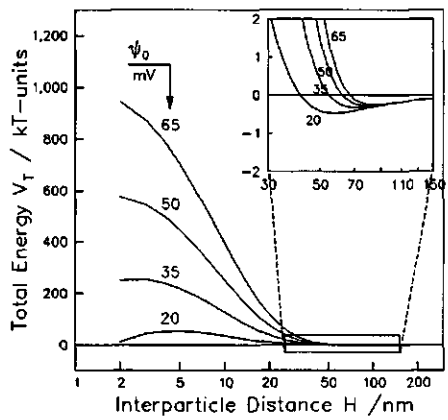

Fig. 4.13: DLVO-energy curve for particles in a low-polar medium; the effect of **surface potential** ψ_0. For parameters see text.

The effect of the **Hamaker constant** $A_{11(3)}$ is illustrated in Fig. 4.14. The constant parameters used in the calculation were: $\varepsilon = 6$, $c_i = 0.1$ mM, $\psi_0 = 65$ mV and $a = 5$ μm. From the graph it can be seen that the effect of the Hamaker constant on the repulsion is small. At the smallest distances, not shown, the effects are larger (see Fig. 3.3). The depth of the secondary minimum, however, varies proportionally with the Hamaker constant.

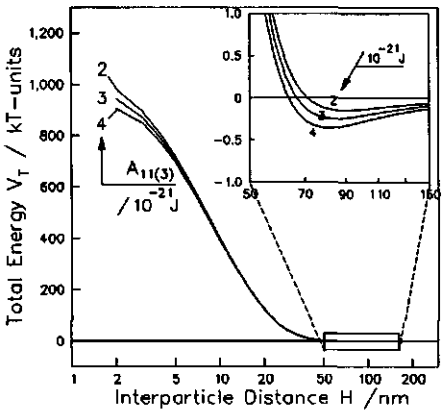

Fig. 4.14: DLVO-energy curve for particles in a low-polar medium; the effect of the **Hamaker constant** $A_{11(3)}$. For parameters see text.

The effect of the last parameter that was varied, the **particle size** a, is shown in Fig. 4.15. Calculations have been carried out at constant values of $\varepsilon = 6$, $c_i = 0.1$ mM, $\psi_0 = 65$ mV and $A_{11(3)} = 0.3 \times 10^{-20}$ J. From Fig 4.15 it can be seen that V_T increases proportionally with the size of the particles. This conclusion is the basis for the remark that, when suspended in hydrocarbon, only for larger than colloidally-sized particles repulsive forces are sufficiently large to give electrostatic stabilization (see sect. 4.3.1.2). The picture supports the remark made earlier that with micron-size particles the changes between repulsion and attraction vary more strongly with distance than with colloidal particles.

4.4.2 DLVO-force curves

An example of a DLVO-force curve, at various **ionic strengths** c_i is given in Fig. 4.16. For the calculation of these curves we used Eqs. 3.15, 3.17 and 4.38. The effect of retardation has been taken into account. The same parameters have been varied as in the calculation of the energy curve of Fig. 4.12. Since the force curve is the first derivative of the energy curve, the secondary minimum in the energy curve is positioned at the distance where the force curve intercepts the x-axis. The maximum in the force curve is at the abscissa of the inflection point of the energy curve.

The growth of the height of the force barrier with increasing ionic strength is clearly seen. Hence, stimulation of the dissociation in non- or low-polar media leads (within limits) to an increase of the repulsive barrier. At even higher ionic strengths, however, there is a risk that the distance of the repulsion becomes so small that coagulation occurs. Since the attraction between the inorganic solids in nonionic is

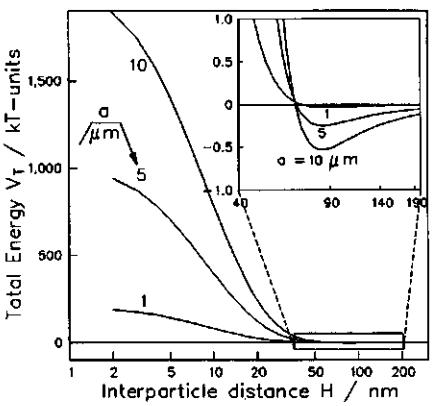

Fig. 4.15: DLVO-force curve for particles in a low-polar medium; the effect of the **particle size** on the energy of interaction (V_T). For parameters see text.

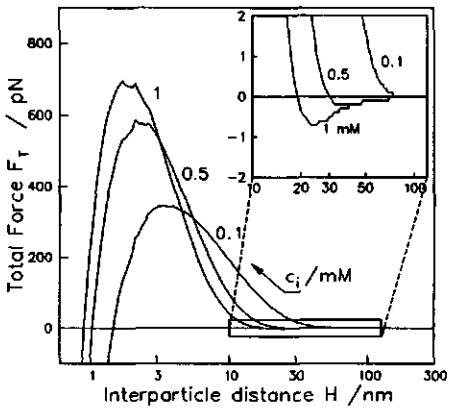

Fig. 4.16: DLVO-force curve for particles in a low-polar medium;the effect of **ion concentration** on the force of interaction. For parameters see text.

weak (sect. 3.3.3), this last mentioned effect will be found only at relatively high ionic strengths. At increasing ionic strength the secondary minimum, being responsible for the reversible coagulation and occurring at the interparticle distances in the horizontal plane of a sediment, becomes deeper.

The force curves generally demonstrate that large net repulsive forces are operational in media with low dielectric constant. They may readily attain values of a few hundreds of pN already at ionic strengths $c_i \geq 0.1$ mM. The corresponding repulsive pressures, that can be calculated on using Eq. 4.44, are of an order of 1000 to 1500 Pa. These values are larger than the pressures we find at the bottom of suspension sediments of inorganic solids in nonionics up to 1 m high.

4.5 SUMMARY

The electrostatic theory for interactions models of plates and spherical particles in suspension, is evaluated for its applicability to particles of crystalline detergent solids in non-aqueous media. For both models it is concluded that for the calculation of the repulsive energies and forces, approximate equations for 'weak overlap' can be used. The approximate equations result in repulsive energies, pressures and forces, which are in good agreement with the results of exact computations. However, at distances $\leq$ 10 nm, i.e. at strong double-layer overlap, the approximated equations give values that are 20 % or more too high.

'Low polar' media, including the nonionics, are defined as those having a dielectric constant between 5 and 12. From Fuoss's theory it can be derived that, at these dielectric constants, the dissociation of electrolytes is low, but higher than in the 'non-polar' hydrocarbons more commonly applied. At concentrations of 0.3 to 1 % w/w Debye lengths are estimated to be $\leq$ 40 nm, i.e. in the same range as in aqueous media. The electrolyte dissociation in nonionics may be further enhanced by ion solvation or inverse micelle formation.

Energy- and force-curves have been constructed for conditions relevant for nonionic media and have been depicted. They demonstrate the dependence of the repulsion on five governing parameters, viz. the dielectric constant, the ionic strength, the electric surface potential, the Hamaker constant and the particle size.

For our suspensions at ionic strengths between 0.02 and 2 mM significant repulsion develops already with surface potentials $\geq$ 20 mV and at distances between 2 and 40 nm. The repulsion is higher than the van der Waals attraction and causes much larger repulsive barriers than those usually reported for non-polar, non-aqueous media with a dielectric constant smaller than 5. The repulsive barrier increases with increasing surface potential, ionic strength and particle radius. The repulsion is expected to influence the resistance against coagulation under pressure in suspension sediments and to cause colloidal stabilization of nonionic suspensions.

The role of the secondary minimum is that in a suspension sediment it influences coagulation in the horizontal plane. Because of the long range of the repulsion, retardation causes the energies in the secondary minima to be only a few kT. Secondary minimum coagulation can only be expected at relatively high ionic strengths.

4.6 BIBLIOGRAPHY

4.1 **Theory of the stability of lyophobic colloids. The interaction of sol particles having an electric double layer.** Verwey, E.J.W.; Overbeek, J.Th.G.. (Elsevier, Amsterdam). **1948.**

4.2 **Surfactant Science Series. Vol. 15: Electrical Phenomena at Interfaces. Fundamentals, Measurements and Applications. Ch.2: Electrical Double Layer.** Usui, S.; Hachisu, S.. Kitahara, A.; Watanabe, A.; Editors (Marcel Dekker, New York). **1984.**

4.3 **Colloidal Dispersions. Ch.3: Fundamentals of Electrical Double Layers in Colloidal Systems.** Lyklema, J.. Goodwin, J.W.. Editor. (Spec. Publ. 43, Royal Society Chem., London). **1982.**

4.4 **Intermolecular and surface forces: with applications to colloidal and biological systems.** Israelachvili, J.N. Editor. (Academic Press, London). **1985.**

4.5 **Principles of colloid and surface chemistry. 2nd ed. Revised and Expanded.** Hiemenz, P.C.; Editor (Marcel Dekker, New York). **1986.**

4.6 **Foundations of colloid science. Vol. I.** Hunter, R.J.. Editor (Clarendon Press, Oxford, UK). **1987.**

4.7 **Principles of the Stability of Lyophobic Colloidal Dispersions in Non-Aqueous Media.** Lyklema, J.. *Adv. Colloid Interface Sci.*, **1968,** 2, 65-114.

4.8 **Stability and electrophoretic deposition of suspensions in non-aqueous media.** Koelmans, H.; Overbeek, J.Th.G.. *Disc. Faraday Soc.* **1954,** 18, 52-63.

4.9 **Stability of Colloidal Dispersions in Non-aqueous Media. Vol 10: Surface and Colloid Science.** Parfitt, G.D.; Peacock, J.. Matijevic, E. Editor. (Plenum Press, London). **1978.**

4.10 **Surfactant Science Series. Vol. 15: Electrical Phenomena at Interfaces. Fundamentals, Measurements and Applications. Ch.5: Non-aqueous Systems.** Kitahara, A.. Kitahara, A.; Watanabe, A.. Editors (Marcel Dekker, New York). **1984.**

4.11 **Stability of Coarse Suspensions in Nonpolar Media: Effect of Gravity on the Interaction between Particles.** Mil, P.J.J.M. van; Crommelin, D.J.A.; Wiersema, P.H.. *J. Colloid Interface Sci.* **1984,** 98(1) 61-71.

4.12 **Stability of emulsions of water in oil. I. The correlation between electrokinetic potential and stability.** Albers, W; Overbeek, J.Th.G.. *J. Colloid Sci.* **1959,** 14, 501-509.

4.13 **Stability of non-aqueous dispersions. I The relationship between surface potential and stability in hydrocarbon media.** McGown, D.N.L; Parfitt, G.D.; Willis, E.. *J. Colloid Sci.* **1965,** 20, 650-664.

4.14 **The effect of water on electrokinetic potential and stability of suspensions in nonpolar media.** Kitahara, A.; Karasawa, S.; Yamada H.. *J. Colloid Int. Sci.* **1967,** 25, 490-495.

4.15 **Zeta potential in non-aqueous media and its effect on dispersion stability.** Kitahara, A.. *Progress Organic Coatings* **1973/1974,** 2, 81-98.

4.16 **The concentration effects of surfactants on zeta-potential in non-aqueous dispersions.** Kitahara, A.; Amano, M.; Kawasaki, S.; Kon-no, K.. *Colloid Polymer Sci.* **1977,** 255, 118-1121.

4.17 **Properties of charged non-aqueous colloids in a low conductivity regime.** Novotny, V.. *Colloids Surf.* **1981,** 2, 373-385.

4.18 **The dispersibility and stability of carbon black in media of low dielectric constant. 1. Electrostatic and steric contributions to colloidal stability.** Pugh, R.J.; Matsunaga, T. ; Fowkes, F.M.. *Colloids Surf.* **1983,** 7, 183-207.

4.19 **Stability of Concentrated Colloidal Dispersions in Apolar Media.** Green, J.H.. Thesis. (Pittsburgh, Pennsylvania) **1985;**
Charge stabilization of Concentrated Dispersions in Apolar Media. Green, J.H.; Parfitt, G.D.. in **Flocculation, sedimentation and consolidation.** Moudgil, B.M.; Somasundran, P.. Editors. (Proc. Engng. Found. Conf.,Georgia) **1985;**
Stability of Non-aqueous Dispersions. Paper 7. Electrostatic Stabilization of Concentrated Colloidal Dispersions. Green, J.H.; Parfitt, G.D..*Colloids Surf.* **1988,** 29, 391-402.

4.20 **The use of zeta-potential measurements in organic solvents to determine the donor-acceptor properties of solid surfaces.** Labib, M.E.; Williams, R.. *J. Colloid Interface Sci.* **1984,** 97(2), 356-366;
An experimental comparison between the aqueous pH scale and the electron donicity scale. ibid. *Colloid Polymer Sci.* **1986,** 264, 533-541.

4.21 **The origin of the surface charge on particles suspended in organic liquids.** Labib, M.E.. *Colloids Surf.* **1988,** 29, 293-304.

4.22 **The Double-layer Interaction of Two Charged Colloidal Spherical Particles of a Concentrated Dispersion in a Medium of Low Dielectric Constant.** Féat, G.R.; Levine, S.. *J. Colloid Interface Sci.* **1976,** 54(1), 34-44.

4.23 **Dispersion Polymerization in Organic Media. The Theoretical Basis for the Steric Stabilization of Polymer Dispersions Prepared in Organic Media.** Osmond, D.W.J.; Waite, F.A.. Barrett, K.E.J.; Editor. (John Wiley, New York). **1975.**

4.24 **Polymeric Stabilizations of Colloidal Dispersions. Basic Concepts of Colloid Stability.** Napper, D.H.; Editor. (Academic Press, London). **1983.**

4.25 **Mechanism of Electric Charging of Particles in Nonaqueous Liquids. Ch.15. Colloids and Surfaces in Reprographic Technology.** Fowkes, F.M.; Jinnai, H.; Mostafa, M.A.; Anderson, F.W.; Moore, R.J.. Hair, M.; Croucher, M.D. Editors. (ACS Symposium Series 200, New York) **1982.**

4.26 **Steric and electrostatic contributions to the colloidal properties on non-aqueous dispersions.** Fowkes, F.J.; Pugh, R.J.. Polymer adsorption and dispersion stability., Amer. Chem. Soc. Symp. Series 240, **1984.**

4.27 **Electrostatics in the petroleum industry. The prevention of explosion hazards.** Klinkenberg, A; van der Minne, J.L.. Shell Research and Development Report. (Elsevier, Amsterdam). **1958.**

4.28 **Conductivity and Debye Length in Aerosol-OT Hexane/Liquid Paraffin Solutions.** Mil, P.J.J.M. van; Crommelin, D.J.A.; Wiersema, P.H.. *Ber. Bunsenges. Phys. Chem.* **1982,** 86, 1160-1165.

4.29 **Nonaqueous solution chemistry.** Popovych, D.; Tomkins, R.T.. (John Wiley, New York) **1981.**

4.30 Doscher, T.M.. *J. Phys. Chem.* **1949,** 53, 1362.

4.31 **Metal Ion Complexes of Polyoxyalkylene Chains. Vol. 19. Surfactant science series. Chemical analysis.** Cross, J.. Editor. (Marcel Dekker, New York). **1987.**

4.32 **The Interaction of Polar Molecules, Micelles and Polymers in Nonaqueous Media.** Fowkes, F.M.. **Surfactant Science Series. Vol 2. Solvent properties of Surfactant Solutions.** Shinoda, K.. Editor. (Marcel Dekker, New York) **1967.**

4.33 **The Formation of Micelles in Nonaqueous Solution.** Shinoda, K.. **Colloidal Surfactants.** (Academic Press, New York) **1963.**

4.34 **Micelle formation and Catalysis in Nonaqueous Media.** Kon-no,K.; Kitahara, A.; ElSeoud, O.A.. **Surfactant science series. Vol. 2. Nonionic Surfactants: Physical Chemistry.** Schick, M.J.. Editor. (Marcel Dekker, New York) **1987.**

Chapter 5

EXPERIMENTAL:

MATERIALS AND METHODS

5.1 INTRODUCTION

Our study of non-aqueous suspensions can be roughly divided into two main areas. These are
1. the study of the electric and dielectric parameters of low-polar solvents, solids and mixtures of these two, and
2. the study of the macroscopic mechanical properties of the suspensions.
It is the main objective of our research programme to establish the qualitative and quantitative relations between the electric and dielectric parameters on the one hand side and the mechanical properties on the other.

The current chapter gives insight into the methods selected and applied in our non-aqueous liquids studies. Most of these methods are already available and could be used without further adaptation. In a few cases methods and apparatus had to be developed. The emphasis of the current study is on the nonionics Plurafac LFRA30 and Imbentin C91/35, on DoBS acid and on the crystalline detergent solids. However, these ingredients are chosen so that the findings may be of wider applicability.

5.2 NONIONICS AND DOBS ACID

5.2.1 Materials and methods

Our nonionics are freed from ionic admixtures by consecutive cation and anion exchanging (Biorad AG/1X2 and Biorad AG 50W/X8). After ion exchanging the water content is reduced to below 0.1 % by drying in a microwave oven. The extent of purification was monitored by elementary analysis (see sect. 5.4.1.1) and by conductivity measurements (see sect. 5.4.1.2). An estimation of the residual ionic strength in the nonionics is given in chapter 6. In the course of our work it was discovered that the conductivity and water content could also be reduced to almost equally low values with activated Al_2O_3 column chromatography (Act.I, Merck). The water content was measured by an automated Karl-Fischer titration, monitoring the titration end-point coulometrically (Metrohm, 652). Results of average molecular compositions, water content and molecular weights, as determined with proton NMR, have already been given in Table 2.1 and Fig. 2.2.

The main characteristics of the DoBS acid (or HDoBS) additive, Marlon AS3, have been discussed previously (sect. 2.2.4). It was used without purification. Its proton NMR spectrum confirmed the bulk composition of the dodecylbenzene chain, i.e. $C_{12}H_{25}C_6H_4$; its average molecular weight estimated by acid-base titration is repeatedly found to be 324.9 $\pm$ 1.5 (nominal: 326.5). From earlier analyses using the method reported by Reid, et al. (1967) [5.1], Marlon AS3 was found to contain 97.7 % DoBS acid, 0.39 % H_2SO_4 and 1.79 % other organic matter.

The specific densities of the liquids were measured by a resonance frequency 'tuning fork' method (Paar DMA 35, Mettler).

Viscosities of liquids, i.e. pure nonionics, solutions of DoBS acid in nonionic, as well as supernatants of suspensions, were measured with a Bohlin CS rheometer (see sect. 5.5.2.1). With the cone and plate geometry volumes of only 1.5 cm^3 were needed for these measurements. At the temperature of the measurement (25 °C) the liquids all show Newtonian viscosity behaviour. The viscosities of the nonionics used have already been given (Table 2.1) and are in the range of 30 to 60 mPa s. Addition of up to 10 % of HDoBS to the nonionics led to a viscosity increase of ca. 3 mPa s per added volume percent of acid.

5.2.2 Dielectric properties and conductivity

The refractive indices of the nonionic solutions were measured with an Abbe refractometer (Zeiss) at 25 °C, using a Na_D-line compensator.

Dielectric constants and electrical conductivities of low-polar liquids were measured simultaneously in a cell with electrodes of which the distances can be adjusted. The cell is similar to the one described by Lockhart et al. (1978) [5.2], but adapted in such a way that the contents can be thermostatted. In the bottom part, instead of a Teflon bus, an Araldite bus with molten-in electrodes is mounted. The plate distances in the cell can be adjusted by a micrometer, with a reading accuracy of 0.002 mm. To avoid current leakages, the walls of the cell are made of Teflon. The temperature can be stabilized with an accuracy of 0.1 °C. Prior to every measurement, the cell is cleaned by rinsing with petroleum ether. The impedance was measured in a circuit with a Hewlett Packard HP4284A precision LCR meter. At the low-frequency side in our experimental frequency range we always observed a frequency- independent portion of the real part ε' of the permittivity. The corresponding value for ε' we interpret as *the* dielectric constant ε. For the measurement of the dielectric constant the frequency range between 600 kHz and 1 MHz was used; for the conductivity that between 15 and 50 kHz. Details of the calculation method are given below.

For the evaluation of the dielectric constant ε and the specific electric conductivity K, the liquid in the cell is considered as an RC-circuit, with a condenser and a resistor in parallel. The impedance Z and the phase shift θ are measured. As the absolute distance between the measuring plates is less accurately known than the

changes thereof, a differential method is applied, using plate distances δ of 1.000 and 0.900 mm. The 'cell constant' (δ/A, where A is the plate surface area) was 0.9004 m^{-1}. It was determined using various non- and low-polar solvents as reference liquids (n-octane: ε = 1.94, 2-methylbutane 2-ol: 5.82, tetrahydrofuran: 7.60, 2-butanol: 15.80, 2-propanol: 18.30). Using this cell constant the average difference between the values of the reference liquids and experimental values were found to be smaller than ca. 2 %.

To evaluate the specific electric conductivity K (SI units: S m^{-1}) of the liquid, two successive measurements are carried out with the same sample but at slightly differing electrode distances. When this distance is δ, K is found by

$$K = \frac{\delta}{A} \frac{1}{(|Z_1| - |Z_2|)\left(\sqrt{\tan^2\theta + 1}\right)} \qquad [5.1]$$

where $|Z_1|$ and $|Z_2|$ are the absolute values of the measured impedances in positions 1 and 2, respectively, and θ the average phase angle of both measurements. The phase angle is independent of the plate distance and given by

$$\tan\theta = -\omega R C \qquad [5.2]$$

where ω is the angular frequency. The resistance R can be written as

$$R = \frac{d}{A}\frac{1}{K} \qquad [5.3]$$

and the capacitance C as

$$C = \frac{\varepsilon_0 \varepsilon A}{d} \qquad [5.4]$$

where ε_0 is the dielectric permittivity of vacuum and ε the (relative) dielectric constant. Combining Eqs. 5.2 to 5.4 one obtains

$$\tan\theta = -\frac{\omega \varepsilon_0 \varepsilon}{K} \qquad [5.5]$$

Finally, the relative dielectric constant ε is found from the capacitive part

$$\varepsilon = \frac{\delta}{\varepsilon_0 A}\frac{C_1 C_2}{C_1 - C_2} \qquad [5.6]$$

where C can be obtained from

$$C = \frac{\tan\theta}{\omega |Z| \left(\sqrt{\tan^2\theta + 1}\right)} \qquad [5.7]$$

The dielectric constants ε of the liquids in this study are in the range of 4 to ca. 18; the conductivities K are in the range 0.1 to 500 $\times 10^{-6}$ S m^{-1}. The lower values were found with pure nonionics and the higher ones in systems with the highest HDoBS concentrations.

5.3 SOLIDS

5.3.1 Particle density, size, shape and porosity

All solid materials were used without further purification. The calcite, Zeolite 4A and the oxides were used as received; the other solids were dry-milled in a colloid mill (Alpine 160Z, Augsburg) to a particle size of approximately 5 μm. Particle size measurements of the solids are carried out with the Malvern particle sizer (3660D), after dispersion in a mixture of ethylacetate and toluene. This liquid mixture was selected because it has a refractive index of 1.450, thus having sufficient difference with that of the solids dispersed. The Malvern particle sizer has the inherent restriction that particles smaller than 1 μm are not measured. The distribution of particle sizes indicates that a fractionbetween 0.01 and 0.03 of the total solids volume is present as particles $\leq$ 1 μm. This means that, although the volume fractions are low, the number of small particles in some of the solids can be significant.

The water content of most of the solids is measured from the weight loss after drying until constant weight, at 135 °C for 5 hours. However, for perborate, the drying was carried out at 45 °C for 72 hours at reduced pressure, whereas for Zeolite 4A drying was carried out during 3 hours at 800 °C.

Particle densities are derived from the densities of the suspensions in nonionic. The densities were measured with the resonance frequency or 'tuning fork' method (Paar, Mettler). For some solids (α-Alumina, Anatase and Lime) the Penta Pycnometer (Quantachrome) was used to estimate the density. Particle size, water contents and specific density of the solids have already been given in Table 2.2 together with the names of the suppliers. In general the agreement with literature values was excellent. Only for Zeolite and α-Alumina lower densities are found, probably due to the presence of very small pores.

A further characterization of the particles has been carried out by X-ray powder diffractometry (X.R.D) (Philips PW1700, System 1). The results showed that most solids are crystalline and have diffraction patterns in agreement with the chemical formula given. Only the sodium trisilicate ('Soluble M') is amorphous. Its composition was checked by quantitative analysis of Na, Si, H and H_2O. The X-ray diffraction results of the powders are collected in Table 5.1, together with the results of measurements of the specific surface area, pore size and axial ratio.

Specific surface area and porosity in the dry powder, i.e. the volume of pores per weight, are measured using the BET nitrogen adsorption method (Autosorb-6,

Quantachrome). With this method also the very small pores in the solids are measured. Results are included in Table 5.1. For the oxides having high fractions of larger pores, the pore volume was measured by mercury porosimetry (Autopore II 9220, Micromeritics). With this method, which is based on the measurement of the intrusion volume under pressure, also the 'particle bed porosity' is included.

Table 5.1: Crystal type, specific surface area, porosity and axial ratio of the particles used in the current study (see also data given in Table 2.2).

	Chemical formula	Crystal (identified by X-ray)[a]	Specific surface[b] /10^3 m^2 kg^{-1}	Pore volume /10^{-3} m^3 kg^{-1}	Axial ratio r_e[c]
1	TiO_2	Anatase[e]	11	0.34[d]	0.66
2	Al_2O_3	α-Alumina[e]	150	0.24[b]	0.67
3	MgO	Periclase[f]	166	0.42[d]	0.67
4	CaO	Lime[g]	2.3	0.10[d]	0.67
5	$CaCO_3$	Calcite[e]	85.3	0.62[d]	0.65
6	$NaBO_3$ H_2O	Perborate monohydrate[h]	0.3	0.003[b]	0.67
7	$Na[AlO_2.SiO_2].(H_2O)_{0.3}$	Zeolite 4A 'activated'[e]	2.9	0.03[b]	0.63
8	Na_2CO_3	Soda ash[e]	2.1	0.01[b]	0.66
9	$Na_5P_3O_{10}$	STP[i]	1	0.005[b]	0.64
10	$Na_2O.(SiO_2)_3.(H_2O)_{2.5}$	Soluble M[j]	0.3	0.002[b]	0.63

[a] powder diffractometry; [b] N_2 adsorptiometry; [d] Hg porosimetry; [c] IBAS results (see text); [e] pure, crystalline; [f] peak intensity MgO/$Mg(OH)_2$: 90/10; [g] CaO (Lime)/ CaO: 99/1; [h] $NaBO_3.H_2O/NaBO_2.(H_2O)_2$: 93/7; [i] Phase I/Phase II: 79/21; [j] amorphous, based on chemical analysis of Na, Si, H and H_2O.

In addition, a particle shape factor, i.e. the axial ratio r_e, was determined with an interactive image analyzer (IBAS, Kontron). The results showed that on the average the particles can be considered as approximately spherical (Table 5.1). [Note: From electron microscopic pictures it appears that most particles have rough surfaces and contain protrusions with a size of 20 to 100 nm. However, in the image analysis which gives a macroscopic picture, these protrusions have only an insignificant influence on the average particle shape factors obtained.] From the observed r_e values it can be derived that the theoretical intrinsic viscosities [η] are

all around 2.6 (Goodwin, 1981; Leal an Hinch, 1971) [5.3]. For one example case (STP in Plurafac) the intrinsic viscosity obtained in this way, will be compared with that obtained using rheometrical methods (see sect. 5.5.2.3).

5.3.2 Dielectric parameters

5.3.2.1 Dielectric constant

Dielectric measurements of solids have been carried out by means of a Wayne-Kerr radio-frequency bridge (1 MHz), using the method described by Rosen (1963) [5.4]. According to this method, the solid powder is compressed in a die (more familiarly known as an 'infra red press') to form a small, plan-parallel disc (diameter 15 mm). The capacitance of this solid disc is measured by a LCR meter (Hewlett-Packard 4271A). From the accurately measured weight and thickness, and from the density of the solids, the volume fractions of solids and air in the disc are calculated. The dielectric constants of the solids are computed from the measured capacitance using Eq. 5.4, assuming that the contributions to the capacitance of solids and air in the disc are in parallel. The results are used, together with those of the refractive index, for the calculation of the Hamaker constants of the solids (see sect. 6.4.1).

5.3.2.2 Refractive index

The refractive indices of the solid particles were measured using a method in which the refractive index of a crystalline solid is matched with that of an immersion liquid of known refractive index made of mixes of solvents of known refractive index. The judgement whether the refractive index of the particle is higher or lower than that of the immersion liquid is carried out with help of 'Becke-lines' (McCrone, et al., 1978) [5.5]. A Becke line is a bright halo near the boundary of a transparent particle, which moves with respect to that boundary when the microscope is moved up and down. The halo will always move up to the higher refractive index medium as the position of the focus is raised. The halo crosses the boundary to the lower refractive index medium when the microscope is focused in downward direction.

From a comparison of the results obtained with pure, isotropic crystalline solids with known refractive indices (NaCl, $CaCO_3$), it was found that the refractive index obtained was accurate within $\pm$ 0.002. However, because the method gives only an average refractive index from a contribution of various directions, it is less accurate for anisotropic crystals. Since the span of refractive indices between the different solids (1.45 to ca. 1.70) is larger than the accuracy of $\pm$ 0.005 estimated for the anisotropic crystals, the method allows the distinction of different classes of solids.

5.3.3 Microscopy

Light microscopy of the solids is carried with an Axoplan microscope (Zeiss, MC100). Microscopic measurements were used to check particle size distributions and to determine the refractive indices of the solid materials (see sect. 5.3.2.2)

5.4 SUPERNATANTS AND SOLIDS IN SUSPENSION

5.4.1 Supernatants

5.4.1.1 Atomic analysis

The liquid phase in equilibrium with the suspended solids, i.e. the supernatant, is supposed to represent the bulk of the liquid phase and can be obtained by decanting a suspension sediment formed under gravity or after centrifugation. The supernatants were analyzed quantitatively by various spectroscopic methods after filtration over a millipore filter of 0.22 μm (Millex GS) or, occasionally, after centrifugation. [Note: There is a risk that centrifugation causes compression of double layers and may lead to higher concentrations in supernatants. However, differences in results of decanted samples and of centrifuged samples have not been observed and are within the experimental error of the procedures applied.]

Samples of supernatants were analyzed for their Na, K and Li content by flame Atomic Absorption Spectroscopy (A.A.S) (Perkin Elmer 2100); Ca, Mg, B, Al, P, Al, Si, Ti, Fe and Zn were analyzed by Plasma Emission Spectroscopy (P.E.S.) (Perkin Elmer ICP/5500); S and Cl were analyzed by using X-ray Fluorescence Spectroscopy (X.F.S.) (Philips PW1404). A more detailed discussion of most experimental results is given in Chapter 6. However, because of its importance for the experimental methods and procedures discussed further in this chapter, one important result is already given here. It refers to suspensions of sodium salts in nonionics, for example such systems as discussed in sect. 1.4, to which variable amounts of DoBS acid are added.

In these systems it was found in the supernatants that no protons could be recovered already half an hour after acid addition. At that time the molar concentration of sodium recovered in the supernatant is approximately equal to the molar concentration of acid added. At the same time the concentrations of other atoms, such as phosphorous, remained low. The sulphur concentration in the supernatant, representing the HDoBS amount, however, appeared to be proportional to the amount of DoBS
acid applied. A graphical representation of these two findings, whereby the sodium and the sulphur concentrations are plotted as functions of the added DoBS acid concentration, over a number of detergent solids, is given in Figs. 5.1a and Fig. 5.1b, respectively.

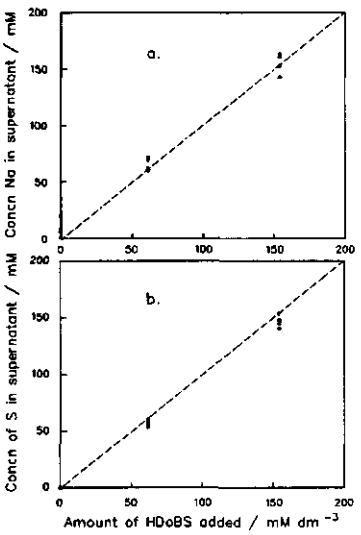

Fig. 5.1: Sodium (a) and sulphur concentrations (b) in the supernatants of suspensions of different Na salts in Plurafac nonionic; sampling half an hour after preparation.

dissolution of the solid had occurred. It is possible that the mechanism of this heterogeneous exchange reaction proceeds via an adsorption of HDoBS on the solid surface prior to a desorption of the neutral anionic. The small differences between amounts added and recovered and the finding in the supernatant of a sulphur concentration independent of the exchange indicate, however, that only a small amount of DoBS acid remains adsorbed. [Note: From the differences in concentration before and after introduction of solids the adsorption levels can be estimated. On doing this we have measured adsorptions ranging from 3 to 7 μM m^{-2} on using 5 % w/w DoBS acid. Lower adsorptions were found when lower DoBS acid amounts were added. These results indicate that we may have to do with monolayer adsorption of DoBS acid. However, the inaccuracy of our analytical methods at present do not allow to come to a firmer conclusion.]

The results indicate that, after addition of HDoBS to the nonionic suspension, hydrogen and sodium are exchanged leading to an in situ formation of the anionic NaDoBS in a concentration which is (almost) equivalent to the DoBS acid added into the suspension. The reaction path representing this ion exchange reaction is given in Fig. 5.2a. This reaction scheme also shows that the exchange reaction requires part of the surface -ONa groups to become converted into hydroxyl groups, to an extent that is related to the amount of acid added. No dissolution of the solid in the continuous phase was observed, at least when the acid levels remained smaller than 2 %. Also with levels ≈ 5 % the dissolution remained limited to levels slightly higher than the detection limit of the analysis. It is found by atomic analysis of the supernatants, that only at levels of ≥ 10 % of DoBS acid significant

a. Ion exchange reaction :

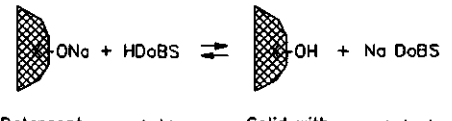

b. Anionic dissociation :

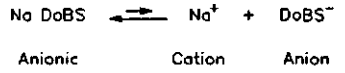

Fig. 5.2: a. Proposed mechanism of the exchange reaction after addition of DoBS acid to a suspension of Na salt in low-polar solvent. b. Dissociation of NaDoBS.

5.4.1.2 Conductivity and ionic strength

In sects. 4.3.1 and 4.3.2 the dissociation of anionic electrolytes in low-polar media (see Fig. 5.2b) and the role of dissociation-enhancing factors have been discussed extensively. To evaluate the ionic strengths in nonionic liquids, conductivity measurements of supernatants have been carried out. For these measurements we used the same arrangement as for the measurements of the dielectric constants (see sect. 5.2.2). From Fig. 5.1 the conclusion can be drawn that the anionic NaDoBS can be present in significant amounts in the solution. In sect. 4.3.2.1 it was hypothesized that the anionic could also contribute to a conductivity rise. This aspect will be discussed further in this section. The results of the conductivity measurements and discussed in terms of ionic strengths will be discussed in sect. 6.2.2.2.

According to the Arrhenius-Ostwald theory (Fuoss and Shedlovsky, 1949, [5.6]; Kitahara et al., 1967) [5.7], the degree of dissociation α of an electrolyte in a low-polar solvent can be given by

$$\alpha = \frac{\Lambda}{\Lambda_0} s(z) \qquad \textbf{[5.8]}$$

where, Λ is the molar conductivity, defined by K/c_0, and Λ_0 the molar conductivity at infinite dilution, i.e. the limiting molar conductivity, defined as

$$\lim_{c_0 \to 0} \frac{K}{10^3 c_0} = \Lambda_0 \qquad \textbf{[5.9]}$$

where c_0 is the molar concentration in M dm^{-3} (M) of anionic NaDoBS in the nonionic. In Eqs. 5.8 and 5.9, Λ and Λ_0, have the units S m^2 mol^{-1}. In Eq. 5.8, $s(z)$ is the Shedlovsky crowding factor (Shedlovsky, 1938, [5.8], Popovych and Tomkins, 1981, [5.9]). It is defined as

$$s(z) = \left[\frac{z}{2} + \left(1 + \left(\frac{z}{2}\right)^2 \right)^{\frac{1}{2}} \right]^2 \qquad \textbf{[5.10]}$$

where

$$z = \left(a \Lambda_0 + b\right) \Lambda_0^{-\frac{3}{2}} \left(c_0 \Lambda\right)^{\frac{1}{2}} \qquad \textbf{[5.11]}$$

in which a and b are related to the Debye-Hückel ion interaction parameters, defined by

$$a = \frac{8.204 \times 10^5}{(\varepsilon T)^{\frac{3}{2}}} \qquad [5.12]$$

and

$$b = \frac{8.2501 \times 10^{-4}}{\eta_c (\varepsilon T)^{\frac{1}{2}}} \qquad [5.13]$$

with T in Kelvin and η_c, the viscosity of the continuous phase in mPa s. It is found for our nonionic systems that $s(z)$ ranges from 1.03 to 1.6 at room temperature. When the value of Λ_0 for a given solvent is known, from the measured specific conductivity K and the concentration of the anionic NaDoBS c_0, the degree of dissociation α can be evaluated from Eq. 5.8 and, hence, the required ionic strength c_i (in M) according to

$$c_i = \alpha c_0 \qquad [5.14]$$

For low ionic strengths, i.e. when the crowding parameter $s(z) \rightarrow 1.0$, substitution of Eq. 5.8 in Eq. 5.14 leads to

$$c_i \approx \frac{K}{10^3 \Lambda_0} \qquad [5.15]$$

This equation allows the approximate evaluation of c_i, in M, directly from the measured specific conductivity K and the limiting molar conductivity Λ_0.

5.4.1.3 Limiting molar conductivities in nonionics

Values of Λ_0 for NaDoBS in nonionic and necessary for the evaluation of c_i are not available in the literature. Hence, the values of Λ_0 were experimentally determined in a dilution series of NaDoBS in the nonionics Plurafac and Imbentin. The starting solutions in these nonionics had concentrations of NaDoBS of 3.62 and 3.66 mM, which were diluted in seven steps to a lowest concentration of 0.30 and 0.31 mM, respectively. From the conductivities of these solutions the limiting molar conductivities have been derived.

Based on the Arrhenius-Ostwald relationship, modified by Shedlovsky, the following equation has been derived

$$\frac{1}{\Lambda s(z)} = \frac{C_0 \Lambda f_\pm^2 s(z)}{\Lambda_0^2 K_D} + \frac{1}{\Lambda_0} \qquad [5.16]$$

In this equation K_D is the dissociation constant, defined by

$$K_D = \frac{\alpha^2 c_0 f_\pm^2}{(1 - \alpha)} \qquad [5.17]$$

and $f_\pm$ is the mean ionic activity coefficient, for which in the Debye-Hückel approximation

$$-\log f_\pm = \frac{A c_i^{1/2}}{1 + B r c_i^{1/2}} \qquad [5.18]$$

where r is the ion-pair radius and A and B are given by

$$A = \frac{1.8123 \times 10^6}{(\varepsilon T)^{3/2}} \qquad [5.19]$$

and

$$B = \frac{5.0288 \times 10^{11}}{(\varepsilon T)^{1/2}} \qquad [5.20]$$

Including the combinations of Eqs. 5.8 and 5.14, of Eqs. 5.10 to 5.13 and including also Eq. 2.5, we have a set of six non-linear equations and six unknowns, viz. Λ_0, K_D, $f_\pm$, $s(z)$, c_i and r. From these equations Λ_0 can be obtained, substituting the experimental parameters ε, T and η, at any combination of c_0 as the independent and Λ as the dependent variable. To find the average values of the constants Λ_0, K_D and r with a number of combinations of c_0 and Λ, a procedure is followed that is proposed by Shedlowsky (Popovych and Tomkins, 1981 [5.9]). The procedure involves a plot of $1/(\Lambda s(z))$ against $c_0 \Lambda f_\pm^2 s(z)$ (see Eq. 5.16), whereby the correlation coefficient of a straight line is maximized. The average value of $\Lambda_0^2 K_D$ is then derived from the slope, allowing, in combination with Eq. 5.17, the evaluation of the individual values for Λ_0 and K_D.

Graphs are given in Fig. 5.3. It was found that the highest correlation coefficients for Plurafac and Imbentin were 0.98 and 0.99, respectively. These correlation coefficients suggest that it is reasonable to assume that Λ_0, K_D and r are constants. The average results of the limiting molar conductivity Λ_0, the dissociation constant K_D and the ion-pair radius r are in this order: 1.02×10^{-4} S m^2 mol^{-1}, 5.6×10^{-8} M dm^{-3} and 5.4×10^{-10} m in Plurafac, and 1.02×10^{-4} S m^2 mol^{-1}, 2.5×10^{-6} M dm^{-3} and 5.9×10^{-10} m in Imbentin. The results show that NaDoBS has a larger ion-pair radius and dissociates more in Imbentin than in Plurafac. It was further found that $f_\pm$ varied from 0.79 to 0.90 in Plurafac and from 0.61 to 0.80 in Imbentin; $s(z)$ dropped from 1.06 to 1.03, and from 1.17 to 1.09, respectively, in the two nonionics at the same time.

Values of Λ_0 for NaDoBS in nonionic can also be derived from the conductivities at infinite dilution of NaDoBS in water Λ_0^{water} and using Walden's rule

$$\Lambda_0^{water}\,\eta_0^{water} = \Lambda_0\,\eta_0 = \text{constant} \qquad [5.21]$$

From conductivity measurements in water, obtained for a series of NaDoBS concentrations, we derived that Λ_0^{water} has a value of $(75 \pm 4) \times 10^{-4}$ S m^2 mol^{-1}. From the difference with the known molar conductivity of the cation (λ_+) in water, i.e. 50×10^{-4} S m^2 mol^{-1}, the molar conductivity of the anion (λ_-) is found to be 25×10^{-4} S m^2 mol^{-1}. For the liquid nonionics Plurafac and Imbentin, with viscosities of 51.6 and 33.6 mPa s, respectively, this leads for NaDoBS to $\Lambda_0 = 1.49$ and 2.29×10^{-4} S m^2 mol^{-1}, respectively. Since, the experimental values in the nonionics are 0.69 and 0.44, respectively, of the estimates derived from the molar conductivities in water, this result indicates that the mobilities of the Na^+ and $DoBS^-$ ions are more reduced by the nonionics than by water and that solvation in nonionics is stronger. The results further suggest that solvation effects in Imbentin are stronger than in Plurafac.

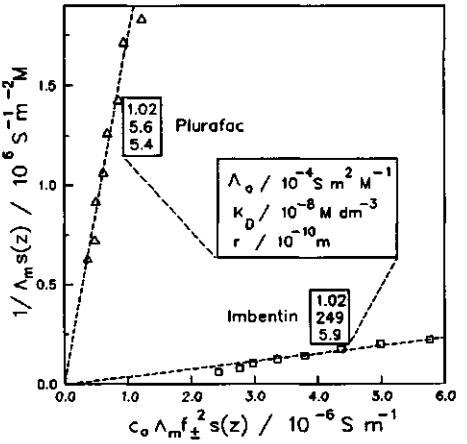

Fig. 5.3: Shedlowsky plots and plot parameters for a dilution series of NaDoBS in Plurafac and Imbentin.

5.4.1.4 Coefficients of self-diffusion

Some evidence concerning the correctness of the values of Λ_0 could be obtained by measuring the coefficients of self-diffusion of DoBS acid, in the nonionics. This can be accomplished by pulse field gradient (pfg) NMR. Pulse field gradient NMR measurements were performed on a Bruker MSL 300 spectrometer, in combination with a $^1H/^{19}F$ 5 mm dual frequency probe, with z-gradient coils. The field gradient pulse generator was home-designed and -made. All spectra were measured by the 'pulsed field gradient Fourier Transform Stimulated Echo' (pfg-FT-STE) technique developed by Tanner and Stejskal (1968/1970) [5.10] and reviewed by Stilbs (1987) [5.11]. The two field gradient pulses were spaced 50 to 675 ms apart. The 90 pulse time was about 8 μs. Typically 32 scans were acquired of 229 ms each with a dwell time of 56 μs. The field gradient was calibrated with 1-octanol, which has a known coefficient of self-diffusion of 1.4×10^{-10} m^2 s^{-1} at 25 °C. Typical gradient strengths of 0.11 T m^{-1} were obtained. The echo attenuation ratios R were determined for each peak individually on the basis of the areas of the resonances peaks. The coefficient of self-diffusion D was obtained from the slope of the experimental R values.

From the pfg-NMR measurements it is found for DoBS acid that, in the nonionics Plurafac and Imbentin, $D = (0.9 \pm 0.1) \times 10^{-11}$ and $(1.3 \pm 0.2) \times 10^{-11}$ m^2 s^{-1},

respectively. When it is assumed that the non-dissociated DoBS acid and the DoBS anion have equal friction coefficients, the molar conductivity of the anion λ_- follows from the diffusion coefficient D, using

$$\lambda_- = D\frac{N_A e^2}{k_B T} \qquad [5.22]$$

From the coefficients of self-diffusion, using Eq. 5.22, values of λ_- are found to be $(0.32 \pm 0.03) \times 10^{-4}$ and $(0.51 \pm 0.07) \times 10^{-4}$ S m^2 mol^{-1} in Plurafac and Imbentin, respectively. Walden's rule predicts λ_- values in Plurafac and Imbentin of 0.47 and 0.68 $\times 10^{-4}$ S m^2 mol^{-1}, respectively. Hence, these experimental values in nonionics are again lower than those derived from the molar conductivities of the DoBS anion in water. The results agree with the earlier observation that the nonionics solvate the ions of NaDoBS better than water. [Note: In the dilution series the values for Λ_0 found experimentally were 1.02×10^{-4} S m^2 mol^{-1} in both nonionics. Using these values and the above values for λ_-, it can be derived that $\lambda_+ = 0.80 \times 10^{-4}$ and 0.51×10^{-4} S m^2 mol^{-1} in Plurafac and Imbentin, respectively. The difference in λ_+ values in the two nonionics suggests that the larger difference of the molar conductivity of NaDoBS in Imbentin compared to the predicted values is mainly the result of the lower mobility and stronger solvation of Na^+ ions in Imbentin.]

5.4.2 Suspended Particles

5.4.2.1 Electrophoretic mobility

The surface potentials ψ_0 of particles have been evaluated by measuring the mobility of particles in an electric field, assuming the electrokinetic potential $\zeta = \psi_0$ (see sect. 4.3.1). To this end the concentrated suspension was diluted with supernatant from an original volume fraction ϕ of 0.32 to a ϕ of 0.002 to 0.0008. The dielectric constant ε, specific conductivity K and viscosity η of these diluted suspensions were all measured separately and used for the calculation of the ζ-potential.

The original electrokinetic measurements were carried out on a Rank Brothers Mark 2 equipment supplied with a flat quartz cell for micro-electrophoresis, having a depth of 1.0 mm and a path length of 9.5 cm. Potentials over the cell were measured with two Ag/AgCl electrodes. Viscosities of nonionics are rather high. Hence, to obtain measurable velocities in media of low dielectric constants, these experiments were carried out at slightly elevated temperature (40 °C), obtained by placing the cell in a thermostatted paraffin oil bath and at field strengths of 30 to 110 kV m^{-1}. The latter was realized by using a high voltage power supply unit (Wallis, type A.C.S. 303/1) and a safety voltage transfer and measuring unit. Under these conditions the mobility is independent of the field strength. It took about 1 to 2.5 hours per suspension to measure seven points of the velocity distribution, which appeared to be parabolic.

Later experiments were carried out at room temperature, using a Laser Doppler electrophoresis equipment with a 0.8 cm^3 micro cell suitable for measurements of non-aqueous media (Coulter, Delsa 440). To prevent polarization, the direction of the static electric field is alternated, with field-off times in between, to reduce heat dissipation. The field-on and field-off times used were 5.2 and 2.5 s, respectively. During 120 s the mobility is measured eight times in two directions. As the velocity of a particle is derived from the Doppler shifts of the reflected laser beams under four different angles, a fairly accurate distribution of velocities emerges. In all cases the measurements were carried out at four field strengths, viz. 5, 10, 20 and 30 kV m^{-1}; in this range the mobility was independent of the field strength applied.

As already discussed (sect. 4.3.1.3), in our low-polar systems, the Debye lengths $1/\kappa$ are $\leq$ ca. 20 nm, whereas particle radii are approximately 5 μm. Hence, in such media κa is large so that calculation of the ζ-potential from the electrophoretic mobility can be carried out by simply using the Henry equation (Hunter, 1987 [5.12])

$$\zeta = \frac{1.5\, u_e\, \eta}{\varepsilon\, \varepsilon_0\, f(\kappa a)} \qquad [5.23]$$

Since $\kappa a \geq 200$, $f(\kappa a) \rightarrow 1.5$, therefore Eq. 5.23 becomes

$$\zeta = \frac{u_e\, \eta}{\varepsilon\, \varepsilon_0} \qquad [5.24]$$

In Eqs. 5.23 and 5.24, u_e is the velocity of a particle per unit of field strength. It has the dimensions $m^2\ s^{-1}\ V^{-1}$. The typical range of u_e is from 1 to 14 $\times 10^{-11}$ $m^2\ s^{-1}\ V^{-1}$ in our experiments.

5.5 SUSPENSIONS

5.5.1 Sediments

5.5.1.1 Sediment formation

Sedimentation experiments have been carried out with concentrated suspensions in calibrated and stoppered Pyrex glass cylinders of 250 cm^3. It was found with unstable suspensions in smaller vessels that wall effects can cause an irregular sedimentation behaviour. Before filling the cylinders with the suspension, they were cleaned and rinsed three times with tap water and three times with demineralized water.

In most suspensions a clear layer develops after an incubation period of a few hours and no particles are observed in the upper layer. Only in a few suspensions of oxides a slight haziness in the upper layer was seen. This points to a generally

fast rate of coagulation prior to sedimentation. It suggests that in DoBS acid stabilized suspensions some (secondary minimum) coagulation may occur. The rate of formation of the clear layer was followed by recording the position of the boundary layer with time. In most cases a steady state with a constant rate of sedimentation can be defined after the incubation period. At longer time scales an exponential decay with time is found. The sedimentation continues until a final equilibrium volume is reached. For some strongly coagulating solids the equilibrium is reached already after a few days. However, in other cases (activated Zeolite 4A, Calcite) settling to equilibrium takes more than half a year.

From the final settled volume, the volume fraction in the sediment ϕ_{sed} was evaluated. It has to be noted here that this method gives an **average** value of the volume fraction ϕ_{sed}. Thus gradients in packing fraction from top to bottom of the sediment, which for example can occur under the increasing pressure of a growing sediment, are not taken into account. Since the sediments are non-transparent, it is not easy to obtain an indication of this gradient by using optical methods. However, values of local volume fractions can be obtained from measurements of the absorption of soft γ-radiation, making use of the differences in absorption between the solid and the liquid.

5.5.1.2 Volume fractions in sediments

Measurements of γ-ray absorption can be carried out at any height in the sediment, thus allowing the measurement of a packing gradient and, when the particle size is known, also the particle number concentrations. The method applied is similar to that described by Blake and Colombera (1977) [5.13]. For the absorption of a beam of γ-radiation through a suspension, assuming a homogeneous particle distribution in the irradiated volume, it can be derived that

$$\ln(\frac{I_0}{I}) = (\mu_s - \mu_l) d_s + \mu_l d \qquad [5.25]$$

where I_0 is the number of photons of the radiation that enters the sample, I is the number of photons that leaves the sample after crossing a sample with path length d, d_s is the path length through the solids suspended, and μ_s and μ_l (dimension: m^{-1}) the absorption coefficients for γ-radiation of the solid phase and the liquid phase, respectively.

When ϕ is the volume fraction of the solids then $\phi = d_s/d$ and substitution into Eq. 5.25 gives

$$\ln(\frac{I_0}{I}) = (\mu_s - \mu_l) \phi d + \mu_l d \qquad [5.26]$$

Hence, when for a solid the values of I are measured as a function of volume fraction ϕ, a plot of the absorbance $\ln(I_0/I)$ against ϕ gives a straight line with slope $(\mu_s - \mu_l)d$ and intercept $\mu_l d$. Since in a fixed arrangement d is known and constant, the procedure allows the calculation of μ_s and μ_l. A schematic diagram of

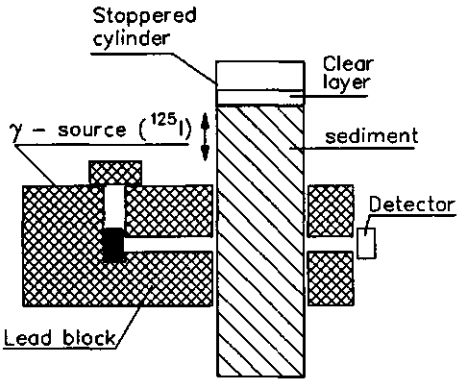

Fig. 5.4: Arrangement for the measurement of solid volume fractions in sediments with weak γ-radiation.

curves have been measured and values of μ_s and μ_l calculated. These calibration curves are used to establish the volume fractions in settled sediments from top to bottom. To avoid disturbances due to sedimentation during the calibration, the measurements were carried out immediately after preparation of the suspension, i.e. in the sedimentation incubation period. An example calibration curve is given in Fig. 5.5. With the help of such curves the volume fraction of any sediment of a solid can be determined. This method is used to establish the solid volume fractions as a function of height in sediments. The power of the method to detect all solids suspended in the volume is convincing: It is found that, averaged over 33 sediments, 98.0 % of the solids is detected.

the home-made measuring device is given in Fig. 5.4. It consists of a lead block of 5 × 10 × 10 cm, with a vertical cylindrical opening through which the cylindrical flasks (250 cm^3) can be moved vertically. A second smaller vertical hole contains the glass tube with a solution of the γ-source (Na^{125}I, ex Amersham, UK), which emits monochromatic radiation of 35.49 keV. The radiation is led through a cylindrical channel with a diameter of 7 mm, which connects the two vertical holes, passing the centre of the cylinder with the suspension to the NaI scintillation counter which is used as the detector (Mini Assay, Mini Instruments Ltd.).

For all the solids studied, calibration

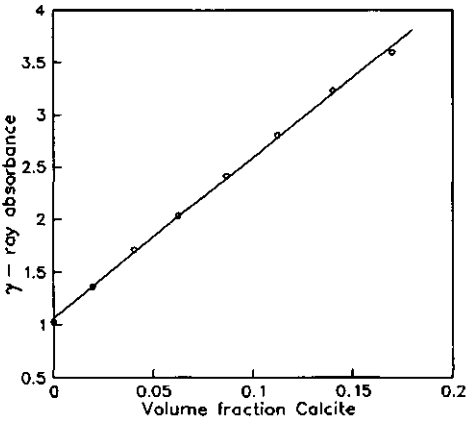

Fig. 5.5: Example calibration curve. Calcite suspension sediment in Plurafac. Plot parameters: Intercept = 1.05; R^2 = 0.9996.

From the volume fractions measured in the consecutive sediment segments from top to bottom the (increasing) static pressure can be evaluated. Since volume fraction ϕ and the pressure are related, the pressure at volume fraction ϕ is denoted as $\Pi(\phi)$. The plot of $\Pi(\phi)$ as a function of the volume fraction gives a

direct insight in the strengths of the coagulative forces (see sect. 7.5). The network compression modulus $K(\phi)$ and defined as

$$K(\phi) = \phi \frac{d\,\Pi(\phi)}{d\,\phi} \qquad [5.27]$$

can be derived further from these data (Buscall, et al. 1982 [5.14]; Sonntag and Strenge, 1987 [5.15]).

5.5.1.3 Centrifugation method

To establish the maximum volume fractions of non-aqueous suspensions a number of centrifuge experiments have been carried out. The centrifuge used is a High Speed Centrifuge (MSE, type Europa 24) and is used at 12.500 rpm, corresponding with a sedimentation force of approximately 10.000 × g. The centrifugation tubes used for these experiments are made of hard polypropylene (Sorvall).

5.5.1.4 Confocal Scanning Laser Light Microscopy

Confocal scanning laser light microscopy (C.S.L.M) is a technique where laser light is focused very accurately on a plane inside a suspension, at penetration depths up to ca. 20 μm. Positions of particles in sediments can thus be observed. Our experiments were carried out with a combination of a Biorad MRC 600 CSLM and a Zeiss inverted microscope. The in-depth resolution of the arrangement is approximately 0.5 μm. With reflection microscopy it is possible to observe the reflective areas of particles in a suspension and to get a stereoscopic microscopic picture. By mounting the microscope vertically, we applied the method to look inside a suspension through the bottom of a vessel and to observe the positions of suspended particles. Focusing at planes at increasing depths, with increments of 0.7 μm, allowed us to observe the organisation in the bottom of a suspension over a distance of a few particle diameters. Although the many reflective surface parts prohibited unambiguous interpretation of the pictures, movement of particles, i.e. movement of reflective areas from the primary particles, could be observed. The pictures confirmed that particles are organized in stacks resting at their points of contact, when a sediment is in equilibrium. Over a period of 3 days only minor changes in positions are observed.

5.5.1.5 Scanning Electron Microscopy

Samples of suspensions are frozen in liquid nitrogen in a special holder that permits fracturing of the frozen sample to exhibit the internal structure (Cryo-SEM). After fracturing the samples are coated with Pt/C in a freeze-etching device (Balzers BAF 400). Via a Hexland cryo system the samples are transported into a Scanning Electron Microscope (Philips SEM 515). The samples are inspected at a temperature $\leq$ - 100 °C using a solid state backscatter detector (KE Developments). The backscatter signal allows us to discriminate between features

having different mean atomic numbers. In our suspensions, the crystalline detergent solid particles appear light in the dark continuous phase.

5.5.2 Viscosity

5.5.2.1 Methods

Samples for viscosity measurements were prepared by adding the solid to the liquid, while stirring gently, to the target volume fraction. Optionally, DoBS acid is added. The samples are de-aerated under vacuum and stored in glass containers. The viscosity measurements were performed with two different types of viscometers. In the first one (Haake RV20) the shear rate was controlled and the shear stress measured. This instrument was used for measurements in the intermediate and high shear rate range, i.e. from 0.05 to 500 s^{-1}. For measurements which required greater sensitivity (low shear rate measurements or samples with low viscosities) the second one, a controlled shear stress rheometer (Bohlin CS) was used. The temperature (adjustable between 5 and 90 °C) was kept constant by means of a water jacket.

All suspensions were measured between concentric cylinders, provided with grooves in order to prevent wall slip. On the Bohlin CS rheometer only the bob was grooved, the cup was roughened by sand blasting. The grooves are of a block type as found on some commercial bobs (Haake, MVIIP and SVIIP).

Viscosity measurements were carried out at a number of shear rates or shear stresses. The measurement at a given condition is maintained until the reading does not change any more with time (steady state conditions), meaning that in suspensions that are structured by attraction forces between the particles, the velocities of rupture and rebuilding of the structure are equal. The measurements were carried out from low to high shear rate or shear stress. No special precautions were taken in introducing the sample into the viscometer, although some time was allowed for temperature equilibration.

5.5.2.2 Influence of shear rate

As is mentioned before in sect. 2.4.2 a well known property of suspensions is that they exhibit non-Newtonian behaviour. This means that the viscosity η (dimensions: Pa s), which is the proportionality constant between the shear stress (τ, dimensions: Pa) and the shear rate ($\dot{\gamma}$, dimensions: s^{-1})

$$\eta = \frac{\tau}{\dot{\gamma}} \qquad \textbf{[5.28]}$$

is not a constant, but dependent on the shear rate. This phenomenon is called shear-thinning if the viscosity is lowered when higher shear rates are applied. When the viscosity rises with increasing shear rates the suspensions are called shear-thickening. At extremely low and high shear rates the viscosity is indepen-

dent of the shear rate. For suspensions of particles which interact with each other this influene can be explained in the following way: At rest the particles are ordered in a three dimensional array, such as in a crystal lattice. An extremely low shear will not be sufficient to break down this structure significantly. In other words, the relaxation time of the structure is much shorter than the characteristic (shear rate) time, i.e. $1/\dot{\gamma}$. Hence, the viscosity is unaffected by the rate of shear. This plateau value of the 'creep' viscosity in the viscosity-shear rate curve (η_0) is called the 'first Newtonian plateau'. The value is supposed to be completely determined by the colloidal, attractive and repulsive, interparticle forces. In our suspensions the constant viscosity of the 'first Newtonian plateau', is usually not reached, even not after reducing the shear rate to values of 10^{-4} to 10^{-5} s^{-1}.

When a higher shear is applied to this ordered structure it is partially broken down leading to a lower viscosity and resulting in shear- thinning. Eventually, at a very high shear rate, the three-dimensional structure will be completely lost, and particles tend to arrange in two-dimensional, plate-like structures with liquid layers separating the plates. Once this structure is formed the viscosity will again no longer depend on the shear and the viscosity of the 'second Newtonian plateau' η_∞ is reached. This viscosity is purely determined by hydrodynamic interactions induced by the applied shear. Therefore, η_∞ only depends on the viscosity of the liquid phase η_c and on the effective volume fraction of the suspended solids ϕ. The ϕ includes also the influences of particle shape and porosity.

One of the equations that predicts the full coarse of the shear-thinning curve is the one derived by Cross (1965) [5.16]. For suspensions of interacting particles he derived an equation equivalent to

$$\frac{\eta_0 - \eta}{\eta - \eta_\infty} = (k\dot{\gamma})^m \qquad \textbf{[5.29]}$$

where k is a constant parameter with the dimensions of time and m is a dimensionless constant (Barnes, 1990) [5.17].

For systems where the viscosity remains in the shear thinning part of the viscosity curve in-between the two plateaus, i.e. $\eta_0 >> \eta >> \eta_\infty$, after a redefinition of the parameters, the Cross model reduces to the well-known 'power law' model

$$\eta = K\dot{\gamma}^{(n-1)} \qquad \textbf{[5.30]}$$

where n is the power-law index and K is called the consistency, with the dimensions Pa s^n.

For viscosities lower than the 'first Newtonian plateau', i.e. $\eta_0 >> \eta$, Eq. 5.29 reduces to the Sisko model

$$\eta = \eta_\infty + K\dot{\gamma}^{(n-1)} \qquad \textbf{[5.31]}$$

These two equations both describe the viscosity in the shear-thinning area of our suspensions in nonionics equally well. However, since the latter one includes also the accessible constant viscosities in the ('infinitely') high shear rate area, Eq. 5.31 is preferred.

Experimental results of η as a function of $\dot{\gamma}$ are usually plotted logarithmically. In doing so, η_∞ shows up as a plateau at the high shear rate end (see Fig. 2.7). Fitting of Eq. 5.31 over experimental results leads to the fit parameter K, the 'consistency', which indicates the position of the shear-thinning area with respect to the $\dot{\gamma}$ axis. With increasing consistency, the curve shifts to the high shear rate end of the plot and vice versa. The consistency K has a relation with the attraction between particles: strong attraction is reflected in a high K value and conversely (see Fig. 2.7, sect. 2.4.2).

The exponent $(n\text{-}1)$ is proportional to the slope of the shear thinning part of the curve. Note that the slope is negative, so $0 \leq n \leq 1$. Two extreme situations can be distinguished with respect to the value of n. In the situation that $n = 1$ the liquid behaves Newtonian. When $n = 0$, after substitution of Eq. 5.28, Eq. 5.31 simplifies to

$$\tau = \eta_\infty \dot{\gamma} + K \qquad [5.32]$$

Equation 5.32 is the Bingham yield stress equation, where η_∞ is now the 'plastic viscosity' and K the stress at which the network 'yields'. Hence, for the situation of $n = 0$, the consistency K is equivalent to the well-known 'Bingham yield stress'. In our non-aqueous suspensions, we usually find values of n = approx. 0.1. Hence, the Bingham yield stress concept for our suspensions is considered to be an idealization (Barnes, 1985) [5.18]. The data in our work will therefore be analyzed with the Sisko equation (Eq. 5.31). The found value of n indicates that our systems are very shear sensitive.

5.5.2.3 Influence of solids volume fraction

Already in the beginning of this century Einstein derived an relation between the viscosity η of a suspension, the viscosity of the continuous phase η_c and the volume fraction ϕ for hard, non-interacting spheres in the limit of infinite dilution.

$$\frac{\eta}{\eta_c} = 1 + 2.5\,\phi \qquad [5.33]$$

The equation has been shown to describe viscosities accurately up to $\phi = 0.01$. More recent attempts have led to equations which are valid up to higher ϕ values. However, none of these equations proved useful for our suspensions. A great number of empirical relations have been reported. One of the most successful, which has some theoretical justification is the Krieger-Dougherty relation (Barnes, 1990 [5.17], Goodwin, 1985, [5.19])

$$\frac{\eta}{\eta_c} = \left(1 - \frac{\phi}{\phi_m}\right)^{-[\eta]\phi_m} \qquad [5.34]$$

In this equation, ϕ_m is the maximum volume fraction of solids which can be suspended, i.e. the maximum packing, and $[\eta]$ the intrinsic viscosity, a parameter which depends on the volume fraction and the width to length ratio of the particles r_e. For hard spheres $[\eta] = 2.5$, whereas for non-spherical particles $[\eta] > 2.5$. The maximum volume fraction ϕ_m reported for non-interacting, homodisperse spheres is ≥ 0.71, but for interacting, polydisperse particles values of ϕ_m have been reported which range from 0.25 to 0.7. For such systems $[\eta]$ can vary between 2.7 to 10.

Although in principle also valid for lower shear rates, we use Eq. 5.34 only for the relation of the 'infinite' shear rate viscosity η_∞ and the volume fraction ϕ. Namely, due to changes in particle arrangement ϕ_m will vary with shear rate $\dot{\gamma}$. A plot of measured η_∞ versus ϕ, and a plot of Eq. 5.34 over the experimental data will allow the evaluation of both the maximum volume fraction ϕ_m and the intrinsic viscosity $[\eta]$ (see sect. 5.2.1).

Another route to evaluate $[\eta]$ follows directly from its definition

$$[\eta] = \lim_{\phi \to 0}\left(\frac{\eta/\eta_c - 1}{\phi}\right) \qquad [5.35]$$

This equation shows that the intrinsic viscosity can be obtained from a plot of the reduced viscosity versus the volume fraction ϕ.

5.5.2.4 Shear moduli from creep and relaxation

Creep and elastic relaxation measurements are carried out on the Bohlin CS rheometer using a concentric serrated, cylindrical geometry in order to prevent wall slip. For these measurements, a sample was introduced into the viscometer and left for about ten minutes to allow the structure to relax and the temperature to equilibrate. Curves for the deformation as function of time in creep and in elastic relaxation were recorded at a number of increasing shear stresses. Especially at the lowest stresses it could take more than 10 minutes before a constant shear rate was observed.

For the evaluation of the shear modulus G_0 from creep results, the viscoelastic deformation as a function of time data was fitted to the equation

$$\frac{\gamma}{\sigma} = \frac{1}{G_0} + \frac{1}{G_1}\left(1 - \exp\left(-\frac{t}{\tau}\right)\right) + \frac{t}{\eta_0} \qquad [5.36]$$

where γ is the deformation or strain, σ is the shear stress, G_0 and G_1 are the time-independent and the time-dependent parts of the shear modulus, respectively, t is

the time, τ the characteristic time and η_0 the viscosity at low shear rate. The quotient γ/σ is sometimes denoted as the compliance J (Pa^{-1}). Only deformations observed in the first two minutes were analyzed.

For the evaluation of the shear modulus G_0 from the relaxation data, the data of the deformation as a function of time were fitted to the equation

$$\frac{\gamma}{\sigma} = \frac{1}{G_0} + \frac{1}{G_1}(1 - \exp(-\frac{t}{\tau})) \qquad [5.37]$$

The values for G_0 obtained from these fits were plotted as a function of the applied shear stress σ. It was generally found that as the shear stress σ increases, G_0 from creep increased, whereas G_0 from relaxation decreased. The plateau values, which in case of linear elastic compliance are identical, are considered to be the linear visco-elastic domain.

5.6 SUMMARY

The solids, the liquid nonionics and the anionic acids, used in the current non-aqueous liquids research project, have been characterized. Details of the analytical methods are given. The techniques include measurements of the molecular and crystalline structure, specific density, specific surface area, porosity, axial ratio and water content. The methods to measure the refractive indices and dielectric constants of the liquids and solids are discussed. Accurate analysis of the supernatants of our suspensions is carried out, by Atomic Absorption, by Plasma Emission and by X-ray Fluorescence Spectroscopy. It is demonstrated that, when sodium salts are suspended in the nonionic, added DoBS acid is quantitatively converted into anionic NaDoBS. A mechanism for the exchange reaction is proposed.

Details are given of the methods applied for the electrostatic characterization of the starting materials and of the suspension supernatants. From conductivity measurements the limiting molar conductivity of NaDoBS was derived. In both nonionics Plurafac LFRA30 and Imbentin C91/35 the limiting molar conductivity was 1.02×10^{-4} S m^2 mol^{-1}, which value is lower than predicted from limiting molar conductivities in water. The results indicate that solvation interactions of Na^+ and $DoBS^-$ ions in nonionics are stronger than in water and stronger in Imbentin than in Plurafac. Using the limiting molar conductivity, the ionic strengths of supernatants can be evaluated from their conductivities. The method for the measurement of the ζ-potentials is also discussed.

Suspension sediments are characterized by a γ-ray absorption method and by rheological methods. By γ-ray absorption the volume fractions as a function of height can be measured in static sediments. From the results the relation between the static pressure $\Pi(\phi)$ and the volume fraction ϕ and also the network modulus $K(\phi)$ are derived. Rheology is used to measure the mechanical properties of suspensions under dynamic conditions. The methods are discussed to derive the

consistency and shear thinning index from the Sisko model, and the intrinsic viscosity and maximum particle packing from the Krieger-Dougherty equation. The method to derive the elastic shear modulus G_0 from creep and elastic relaxation measurements is explained.

5.7 BIBLIOGRAPHY

5.1 **Determination of Anionic-Active Detergents by Two-phase Titration.** Reid, V.W.; Longman, G.F.; Heinerth, E.. *Tenside,* **1967,** 4 (9), 292-304.

5.2 Lockhart, N.C.; Snaith, *J. Phys. E: Sci. Instrum.* 11, 1011 **1978**; Lockhart, N.C.. *J. Phys. E: Sci. Instrum.*. 12, 433 **1979**; adapted by P.W.M. van der Zon and G.A. van Koppen, URL Vlaardingen.

5.3 **Some uses of rheology in colloid sciences.** Goodwin, J.W.. **Ch. 6. Colloidal dispersions.** Goodwin, J.W.. Editor. Spec. Publ. 43. (Royal Society Chem., London). **1981**; Leal, L.G.; Hinch, E.J.. **The effect of weak Brownian rotations on particles in shear flow.** *J. Fluid Mech.* **1971,** 46 (4), 685 - 703.

5.4 Rosen, D.. *Trans. Far. Soc.* 59, 2178-2191, **1963.**

5.5 **Polarized light microscopy.** McCrone, W.C.; McCrone, L.B.; Delly, J.G.. (Ann Arbor Science Publishers Inc., Ann Arbor, Michigan, USA), **1978.**

5.6 **Extrapolation of Conductance Data for Weak Electrolytes.** Fuoss, R.M.; Shedlovsky, Th.. *J. Am. Chem. Soc.* **1949,** 71, 1496-1498.

5.7 **The Effect of Water on Electrokinetic Potential and Stability of Suspensions in Nonpolar Media.** Kitahara, A.; Karasawa, S.; Yamada, H.. *J. Colloid Int. Sci.* **1967,** 25, 490-495.

5.8 **The computation of ionization constants and limiting conductance values from conductivity measurements.** Shedlovsky, Th.. *J. Franklin Inst.* 225, 739-743, **1938.**

5.9 **Transport Properties.** Popovych, D; Tomkins, R.T.. **Ch. 7. Nonaqueous Solution Chemistry.** (John Wiley, New York). **1981.**

5.10 **Restricted Self-Diffusion of Protons in Colloidal Systems by th Pulsed-Gradient, Spin-Echo Method.** Tanner, J.E.; Stejskal, E.O.. *J. Chem. Phys.* **1968,** 49, 1768; **Use of the Stimulated Echo in NMR Diffusion Studies.** Tanner, J.E.. *J. Chem. Phys.* **1970,** 52, 2523.

5.11 **Fourier transform pulsed-gradient spin-echo studies of molecular diffusion.** Stilbs, P.. *Progress in NMR spectroscopy.* **1987,** 19, 1.

5.12 **Foundations of colloid science. Volumes I and II.** Hunter, R.J.. Editor. Clarendon Press, Oxford, UK). **1987.**

5.13 **Sedimentation: A comparison between theory and experiment.** Blake, J.R.; Colombera, P.M.. *Chem. Engineering Sci.* 32 221, **1977.**

5.14 Buscall, R.; Goodwin, J.W.; Hawkins, M.W; Ottewill, R.H.. **Viscoelastic Properties of Concentrated Latices. Part 2 - Theoretical Analysis.** *J. Chem. Soc., Faraday Trans. 1.* **1982,** 78, 2889-2899.

5.15 **Coagulation Kinetics and Structure Formation.** Sonntag, H.; and Strenge, K.. (Plenum Press, London, UK). **1987.**

5.16 **Rheology of Non-Newtonian fluids: A new flow equation for pseudoplastic systems.** Cross, M.M.. *J. Colloid Sci.* **1965,** 20, 417-437.

5.17 **An introduction to rheology.** Barnes, H.A.; Hutton, J.F.; Walters, K..(Elsevier, Amsterdam). **1989.**

5.18 **The yield stress myth.** Barnes, H.A.; Walters, K.. *Rheologica Acta* 24, 323, **1985.**

5.19 **Colloidal Dispersions: Ch. 8. Some Uses of Rheology in Colloid Science.** Goodwin, J.W.. Goodwin, J.H. Editor (R. Soc. Chem. - Spec. Pub. 43, London, UK). **1981.**

Chapter 6

EVALUATION OF FACTORS DETERMINING PARTICLE INTERACTIONS

6.1 INTRODUCTION

By the macroscopic mechanical properties of a concentrated suspension are meant those properties which are important for the behaviour of a suspension in use. Representative properties are the viscosity and the rate of sedimentation, which determine the pourability and the clear layer formation, respectively. These properties should be constant over the whole height of a suspension sediment and should remain so during storage, also at elevated temperature. Hence, the first condition for acceptable mechanical properties of a suspension is that its colloidal stability is obtained and maintained (see chapters 1 and 2).

An inventory has led to the insight that the mechanical properties of the suspension are mainly influenced by:
a. The density difference between the solid and the liquid phase. This is one of the parameters influencing the rate of clear layer formation.
b. The viscosity of the liquid phase, which is directly proportional to the viscosity of the suspension (see Eq. 5.34), and
c. The solid - solid interactions.
The last factor is the result of the van der Waals attraction and the (electrostatic or steric) repulsion. For a given suspension the repulsion is the only variable that can be changed.

In Chapter 3 the theory of van der Waals attraction was discussed. Using this theory an estimation can be made of the Hamaker constants and the van der Waals attraction for our systems studied. In Chapter 4 we have dealt with the theory of electrostatic repulsion in non-aqueous suspensions. In Chapter 5 the experimental methods were discussed. In the current chapter we give the results of our electric and dielectric measurements. In this study we have concentrated on the behaviour of two low-polar nonionics, which are representative for two important groups. These are Plurafac LFRA30, an EO/PO nonionic with a dielectric constant of $\leq$ 6, and Imbentin C91/35, an all-EO nonionic with a dielectric constant $\geq$ 6 (see sect. 2.2.1). The suspension stabilizer is dodecylbenzene sulphonic acid, DoBS-acid or HDoBS (see sect. 2.2.4 and sect. 5.2.1), i.e. an ingredient which in combination with a detergent solid in suspension is quantitatively converted into the sodium salt NaDoBS (see sect. 5.4.1.1).

The present chapter contains three sets of data. The first involves the results of electric and dielectric measurements of the supernatants of suspensions. The

second set includes electrokinetic (ζ-) potentials. These two sets allow the calculation of the electrostatic repulsion. The third set comprises the evaluation of Hamaker constants from refractive indices and dielectric constants. The results of the three sets will be combined to construct the energy and force DLVO curves, which will be used in Chapter 7 to interpret the mechanical properties.

6.2 IONIC STRENGTHS AND DIELECTRIC CONSTANTS IN NONIONICS; DEBYE LENGTHS

6.2.1 Elemental analysis and conductivities in suspension supernatants

6.2.1.1 Unstable nonionic suspensions

When an electrical field is applied to the 'pure' nonionics Plurafac and Imbentin a small current can be measured. This observation of a non-zero conductivity is an indication of the presence of ions, in spite of our attempts to remove all dissolved ionic species in a series of ion-exchange steps (sect. 2.2.2). If these nonionics are the supernatants of suspensions, usually even higher conductivities can be found. To identify the dissolved ionic species elemental analysis is carried out. The ion formation is quantified by the measurement of conductivities in supernatants of unstable and of stabilized suspensions.

A first indication of the non-zero solubility of a particular crystalline detergent solid, viz. STP in Plurafac and Imbentin, was given already in Table 2.3. That work was extended to the other solids suspended in these two nonionics. Elemental analysis was carried out in supernatants of concentrated suspensions, which were equilibrated for more than six months. The applied procedures and the analytical methods are discussed in sect. 5.4.1.1.

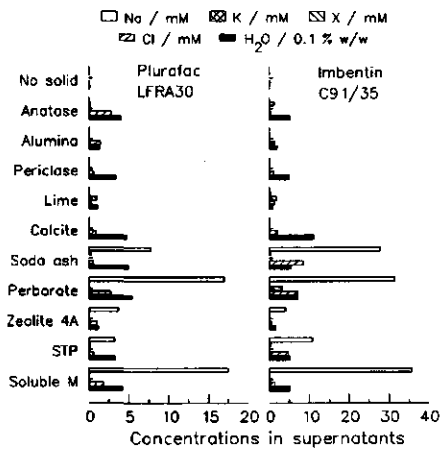

Fig. 6.1: Concentrations of Na, K, X, Cl and H_2O in supernatants of suspensions in Plurafac and Imbentin (X refers to the central atoms, i.e. STP: X=P, Alumina: X=Al, etc.)

After elemental analysis of supernatants of crystalline detergent salts it is found in both nonionics that sodium is the only cationic element present in significant amounts. The results of the analysis of all the solids applied are shown in Fig. 6.1. To our great surprise, in the supernatants of suspensions of Na perborate, Na phosphate, Na silicate or Zeolite 4A, the concentrations obtained by elemental analysis of B, P, Si and Al, respectively (indicated in Fig. 6.1 by

X), hardly exceeded the detection limits. Hence, we could not find concentrations of elements that could indicate the presence of dissolved crystalline detergent salts. The concentrations found showed that the solubilities of these solids in the nonionic are maximally 0.01 % w/w (Perborate in Imbentin).

The only other element that was found in significant amounts was chlorine. However, also for this element in all cases the concentrations remained low in comparison to the Na concentrations found. Since carbon atoms cannot be determined by the analytical procedures applied, ion levels from this element (such as expected from soda ash) could not be given. Carbonate may thus be present and also act as a compensating ion for the Na atoms. The detection of water in most supernatants in concentrations $\leq$ 0.5 % w/w makes it also possible, that compensating ions are present in the form of hydroxyl groups. Hence, the species in the nonionic supernatants in equilibrium with the detergent solids is supposed to consist of a mixture of NaCl, Na_2CO_3 or NaOH, henceforth collectively denoted as NaR.

In the suspensions of the oxides and Calcite, the elemental analysis of nonionic supernatants showed no detectable concentrations of Ti, Al, Mg, Ca (X in Fig. 6.1) in suspensions of Anatase, Alumina, Periclase, Lime or Calcite, respectively. In these suspensions also no Na atoms could be detected.

The ion formation in the supernatants of unstable suspensions was monitored by measuring the conductivities (see sect. 5.4.1.2). The results of the conductivity measurements are summarized in Fig. 6.2. In the supernatants of suspensions of oxides and Calcite the conductivities are found to be all very low. They range from 0.1 to 1.9 $\times 10^{-6}$ S m^{-1} in Plurafac and from 0.6 to 18 $\times 10^{-6}$ S m^{-1} in Imbentin. They have the same magnitude or are only slightly higher than the conductivity of the nonionics without solids. However, after addition of the crystalline detergent solids to the nonionics the conductivities of the supernatants rose, but in Plurafac less than in Imbentin. [Note: For STP suspensions this was shown already in Table 2.3.]

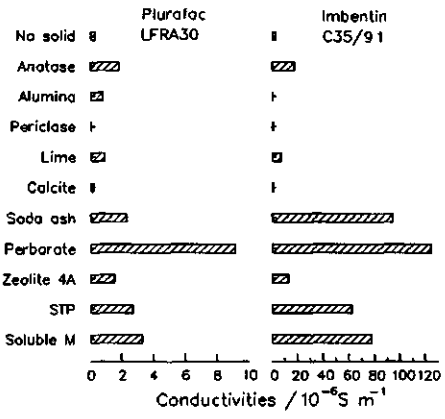

Fig. 6.2: Conductivities in supernatants of suspensions of detergent solids and oxides in nonionics Plurafac and Imbentin.

6.2.1.2 HDoBS-stabilized suspensions

The effect of NaDoBS on dissociation and ion formation in Plurafac and Imbentin is monitored by measuring the conductivities in these two nonionics in a dilution series, using NaDoBS from a stock solution. The results are represented graphically in Fig. 6.3, where results are plotted on logarithmic scales. Results are also given for the case NaDoBS is formed in situ from HDoBS and suspended STP or Soda ash. In Plurafac and Imbentin the curves of NaDoBS formed in situ from HDoBS and the different solids largely coincide with the curves found with NaDoBS from stock solution. This demonstrates that our method is consistent and that NaDoBS is indeed the reason for the increase in conductivity.

Two observations in the conductivity patterns obtained are of interest:The first is that the conductivities rise continuously with the NaDoBS concentrations in both nonionics. In this sense the conductivity - concentration curves of the anionic NaDoBS in nonionic are completely different from those of the same ingredient in water, where a constant conductivity is found beyond the critical micelle concentration. A sharp discontinuity indicative for such a critical micelle formation is not found in our nonionics in the concentration range studied.

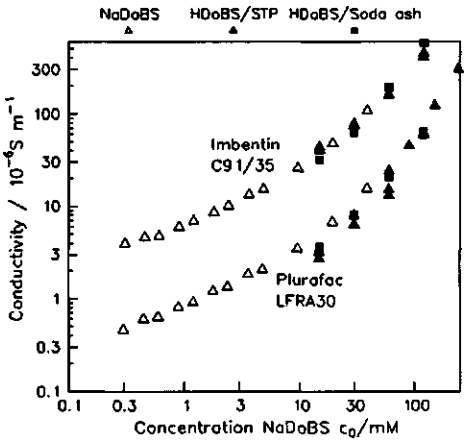

Fig. 6.3: Conductivities with NaDoBS in Plurafac and Imbentin. NaDoBS formed in situ from HDoBS added to suspensions of crystalline detergent solids and NaDoBS from stock solution.

The second interesting observation is that the conductivities in both nonionics tends to rise more than proportionally with the concentration of NaDoBS. This means that a minimum had developed, if a molar conductivity - concentration curve would have been constructed. Qualitatively, this observation is in line with the results of van Mil et al. (1982) [6.1], who, for NaAOT in hexane/paraffin mixtures, postulated an ion-stabilizing influence from NaAOT ion-pairs and leading to triple ions (see sect. 4.3.2.3). However, as the concentration range in which we observe the effect is much higher ($>$ 30 mM against $\leq$ 1 mM), this is not a very likely explanation in our case. Klinkenberg and van der Minne (1958) [6.2] also observed similar results for solutions of various electrolytes (i.e. Dips (Di-isopropyl salicylate), Tiap (Di-isoamyl ammonium picrate) or of CPB (Cetyl pyridinium bromide)) in non-polar hydrocarbons. They explained their results from the formation of 'large molecular associates' which enhanced the dissociation (sect. 4.3.2.3). It is possible that under our conditions associated NaDoBS, e.g. when involved in a slow micelle formation, binds other ions and stabilize ions similarly. However, we think that the formation of molecular

associates is not necessary to explain the more than proportional increase of the conductivity in our suspensions. An alternative explanation is that an increase in the NaDoBS concentrations also leads to an increase in the dielectric constant of the liquid phase (see sect. 6.2.3). According to Fuoss's equation (Eq. 2.5), simply this element can contribute already to the increase of the dissociations and ionic strengths. This will be quantified further in sects. 6.2.3.2 and 6.2.2.3.

6.2.2 Ionic strengths in supernatants

6.2.2.1 Unstable nonionic suspensions

When the dissociating species in the nonionics that cause the increased conductivity may be called NaR, its ionic strength might be estimated from its limiting molar conductivity, applying Eq. 5.15. Limiting conductivities of NaR in nonionics are not available, but can be derived roughly from the known values in water and applying Walden's rule (Eq. 5.21). They are estimated in Plurafac and Imbentin to be about 3.5 and 7 $\times 10^{-4}$ S m^2 mol^{-1}, respectively. When it is supposed that all Na is present in the form of Na_2CO_3, the ionic strengths are estimated to range from 0.002 to maximally 0.04 mM in Plurafac and from 0.002 to 0.25 mM in Imbentin. These estimated ionic strengths in pure nonionics are usually lower at least by a factor of ten than those obtained in HDoBS-stabilized suspensions at the levels of $\geq$ 10 mM (i.e. 0.3 %) (see sect. 6.2.1.2). This contribution to the ionic strengths is therefore ignored.

6.2.2.2 Nonionic suspensions stabilized with HDoBS

In suspensions of crystalline detergent solids with added HDoBS, from the measured specific conductivities K of the supernatant, the ionic strengths in the bulk of the liquid phase c_i can be directly derived from the established limiting molar conductivities Λ_0 of NaDoBS in Plurafac and Imbentin being both 1.02 $\times 10^{-4}$ S m^2 mol^{-1}. The Shedlovsky crowding factor $s(z)$ and the degree of dissociation α can be evaluated from the experimental data for the dielectric constants ε and the supernatant viscosities η_c (see sect. 5.4.1.3). Ionic strengths thus obtained for a number of supernatants of practical suspensions in Plurafac and Imbentin are given in Fig. 6.4.

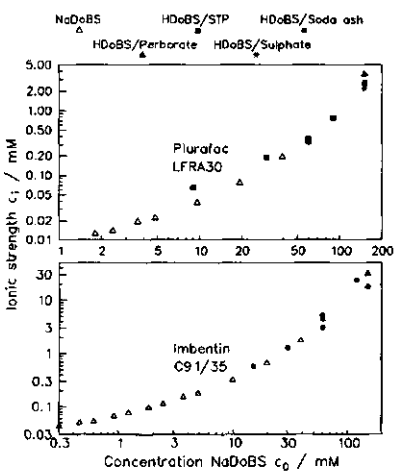

Fig. 6.4: Ionic strengths as a function of the concentration NaDoBS in Plurafac and Imbentin. NaDoBS formed in situ or added from stock solution.

The results show that for NaDoBS concentrations between 10 mM and 150 mM, the ionic strengths increase

from roughly 0.05 to 4 mM in Plurafac or from 0.3 to 30 mM in Imbentin. The results indicate that the degree of dissociation α is about 0.01 in Plurafac and 0.15 in Imbentin. The observed ionic strengths are all much higher than usually reported in non-polar non-aqueous media. The experimental results show that ionic strengths between Plurafac and Imbentin can differ by an order of magnitude at equal electrolyte concentrations.

6.2.2.3 Theoretical prediction by Fuoss's equation

From the ionic strengths, the dissociation constants of NaDoBS in the nonionics Plurafac and Imbentin are calculated, using a rearranged form of Eq. 4.48. The procedure is applied with NaDoBS predissolved in a stock solution and with NaDoBS formed in situ from addition of HDoBS to a suspension of STP in Plurafac or to a suspension of Soda ash in Imbentin. The dissociation constants are plotted as a function of the dielectric constant of the liquid phase in Fig. 6.5. The results are also compared with the theoretical dissociation constants obtained from the Fuoss equation (Eq. 2.5), using the ion pair radii given in sect. 5.4.1.3.

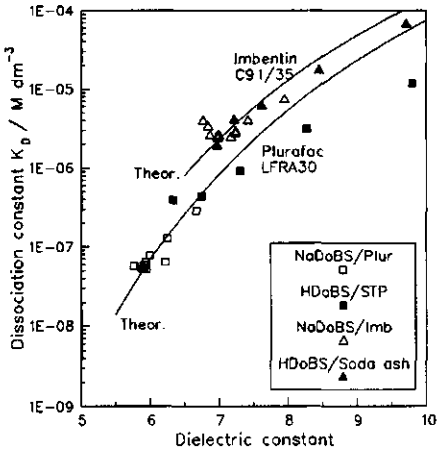

Fig. 6.5: Dissociation constants of NaDoBS in the nonionics Plurafac and Imbentin; experimental values compared with theoretical values (drawn curves). NaDoBS formed in situ or from stock solution.

Figure 6.5 shows that, for Imbentin as well as for Plurafac, the dissociation constants can be predicted reasonably well from the Fuoss theory, although at higher values of the dielectric constant the experimental results are lower than theoretically predicted. It has to be noted here that the higher dielectric constants are obtained with higher levels of NaDoBS (see Fig. 6.7), which is predominantly present in an undissociated form. Hence, the observed enhanced dissociation on increased NaDoBS levels can to a large extent be ascribed to a macroscopic effect, i.e. the enhancing influence of NaDoBS on the dielectric constant. Microscopically, the effect may be related to a stimulated dissociation due to solvation of the Na^+ and $DoBS^-$ ions by excess ion-pairs of Na^+DoBS^-, which is analogous to the triple ion formation proposed by van Mil et. al (1982) [6.1] (see Fig. 4.9).

At higher dielectric constants the dissociations are lower than predicted by the Fuoss theory (Fig. 6.5). This deviation may be ascribed to a reduced efficacy of the solvation process at higher NaDoBS concentrations. This may occur when NaDoBS is organized in molecular associates. It is striking that the solvation efficacy is more reduced in Plurafac than in Imbentin. This would suggest that the molecular associate formation occurs more easily in Plurafac than in Imbentin,

whereas Imbentin solvates the NaDoBS more strongly so that molecular associates are less easily formed. This stronger solvating influence of Imbentin is consistent with the higher dissociations and with the lower mobilities of Na^+ and $DoBS^-$ ions found in this nonionic (sect. 5.4.1.3).

6.2.3 Dielectric constants of the supernatants

6.2.3.1 Unstable suspensions

The influence of the presence of solids on the dielectric constant of the supernatants is also measured in supernatants of unstable suspensions in the two nonionics Plurafac and Imbentin. Results are given in Fig. 6.6.

The presence of oxides leads in some cases to a rise of the dielectric constant. Occasionally this increase was larger than the accuracy of the experiments, which had an average standard deviation of $\pm$ 2 %. It is assumed that the rise observed is a result of a release of water from the oxides. Since, the dielectric constant of water is ca. 13 times higher than that of the nonionics, an increase of the water content in the nonionic by 0.6 % is already sufficient to cause a rise of the dielectric constant that is larger than the experimental error. The finding, with some oxides, of a decrease of the dielectric constant may be a result of the fact that some oxides are able to withdraw water from the nonionic. With the crystalline detergent solids also an increase of the dielectric constant of the supernatants was detected. As for the oxides, the rise is ascribed to a release of water from the detergent solids (see sect. 6.2.1.1). Unfortunately, the accuracy of the measurement of the dielectric constants is not sufficient to come to firmer conclusions, at this moment.

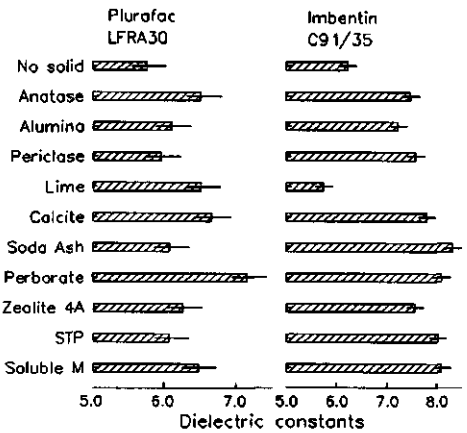

Fig. 6.6: Dielectric constant of supernatants of suspensions of crystalline detergent solids and oxides in nonionics Plurafac and Imbentin. [Note: The lines in the bars indicate the average error.]

6.2.3.2 Stabilized suspensions

The dielectric constant ε of the liquid phase is one of the parameters which determines the electrostatic repulsion (see sect. 4.3.1.3). Having a dielectric constant of 36.8, NaDoBS is considerably more polar (see Table 6.3) than the nonionics and it was expected that its presence had an enhancing influence on the dielectric constant of the continuous phase. To quantify this, the dielectric constants were measured in supernatants of NaDoBS in nonionic. Again, the effect

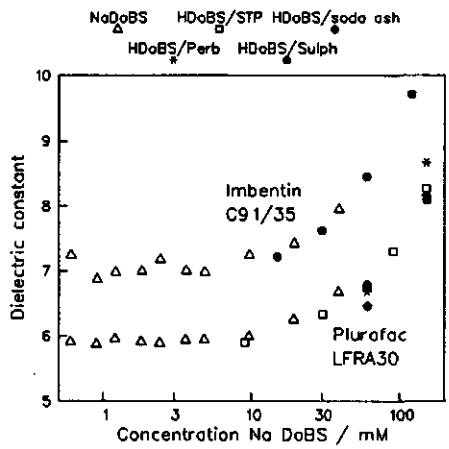

Fig. 6.7: Dielectric constant as a function of NaDoBS concentration in Plurafac and Imbentin. NaDoBS formation in situ or NaDoBS from stock solution.

stimulating influence on the dissociations. was measured by addition of NaDoBS formed in situ as well as by addition of preformed anhydrous NaDoBS.

From the results, given in Fig. 6.7, it can be derived that the dielectric constant of the nonionic liquid is increased with approximately half a unit with every added 30 mM (1 % w/w) of NaDoBS. Moreover, it can be concluded that it makes no difference whether the NaDoBS is formed in situ or whether it is preformed, demonstrating that in the three component systems the presence of the solids has no influence on the dielectric constant of the continuous phase. It was shown already in sect. 6.2.2.3 that the enhancement of the dielectric constant by NaDoBS has a

6.2.4 Debye lengths in nonionics

The Debye lengths of NaDoBS in the nonionics Plurafac and Imbentin are calculated using Eq. 4.3, applying the experimental results for the dielectric constant and for the ionic strengths. The ionic strengths were derived from the conductivities (sect. 6.2.2.2) and from the limiting molar conductivity (sect. 5.4.1.3).

The Debye lengths are presented as function of the NaDoBS concentration in Fig. 6.8. Again the plot is given for solutions of NaDoBS prepared separately, as well as for NaDoBS formed in situ, i.e. from HDoBS added to a suspension. Figure 6.8 shows that the Debye lengths in Plurafac range from 33 to 1 nm and in Imbentin from 13 to 1 nm, dependent on the NaDoBS concentration. To our knowledge it is the first time that such short Debye lengths are reported in media in this range of dielectric constants.

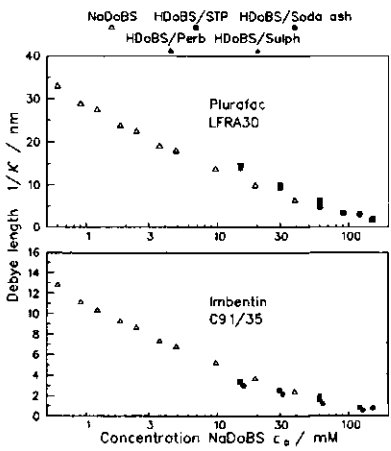

Fig. 6.8: Debye length as a function of NaDoBS concentration in the nonionics Plurafac and Imbentin. NaDoBS prepared in situ from addition of HDoBS to suspensions of solids and NaDoBS from stock solutions.

6.3 ZETA POTENTIALS

6.3.1 Influence of DoBS acid concentration

6.3.1.1 Results

Electrophoretic mobilities of a number of crystalline detergent solids in nonionic are measured with particles from different suspensions with varying amounts of HDoBS. The procedure of measurement is given in sect. 5.4.2.1. The electrophoretic mobilities are converted to ζ-potentials using Eqs. 5.23 or 5.24. Results obtained in Plurafac and Imbentin are given in Fig. 6.9 (top) and (bottom), respectively.

As a function of HDoBS concentration a rather sharp change in ζ-potentials is found in both nonionics which levels off already after addition of 0.5 % DoBS-acid (i.e. 15 mM dm^{-3}). The ζ-potentials start with a negative value in Plurafac. Depending on the nature of the solids, ζ varies from -30 to -22 mV, and changes upon addition of HDoBS to positive, i.e. up to +45 to +75 mV. In Imbentin, after addition of HDoBS, ζ-potentials for soda ash reaches similar positive values, however, those of STP remain lower. Contrary to Plurafac, the initial ζ-potentials in Imbentin are near zero or slightly positive.

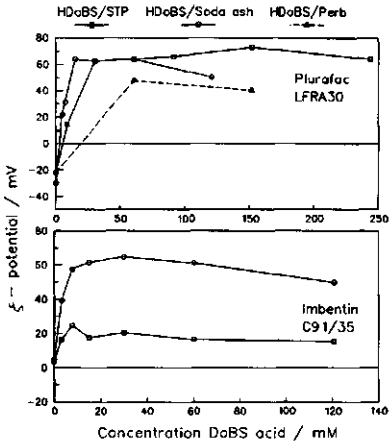

Fig. 6.9: ζ-potentials of crystalline detergent solids as a function of HDoBS concentration in the nonionics Plurafac and Imbentin.

6.3.1.2 Discussion; a mechanism proposed for surface charging

The observations of positive ζ-potentials and the formation of NaDoBS after the addition of HDoBS to a suspension in nonionic, are assumed to be a result of the preferential adsorption of H^+ ions on the surface. This causes the surfaces to become positively charged. A proposed mechanism is given in Fig. 6.10a. Alternatively, the final situation can be described as the result of adsorption of Na^+ ions by a (by HDoBS) hydroxylated surface (see Fig. 5.2). The distribution of ions over surface and double layer is presented graphically in Fig. 4.1. [Note: It may also be that the positive surface charging rises because of an increasing affinity of the $DoBS^-$ anion for the continuous phase. This point of view is in agreement with the observation that for small anions, such as from adsorbed water, the affinity of the OH^- ion for the continuous phase is much smaller and does not lead to the formation of such high positive surface charges.]

The charging process is more efficient with H^+ than it is with Na^+. This is concluded from the observation that by using NaDoBS instead of HDoBS, the positive ζ-potentials are much lower. This result could be a reflection of the stronger (Lewis) acidity of H^+ in comparison to Na^+ ions with respect to the surface, which is supposed to be of (Lewis) basic nature. The proposed mechanism of surface charge formation in our system is analogous to that proposed by various researchers of charge formation by NaAOT and 'polar' surfaces or oxide particles suspended in hydrocarbons (Koelmans and Overbeek, 1954 [6.3], Lyklema, 1968 [6.4], McGown, Parfitt and Willis, 1965 [6.5]; Kitahara, 1967 [6.6], 1973 [6.7] and 1977 [6.8], Parfitt and Peacock, 1978 [6.9] and van Mil, Crommelin and Wiersema (1984) [6.10].

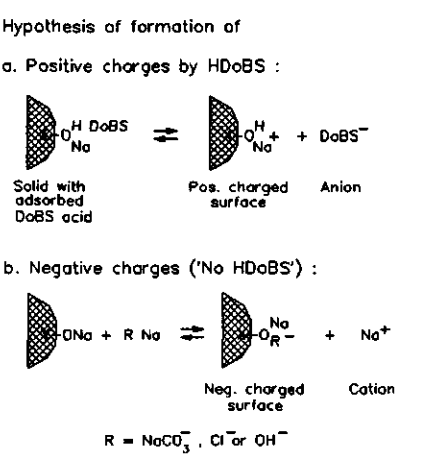

Fig. 6.10: Mechanisms explaining the charge formation of crystalline detergent solids in nonionic: a. after the addition of HDoBS, b. in unstable suspensions ('No HDoBS').

Still another interesting observation emerges from Fig. 6.9: The ζ-potentials in the zero acid situation are different. In Plurafac they are clearly negative whereas in Imbentin they are near zero or slightly positive.

It is assumed that the negative ζ-potentials observed in Plurafac are due to a surface affinity of R^- ions (see Fig. 6.10b) and caused by the weak ion-solvating properties of Plurafac for the R^- ions (see sect. 6.2.2.3). An alternative hypothesis is that the negative ζ-potentials originate from an abstraction by the nonionic of Na^+ ions from the detergent solid. The nonionic would then act as a crown-complexant (see sect. 4.3.2.2) or in Lewis terms as a base, similar to the observation by Labib and Williams regarding strongly electron-donating solvents (1984/1986 [6.11], 1988 [6.12]). Because of the high ionic mobilities and weak complexing properties of Plurafac for cations observed (i.e. its weak Lewis basicity) this hypothesis is less likely.

Contrary to Plurafac, in Imbentin no negative ζ-potentials are found in the zero acid situation. That in this nonionic no preferential surface adsorption of R^- ions occurs is ascribed to the stronger affinity of this medium for R^- ions. This observation is consistent with the stronger solvation of ions in Imbentin and which was inferred from the reduction of the ion mobilities (sect. 6.4.1.3). The (small) positive ζ-potentials found in Imbentin, suggest that the affinity of the surface for the Na^+ ions is (slightly) higher than that of the nonionic. The values of ζ for suspensions without HDoBS show that the balance between the surface affinity for R^- or Na^+ ions, relative to the solvating character of the nonionic for these ions, determines the magnitude and the character of the surface charge. This subtle

balance is disturbed by addition of DoBS acid. Surface charging it the third effect of HDoBS and next to the increase in ionic strength and in dielectric constant.

6.3.2 Influence of solvation enhancing additives

The Gibbs free energy of solvation can be influenced by 'additives' of the liquid phase. Since the Gibbs energy of adsorption does not change, according to the mechanism of charge formation proposed in sect. 6.3.1.2, additives could have a considerable influence on the ζ-potential. Two additives of interest for these systems will now be particularly considered: viz. a crown-ether and water.

6.3.2.1 A crown-ether additive

The crown-ether 15-Crown-5 has particularly strong complexing properties for Na^+ ions (Fig. 6.11) and is soluble in nonionic. It was added to Plurafac to enhance its solvating power in amounts up to maximally 10 % w/w of the liquid phase. At that concentration it caused a (limited) increase of the dielectric constant of approximately one unit, whereas proportionally lower dielectric constants were found with lower levels. Based on its properties it was

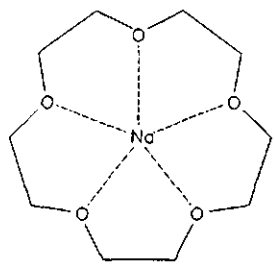

Fig. 6.11: Molecular structure of a crown complexant, i.e. 15-Crown-5. For clarity C- and H-atoms are omitted.

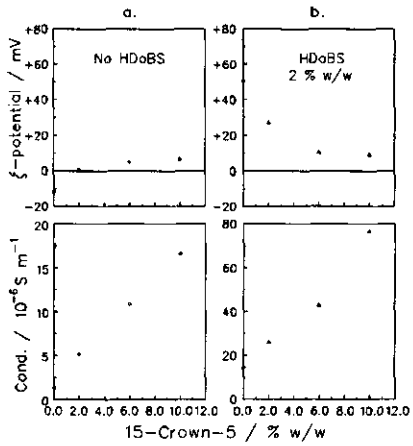

Fig. 6.12: Influence of crown complexant (15-Crown-5) on the ζ-potential and conductivity of a suspension of STP in Plurafac a. with no added HDoBS, b. with 2 % w/w HDoBS.

expected that the crown-ether would particularly enhance the solvating power for Na^+ ions of the Plurafac continuous phase. Experiments are carried out in STP suspensions free of HDoBS and in STP suspension stabilized with 2 % w/w HDoBS. Results are given in Fig. 6.12a and b, respectively. In these figures the results of the measurements of the ζ-potential (top curves) and of the conductivity (bottom curves) are shown.

In HDoBS-stabilized suspensions (Fig. 6.12b) the predicted effect of a higher crown-complexant concentration is that of an enhanced dissociation of NaDoBS, resulting in a higher

conductivity, a stronger solvation and lower mobility of ions and hence a lower positive ζ-potential. The results demonstrate that the conductivity and ζ-potential patterns observed are in agreement with the predictions. The results are consistent with the mechanism of charge formation in the presence of DoBS acid given in Fig. 6.10a and discussed in sect. 6.3.1.2.

In HDoBS-free suspensions the influence of the crown-ether additive is more complex. Addition of the crown-ether results in a rise of the conductivity (see Fig. 6.12a, bottom curve) demonstrating the expected stimulation of the dissociation of NaR (see sects. 6.2.1.1 and 6.2.2.1). The negative ζ-potential, typical for unstable suspensions in Plurafac, decreases on addition of the crown-ether. This is in agreement with the increased solvation of Plurafac and consistent with the behaviour of Imbentin (sect. 6.3.1.2), having also a stronger solvation of ions and inferred from its reduction of the ion mobilities (sect. 6.4.1.3). The reason for the (slightly) positive ζ-potentials on further addition of the crown-ether is not well understood. It demonstrates that the affinity of the continuous phase for R^- slightly increases from the addition of the crown-ether. It may that this is the result of the higher Na^+ and R^- ion concentrations in the liquid phase.

6.3.2.2 The influence of water as additive

The second additive investigated is water. The role of water in the dissociation and charge formation in non-aqueous media is often complex. In various studies it is shown that moisture in non-aqueous media has a variable effect on the formation and sign of the surface charges (McGown, Parfitt and Willis, 1965 [6.13]; Labib and Williams, 1986 [6.14]; Logtenberg and Stein, 1986 [6.15]; Goodwin, et al., 1988 [6.16]). In some of these studies it was noted that water is essential to obtain positive charges with NaAOT.

Small amounts of moist liberated from the solids sometimes result in a water content of the nonionic which is considerably higher than that of the starting nonionic (see Fig. 6.1). Hence, small amounts of water, particularly in practical systems, cannot be excluded completely and may therefore affect the charge stabilization mechanism. In our HDoBS-stabilized nonionic suspensions it is found that the mechanical properties of the suspensions did not change very much at water levels lower than 1 % w/w. Even at slightly higher levels sometimes good pourability was maintained.

It had to be expected that addition of water to the nonionic would lead to more dissociation, a strong solvation and reduced ion mobilities for Na^+ and R^- ions. In HDoBS-stabilized systems the predicted effect of water is like that of the crown-ether, i.e. a larger affinity of the solvent for Na^+ ions, a decreased mobility and a reduced positive ζ-potential.

The results of the experiments, with water deliberately added to a suspension of STP in Plurafac stabilized with 2 % HDoBS, having an initial water content of 0.3 % w/w, confirms this (Fig. 6.13, top graph). However, the conductivity results in these experiments were unexpected. As is shown in Fig. 6.13 (bottom graph) the

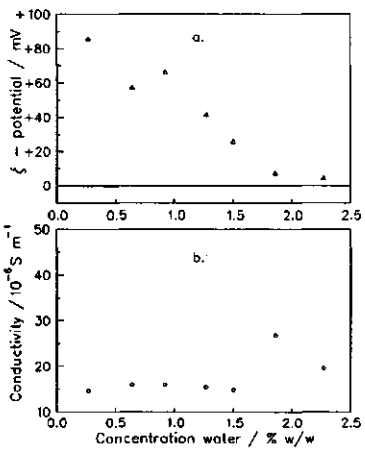

Fig. 6.13: Influence of water concentration a. on the ζ-potential and b. conductivity of a suspension of STP in Plurafac.

conductivity up to ≥ 1.5 % w/w did not increase with rising concentrations of water. Hence, in this experiment no clear increase of the solvating power of the nonionic liquid upon addition of water is observed that is in agreement with the decrease of the ζ-potential. There may be two explanations for this observation: The ζ-potential decreases because of an increased binding of water to the surface. This could cause an increased concentration of counterions ($DoBS^-$ or R^-) in the Stern-layer surrounding the particles. Another explanation could be that there is an enhanced dissociation in the liquid phase leading to more Na^+ ions, but the effect on dissociation is reduced by a reduced mobility due to an enhanced solvation. When these two effects compensate each other, no change in the conductivity will be seen. The effects of water on the ζ-potential seem qualitatively correlated with the pourability results (see also sect. 7.3.1.2).

6.3.3 Solids with other positive ions

6.3.3.1 Mica

Electrophoretic mobilities are measured of 4 μm mica particles (ex Norwegian Talc) suspended in Plurafac. Mica is a potassium alumina-silicate mineral (Muscovite) with the overall chemical structure $KAl_2Si_3AlO_{10}(OH,F)_2$. The suspensions of mica were made in the absence and in the presence of 5 % w/w HDoBS.

The results, given in Fig. 6.14a, show that in the absence of HDoBS, as with the crystalline detergent solids, with mica a negative ζ-potential is found of -32 mV. Elemental analysis of unstable mica suspensions demonstrated that in the supernatant K is the dominant element, whereas Al and Cl concentrations remained below

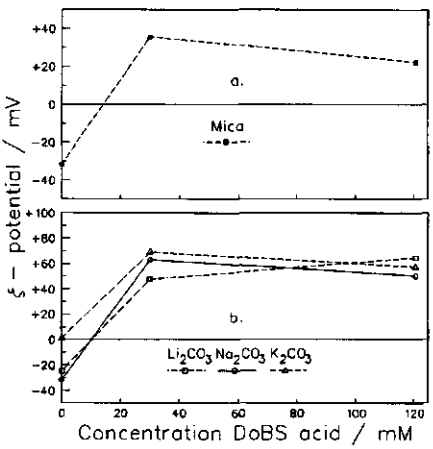

Fig. 6.14: ζ-potential as a function of HDoBS concentration in Plurafac of suspensions of a. mica, and b. lithium, sodium and potassium carbonate.

the detection limits. The concentration of K in the supernatant was even ten times as high as that of Na. The results suggested that a K salt (K_2CO_3?) is the dominating dissolved species and, after dissociation, responsible for the conductivity in the absence of acid.

In HDoBS-stabilized mica suspensions a ζ-potential is found of +36 mV. Hence, analogous to the behaviour of the crystalline detergent solids addition of HDoBS changes the sign of the surface charge. The positive ζ-potential is lower than that of the sodium salts in Plurafac discussed earlier (see Fig. 6.9). It suggests a weaker affinity of the hydroxylated mica surface for K^+ ions, as compared with the affinity for Na^+ ions in detergent solids (see Fig. 6.10a).

6.3.3.2 Lithium and potassium carbonate

In order to obtain insight into the influence of the size of the positive ion on the surface charge formation, electrophoretic mobilities are measured of lithium carbonate (Li_2CO_3) and potassium carbonate (K_2CO_3) particles in Plurafac. The suspensions of these carbonates were made in the absence and in the presence of 1 and 4 % w/w HDoBS. The results are given in Fig. 6.14b. [Note: The ionic strengths in the supernatants were estimated from the conductivity and an estimated limiting molar conductivity. Since the limiting conductivities were not available they were derived from the limiting conductivities in water and Walden's rule. The ionic strengths obtained were used to estimate κa and to evaluate the ζ-potentials. Because of the uncertainty in the ionic strengths, the results can have only indicative value.]

The results show that, in the absence of HDoBS, again negative ζ-potentials were obtained: with the Li salt the potential was -25 mV, i.e. in same range as the Na salt, and with the K salt -1 mV. The results demonstrate that the affinity of the solvent for the anion (R^-) is stronger in case of a potassium salt than in case of a lithium salt. The small differences in positive ζ-potentials emerging after application of HDoBS, suggests that there is no difference in affinity of the hydroxylated solids for the different alkali metal ions. The results suggest that the solvation of the $DoBS^-$ anion in the nonionic is the dominant factor controlling the ζ-potential.

6.3.4 Surface charge densities

The electrokinetic results allow the determination of the surface charge densities σ_0 (C m^{-2}). It can be derived from the Gouy-Chapman theory, that the charge density on a flat surface σ_0 can be obtained from (Verwey and Overbeek, 1948 [6.17])

$$\sigma_0 = 4 n_i e \frac{1}{\kappa} \sinh \frac{e \psi_0}{k_B T} \qquad [6.1]$$

With this equation the surface charge density can be calculated from the ionic strengths and the dielectric constant, substituting ζ for the surface potential ψ_0. For

suspension stabilized with 2 % w/wHDoBS, i.e. at c_0 = ca. 60 mM, it is found in this way that surface charge densities range from 0.4 to 1 $\times 10^{-3}$ C m^{-2} in Plurafac and from 1 to 2 $\times 10^{-3}$ C m^{-2} in Imbentin. These values are at least one order of magnitude lower than those usually found in aqueous media.

6.4 HAMAKER CONSTANTS

6.4.1 Inorganic solids (crystalline detergent salts and oxides)

Dielectric constants and refractive indices of the inorganic solids used in this study are given in Table 6.1. For the crystalline detergent solids the data are obtained with the methods described in sects. 5.3.2.1 and 5.3.2.2; the values for the oxides are taken from the CRC Handbook (1987, 67th. Ed), except those for Anatase (Pascal, 1963 [6.18]). The dielectric constants of the crystalline detergent solids and of the oxides (except Anatase) appeared to be in the same range as those

Table 6.1: Refractive indices and dielectric constants of solids (crystalline detergent salts and oxides) used in the present study.

	Solid	Refractive index[a] (25°C) n	Dielectric constant[a] (25°C) ε
1	Anatase	2.53[b]	48[c]
2	α-Alumina	1.764[b]	6.5[b]
3	Periclase	1.736[b]	9.7[b]
4	Lime	1.838[b]	7.5[b]
5	Calcite	1.581	8.3[b]
6	Perborate monohydrate	1.500	6.5
7	Zeolite 4A 'activated'	1.439	14.5
8	Soda ash	1.492	8.4[b]
9	STP	1.478	6.3
10	Soluble M	1.486	4.7

[a] Results of this work (see sects. 5.3.2.1 and 5.3.2.2);
[b] Data ex Handbook (CRC); [c] Pascal, 1963 [6.18].

of the nonionics (see Table 2.1) and show that all solids except Anatase are all fairly poor conductors.

From the dielectric constants and refractive indices of Table 6.1, the Hamaker constants for interactions in vacuum of the crystalline detergent solids and of the oxides are evaluated. The Hamaker constants are calculated using the macroscopic Lifshitz-Israelachvili theory and the (modified) microscopic Hamaker-de Boer-Slater-Kirkwood theory. The results are given in Table 6.2.

Table 6.2: Hamaker constants in vacuum (A_{11}) of solids used in the present study.

	Solid	Hamaker constant (Macr.)[a]	s[b]	Hamaker constant (Micr.)[c]	Hamaker constant (Lit.-data)
		$A_{11}/10^{-20}$ J		$A_{11}/10^{-20}$ J	$A_{11}/10^{-20}$ J
1	Anatase	38.2	2.7	35.8	19.7[d] 20.5[e]
2	α-Alumina	14.1	2.4	18.9	15.5[d] 11.9[f] 15.6[g]
3	Periclase	13.3	2.0	15.5	10.6[d] 7.7[f]
4	Lime	16.3	2.0	15.9	12.4[d]
5	Calcite	9.1	2.4	11.8	10.1[g]
6	Perborate monohydrate	7.0	1.7	8.3	
7	Zeolite 4A 'activated'	5.6	2.3	6.5	
8	Soda ash	6.8	2.0	9.3	
9	STP	6.5	2.2	8.8	
10	Soluble M	6.7	2.3	8.3	

[a] Calculated using data from Table 5.1 and Eq. 3.18; [b] s: the avg. number of bonding electrons per atom, Eq. 3.29; [c] Calculated from data of Tables 2.2 and 5.1, and Eqs. 3.27, 3.29 and 3.4; [d] Visser (1973) [6.19]; [e] Vincent (1973) [6.21]; [f] Visser (1976) [6.20]; [g] Hough and White (1980) [6.22].

Hamaker constants of altogether a dozen of inorganic substances have been reported by Visser (1973) [6.19], (1976) [6.20], Vincent (1973) [6.21] and Hough and White (1980) [6.22]. Relevant literature values

are also included in Table 6.2. The results of our calculations were used before to create Fig. 3.6. The two methods applied give results which differed by less than a few dozen of a percent. From Table 6.2 it appears further that crystalline detergent solids tend to have lower Hamaker constants than the metal oxides (see also Fig. 3.6). From the comparisons with the data in the referred literature it is suggested that Eq. 3.18 overestimates the Hamaker constants. However, when compared with the results of more recent exact computations, Israelachvili showed for inorganic solids (1985, [6.25], Table XV) that Eq. 3.18 (and thus also the combination of Eqs. 3.27, 3.29 and 3.4) still underestimates the Hamaker constants. In the light of the uncertainties generally encountered in evaluations of Hamaker constants it is concluded, however, that both procedures for the evaluation of the Hamaker constants are satisfactory approximations for the present purposes.

6.4.2 Low-polar nonionic liquids

For the liquid nonionics the Hamaker constants are evaluated from the Lifshitz-Israelachvili theory (Eq. 3.18) using the refractive indices and dielectric constants given in Table 2.1 (see also sect. 5.2.2). The results are collected in Table 6.3. With the aim to indicate the reliability of this procedure the method of calculation was also applied to water and n-dodecane, for which also various literature values are available (Visser, 1973 [6.19], 1976 [6.20]; Churaev, 1972 [6.23]; Vincent, 1973 [6.21]; Hough and White (1980) [6.22], Parsegian and Weiss (1981) [6.24]; Israelachvili (1985) [6.25] and Prieve and Russell (1988) [6.26].

There is a good agreement between the results of Eq. 3.18 and the values given in the literature for water and n-dodecane (Table 6.3), which supports the applicability of Eq. 3.18 for organic substances (see sect. 3.3.1). Hamaker constants of the nonionics Plurafac and Imbentin are found to have both a magnitude of 5.9×10^{-20} J. A value which is slightly higher than the value of 5.5×10^{-20} J for C_8E_6 nonionic reported by Mathai and Ottewill (1968) [6.27].

6.4.3 Inorganic solids immersed in nonionics liquids

6.4.3.1 Crystalline detergent solids and oxides in nonionics

A comparison of the Hamaker constants of the solids and liquids in Tables 6.2 and 6.3, respectively, demonstrates that the crystalline detergent solids, except Zeolite 4A, all have a Hamaker constant different from that of the nonionic. This was already apparent from their higher optical densities. Hence, when these solids are dispersed in nonionic they will experience a van der Waals attraction between the particles and hence tend to coagulate immediately after dispersion. The higher Hamaker constants of oxides reflect that particles of these solids will show an even stronger interaction when dispersed in a low-polar nonionic.

Table 6.3: Hamaker constants in vacuum (A_{11}) of nonionics used in the present study, evaluated using the macroscopic theory. For comparison also the results of water and of n-dodecane are included.

	Liquid	Refract. index (Na_D) (25°C) (n)	Dielectric constant[a] (25°C) (ε)	Hamaker constant (Macr.) $A_{11}/10^{-20}$ J	Hamaker constant (Lit.- data) $A_{11}/10^{-20}$ J
1	Plurafac LFRA30	1.4529[a]	5.70[a]	5.9	
2	Imbentin C91/35	1.4528[a]	6.23[a]	5.9	5.55[k]
3	Na DoBS	1.519[b]	36.8[b]	7.5	
4	n-Dodecane	1.411[b]	2.01[b]	5.0	4.6-5.0[c] 5.04[g] 5.0[i] 4.7[j]
5	Water	1.333[b]	78.54[b]	3.4	4.38[c] 5.1[d] 3.7[e] 3.6[f] 3.7[g] 4.0-6.0[h] 3.7[i] 3.81[j]

[a] This work; methods are given in sect. 5.2.2 (see also Table 2.1); [b] Data ex Handbook (CRC, 67th Ed., 1987); [c] Visser (1973) [6.19]; [d] Churaev (1972) [6.23]; [e] Vincent (1973) [6.21]; [f] Visser (1976) [6.20]; [g] Hough and White (1980) [6.22]; [h] Parsegian and Weiss (1981) [6.24]; [i] Israelachvili (1985) [6.25]; [j] Prieve and Russell (1988) [6.26]; [k] Mathai and Ottewill (1968) [6.27].

The mixed Hamaker constants for the dispersed inorganic solids (nature 1) in the nonionics Plurafac and Imbentin (nature 3), i.e. $A_{11(3)}$, are given in Table 6.4. For the calculation of these Hamaker constants we applied the methods discussed in sect. 3.3.3. On the left-hand-side column the average results are given of method a. (purely macroscopically) and method b. (macroscopically, combined with Eq. 3.30). In the middle column results are given resulting from method c. (the microscopic method, combined with Eq. 3.30). Since in the applied procedures we subtract two close values, each known only with an inaccuracy of a few tens of a percent, this procedure does not allow more than the estimation of an order of magnitude. On the right-hand-side column of Table 6.4 the mean result of the two calculation procedures are given. As for the time being there is no independent

Table 6.4: Hamaker constants of crystalline detergent solids and oxides in nonionic ($A_{11(3)}$), evaluated using the macroscopic and microscopic theories.

	Solid	Hamaker constant (Macr.)[a] $A_{11(3)}$ /10^{-20} J	Hamaker constant (Micr.)[b] $A_{11(3)}$ /10^{-20} J	Hamaker constant Avg. of two methods[c] $A_{11(3)}$ /10^{-20} J
1	Anatase	16.8	12.6	14.6 ± 2.1
2	α-Alumina	2.0	3.7	2.8 ± 0.8
3	Periclase	1.7	2.3	2.0 ± 0.3
4	Lime	2.9	2.4	2.7 ± 0.3
5	Calcite	0.37	1.01	0.7 ± 0.3
6	Perborate monohydrate	0.05	0.19	0.12 ± 0.07
7	Zeolite 4A 'activated'	0.009	0.013	0.01 ± 0.003
8	Soda ash	0.04	0.37	0.20 ± 0.17
9	STP	0.01	0.28	0.15 ± 0.13
10	Soluble M	0.03	0.19	0.11 ± 0.08

[a] Macroscopic: Average of results of Eqs. 3.31, and Eq. 3.18 combined with Eq. 3.30; [b] Microscopic: From Eqs. 3.4, 3.27 and 3.39, combined with Eq. 3.30; [c] Average of Macroscopic and Microscopic results.

way to prefer one of the computation procedures over the other we used the results of the latter column throughout in our further calculations.

As was remarked before (sect. 3.3.3), the Hamaker constants of dispersed solids in nonionic obtained from the macroscopic method tend to be systematically lower than those of the microscopic method. In spite of these differences, the main trends, viz. that oxides have a higher Hamaker constant than the crystalline detergent solids, with Calcite in between, is found with both methods. The average Hamaker constants found for the crystalline detergent solids range between 0.11 to 0.20 $\times 10^{-20}$ J and is of the same magnitude as the literature values for dispersions of inorganic solids in non-aqueous solvents (see sect. 3.3.3). With the exception of activated Zeolite 4A, from the Hamaker constants evaluated we could not conclude that there are significant differences between the various detergent solids.

6.4.3.2 The influence of particle porosity

It has to be noted here that some of the inorganic solids we applied in the current studies are porous. Their pore volumes have been given in Table 5.1. From that table it can be seen that high porosities are particularly found with the oxides and with Calcite, i.e. materials which, according to Tables 6.2 (and 6.4), also have a relatively high Hamaker constant. We think that this relation is not fortuitous. It is possible that this is caused by the fact that the Hamaker constant has had an important influence on the van der Waals attractions which played a role during the solids preparation process and that this influence is maintained in the form of particle porosity during the further course of the particle processing. In agreement with this concept high Hamaker constants would than lead to 'agglomerate particles' whereas low Hamaker constants lead to 'aggregate particles' (see Fig. 2.1). This influence may be analogous to the reasons why strong and reduced van der Waals attraction forces lead, respectively, to more openly spaced and to more densely packed suspension sediments (see sect. 2.3.1).

In suspensions of porous particles the effective Hamaker constant has to be taken into account (see Eq. 3.32). For example, this means for calcite particles, with a pore volume fraction of 0.54, that the effective Hamaker constant is reduced from 0.7 to 0.17 $\times 10^{-20}$ J. For oxide particles a similar effect of porosity on the effective Hamaker constants will be found.

In activated Zeolite 4A, with a pore volume fraction of approximately 0.05, the pores have a size of 0.4 nm and are very small. The pores are so small that nonionic molecules cannot fill them, causing these pores to remain empty when Zeolite particles are immersed in Plurafac. This phenomenon could explain the refractive indices of activated Zeolite 4A particles experimentally found (1.439) (Table 6.1), which is lower than that of the nonionics Plurafac (1.4529) or Imbentin (1.4528). [Note: sodium aluminiumsilicate, the solid constituent of activated Zeolite 4A, has a much higher refractive index (1.537)]. Hence, these Zeolite particles may have a lower effective Hamaker constant than nonionic molecules (Table 6.4). When there is no third phase present this is of no consequence for the overall Hamaker constant and for the van der Waals attraction. However, when air bubbles are whipped in such a suspension, as is observed by Scanning Electron Microscopy (Fig. 6.15), these Zeolite particles pack very densely at the boundary layer of the bubbles. The packing of Zeolite particles around

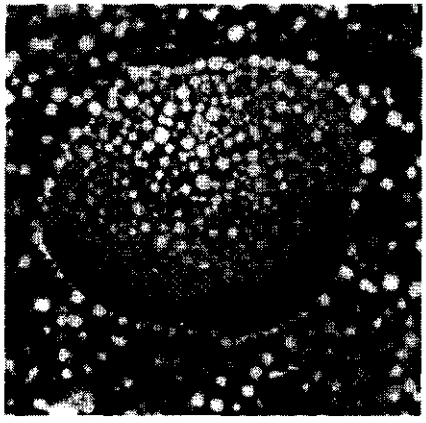

Fig. 6.15: Dense packing of the Zeolite particles at the boundary layer of an air bubble in a suspension of activated Zeolite 4A in Plurafac.

these bubbles is so dense that the bubbles can be kept stabilized for lengthy periods in the suspension. This effect is not found when Zeolite in suspended in Trioxitol, i.e. a nonionic with refractive index lower than that of Zeolite 4A; also not at -40 °C at higher Trioxitol viscosities. These observations are explained from the stronger attraction between nonionic molecules than between Zeolite particles and which causes the Zeolite particles to be expelled from the liquid phase to the liquid - gas boundary layer.

6.5 SUMMARY

Ionic strengths in HDoBS-stabilized suspensions in the nonionics Plurafac and Imbentin are evaluated from the conductivity in the supernatants and from their respective limiting molar conductivities. At HDoBS concentrations between 10 and 150 mM, the ionic strengths are found to range from 0.05 to 4 mM in Plurafac and from 0.3 to 30 in Imbentin. The ionic strengths thus obtained are considerably larger than in supernatants of unstable suspensions and are higher than ever reported in media of such low polarity. The ionic strengths can be explained with the Fuoss theory, whereby the dielectric constant is the main governing parameter. This constant is increased by HDoBS. Only at relatively high dielectric constants, i.e. at high HDoBS concentration, are the ion concentrations lower than theoretically predicted. This could be due to the formation of 'molecular associates'. Partly as a result of the high ionic strengths, in the HDoBS concentration regime between 10 and 150 mM, Debye lengths range from 33 to 1 nm in Plurafac and from 13 to 1 nm in Imbentin.

Electrokinetic (ζ-)potentials of particles of detergent solids suspended in nonionic are found to be a function of the HDoBS concentration, but tend to level off at HDoBS concentrations $\geq$ ca. 20 mM to a maximum value ranging from +25 to +80 mV, depending on the nature of the solids. Addition of water or of a crown-complexant (15-Crown-5), reduces the positive ζ-potential. The formation of positive surface charges can be explained from the larger affinity of the solvent for $DoBS^-$ ions in comparison to that of the nonionic liquid.

Hamaker constants in vacuum of crystalline detergent solids are evaluated from their dielectric constants and refractive indices. The results showed the Hamaker constants for the detergent solids (except activated Zeolite 4A) to exceed those of the nonionics, but to be lower than those of the metal oxides. The differences between the Hamaker constants of crystalline detergent solids and those of nonionics are relatively small, implying that suspensions of detergent solid particles in nonionics can be stabilized easily.

6.6 BIBLIOGRAPHY

6.1 **Conductivity and Debye Length in Aerosol-OT Hexane/Liquid Paraffin Solutions.** Mil, P.J.J.M. van; Crommelin, D.J.A.; Wiersema, P.H.. *Ber. Bunsenges. Phys. Chem.* **1982,** 86, 1160-1165.

6.2 **Electrostatics in the petroleum industry. The prevention of explosion hazards.** Klinkenberg, A; van der Minne, J.L.. Shell Research and Development Report. (Elsevier, Amsterdam, Neth.). **1958.**

6.3 **Stability and electrophoretic deposition of suspensions in non-aqueous media.** Koelmans, H.; Overbeek, J.Th.G.. *Disc. Faraday Soc.* **1954,** 18, 52-63.

6.4 **Principles of the Stability of Lyophobic Colloidal Dispersions in Non-Aqueous Media.** Lyklema, J.. *Adv. Colloid Interface Sci.*, **1968,** 2, 65-114.

6.5 **Stability of non-aqueous dispersions. I The relationship between surface potential and stability in hydrocarbon media.** McGown, D.N.L; Parfitt, G.D.; Willis, E.. *J. Colloid Sci.* **1965,** 20, 650-664.

6.6 **The effect of water on electrokinetic potential and stability of suspensions in nonpolar media.** Kitahara, A.; Karasawa, S.; Yamada H.. *J. Colloid Int. Sci.* **1967,** 25, 490-495.

6.7 **Zeta potential in non-aqueous media and its effect on dispersion stability.** Kitahara, A.. *Progress Organic Coatings* **1973/1974,** 2, 81-98.

6.8 **The concentration effects of surfactants on zeta-potential in non-aqueous dispersions.** Kitahara, A.; Amano, M.; Kawasaki, S.; Kon-no, K.. *Colloid Polymer Sci.* **1977,** 255, 118-1121.

6.9 **Stability of Colloidal Dispersions in Non-aqueous Media. Vol 10: Surface and Colloid Science.** Parfitt, G.D.; Peacock, J.. Matijevic, E. Editor. (Plenum Press, London). **1978.**

6.10 **Stability of Coarse Suspensions in Nonpolar Media: Effect of Gravity on the Interaction between Particles.** Mil, P.J.J.M. van; Crommelin, D.J.A.; Wiersema, P.H.. *J. Colloid Interface Sci.* **1984,** 98(1) 61-71.

6.11 **The use of zeta-potential measurements in organic solvents to determine the donor-acceptor properties of solid surfaces.** Labib, M.E.; Williams, R.. *J. Colloid Interface Sci.* **1984,** 97(2), 356-366;
An experimental comparison between the aqueous pH scale and the electron donicity scale. ibid. *Colloid Polymer Sci.* **1986,** 264, 533-541.

6.12 **The origin of the surface charge on particles suspended in organic liquids.** Labib, M.E.. *Colloids Surf.* **1988,** 29, 293-304.

6.13 **Stability of non-aqueous dispersions. I The relationship between surface potential and stability in hydrocarbon media.** McGown, D.N.L; Parfitt, G.D.; Willis, E.. *J. Colloid Sci.* **1965,** 20, 650-664.

6.14 **The effect of Moisture on the Charge at the Interface between Solids and Organic Liquids.** Labib, M.E.; Williams, R.. *J. Colloid Interface Sci.* **1987,** 115(2), 330.

6.15 **Zeta potentials and coagulation of ZnO in alcohols.** Logtenberg, E.H.P.; Stein, H.N.. *Colloids and Surfaces* **1986,** 17, 305-312.

6.16 **The effect of Trace Water on Non-Aqueous Silica Dispersions.** Goodwin, J.W.; McDonald, F.; Reynolds, P.A.. *Colloids and Surfaces.* **1988** 33 1-9.

6.17 **Theory of the stability of lyophobic colloids. The interaction of sol particles having an electric double layer.** Verwey, E.J.W.; Overbeek, J.Th.G.. (Elsevier, Amsterdam, Neth.). **1948.**

6.18 **Nouveau Traité de Chimie Minérale,** P. Pascal (Masson, Paris). **1963.**

6.19 **On Hamaker constants: A comparison between Hamaker constants and Lifshitz-van der Waals constants.** Visser, J.. *Adv. Colloid Interface Sci.* **1973,** 3, 331-363.

6.20 **Surface and colloid science. Vol. 8. Chapter 1: Adhesion of colloidal particles.** Visser, J.. Mateijevic, E.. Editor. (John Wiley, New York) **1976.**

6.21 **The van der Waals Attraction Between Colloid Particles Having Adsorbed Layers. II Calculation of Interaction Curves.** Vincent, B.. *J. Colloid Interface Sci.* **1973,** 42 (2), 270-285.

6.22 **The calculation of Hamaker constants from Lifshitz theory with application to wetting phenomena.** Hough, D.B.; White, L.R.. *Adv. Colloid Interface Sci.* **1980,** 14, 3-41.

6.23 Churaev, N.V.. *Koll. Zhur.* **1972,** 34, 959.

6.24 Parsegian V.; Weiss, G.H.. *J. Colloid Int. Sci.* **1981,** 81, 1, 285-289.

6.25 **Intermolecular and surface forces: with applications to colloidal and biological systems.** Israelachvili, J.N. Editor. (Academic Press, London). **1985.**

6.26 Prieve, D.C.; Russel, W.B., *J. Colloid Int. Sci.* **1988,** 125, 1, 1-13.

6.27 Mathai, K.G.; Ottewill, R.H.. *Trans. Faraday Soc.* **1966,** 62, 759.

Chapter 7

MECHANICAL PROPERTIES OF HDoBS-STABILIZED SUSPENSIONS

7.1 INTRODUCTION

In Chapter 6 results are given of measurements of the electric and dielectric parameters of a number of nonionic suspensions. It was reported that addition of DoBS acid to suspensions of detergent solids had three important consequences: it led to the formation of positive surface potentials, and in the continuous phase it increased the ionic strength and the dielectric constant. In Chapter 5 it was shown on theoretical grounds that, as a consequence of these three effects, considerable repulsive barriers may develop. Given the Hamaker constants collected in Table 6.4 it was further also found that detergent solid particles exhibit only weak attraction in nonionics so that electrostatic stabilization can be achieved.

This chapter deals with a discussion of the macroscopic mechanical properties of the suspensions, more specific
a. the viscosity at 'infinitely' high shear rate,
b. the viscosity at lower shear rates,
c. the creep compliance measurements, and
d. the volume fractions in settled sediments, i.e. suspensions in rest.
The latter three subjects are discussed particularly in relation to the influence of DoBS acid on the interactions of the particles. The experimental methods have already been discussed in Chapter 5. The current chapter will be concluded with a general discussion of the stabilization mechanism.

In our study we payed attention to variables as the volume fraction, the temperature and the DoBS acid concentration. Since a discussion of all these variables in combinations with all the solids studied in the two nonionics is beyond the scope of the present chapter, we decided to limit the considerations to a few characteristic systems under typical conditions.

7.2 SUSPENSION PROPERTIES AT 'INFINITE' SHEAR RATE

7.2.1 Introduction

Viscosities η of suspensions are measured as a function of the shear rate $\dot{\gamma}$. The experimental methods are described in sect. 5.5.2. Typical examples showing the characteristic shear thinning behaviour are given in Fig. 7.1. The example system

is an unstable suspension of soda ash in Imbentin at three different volume fractions ϕ. In viscosity measurements of nonionic suspensions of crystalline detergent solids at high shear rates a tendency to reach a plateau value is always observed. It is generally found for unstable suspensions that to reach the (second Newtonian) plateau value of the viscosity η_∞, shear rates $> 440\ s^{-1}$ are necessary. For HDoBS-stabilized suspensions the viscosity at 'infinite' shear rate η_∞ is often reached already when shear rates are $\geq 200\ s^{-1}$ (see for example Fig. 7.6).

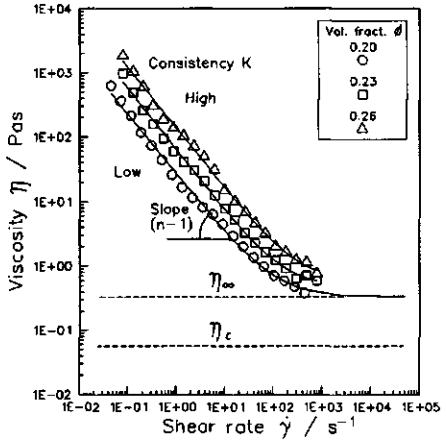

Fig. 7.1: Viscosity as a function of the shear rate for unstable suspensions of Soda ash in Imbentin at three different volume fractions. Best fits are made with the Sisko model.

According to the model discussed in sect. 5.5.2.2, at 'infinitely' high shear rates a break-down of the three-dimensional structure occurs, whereas the coagulative forces are not strong enough to influence viscosity. At these high rates only hydrodynamic factors determine the viscosity. In Fig. 7.1 the viscosity of the (Newtonian) liquid phase η_c is also indicated.

A fit of the Sisko equation (Eq. 5.31) to the experimental results allows the evaluation of three parameters, viz. the shear thinning index n, the viscosity at 'infinite' shear rate η_∞ and the consistency K (5.5.2.2). The consistency K has a relation with the interactions between particles. Cross (1965) [7.1] and Sonntag and Strenge (1985) [7.2] mentioned specifically that K contains the rate constants for rupture and rebuilding of linkages between particles.

Figure 7.1 demonstrates that in the shear thinning area the curves for the three suspensions are parallel. Hence, values for $(n - 1)$ are approximately equal, whereas the consistencies K differ. [Note: For all the suspensions in nonionics studied so far the values of n seem to be constant and amounting on the average to 0.1 ± 0.1. This value is in the same range as for example that of lubricating grease or skin cream, although those substances have higher consistencies (Barnes, Hutton and Walters, 1990) [7.3].] It is further clear from Fig. 7.1 that K increases with the particle number concentration. This supports the view that K, apart from the strength, also depends upon the number of interactions.

In the coming sections first the influence on η_∞ of the volume fraction, the nature of the solids and the temperature will be discussed. To correct the viscosity results for the influence of the continuous phase η_c, we henceforth plot the curves in terms of the quotient η_∞/η_c, i.e. the *relative* viscosity at 'infinite' shear rate. In section 7.3 the factors influencing K will be dealt with.

7.2.2 Factors influencing the 'infinite' shear rate viscosity

7.2.2.1 Solids volume fraction

An important relation which gives insight into the hydrodynamic interactions between particles is the Krieger-Dougherty equation (sect. 5.5.2.3), relating η_∞/η_c and the volume fraction solids ϕ. In Fig. 7.2a η_∞/η_c is plotted against ϕ for suspensions of soda ash in Imbentin. In Fig. 7.2b the corresponding results are given for STP in Plurafac. In both graphs results for unstable ('No acid') and for HDoBS-stabilized suspensions are included. The results demonstrate that for the suspension of soda ash in Imbentin the addition of DoBS acid has no effect on η_∞/η_c. This trend is also observed for most other combinations of detergent solids and nonionic liquids, provided the volume fractions are lower than 0.3 to 0.4. The fact that DoBS acid does not influence η_∞/η_c is to be expected. All colloidal bonds being broken, this quotient is entirely determined by hydrodynamic interactions. However, for the suspension of STP in Plurafac there is some tendency that the relative viscosity at high shear rates is influenced by the presence of acid (Fig. 7.2b). A possible explanation for this deviating behaviour may be related to the fact that in the latter case the volume fractions are higher. Then interparticle distances are smaller causing that some interparticle interaction remains. The persisting coagulates are porous and contain voids which are filled with liquid that is entrained, causing the effective volume fraction of particles to be larger than ϕ. Apparently, DoBS acid is able to break down these coagulates, at least to some extent and, hence, causes an increase in the volume fraction.

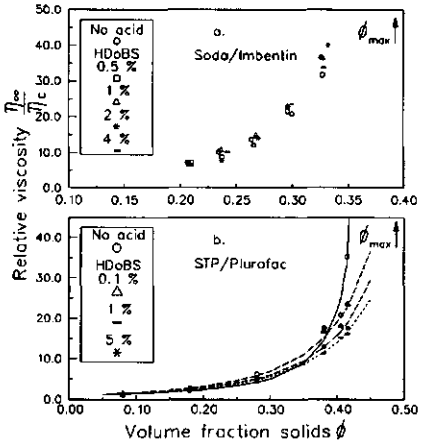

Fig. 7.2: KriegerDougherty plots for unstable and DoBS acidstabilized suspensions a. of Soda ash in Imbentin and b. of STP in Plurafac.

When the Krieger-Dougherty model (Eq. 5.34) is used to fit to the results given in Fig. 7.2b, the effect of DoBS acid is reflected in the plot parameters ϕ_m, i.e. the maximum volume fraction, and $[\eta]$, i.e. the intrinsic viscosity. The parameters thus obtained were used to draw the curves in Fig. 7.2b. In spite of the relatively good fitting curves in the observation range, the fit parameters appeared to be puzzling. For example, the values obtained for HDoBS-stabilized suspensions suggest that ϕ_m approaches about 0.7, whereas in centrifugation experiments for STP suspensions never a value is found exceeding 0.525. Also the obtained values for $[\eta]$ do not agree with other observations (see later sect. 7.2.3). The Krieger-Dougherty fit parameters have therefore not been used for the determination of the maximum volume fractions of our suspensions.

7.2.2.2 Solids nature

Viscosities at 'infinite' shear rate as a function of volume fraction are measured for Periclase and also for a number of other crystalline detergent solids suspended in Plurafac nonionic, both for unstable and for three HDoBS-stabilized suspensions, using 0.1, 1 and 5 % w/w DoBS acid. The results obtained showed only small differences as a function of the DoBS acid concentration, therefore it sufficed to only report data at 1 % w/w level. From Fig. 7.3 it can be seen that all relations have approximately the same characteristic shapes and rise steeply when the volume fractions increase, meaning that with increasing volume fractions these suspensions all become pasty. However, the maximum volume fractions remain much lower than those for hexagonal close packing (0.74), random close packing (0.64) or simple cubic packing (0.52). Moreover, there are substantial qualitative differences between the various solids. For example, for Periclase it is found that very high viscosities are already found when the solids volume fraction is only 0.15. From the results given before (see Table 5.1) it can be derived that the voids fraction of Periclase is 0.56. When these internal voids are taken into account the maximum effective particle packing for Periclase is approximately 0.40, which is not much different from that of the detergent solids any more. It is likely that this high voids level of the Periclase agglomerates is to a large extent responsible for the low maximum volume fractions. Evidently, the Periclase agglomerates are strong enough to survive the high shear forces applied to measure η_∞.

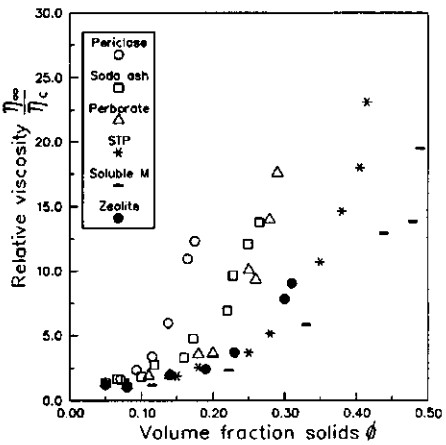

Fig. 7.3: KriegerDougherty plots of suspensions in Plurafac of various solids, stabilized with 1 % w/w DoBS acid.

Since the crystalline detergent solids were found to have no internal voids (Table 5.1), the low volume fraction where they pack maximally cannot be attributed to persisting agglomerates. The exact reason for the behaviour of these solids is not known, but it is likely that it is caused by the presence of protrusions and surface irregularities, causing them to occupy a larger hydrodynamic volume. The differences between the detergent solids are interpreted as attributed to the variations in size and frequency of the protrusions; the variation with respect to the shapes of the particles being too small to be responsible for this observation (sect. 7.2.3). [Note: The magnitude of this influence can be illustrated with Zeolite particles. Zeolite particles are almost perfectly cubically shaped and their corners can be considered as the protrusions of an enclosed sphere. For such particles the effective volume occupied by a surrounding sphere is $(\pi/3)\sqrt{2} = 1.48$ times the volume of the cube. This means that even in a situation of a random, effective close packing the actual volume fraction is not more than ca. 0.43.] For spherical particles protrusions on surfaces and

variations in macroscopic surface roughness may have a similar influence. When the differences between the detergent solids are attributed to protrusions, a conclusion of Fig. 7.3 is that the surface irregularity, defined in this way, increases in the order Soluble M < STP < zeolite < perborate < soda ash < periclase. This result is in qualitative agreement with the EM pictures of the solids.

Increased limiting relative viscosity as function of volume fraction was also observed by Buscall, et al. (1990) [7.4] for systems of weakly interacting spherical particles with a diameter of 3.5 μm. They found that for particles of that size the limiting viscosity in the Krieger- Dougherty curve is enhanced substantially, as is found in fully irreversibly aggregated systems. They suggested that the increase of the attractive force with particle size is stronger than normally observed for colloidal particles, which may point to a transition from weak reversible agglomeration to irreversible aggregation.

Qualitatively, the results of Fig. 7.3 demonstrate that detergent solids immersed in nonionic have a low tendency to coagulate. Therefore relatively high solid fractions can be introduced before the suspensions become pasty. It is assumed that this is due to the low Hamaker constant (Table 6.4), which is basically the same reason why detergent solids can be stabilized relatively easily (sect. 3.3.3). In line with this it was observed that Anatase and Alumina, both insoluble oxides with a much higher Hamaker constant (Table 6.2), become pasty at volume fractions as low as 0.02 or 0.04, respectively.

7.2.2.3 Temperature

The influence of the temperature on the viscosity was studied in separate experiments using HDoBS-stabilized suspensions of STP in Plurafac, which varied with respect to volume fraction and particle size. The temperature was varied over the range 5 to 45 °C, with steps of 10 °C. In Fig. 7.4a shear thinning curves are given at the temperatures studied. The results show that the temperature has only an influence on the 'infinite' shear viscosity η_∞ but not on the consistency K, or the shear-thinning index n.

In Fig. 7.4b, the viscosities at 'infinite' shear rate η_∞ of three suspensions, varying in volume fraction and particle size, is plotted on a logarithmic scale against the reciprocal of the absolute temperature ('Arrhenius plot'). Parallel straight lines were found with all three suspensions. The

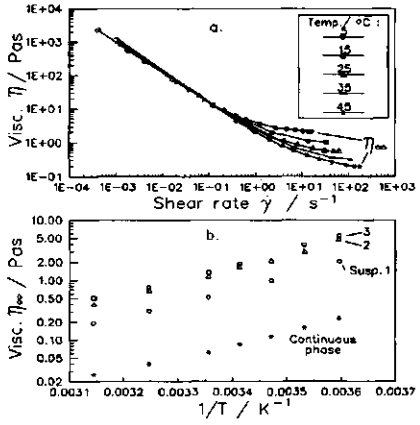

Fig. 7.4: Viscosity as a function of temperature of suspensions of STP in Plurafac, stabilized by HDoBS. a. Viscosity as a function of shear rate, b. 'Infinite' shear rate viscosities.

results reflect the fact that the 'infinite' shear viscosity and the absolute temperature are related by $\eta_\infty \propto \exp(\Delta G^+/T)$, where ΔG^+ is the free enthalpy of activation. The lines were also parallel to that of the (Newtonian) viscosity of the continuous phase plotted in the same way. This result proves that the temperature dependency of HDoBS-stabilized suspensions can be completely ascribed to temperature dependency of the continuous phase. [Note: This independence of the temperature of stabilized suspensions is completely different from the viscosity behaviour of unstable suspensions, which was reported to increase considerably with temperature (Fig. 1.4).] From the slopes it was derived that the value of $\Delta G^+ = 36 \pm 2$ kJ mol^{-1}, which is approximately twice the value of the formation of a hydrogen bond (van Duijneveldt, et al., 1987) [7.5]. The results suggest that the structural organisation of the nonionic, which leads to viscosity increase when the temperature decreases, results from the formation of two hydrogen bonds per molecule.

7.2.2.4 Particle size

In separate experiments the influence of the particle size on the relative viscosity at 'infinite' shear rate has been studied. In these studies the sizes of particles have been varied by changing the milling times. In this way we obtained for five suspensions a range of average particle radii varying from 5.5 to 3.3 μm and at two different volume fractions. In all cases it was found that η_∞/η_c did not depend on size, confirming the expectation that the plateau viscosity is purely a result of the hydrodynamic interactions and not influenced by the factors related to the particle size.

7.2.3 Intrinsic viscosity and particle shape

From Krieger-Dougherty plots to the experimental data of Fig. 7.2b it is found that the intrinsic viscosities $[\eta]$ for STP vary between 3.4 and 4.9 (see sect. 7.2.2.1). Intrinsic viscosities of that order would mean that the STP particles are very anisometric, with axial ratios r_e of the order of 0.1. However, from image analysis of microscope photographs this ratio was rather found to be 0.6 to 0.7 (see Table 5.1) meaning that the particles are more spherical and ought to have $[\eta]$ around 2.55 (Leal and Hinch, 1971; Goodwin, 1981 [7.6]). To solve this controversy, values for $[\eta]$ are collected at low volume fractions for an unstable and a HDoBS- stabilized STP suspension. Alike for the

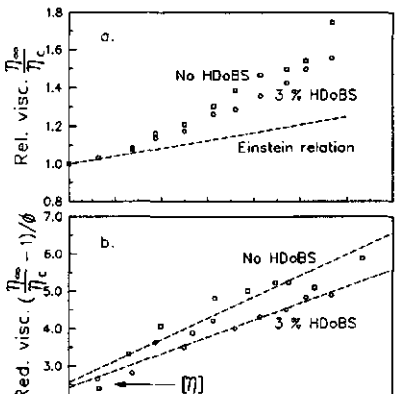

Fig. 7.5: Relative (a) and reduced (b) viscosities as a function of the volume fraction in dilute suspensions. Extrapolation of the reduced viscosity to zero volume fraction leads to the intrinsic viscosity.

concentrated suspensions, values of η_∞/η_c for these dilute suspensions were obtained from the Sisko plot. The relative viscosities obtained in this way are given in Fig. 7.5a; the reduced viscosity is plotted as a function of the volume fraction ϕ in Fig. 7.5b (see Eq. 5.35). A comparison in Fig. 7.5a of the relative viscosities with those predicted by Einstein's equation for non-interacting hard spheres (Eq. 5.33) shows, as expected, that the Einstein slope (2.5) is approached at very low ϕ. Hence, the high values for $[\eta]$ found before must be attributed to aggregation. HDoBS-stabilized suspensions more closely follow the Einstein relation, indicating that the interactions are diminished due to acid addition.

From Fig. 7.5b, upon extrapolation a value of $[\eta] = 2.55 \pm 0.05$ is found. This result shows that STP particles behave as if they are virtually spherical, which is in agreement with the results of the image analysis. Based on this result it is supposed that the particles of the other solids, which in image analysis were found to have similar axial ratios as STP (see Table 5.1), can also be considered as spherical. The results prove as well that, although the Krieger-Dougherty equation generally fits the experimental data well, unfortunately for our rough particles the obtained fit parameters for $[\eta]$ bear no relation to the actual particle shape.

7.3 SUSPENSION VISCOSITIES AT LOW SHEAR RATES

7.3.1 The influence of HDoBS

7.3.1.1 Introduction

In a number of experiments the effect of DoBS acid on the shear thinning part of the viscosity-shear rate curve was studied. The DoBS acid concentration was 0.5, 1, 2 or 4 % w/w. An example of a shear thinning curve is shown in Fig. 7.6.

The results demonstrate that the viscosity drops considerably upon the addition of DoBS acid. Already 0.5 % w/w HDoBS produces the main effect. Only at low shear rates, where weaker interactions are monitored, a minor influence of the DoBS acid concentration remains visible above 0.5 % w/w. For practice, the effect of such small additions of HDoBS is dramatic: the suspension changes from pasty to easily pourable. Similar results were

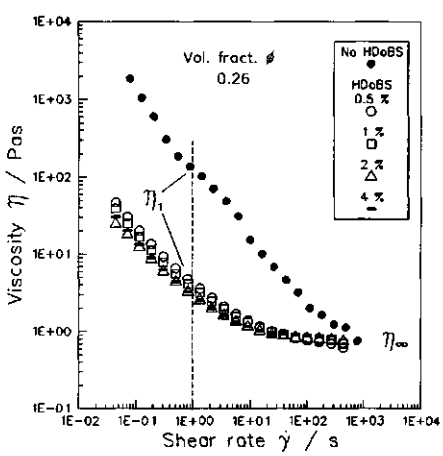

Fig. 7.6: Viscosity as a function of shear rate (Sisko plot) of suspensions of Soda ash in Imbentin with increasing HDoBS amounts added.

obtained for STP in Plurafac (sect. 1.4) and other suspensions. Hence, we are dealing with a general phenomenon.

7.3.1.2 The consistency - ζ-potential relation

The consistency K has a relation with the Bingham yield stress and is a reflection of the colloidal interactions between particles (sect. 5.5.2.2). K can be derived from the viscosity-shear rate results by fitting to the Sisko model (Eq. 5.31). Figure 7.1 demonstrates that K depends on η_∞ (see sect. 7.2.1). An expression independent of η_∞ can be obtained by introducing the quotient K/η_∞. If a viscosity η_1 is defined at a shear rate $\dot{\gamma} = 1$ it follows from Eq. 5.31

$$\frac{\eta_1}{\eta_\infty} = 1 + \frac{K}{\eta_\infty} \qquad [7.1]$$

The quotient K/η_∞ is dimensionless and equal to $(\eta_1/\eta_\infty - 1)$. We shall henceforth refer to it as the 'normalized' consistency. It has as the advantage that it reflects the interparticle interactions only, because hydrodynamic contributions have been eliminated.

In Fig. 7.7, K/η_∞ values obtained for suspensions of soda ash and STP in Imbentin and Plurafac are given as a function of the DoBS acid concentration. These results are averages obtained at five volume fractions, ranging from 0.2 to 0.32. The variation over these five volume fractions was found to be approximately $\pm$ 20 %, which is sufficiently low for the present purpose. The curves show that K/η_∞ falls sharply upon addition of as little as 15 mMol dm^{-3} HDoBS (0.5 % w/w) [Note the logarithmic scale.] Further addition of DoBS acid usually has only a limited influence. The addition of DoBS acid can be interpreted as leading to a reduction of the rate of rebuilding of interparticle linkages and hence to colloidal stabilization.

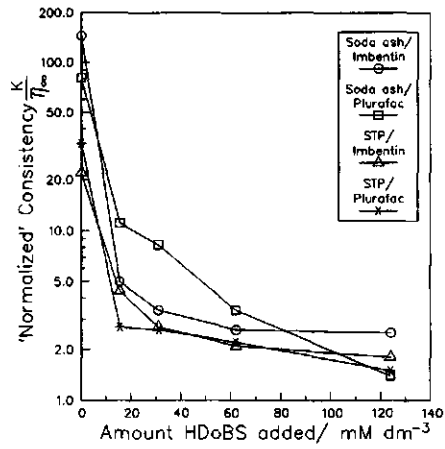

Fig. 7.7: 'Normalized' consistency as a function of HDoBS concentration for suspensions of soda ash and STP in Imbentin and Plurafac. Average results of 5 volume fractions.

The effect of DoBS acid, when added to unstable suspensions of crystalline detergent solids in nonionic, was mentioned previously to increase the ζ-potential. The main rise in the ζ-potential was found to occur already after the addition of 0.5 % w/w of HDoBS, after which further addition of DoBS acid had little influence (see Fig. 6.9). This result is at least in qualitative agreement with the consistency pattern. This agreement strongly supports the view that the ζ-potential

and the consistency are related and that the stabilization obtained is electrostatic in nature.

7.3.1.3 The consistency - electrostatic force relation

Further addition of HDoBS > 0.5 % w/w tends to reduce the consistency somewhat (Fig. 7.7), whereas on the other hand the corresponding influence on the ζ-potential is minimal or even slightly negative (Fig. 6.9). Further addition of DoBS acid was found earlier to also increase the ionic strength and the dielectric constant (Figs. 6.4 and 6.7). Both factors increase the steepness of the repulsive energy curves and thus cause an enhanced electrostatic repulsive force. This observation led to the insight that the observed further decrease of the consistency occurring at DoBS acid concentrations above 0.5 % w/w could also be due to the rise of the electrostatic interparticle repulsion. In order to make this picture quantitative, we evaluated the electrostatic repulsive forces by applying the (approximated) equations for the repulsive forces between spheres given in Chapter 4. Attractive forces were calculated using the equations given in Chapter 3, substituting the Hamaker constants of Table 6.4. The theoretical net repulsive force was found from the sum of these two forces.

In Figs. 7.8 the results are given. The variation is obtained by using 0, 0.1, 0.25, 0.5, 1, 2 and 4 % w/w HDoBS. The maximum total force F_T reflects the steepest part of the energy curve (see for example Fig. 4.13), coinciding with the point where the modulus, i.e. a function of the second derivative of the pair energy, i.e. dV_T^2/dH^2 (see sect. 7.4.2.3), is zero. The normalized consistency K/η_∞ and the maximum force F_T are plotted both on log scales. The force is calculated using the Hamaker constants derived from the macroscopic method (closed symbols). Unfortunately, these results are not accurate enough to allow a conclusions on the preferred Hamaker constants.

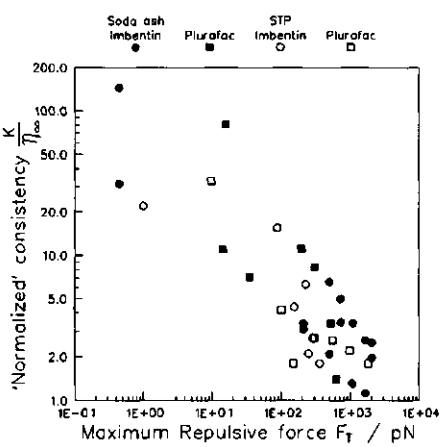

Fig. 7.8: 'Normalized' consistency of STP and soda ash suspensions in Plurafac and Imbentin as a function of the maximum repulsive force. Results using the macroscopic Hamaker constants.

The results show that for both solids the decrease of the consistency can be explained reasonably well from the increased electrostatic force: The higher the repulsive force the lower the normalized consistency. The decreasing influence of the repulsive barrier is, however, larger in STP than in soda ash suspensions. It is possible that the explanation has to be also sought in the presence of more protrusions on soda ash particles (sect. 7.2.2.2). The correlation between the normalized consistency and the maximum repulsive force is encouraging, particularly when it

is realized that the consistency reflects the multiparticle interactions, whereas the repulsive forces, evaluated with the DLVO theory, apply to pair interactions.

Buscall, McGowan and Mumme-Young (1990) [7.4] showed that the Bingham yield stress, which is related to the consistency K (Eq. 5.32), is correlated to the depth of the pair energy in the secondary minimum. The depth of the secondary minimum increases with ionic strength (see Fig. 4.12). Considering the weak influence of further acid addition on the normalized consistency, it becomes apparent that the influence of the increase of the secondary minimum is not noticed in our results. The conclusion must be that the secondary minimum must be very shallow. This is in agreement with the low Hamaker constants of the detergent solids. [Note: We calculate low secondary minimum energies of 2 kT at maximum, when the Hamaker constants from the macroscopic method are used. The Hamaker constants derived from the microscopic method result in secondary minimum energies which are 10 to 20 kT. These calculation results suggest that the Hamaker constants from the macroscopic method are in better agreement with the normalized consistencies found than that of the microscopic method.] Possibly, for our systems the influence of the secondary minimum is found only at shear rates lower than those applied.

7.3.2 Influence of hydrodynamic energy in stabilized suspensions

7.3.2.1 The temperature and the particle size

It has been shown already that the consistency is not influenced by the temperature (Fig. 7.4). Because the van der Waals attraction is almost independent of the temperature (sect. 3.3.5) and since the electrostatic repulsion increases only slightly with the temperature (see e.g. Eq. 4.14), the repulsive barrier increases little on temperature rise. Evidently the DLVO effect is too small to be noticed in the consistency values. In chemical interactions much higher energies are involved and are therefore much more sensitive to the temperature. Hence, the small temperature effects in stabilized suspensions on the consistency demonstrate that there are no chemical interactions between the particle surfaces.

The influence of the particle size on the consistency K was studied. This influence is particularly interesting because the consistency is expected to be related to the rate constants for rupture and rebuilding of linkages between particles, which are related to the particle dimensions. The systems used for this part of the study are two HDoBS-stabilized suspensions of STP in Plurafac with volume fraction solids of 0.37 and 0.33. They are identical to those considered in the study the effect of the particle size on η_∞, where no size influence on the hydrodynamic interactions was found (sect. 7.2.2.4). The viscosities of the suspensions were measured in the temperature range of 5 to 45 °C. The consistency as a function of the particle size is given in Fig. 7.9, where both variables are plotted on a logarithmic scale.

From Fig. 7.9 it can be seen that the particle radius a has a significant influence on the K. The straight lines in the double logarithmic plots have slopes -2.5 and -

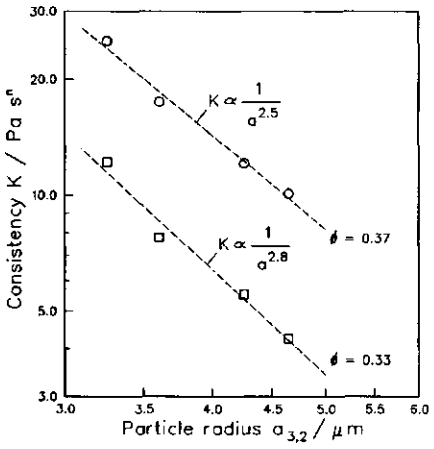

Fig. 7.9: Consistency as a function of particle size for two HDoBSstabilized suspensions of STP in Plurafac. The volume fraction is indicated.

2.8, which are both close to 3, suggesting that the consistency is related to the volumes of the particles. [Note: For the current plots the surface-weighted mean particle radius $a_{3,2}$ is used. Plotting instead of the arithmetic mean particle radius $a_{1,0}$ gave slopes of -3.1 and -3.2, for the two volume fractions, respectively. In the latter particle size average, smaller particles play a more important role than in the former. This result therefore suggests that the small particles, due to their larger number and higher mobility, tend to influence the low shear rate interactions more strongly than the bigger ones.]

7.3.2.2 The Péclet number

It is common practice to plot, instead of η/η_c versus $\dot{\gamma}$, η/η_c versus the dimensionless Péclet number $\eta_c a^3\dot{\gamma}/k_BT$ (Russel, 1980 [7.7]; Goodwin, 1981 [7.6]). A plot of these parameters for HDoBS-stabilized suspensions of STP in Plurafac at two volume fractions of solids is given in Fig. 7.10. All suspensions contained 3 % w/w of DoBS acid, hence all had the same repulsive force. The results include systems with two particle radii, 3.6 and 4.7 μm, whereas the viscosity determinations are carried out in the temperature range between 5 and 45 °C. The results show that, for a constant volume fraction solids, the relative viscosity scales well with the Péclet number.

The Péclet number is a measure of the ratio between the timescales for Brownian motion $\eta_c a^3/k_BT$ and that for shear, i.e. $1/\dot{\gamma}$. In our systems, where the contribution of translational Brownian motion to the movement of particles is not very important, this concept is less useful. It is better therefore to consider for our systems the Péclet number as a dimensionless energy number, where the numerator, i.e. $\eta_c a^3\dot{\gamma}$, is proportional to the amount of hydrodynamic energy applied to the suspension by the shear

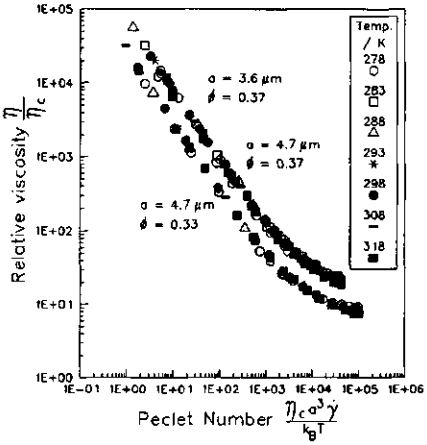

Fig. 7.10: Relative viscosity as a function of the Péclet number for HDoBSstabilized suspensions of STP in Plurafac.

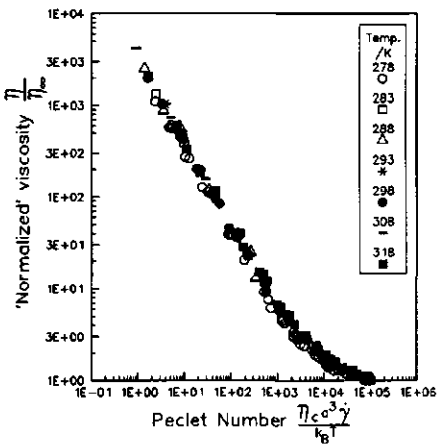

Fig. 7.11: 'Normalized' viscosity as a function of the Péclet number of HDoBSstabilized suspensions of STP in Plurafac. Average over two particle sizes, two volume fractions and seven temperatures.

of the rheometer. Hence, the Péclet numbers indicate the amount of energy, in kT-units, supplied to the suspension. Its value reflects the amount of energy required to maintain a constant ratio of the rates of bond formation and rupture and this energy can be compared to the energies of interaction of the DLVO curves for pairs of particles. The observation in the previous sections that the consistency K is about inversely proportional to the cube of the particle radius a, and that the 'infinite' shear viscosity scales with the continuous phase viscosity η_c and is proportional to $1/T$ is consistent with Fig. 7.10.

That we have two separate sets of results in Fig. 7.10 is only due to the differences in volume fraction, which causes differences in the hydrodynamic interactions. Since the effects of the hydrodynamic interactions are reflected in the infinite shear viscosity η_∞, its influence can be taken into account by plotting, instead of η/η_c, the 'normalized' viscosity η/η_∞ versus the $\eta_c a^3\dot{\gamma}/k_B T$. The results of this procedure are given in Fig. 7.11.

The master curve now obtained represents the Sisko model (Eq. 5.31), modified in such a way that both sides of the equation are divided by η_∞. Then, the Sisko equation can be written as

$$\frac{\eta}{\eta_\infty} = p + q\,\dot{\gamma}^{(n-1)} \qquad [7.2]$$

A fit of this equation to the experimental results in Fig. 7.11 gave $p = 1.00 \pm 0.02$, as expected. The slope of the curve q, is related to the normalized consistency K/η_∞ (sect. 7.3.1.2) and can be written as $q = K\eta_c a^3/\eta_\infty k_B T$. It includes the influences of the particle radius a, the temperature T and the continuous phase viscosity η_c. The influence of the effective volume fraction ϕ, reflecting also the nature of the particles, is implicitly present in η_∞. The value of the exponent $(n - 1)$ was found to be -0.92 ± 0.01 and gives an average flow index $n = 0.08 \pm 0.01$. The results are a clear indication that at Pé $\geq$ 1, i.e. $\dot{\gamma} \geq$ ca. 5×10^{-4} s^{-1}, the HDoBS-stabilized STP suspensions in Plurafac behave as colloidally stable, hard sphere suspensions. The results given in sect. 7.3.1 indicate that this colloidal stability is achieved by electrostatic double layers.

7.4 SHEAR MODULI FROM CREEP COMPLIANCE

7.4.1 Introduction

In a creep experiment a constant shear stress, σ, is applied to the suspension and the strain, γ, is monitored as a function of time. The compliance is defined as γ/σ and has the dimensions of Pa^{-1}. The recovery is measured by monitoring the relaxation of the strain when the stress is removed. Both, creep and recovery versus time curves allow the evaluation of the time-independent part of the shear modulus G_0. It is obtained, respectively, from the plot of the experimental creep results to the model given by Eq. 5.36 and by a plot of the recovery results to Eq. 5.37. Extrapolation to time t=0 leads then to a compliance result which is equal to $1/G_0$.

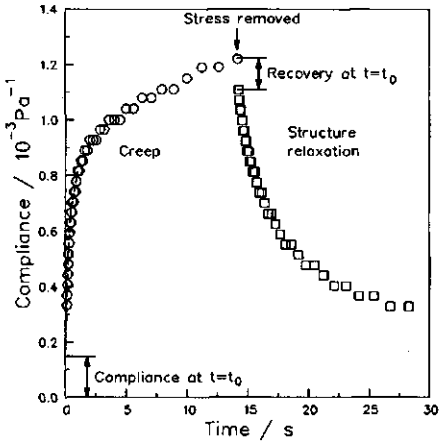

Fig. 7.12: Example of a creep compliance and recovery curve of a HDoBSstabilized suspension (3 % w/w, 93 mM) of STP in Plurafac. Shear stress σ = 6.0 Pa. ϕ = 0.524.

Creep compliance and recovery are measured for a series of suspensions of STP in Plurafac, stabilized by 3 % w/w DoBS acid and are measured at various shear stresses. An example of such a creep compliance-recovery curve is given in Fig. 7.12. The measurements were carried out with solid volume fractions up to 0.525, thus forcing the particles so close together that it is possible to measure the response of the double layers to the applied shear stress.

7.4.2 Shear moduli of STP suspensions

7.4.2.1 As a function of shear stress

The shear moduli G_0, using various shear stresses are collected in Fig. 7.13 for the same HDoBS-stabilized STP/Plurafac suspension. Above a shear stress of approx. 8 Pa, the shear moduli derived from creep and those from recovery deviate. The instantaneous compliance results from creep increase whereas those from recovery decrease. This result is attributed to overstrain occurring when the suspension compliance is not completely elastic. It is found that at stresses $\leq$ 8 Pa, the creep and recovery results converge both at a shear modulus G_0 between 7.0 and 8.5 $\times 10^3$ Pa. Evidently at the low shear stress values the strain is completely elastic. This elasticity is ascribed to interactions of electrostatic double layers, which are considered to be completely recoverable on application of stress.

Figure 7.13 further shows that at higher applied stresses, i.e. at a shear stress of approximately 15 Pa, high recoveries and low G_0 values are found. This is considered as an indication of flow. At the high stresses so much flow is initiated that particles change their relative positions and the suspension yields irreversibly, causing it to become more viscous than elastic.

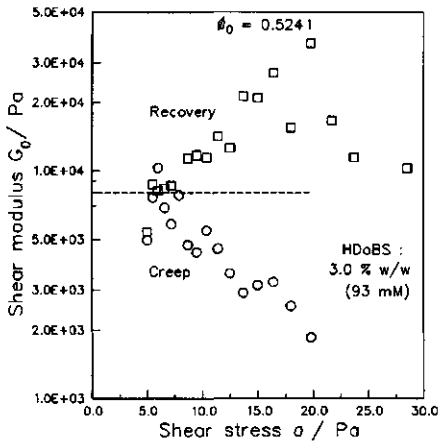

Fig. 7.13: Shear moduli from creep and recovery as a function of shear stress, obtained at a high volume fraction for a HDoBSstabilized suspension of STP in Plurafac.

7.4.2.2 As a function of volume fraction

Shear moduli derived from creep and recovery measurements are evaluated at a number of volume fraction solids ϕ. The results are summarized in Fig. 7.14. They demonstrate, particularly at the lower volume fractions, that the interactions are not completely elastic even at the lowest stresses we could apply in our apparatus. This means that the shear moduli derived from creep are systematically lower than those from recovery. Evidently, completely elastic double layer effects can be monitored only at the highest volume fractions, in situations where the particle distances are small. The shear moduli observed, dependent on volume fraction, are in the range of 0.7 to 8 $\times 10^3$ Pa and are a little higher than the ranges reported for electrostatically stabilized latex suspensions at high volume fractions (Buscall, Goodwin, Hawkins and Ottewill, 1982, [7.8]; Buscall, 1990, [7.9]). The shear moduli for unstable suspensions of STP ('No HDoBS') are also included in Fig. 7.14. In such suspensions creep, but no recovery, can be measured after removal of the stress. With these unstable suspensions completely irreversible compliance and yielding was found. The shear stress required to comply these suspensions is much higher than that of the HDoBS-stabilized suspensions. The results are considered to be indicative for a high degree of irreversible (primary minimum) coagulation in unstable suspensions.

7.4.2.3 Theoretical shear moduli

In Fig. 7.14 the theoretical shear moduli $G_0^{th.}$ are also shown. Following an equation derived by Buscall, et al. (1982) [7.8], for electrostatically stabilized systems it is shown to be directly related to the second derivative with respect to the distance of the pair energy d^2V_T/dH^2 (or the first derivative of the force dF_T/dH), according to

$$G_0^{th.} = \frac{n}{32} \frac{3\phi_m}{R} \frac{d^2 V_T}{d H^2} \qquad [7.3]$$

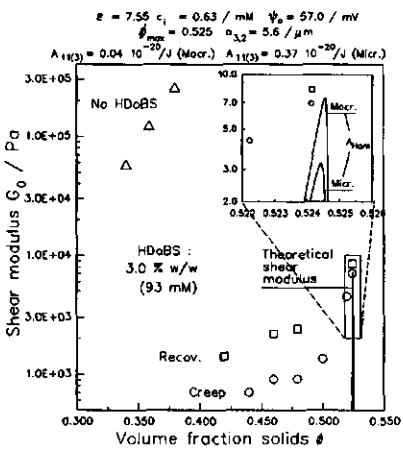

Fig. 7.14: Comparison of theoretical and experimental shear moduli for suspensions of STP in Plurafac at various volume fractions, in the presence (3 %w/w) and in the absence of HDoBS acid.

where ϕ_m is the maximum volume fraction solids and R the distance between the particle centres ($= 2a + H$). The quotient $3\phi_m/R$ represents the surface area per unit of volume in the suspension; n is the coordination number and the quotient $n/32$ is a factor which accounts for the three-dimensional interactions of the double layers. [Note: It has recently been proposed to use instead the numerical constant $n/15\pi$ (Evans and Lips, 1991) [7.10]. The practical consequence for this correction is not significant, however.] Using the approximated equations for the electrostatic repulsion (Eq. 4.41) and for the van der Waals attraction (Eqs. 3.6 and 3.9), taking into account the influence of retardation, from Eq. 7.3 the theoretical shear modulus $G_0^{th.}$ can be evaluated. To this end, we took for the maximum packing ϕ_m and n values of 0.525 and 6, respectively. The evaluation is carried out using the Hamaker constants derived from the macroscopic as well as that from the microscopic theories (Table 6.4).

From the comparison between the maximum theoretical shear modulus and the experimental values (Fig. 7.14) it can be seen that at the high solid volume fractions the experimental shear moduli are in satisfactory accordance with the (approximated) theoretical values, although the experimental results tend to be at the high side. In the suspensions with lower volume fractions the experimental shear moduli are considerably larger than the theoretically predicted. Apparently, the attractive interactions at larger distances are stronger than the theory predicts.

It may be that here we have indications for the influence of secondary minimum coagulation at the points of protrusion, which is not seen in the viscosity measurements at higher shear rates and which is not taken into account in the theoretical derivation. Using the parameters given in Fig. 7.14, the energy of the secondary minima ranges between 0.04 and 2.05 kT, for the microscopic and macroscopic Hamaker constant (Table 6.4), respectively. Although, considering the size of the particles such secondary minima are small, they could play a role. For particles with smooth surfaces the average distances of the secondary minima would be too close to the surfaces to account for the discrepancies between the observed theoretical and experimental data at the lower volume fractions. However, protrusions will keep the particles overall more separated. Theory predicts only weak interactions at these large interparticle distances. However, at the contact points of the protrusions the distances will be short and secondary minimum coagulation may occur at those points. Furthermore, under conditions of low volume fractions

the particles have more possibilities to orient themselves, allowing the number of interactions at the protrusion points to rise.

7.5 PROPERTIES OF SETTLED SUSPENSIONS

7.5.1 Introduction

Network compression moduli $K(\phi)$ give an indication of the strengths of the agglomerative forces in sediments. They can be derived from the packing patterns as a function of sediment height (see sect. 5.5.1.2). The denser the packing, the higher the network compression modulus. Solids such as steel or NaCl have moduli around 10^{11} Pa. Strongly flocculated liquid suspensions of volume fractions of 0.05 of Aerosil in decane, with more open structures, are reported to have network moduli around 10^5 to 10^6 Pa, decreasing with decreasing solids volume fraction and network strength (Sonntag and Strenge, 1987) [7.2]. Buscall, et al. (1982) [7.8] demonstrated that the network modulus of structured dispersions is related to the elastic shear modulus G_0, as determined from the creep compliance measurements and states that it is of the same order of magnitude, with a highest attained value of 5×10^3 Pa (Buscall, 1990) [7.8]. Sonntag and Strenge are of the opinion that the network modulus should exceed the shear modulus, since in contrast to the reversible process of shear deformation, the compression is irreversible, and an essential part of energy is dissipated for the formation of destroyed bonds. In colloidally stabilized, aqueous latex suspensions network compression moduli of the order of 15 Pa have been reported by Okubo (1987) [7.11].

Measurement of the γ-ray absorption in suspensions allows the monitoring of volume fraction solids in consecutive sections of sediments from bottom to top. Usually, the measurements of the volume fraction are carried out after the suspension has settled to apparent equilibrium, i.e. when no visual change in the position of the boundary layer and the super- natant is occurring within a period of two weeks. However, by measure- ments at various stages during the settling process it also is possible to follow the course of the settling with time. The method and the experimental details are discussed in sect. 5.4.1.2. A typical example of experimental results obtained with settled suspensions is given in Fig. 7.15. In this graph the

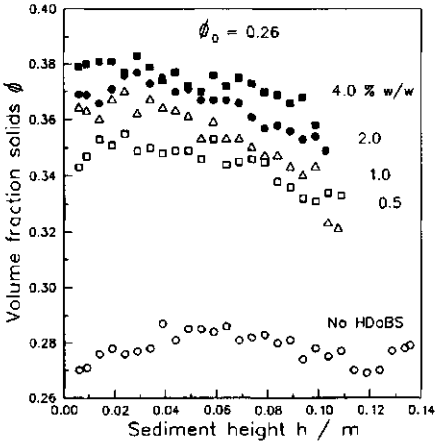

Fig. 7.15: Equilibrium volume fractions in sediments determined by γray absorption in suspensions of soda ash in Imbentin, stabilized with various levels of HDoBS.

volume fractions are plotted as a function of sediment height for suspensions of soda ash in Imbentin in the absence and in the presence of DoBS acid. In Fig. 7.15 to 7.19 the initial volume fractions in the suspension are denoted ϕ_0.

The results of Fig. 7.15 show that the DoBS acid leads to an increase in the average solids volume fraction and hence to a decrease of the interparticle distances. It demonstrates the de-coagulating influence of HDoBS, allowing the particles to move more freely to positions of minimum potential energy. The results are in agreement with those of the provisional experiments for suspensions of STP in Plurafac, reported in Fig. 1.2. The major effect is already attained for 0.5 % w/w; the relative influence from further addition of DoBS acid is less pronounced. This dependency is in line with that for the consistency (sect. 7.3.1.2) and the ζ-potential (Fig. 6.9).

In spite of significant compaction, a random close packing with a volume fraction of 0.64 is, even under the highest pressures at the bottom of the sediment, not reached. [Note: Although centrifugation does lead to a further consolidation, γ-ray absorption shows that higher packings than ca. 0.48 can never be obtained.] It is not known precisely what the reason is for this phenomenon, but it is supposed that the low volume fractions observed are caused by particle protrusions and by particle anisodimensionality, both factors which prohibit a closer packing. Possibly this effect is further reduced by a residual degree of weak secondary minimum coagulation occurring at the points of close contact (sect. 7.4.2.3). [Note: Non-homodispersity is not a reason for the low volume fractions observed. Fractions of small particles may on the contrary lead to higher volume fractions when they fill the voids in a particle bed.]

Two interesting observations emerge further from Fig. 7.15. The first is that at the bottom of the suspensions, volume fractions are found which are lower than in the middle. This phenomenon is the more apparent the stronger the degree of coagulation. It suggests a selective sedimentation of more loosely packed coagulates of the heaviest particles in the first stages of the sedimentation process. Apparently, these coagulates are strong enough to survive the bottom pressure. The second observation is that of a concentration gradient leading to a more dense packing at the bottom than at the top. This effect is more apparent in stabilized suspensions. In accordance with the steeper slope of their repulsive barriers, suspensions with the highest acid concentration, have the smallest gradient.

7.5.2 Volume fractions in sediments

7.5.2.1 Sediment pressures as a function of interparticle distance

The volume fraction-height curves, such as those given in Fig. 7.15, allow the evaluation of the static pressures in the sediments as function of height. The procedure is that the total sediment from top to bottom is divided into slices, in number equal to the number of volume fraction observations. The slices begin and end half-way between two consecutive volume fractions, with the exception of the

top and bottom slice which are extended to their boundaries. The pressures exerted by the particles in a slice are calculated from the density difference of particles with the liquid between the particles, the measured volume fraction and from the volume of the slices. Starting at the top, where the hydrostatic pressure is zero, the consecutive pressures are summed up to find finally at the bottom the highest pressure of the total suspension. A check of the quality of the summation procedure is obtained by summing up all solid volumes in the slices and by comparing the sum with the solids volume introduced. On average the recovery is 100 ± 1.5 %. A plot of the pressures thus obtained (not given here) shows a continuous rise of the pressure with decreasing height.

A plot of the pressure against the volume fraction ϕ, or against $\phi^{-1/3}$, reflects how an increase of the pressure affects the local volume fractions or the distances between the particles, respectively. Hence, the pressure-volume fraction relations are indications of the coagulative forces which keep the coagulates intact and which cause the resistance against the static pressure. [Note: The shortest interparticle distance H of spherical particles and the volume fractions can be related in various ways with the maximum volume fraction ϕ_{max} (see e.g. Barnes, et al., 1990 [7.3]; Boersma, Laven and Stein, 1990, [7.12]). Since ϕ_{max} is not accurately known in our case, these equations do not permit us to evaluate the real interparticle distance quantitatively. However, the equations mostly have such a form that H scales linearly with $\phi^{-1/3}$ only.]

In Fig. 7.16 the pressure Π has been plotted logarithmically as a function of $\phi^{-1/3}$. The results show that the maximum pressures found for suspensions of ca. 0.1 m high are approximate 500 Pa. In the HDoBS-stabilized suspensions the pressure gradients (ln) Π correlates reasonably well linearly with $\phi^{-1/3}$. This experimental result is in general agreement with the equations for the electrostatic repulsion and in particular with that between the electrostatic repulsive pressure P_R^{flat} and exp $-H$ (Eq. 4.27). In the unstable suspension the interparticle distances show no clear dependency on the pressure, indicating that the coagulating forces in this suspension are stronger than those exerted by gravity. Another important observation in Fig. 7.16 is that with higher DoBS acid levels, at a given pressure, the particles are closer together, whereas also the gradients become steeper. Again, these two results can be considered as in agreement with the action of electrostatic repulsive barriers, which at higher ionic strengths become positioned closer to the surface, whereas at the same time the slopes of the energy barriers become steeper (see Fig. 4.12).

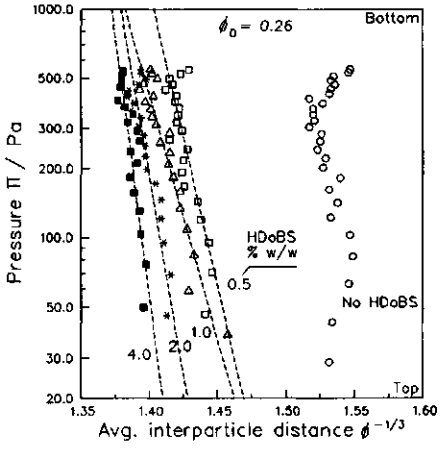

Fig. 7.16: Pressures in equilibrium sediments as a function of average interparticle distance, in unstable and HDoBS-stabilized suspensions of soda ash in Imbentin.

7.5.2.2 Theoretical repulsive pressures in sediments

In Fig. 7.17, the experimental pressures for one of the sediments given in Fig. 7.16, viz. that with 1 % w/w DoBS acid, are compared with the theoretical pressures which develop due to the overlap of the electrostatic double layers. The parameters substituted in the calculation are the same as those given in Fig. 7.16. We recall that they are the results of actual measurements in the supernatants. The repulsive pressure between the particles is calculated using Eq. 4.27. The comparison shows that the electrostatic repulsions which develop upon addition of 1 % w/w of HDoBS are easily sufficient to create a repulsion which cannot be surpassed by the forces exerted by gravity in the sediments. However, from the best guess for the maximum volume fraction $\phi_{max} = 0.40$, the distances at which these electrostatic pressures operate are much shorter than the distances where these pressures develop in the practical suspension. The discrepancy can be explained by again supposing that particle protrusions control the actual interparticle distances. The electrostatic repulsion is supposed to play a role in the interactions of the protrusions and is able to stabilize them against coagulation.

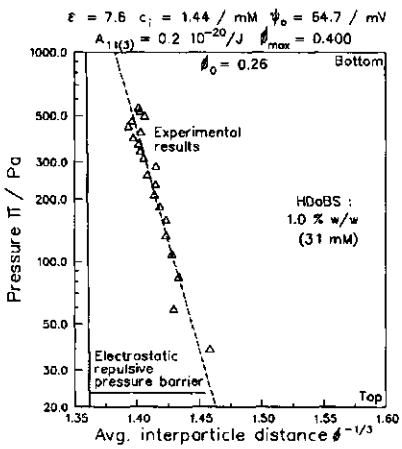

Fig. 7.17: Comparison of the experimental sediment pressure with theoretical computations.

Particularly in horizontal planes in the sediments, where gravity does not press the particles against each other, interparticle distances may be sufficiently large to have a contribution of these secondary minimum interactions.

7.5.2.3 Network moduli as a function of volume fraction

Experimentally it is found from the plot of ln Π versus $\phi^{-1/3}$ that

$$\Pi(\phi) = \mathbf{I} \exp(-\mathbf{S}\, \phi^{-\frac{1}{3}}) \qquad [7.4]$$

where I and S are the intercept and slope of the linear relations in Fig. 7.16, respectively. From the slope S, the network modulus $K(\phi)$, defined as $\phi\, d\Pi/d\phi$ (Eq. 5.27), can directly be evaluated at any combination of the pressure $\Pi(\phi)$ and ϕ, giving

$$K(\phi) = \frac{1}{3}\mathbf{S}\, \Pi(\phi)\, \phi^{-\frac{1}{3}} \qquad [7.5]$$

In Fig. 7.18, again for suspensions of soda ash in Imbentin, the experimental network moduli $K(\phi)$ obtained with various DoBS acid concentrations are plotted against the volume fraction solids. The results show that the network moduli found for our stabilized sediments vary between ca. 2×10^3 Pa at the top to ca. 2×10^4 Pa at the bottom. The results are in same range or a little higher than those derived of the shear moduli by Buscall (1981) [7.8] of electrostatically stabilized latices, but lower than those reported by Sonntag and Strenge (1987) [7.2] of coagulated dispersions of fumed silica in decane. Extrapolation of the network moduli of the unstable suspensions ('No HDoBS') to higher volume fractions suggest that, at the same volume fraction, network moduli of the unstable suspensions are much higher than those of the stable suspensions. This is also observed for the shear moduli. For the HDoBS-stabilized suspensions the network moduli increase with increasing solid concentrations and decrease with increasing amounts of DoBS acid. These results are consistent with the idea that the network modulus depends upon the number and strengths of bonds between particles (Sonntag and Strenge, 1987) [7.2]. At given particle size the number of bonds depends linearly upon the solids concentration, i.e. $K(\phi)$ should increase with increasing ϕ, as is found experimentally. The results are further in line with the idea that upon addition of DoBS acid the product of number and strength of the bonds decreases.

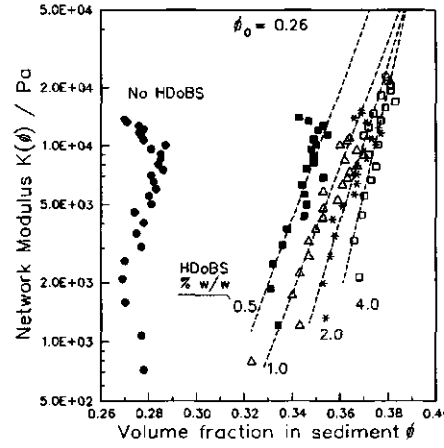

Fig. 7.18: Network Modulus as a function of the volume fraction in sediments of soda ash in Imbentin, stabilized by various levels of DoBS acid.

Unfortunately, the measurements of the shear modulus and those of the network modulus have not been carried out with the same suspensions. Hence, a direct comparison of the two different resulting moduli is not (yet) possible. The higher values of the network modulus found in the soda ash - Imbentin system could therefore not be used to support the theory of Sonntag and Strenge. The difference could also be ascribed to the smaller particle sizes of soda ash particles investigated in the network modulus measurements.

7.5.2.4 Theoretical network moduli in sediments

The theoretical network moduli can be derived from the pressure between two spherical particles. To this end, the attractive force between a pair of spherical particles $F_A^{(sphere)}$, calculated using Eqs. 3.15 and 3.17, is converted to a pressure between two spherical particles using the effective surface area for attraction between two spherical particles (Israelachvili, 1985) [7.13]. For attraction it follows that

$$P_A = \frac{1}{2\pi a H} F_A^{(sphere)} \qquad [7.6]$$

Addition of this joining pressure to the repulsive pressure between two spheres (Eq. 4.44), allows the evaluation of the total pressure between two spherical particles, i.e.

$$\Pi = \frac{1}{\pi a\, 2H} F_A^{(sphere)} + \frac{1}{\pi a \frac{1}{\kappa}} F_R^{(sphere)} \qquad [7.7]$$

The first derivative of the pressure to the volume fraction can be written as

$$\frac{d\Pi}{d\phi} = -\frac{R}{3\phi} \frac{d\Pi}{dH} \qquad [7.8]$$

The theoretical network modulus $K(\phi)$ ($= \phi\, d\Pi/d\phi$) can now be derived from the first derivative of the total pressure Π with regard to the distance, i.e.

$$K(\phi) = -\frac{R}{3} \frac{d\Pi}{dH} \qquad [7.9]$$

and can be numerically computed from Eq. 7.7.

In Fig. 7.19, the experimental network moduli for one of the suspensions considered in Fig. 7.18, viz. that with 1 % w/w DoBS acid, are compared with the theoretical network moduli. The comparison shows that the electrostatic repulsion which develops upon the addition of 1 % w/w of HDoBS, results in network moduli which are much larger than those experimentally found. However, using again a maximum volume fraction $\phi_{max} = 0.40$ to estimate the interparticle distances, the distances at which these moduli become effective are again much shorter than the distances of the experimental results. This observation is consistent with that obtained for the shear moduli and the pressures. It again suggests that, at larger distance than the particle surfaces, there exist contact points between particles where the attraction is stronger than theoretically predicted. This causes stronger bonding and higher moduli. In line with the point made earlier it is suggested that this is due to interactions of the particle protrusions.

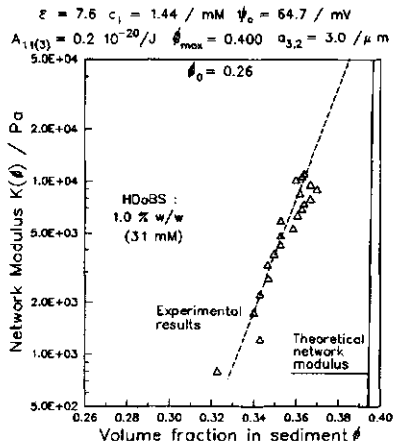

Fig. 7.19: Comparison of the experimental and the theoretical network moduli, derived from the electrostatic parameters in a suspension of soda ash in Imbentin stabilized with 1 % w/w HDoBS.

In conclusion, consolidation of the sediments and the reduction of the network moduli found on addition of DoBS acid, demonstrate an increasing degree of de-coagulation with increasing HDoBS level. However, comparison of the network moduli found in practice, with the literature values suggests that complete de-coagulation on all points of contact is not achieved, even with the highest DoBS acid level. This also follows from the equilibrium volume fractions found in sediments.

7.6 CONCLUDING DISCUSSION: STERIC OR ELECTROSTATIC STABILIZATION ?

Addition of DoBS acid to suspensions of detergent solids leads to de-coagulation and to colloidal stabilization. This follows from the change in viscosity as well as from the compaction of the sediments. At the same time, the ion concentrations in the continuous phase and the surface charge are increased. The DLVO theory was shown to be applicable to low-polar systems. With this theory, using observed electric and dielectric data, it was found that significant repulsive forces and energies could be attained.

Various observations suggest that suspensions of detergent solids as such have only relatively weak attractive interactions. This is caused by the fact that the Hamaker constants of detergent solids which are lower than those of oxides and only a little higher than those of the nonionics. It was further shown that in the presence of DoBS acid the suspensions behave as colloidally stable 'hard sphere' systems. The combination of the large repulsive forces and the small van der Waals attractions could well account for the colloidal stabilization obtained.

A number of observations have led to the conviction that the nature of the colloidal stabilization obtained is indeed electrostatic. The first is that of the correlation between the low shear viscosity and the ζ-potential. Both phenomena undergo a large change upon addition of only 15 mM (0.5 %w/w) of DoBS. The second observation is that the electrostatic repulsive force, calculated using the measured electric and dielectric parameters, relates to the consistency. The third observation is that in creep compliance experiments at low applied stresses, relatively low and completely recoverable moduli could be obtained, which we interpret as indicative of electrostatic interactions. The fourth is that the shear moduli obtained from creep compliance are in good agreement with the maximum values predicted on the basis of the electrostatic repulsion. The fifth is that in settled sediments, pressure patterns show a dependency on the interparticle distance which is in agreement with the equations for electrostatic repulsion: the steepness becomes larger, as well as the distance from the surface was found to become smaller with the rise of the acid concentration. As further circumstantial evidence it may be added that the adsorption of HDoBS is so small that no thick layers can be formed that would be able to produce steric stabilization. Also the complete independence of any temperature effect of the colloidal stabilization makes the possibility of steric stabilization by HDoBS less likely.

In spite of this strong evidence in favour of electrostatic stabilization still a number of questions are remaining. A quantitative explanation for the larger than theoretical interparticle distances emerging from the sedimentation results, from creep compliance results and from the γ-ray absorption work and the large distances at which the repulsive forces are operational could not yet be found. Also in equilibrium sediments the distances are much larger than for smooth particles which rest upon each other's double layers. There are indications that some degree of coagulation in the suspension sediment still remains or, for that matter, that addition of DoBS acid has led only to a partial de-coagulation. It may be that this effect is the result of the presence of protrusions or of the presence of a fraction of small particles which cannot be excluded from our systems. It may be that this is also the reason for the consistency - repulsive force relations which are found to be different for STP and soda ash. These unanswered questions will be an area for further research. Preferably, for that purpose systems we would like to have at our disposal well-defined homodisperse spherical particles.

Accepting that not in all respects a complete quantitative interpretation could be achieved, it is gratifying that so much mechanistic insight into the stabilization of non-aqueous suspensions could be obtained with only moderately characterized systems.

7.7 SUMMARY

Addition of DoBS acid was found to have little or no influence on the viscosity at 'infinite' shear rate of nonionic suspensions. This because this viscosity is governed by hydrodynamic interactions, which are, in turn, determined by the viscosity of the nonionic phase, the temperature and the solids volume fraction. The nature of the solid also has an influence on the 'infinite shear' viscosity. Probably, this is related to the variation in size of the protrusions, causing their effective volumes to be larger than the solids volume. Measurements of the intrinsic viscosity of STP indicated that the particles of this substance are almost spherical.

Low shear rate viscosities monitor effects of interparticle interactions. The consistency, which quantifies the particle interactions, was found to be inversely proportional to the particle volume. Addition of DoBS acid reduces the consistency. The main effect is already obtained from 0.5 % w/w (15 mM dm^{-3}); increase of this concentration has only a limited further influence. In this respect the behaviour of the viscosity is correlated with that of the ζ-potential of the particles. It was also found that the drop in the 'normalized' consistency has a direct relation to the electrostatic force. These results support the conclusion that the nature of the stabilization obtained is electrostatic. The linear dependency of the 'normalized' viscosity on the Péclet number further supports this conclusion. It shows that HDoBS-stabilized systems can as a first approximation be considered as hard-sphere suspensions.

Creep compliance measurements of suspensions of STP in Plurafac at high volume

fractions demonstrate that at low shear stresses the interactions are completely elastic. Under those conditions relaxation of the stress leads to almost complete recovery. The shear moduli as a function of the volume fraction, which are derived from the creep compliance data, drop less steeply than theoretically predicted. It is possible that this effect is a result of secondary minimum coagulation by the particle protrusions.

Measurements of γ-ray absorption demonstrate that the particle concentration from top to bottom in a stable sediment shows a concentration gradient. For HDoBS-stabilized suspensions this gradient is more continuous, whereas in unstable suspensions, due to coagulation, it is very irregular. Pressures show an exponential relation to the interparticle distances. With low levels of DoBS acid the distances between particles are larger than on application of high concentrations of HDoBS. These results are in agreement with the dependency predicted by the electrostatic repulsion, although the experimental pressure drop as a function of distance is much more gradual than the one theoretically predicted. The experimental network moduli derived from the pressure-volume fraction relation also drop much more slowly than theoretically predicted. Again here this may be a result of secondary minimum coagulation occurring by the protrusions.

The overall conclusion is that the suspensions under consideration are electrostatically stabilized with DoBS-acid as the charge-determining electrolyte.

7.8 BIBLIOGRAPHY

7.1 **Rheology of NonNewtonian fluids: A new flow equation for pseudoplastic systems.** Cross, M.M.. *J. Colloid Sci.* **1965,** 20, 417-437.

7.2 **Coagulation kinetics and Structure Formation.** Sonntag, H.; Strenge, K.. (Plenum Press, London, UK). 1987.

7.3 **An introduction to rheology.** Barnes, H.A.; Hutton, J.F.; Walters, K..(Elsevier, Amsterdam). **1989.**

7.4 **Rheology of WeaklyInteracting Colloidal Particles at High Concentration.** Buscall, R.; McGowan, I.J.; Mumme-Young, C.O.. *Faraday Discuss. Chem. Soc.* **1990,** 90, in press.

7.5 Lenthe, J.H. van; Duijneveldt-van de Rijdt, J.G.C.M. van; Duijneveldt, F.B. van.. *Adv. Chem. Phys.* **1987,** 69, 521; **Hoe sterk is een waterstofbrug?** Duijneveldt, F.B. van.; Duijneveldt-van de Rijdt, J.G.C.M. van..*Chem. Mag.* **1990,** 6/7, 333.

7.6 **Some uses of rheology in colloid sciences.** Goodwin, J.W.. **Ch. 6. Colloidal dispersions.** Goodwin, J.W.. Editor. Spec. Publ. 43. (Royal Society Chem., London). **1981**; Leal, L.G.; Hinch, E.J.. **The effect of weak Brownian rotations on particles in shear flow.** *J. Fluid Mech.* **1971,** 46 (4), 685 - 703.

7.7 **Review of the Role of Colloidal Forces in the Rheology of Suspensions.** Russel, W.B.. *J. Rheology.* **1980,** 24 (3), 287-317.

7.8 **Viscoelastic Properties of Concentrated Latices. Part 2. Theoretical Analysis.** Buscall, R.; Goodwin, J.W.; Hawkins, M.W.; Ottewill, R.H.. *J. Chem. Soc., Faraday Trans. 1,* **1982,** 78, 2889-2899.

7.9 **Comments on "Highly Elastic 'Crystals' of Deionized Colloidal Spheres" by T. Okubo.** Buscall, R.. *J. Colloid Interface Sci.* **1990,** 138, 587-588.

7.10 **Concentration Dependence of the Linear Elastic Behaviour of Model Microgel Dispersions.** Evans, I.D.; Lips, A.. *J. Chem. Soc., Faraday Trans.* **1991,** in press.

7.11 **Microscopic observation of ordered colloids in sedimentation equilibrium and important role of Debye-screening length. I. Heavy and monodispersed polystyrene type spheres (specific gravity = 1.50) in aqueous and aqueous-methanol suspensions.** Okubo, T.. *J. Chem. Phys.* **1987,** 86 (4), 2394-2399.

7.12 **Shear thickening (Dilatancy) in Concentrated Dispersions.** Boersma, W.H.; Laven, J.; Stein, H.N.. *J. Amer. Int. Chem. Engng.* **1990,** 36 (3), 321-332.

7.13 **Intermolecular and surface forces. With applications to colloidal and biological systems.** Israelachvili, J.N.. (Academic Press, London, UK) **1985.**

SUMMARY

Concentrated suspensions of detergent powder solids in a liquid nonionic surfactant are considered for practical application as liquid detergent products. If no precautions are taken, upon storage the viscosity of such suspensions increases and the pourability drops because the suspensions are colloidally unstable. It has been found that after the addition of a small amount of dodecylbenzene sulphonic acid (DoBS-acid or HDoBS) good pourability is maintained on storage. All the phenomena observed with such suspensions suggest that the addition of DoBS-acid reduces coagulation and improves colloidal stability. It was hypothesized that the colloidal stability obtained is of an electrostatic nature. In a liquid non-aqueous medium this is unexpected. A study of the mechanism of stabilization is described in this thesis.

After a general introduction to the topic in Chapter 1, in Chapter 2 we discuss the character of the interactions which play a role in nonionic suspensions. The used nonionics are condensates of long chain alcohols and 3 to 9 alkylene oxide units. The dispersed solids are sodium salts as are usually present in current detergent powders, or oxides. They are aggregates or agglomerates of smaller crystalline primary particles and consist of irregular spheroids. The solids, the liquid nonionics and the anionic acid have been characterized with respect to a number of properties, including the molecular and crystalline structure, specific density, specific surface area, porosity, axial ratio and water content. The refractive indices and dielectric constants of the liquids and solids are also measured. Elemental analysis of the supernatants of our suspensions is carried out by Atomic Absorption, by Plasma Emission and by X-ray Fluorescence Spectroscopy. Since analysis of the supernatants indicated only very limited dissolution of the solids, it is concluded that the suspensions are lyophobic. It is demonstrated that, when DoBS-acid is added to a suspension of sodium salts in nonionic, it is converted quantitatively into anionic NaDoBS.

Sedimentation rates, sediment volumes and viscosities are important physical characteristics of concentrated nonionic suspensions; they reflect the interactions between the suspended particles. The interactions follow the DLVO-theory, meaning that they are governed by the balance between attractive and repulsive or 'stabilizing' forces.

The literature on van der Waals attraction (energy and forces) between particles in suspension is discussed in Chapter 3. It shows that for particles in the micron-size range, geometrical parameters (differences in particle size, interparticle distance), retardation and surface roughness are of more importance than in colloidal systems, having smaller particles. This means that the van der Waals bonding energy obtained on approach is larger, but, as a function of increasing interparticle distances, it decays more rapidly.

In the van der Waals attraction, material properties are reflected in the Hamaker constant. Hamaker constants for the inorganic crystalline solids considered in this study are not available in the literature. Therefore it was necessary to evaluate them theoretically. Two approaches have been applied, a macroscopic theory and a microscopic theory. In a comparison they gave identical results within a few tens of percent. For the crystalline detergent solids the constants have been evaluated from their dielectric constants and refractive indices. The results showed the Hamaker constants for the detergent solids (except activated Zeolite 4A) to exceed those of the nonionics, but to be lower than those of the metal oxides. The differences between the constants of crystalline detergent solids and those of nonionics are relatively small, implying that suspensions of detergent solid particles in nonionics can be made to relatively high volume fractions and can be stabilized easily.

In Chapter 4 the electrostatic theory for interactions of particle pairs in suspension is evaluated for its applicability in non-aqueous media, using models of plates and spheres. For both models the conclusion is that, for the calculation of the repulsive energies and forces, approximated equations can be used. They result in repulsive energies, pressures and forces, which are in good agreement with those of exact computations at distances > 10 nm, but underestimate the repulsions at shorter distances.

DLVO energy and force curves have been constructed and demonstrate the dependence of the repulsion on five parameters that govern the behaviour, viz. the dielectric constant, the ionic strength, the electric surface potential, the Hamaker constant and the particle size. For our suspensions with surface potentials ≥ 20 mV, significant repulsions already develop at distances between 2 and 40 nm. The theoretical repulsions are much higher than the van der Waals attractions and cause much larger repulsive barriers than those usually reported for non-polar, non-aqueous media. They are expected to play a role in the colloidal stabilization of nonionic suspensions and to influence the resistance against coagulation under pressures at the bottom of sediments. Secondary minima are only a few kT at most and coagulation is only expected at the protrusion points of contact and at relatively high ionic strengths.

Ionic strengths in HDoBS-stabilized suspensions in the nonionics Plurafac LFRA30 and Imbentin C91/35 are evaluated from the conductivity in the supernatants and from their respective limiting molar conductivities. The methodology is described in Chapter 5. It was found that in both nonionics the limiting molar conductivity was lower than predicted from the values in water assuming Walden's rule applies. The results indicate that solvation interactions of Na^+ and $DoBS^-$ ions in nonionics are stronger than in water and stronger in Imbentin than in Plurafac.

In Chapter 6 the results of the electric and dielectric measurements have been given. It is shown that the dielectric constant of nonionic is increased by HDoBS. Taking this increase into account, the ionic strengths found can be satisfactorily explained from theory. Only at high HDoBS concentration and relatively high

dielectric constants are the ion concentrations lower than theoretically predicted, a feature that could be due to the formation of 'molecular associates'.

From the limiting conductivities, at HDoBS concentrations between 10 and 150 mM, the ionic strengths have been found to range from 0.05 to 4 mM in Plurafac and from 0.08 to 30 mM in Imbentin. These results demonstrate a weak dissociation of the NaDoBS electrolyte. However, the ionic strengths obtained are considerably larger than those in supernatants of unstable suspensions and are higher than ever reported in the 'non-polar' hydrocarbon media, commonly considered in non-aqueous studies. Liquid nonionic media have a dielectric constant between 5 and 12 and are denoted 'low-polar'. At these ionic strengths, and considering the enhancement of the dielectric constant by HDoBS, in the HDoBS concentration regime between 0.5 and 150 mM, Debye lengths range from 33 to 1 nm in Plurafac and from 13 to 1 nm in Imbentin, i.e. in the same range as in aqueous media.

Electrokinetic (ζ-)potentials of particles of detergent solids suspended in nonionics, given in Chapter 6, are found to be a function of the HDoBS concentration. The surface potentials tend to level off at HDoBS concentrations as low as 0.5 % w/w (15 mM dm^{-3}), to a maximum value ranging from +25 to +70 mV, depending on the nature of the solid and the nonionic liquid. Addition of water or of a crown-complexant (15-Crown-5), reduces the ζ-potential. The formation of positive surface charges can be explained from the dissociation of adsorbed HDoBS.

Mechanical properties of concentrated non-aqueous suspensions are discussed in Chapter 7, including their relation to the electrostatic repulsion. Rheology is used to monitor the properties under dynamic conditions. The consistency, which quantifies the particle interactions and shear thinning index was derived from the Sisko model.

Addition of HDoBS was found to have little or no influence on the high shear rate viscosity of nonionic suspensions. This viscosity is governed by hydrodynamic interactions, which are, in turn, determined by the viscosity of the nonionic phase, the volume fraction and the temperature. The nature of the solid also has an influence on the 'infinite shear' viscosity, probably due to variations in protrusion size, causing their effective volumes to be larger than the actual volume. Measurements of the intrinsic viscosity of sodium tripolyphosphate (STP) indicated that the particles of this substance are almost spherical.

Low shear rate viscosities monitor effects of interparticle interactions. The consistency was found to be inversely proportional to the particle volume. Addition of HDoBS reduces the consistency. As with the ζ-potentials, the main effect is already obtained from 0.5 % w/w HDoBS. In this respect the behaviour of the viscosity is correlated with that of the ζ-potential of the particles. It is further found that the drop in the 'normalized' consistency has a direct relation to the electrostatic force. These results support the conclusion that the nature of the obtained stabilization is electrostatic. The correlation of the viscosity with the

Péclet number further supports this conclusion. It shows that under shear HDoBS-stabilized systems can be considered as hard-sphere suspensions.

Creep compliance measurements of suspensions of STP in Plurafac at high volume fractions demonstrated that at low shear stresses the interactions are completely elastic. Under those conditions, relaxation of the stress leads to almost complete recovery. The shear moduli derived from creep compliance, drop less steeply as a function of the volume fraction than predicted from the electrostatic repulsive barrier. It is possible that this difference is a result of secondary minimum coagulation by the particle protrusions.

In static sediments the volume fractions can be measured as a function of height by γ-ray absorption. Measurements of γ-ray absorption shows that the particle concentration from top to bottom in a stable sediment shows a concentration gradient. For HDoBS-stabilized suspensions this gradient is more continuous, whereas in unstable suspensions, due to coagulation, it is very irregular. From these results the relations between the static pressure or the network modulus and the volume fraction are derived. Pressures show an exponential relation with the interparticle distances. With low levels of DoBS-acid the interparticle distances are larger than for high concentrations of HDoBS. These results are in agreement with the dependency predicted by electrostatic repulsion, although the experimental pressure drop as a function of distance is much smoother than that theoretically predicted. The experimental network moduli derived from the pressure-volume fraction relation also drop much more slowly than theoretically predicted. This may again be a result of secondary minimum coagulation occurring by the protrusions.

The overall conclusion is that the suspensions under consideration are electrostatically stabilized with DoBS-acid as the charge-determining electrolyte.

SAMENVATTING

Dit proefschrift betreft een experimenteel onderzoek naar het gedrag van deeltjes, gemengd met een oplosmiddel. Deze deeltjes hebben een grootte van ongeveer vijf micrometer en bevinden zich daarmee op de grens van wat met het blote oog nog zichtbaar is. In hoofdzaak zijn deeltjes bestudeerd, die normaal als vaste ingrediënten in waspoeders aanwezig zijn. Waspoeders, zoals die bijvoorbeeld gebruikt worden voor het reinigen van textiel, voor het wassen van de vaat of voor het schoonmaken van harde oppervlakken. Naast deze wasmiddeldeeltjes zijn ook minerale deeltjes zoals kleideeltjes of poedervormig mica op beperkte schaal toegepast in het onderzoek. Deze vaste stoffen worden allen gekenmerkt door het feit dat het voornamelijk natriumzouten zijn met een zuurrest waarin zuurstof het belangrijkste element is. Ook zijn enkele oxyden van metalen, zoals die soms worden gebruikt in pigmenten en verven, bestudeerd. Meestal zijn de deeltjes opgebouwd uit kleine kristalletjes die samengeklonterd zijn tijdens het produktie-proces. Zij hebben daardoor een ruw oppervlak en zijn meestal nagenoeg bolvormig. Ze zijn soms ook poreus.

De oplosmiddelen waarmee de deeltjes zijn gemengd behoren tot de niet-ionogene oppervlakte-actieve stoffen of 'nonionics'. Nonionics vormen een klasse van meestal vloeibare organische stoffen opgebouwd uit de elementen koolstof, zuurstof en waterstof. Nonionics leveren een belangrijke bijdrage aan de was-werking, in het bijzonder bij de verwijdering van vettig vuil en worden daarom in alle mogelijke wasmiddelen gebruikt. Voorbeelden hiervan zijn de poedervormige en vloeibare wasmiddelen voor de textielwas, shampoos, schoonmaakmiddelen en spoelglansmiddelen voor de machinale vaatwas. In wasmiddelen worden bij voorkeur nonionics gebruikt omdat ze uitstekende eigenschappen hebben wat betreft hun biologische aanvaardbaarheid. Zo zijn ze zeer mild bij direct contact met mens en dier, ze zijn goed biologisch afbreekbaar en na afbraak in het milieu blijft alleen water en CO_2 achter. Nonionics worden in bulk-hoeveelheden geproduceerd door de petrochemische industrie. Zij worden gemaakt uit alcoholen, met een lange alkylstaart, en ethyleen-oxyde.

De vloeibare nonionics die gebruikt zijn voor dit onderzoek, Plurafac LFRA30 en Imbentin C91/35, hebben karakteristieke eigenschappen. Ze zijn goed oplosbaar in water. Zelf zijn ze echter, net als bijvoorbeeld spijsolie, spiritus (methanol) of benzine, bijna geheel vrij van water en worden daarom 'niet-waterige vloeistoffen' genoemd. Ze zijn, ondanks dat ze wat langzamer stromen dan water, goed schenkbaar. Twintig jaar geleden werd al overwogen mengsels van poedervormige wasmiddel-ingrediënten met nonionics te gebruiken als een vloeibaar wasmiddel. Men dacht daarbij aan toepassingsmogelijkheden voor de machinale textielwas, voor de vaatwas en voor de schoonmaak van harde oppervlakken, zoals vloeren en wanden. Een groot voordeel van een dergelijk wasmiddel zou zijn dat het, omdat het watervrij is, uitsluitend actieve ingrediënten bevat en daardoor een klein volume heeft. Ook bleekmiddelen kunnen worden toegepast in zo'n produkt omdat ze door afwezigheid van water niet ontleden. Tot voor kort is het echter niet gelukt

een mengsel van de wasmiddel-ingrediënten met nonionic te maken dat fysisch stabiel was en bleef. De meeste problemen ontstonden doordat de mengsels dik stroperig of zelfs vast werden gedurende de opslag in de winkel. Een probleem dat niet op eenvoudige wijze oplosbaar leek.

Het probleem dat mengsels dik-stroperig worden, schreef men toe aan zogenaamde 'kolloïdale instabiliteit'. Dit is een begrip dat aangeeft dat deeltjes in een vloeistof de neiging hebben bij een onderlinge ontmoeting een verbinding te vormen en zo samen te vlokken tot grotere klonten. Dergelijke samengeklonterde mengsels stromen slechts moeizaam of worden in extreme gevallen volledig stijf en vormen dan een gel. Kolloïdale instabiliteit is een gevolg van aanwezigheid van een aantrekkende kracht tussen de deeltjes, die genoemd is naar de Nederlander Van der Waals. Het is ook deze aantrekkende Van der Waals kracht die er mede voor verantwoordelijk is dat damp condenseert tot een vloeistof.

Zoals beschreven in Hoofdstuk 1 van dit proefschrift, werd in de beginfase van ons onderzoek ontdekt dat toevoeging van een kleine hoeveelheid van een sterk zuur, namelijk DodecylBenzeen Sulfonzuur (verder afgekort tot DoBS-zuur of HDoBS), in staat was het mengsel volkomen 'kolloïdaal stabiel' te maken en dus klontvorming te onderdrukken. Ongeveer 0.5 gewichtprocenten bleken al voldoende voor een drastisch effect. DoBS-zuur is de zure vorm van een ingrediënt, die, net als de vloeibare nonionic, in vele wasmiddel-samenstellingen wordt gebruikt. Het natriumzout van deze verbinding is na gewone zeep waarschijnlijk de meest toegepaste oppervlakte-actieve stof. De gegevens over samenstelling en eigenschappen van DoBS-zuur en van de andere gebruikte grondstoffen zijn beschreven in Hoofdstuk 2. In mengsels van onze vaste stoffen en nonionic werden na de toevoeging van HDoBS goed vloeiende eigenschappen verkregen en deze bleven behouden, ook na langdurige opslag bij verhoogde temperatuur. Deze vinding heeft een nieuwe impuls gegeven aan de ontwikkeling van niet-waterige vloeibare wasmiddelen.

Het effect van DoBS-zuur leidde tot de veronderstelling dat de kolloïdale stabiliteit was verkregen door een door deze toevoeging veroorzaakt afstoting tussen de vaste deeltjes. Dit afstotend effect zou dan leiden tot een vermindering van de invloed van de Van der Waals aantrekking. De geringe hoeveelheid HDoBS, hiertoe nodig, suggereerde dat de afstoting niet direct een gevolg was van de fysieke aanwezigheid van HDoBS, maar van de vorming van een elektrische lading op de oppervlakken van de deeltjes. Dat gelijknamige elektrische ladingen leiden tot afstoting en tot kolloïdale stabiliteit is op zich niets ongewoons en wordt in vele waterige mengsels gevonden. Het speelt in vele processen in de natuur een belangrijke rol. Echter dat dit zou leiden tot kolloïdale stabiliteit in een niet-waterige medium was iets nieuws. Op grond van de tot nog toe beschreven ervaringen in de literatuur was dit niet te verwachten. Er was dus alle aanleiding voor een nader onderzoek naar het werkingsmechanisme. Als dit werkingsmechanisme bekend is kan deze kennis behulpzaam zijn bij het optimaliseren van het effect of zij kan worden toegepast op andere mengsels in niet-waterige media, eventueel ook buiten het gebied van wasmiddelen, zoals bijvoorbeeld bij het bereiden van niet-waterige medicamenten, pigmenten en verven. Andere toepas-

singsgebieden zijn de tertiaire oliewinning, bodemsanering, of keramische materialen.

De resultaten van het experimentele onderzoek naar het werkingsmechanisme van DoBS-zuur in mengsels van onoplosbare vaste stoffen in nonionic vormen het onderwerp van Hoofdstuk 5 tot 7 van dit proefschrift.

Om te kunnen vaststellen of de verandering van de eigenschappen van het mengsel inderdaad veroorzaakt wordt door elektrostatische effecten, moet eerst worden vastgesteld of er reden is voor de aanwezigheid van een elektrostatische kracht. Uit een onderzoek van de literatuur, in Hoofdstuk 4, blijkt dat hiervoor aan twee voorwaarden moet worden voldaan. De eerste is dat er een lading op het oppervlak van de deeltjes wordt gevormd die aanleiding geeft tot een voldoende potentiaalverschil met de vloeistof. De tweede is de aanwezigheid van 'voldoende' ionen in de vloeibare fase. Vooral aan deze laatste voorwaarde wordt in niet-waterige media meestal niet voldaan. In de meeste niet-waterige vloeistoffen zijn de concentraties aan ionen namelijk buitengewoon laag. Zo laag dat zich daardoor, ondanks aanzienlijke potentiaalverschillen, geen voldoend grote afstotende elektrostatische kracht kan ontwikkelen. Een voorbeeld is bijvoorbeeld benzine waarin ionen, afkomstig van verontreinigingen, kunnen voorkomen in concentraties van slechts 1 op de 1.000.000.000 benzine moleculen. In zo'n medium is de opgewekte afstotende elektrostatische kracht tussen deeltjes dan ook buitengewoon klein. De afstotende elektrostatische kracht neemt toe met de concentratie van ionen. Theoretisch onderzoek leerde ons dat voor een voldoende afstotende kracht in niet-waterig milieu er een concentratie van ionen van minstens 1 op de 10.000 moleculen moet zijn. Onderzoek ter bepaling van de oppervlakte-potentiaal van in nonionic gemengde deeltjes is dus even belangrijk als het onderzoek naar de concentraties van de ionen.

De tweede factor die moest worden vastgesteld is of de sterkte van de Van der Waals aantrekking klein genoeg was om te kunnen worden overheerst door de elektrostatisch afstoting. Immers, als de Van der Waals aantrekking heel groot zou zijn zouden misschien onmogelijk grote afstotende krachten noodzakelijk zijn voor een elektrostatische stabilisatie. Een literatuur onderzoek, gegeven in Hoofdstuk 3, voerde ons naar de methoden die gebruikt konden worden om de grootte van de Van der Waals aantrekking te kunnen bepalen.

De toegepaste werkwijzen omvatten voor het merendeel bekende methoden. Ze zijn besproken in Hoofdstuk 5. Slechts in enkele gevallen was het nodig om zelf onze onderzoeksmethoden te ontwikkelen. De potentiaalverschillen werden afgeleid uit metingen van snelheden van de deeltjes in een aangelegd elektrostatisch veld. De ionen concentraties werden bepaald door middel van meting van de geleidbaarheid. De metingen van de brekingsindex en de diëlectrische eigenschappen van de vaste stoffen en vloeistoffen gaf ons een beeld van de aantrekkende Van der Waals kracht. De resultaten van deze metingen zijn weergegeven in Hoofdstuk 6.

De resultaten tonen aan dat HDoBS een zeer grote invloed heeft op de potentiaalverschillen. Het grootste effect daarop wordt al waargenomen na toevoeging van

een hoeveelheid van 0.5 gewichtprocenten HDoBS. Ook de ionenconcentratie neemt door toevoeging van HDoBS sterk toe. Concentraties van 1 op de 1000 moleculen worden gemakkelijk bereikt, vooral omdat door toevoeging van zuur de diëlektrische constante van de vloeistof wordt verhoogd. Als deze invloed in beschouwing wordt genomen blijken de concentraties van ionen bijna volledig theoretisch voorspelbaar. De gevonden ionenconcentraties zijn veel hoger dan men ooit eerder vond in een dergelijk niet-waterig oplosmiddel.

De elektrostatische afstoting die het gevolg is van deze combinatie van effecten van HDoBS is bij concentraties van 0.5 gewichtprocenten op enige afstand van het deeltjesoppervlak veel groter dan de Van der Waals aantrekking en zij is gemakkelijk in staat tot de vorming van grote afstotende barrières. De afstoting is zo groot dat de deeltjes zelfs op de bodem van de mengsels, waar deeltjes door de zwaartekracht een grote kracht op elkaar uitoefenen, niet kunnen klonteren. Een verschijnsel dat wel optreedt bij afwezigheid van HDoBS.

Naast de elektrostatische eigenschappen zijn ook de mechanische eigenschappen van mengsels bestudeerd. Tot de mechanisch eigenschappen van een vloeibaar mengsel behoren de vloeibaarheid ervan en de uitzaksnelheid van deeltjes. Deze beide factoren zijn van belang voor het schenkgedrag en de snelheid van afscheiding van produkten. Toevoeging van een half procent DoBS-zuur heeft een drastische invloed zowel op het stroomgedrag van de mengsels in nonionic, als op het potentiaalverschil. Dit werd al vrij snel duidelijk uit de eerste experimenten. De resultaten suggereerden een directe relatie tussen deze twee factoren. Voorts kon een oorzakelijk verband tussen de opgewekte elektrostatische afstoting en de verandering van de mechanische eigenschappen worden aangetoond. Hiertoe werd de vloeibaarheid van verschillende mengsels bij aanwezigheid van verschillende concentraties DoBS-zuur nauwkeurig bepaald. Uit de resultaten van de metingen, weergegeven in Hoofdstuk 7, kan verder worden geconcludeerd dat de deeltjes in stroming zich inderdaad gedragen als elkaar afstotende bolletjes. Er kon zelfs kwantitatief worden aangetoond dat een vergroting van de elektrostatische afstotende kracht rechtstreeks de kracht die aanleiding geeft tot klonteren doet afnemen. Ook werd, als een zeer kleine kracht werd aangebracht, een elasticiteit gevonden die qua grootte goed overeen kwam met de elasticiteit die direct uit de gemeten potentiaalverschillen en ionen concentraties kon worden afgeleid.

De statische eigenschappen van mengsels in nonionics werden gemeten met behulp van een bundel radioactieve straling. Door de mate van absorptie van deze straling te meten in een mengsel, zijn we in staat de plaatselijke concentraties van deeltjes direct te bepalen. Dit geeft bijvoorbeeld inzicht in de invloed van de zwaartekracht in verhouding tot de aantrekkingskracht tussen de deeltjes. Is de aantrekkingskracht tussen de deeltje klein, dan concentreren zich onderin meer deeltjes dan bovenin. Uit de resultaten van metingen, die eveneens zijn besproken in Hoofdstuk 7, blijkt dat na toevoeging van HDoBS de deeltjes in de mengsels zich inderdaad gemakkelijker bewegen door de gecreëerde vermindering van de aantrekking. De hogere druk onderin wordt veroorzaakt door de sommatie van de gewichten van bovenliggende deeltjes. De druk in evenwicht vertoont een zelfde afhankelijkheid van de afstanden tussen de deeltjes als de elektrostatische afstoting

laat zien. Duidelijk is ook dat de afstanden tussen de deeltjes verkleind worden door toevoeging van meer DoBS-zuur. Dit verschijnsel kan volledig worden verklaard uit de elektrostatische afstotende kracht en de invloed van de hogere ionenconcentraties.

Gezien de resultaten zijn wij overtuigd dat het stabilisatie-mechanisme in dit niet-waterige oplosmiddel elektrostatisch is. Vrijwel in alle gevallen kon een volledige kwantitatieve interpretatie worden bereikt.

CURRICULUM VITAE

Na het behalen van het einddiploma in de afdeling Chemische Techniek aan de Hogere Technische School in Dordrecht in 1965 ben ik in datzelfde jaar in dienst getreden bij het Unilever Research Laboratorium in Vlaardingen. Vervolgens behaalde ik in 1971, op het 'Instituut voor de Opleiding tot Middelbare Akten in de Exacte vakken' verbonden aan de Rijksuniversiteit te Leiden, mijn middelbare akte in de natuur- en scheikunde. In 1972 werd ik benoemd tot 'Research Scientist' in de 'Wasmiddelen divisie' van het Vlaardingse Research Laboratorium. Sinds die tijd heb ik leiding gegeven aan diverse exploratieve en toegepaste projecten in de industriële research. Voorbeelden hiervan zijn: de fotochemische synthese van oppervlakte actieve stoffen, onderzoek naar de massabalans van wasmiddelgebruik in wasmachines, de ontwikkeling van bleekmiddelen geschikt voor gebruik bij lagere temperaturen (TAED), onderzoek naar effecten van een nieuw proteolytisch enzym en een onderzoek naar de toepassingsmogelijkheden van uit oliën en vetten afkomstige gewone zepen. Verder heb ik gedurende een aantal jaren deel uitgemaakt van een "Speculatieve Research Groep'. Het laatste project waar ik sinds 1986 mee belast ben is dat op het gebied van de 'niet-waterige' suspensies. Dit proefschrift beschrijft een deel van de activiteiten die uitgevoerd werden binnen het kader van dit project.